AD-A062 992 OHIO STATE UNIV RESEARCH FOUNDATION COLUMBUS F/G 17/2
TDMA TIMING LOOPS FOR HIGH DATA RATE SYSTEMS.(U)
NOV 78 W G SWARNER, C W CHUANG, R J HUFF F30602-75-C-0061
UNCLASSIFIED OSURF-710300-1(ESL) RADC-TR-78-238 NL

1 OF 3
AD A062992

LEVEL II

RADC-TR-78-238
Interim Report
November 1978

TDMA TIMING LOOPS FOR HIGH DATA RATE SYSTEMS

The Ohio State University ElectroScience Laboratory

W. G. Swarner
C. W. Chuang
R. J. Huff
H. S. Eilts

ROME AIR DEVELOPMENT CENTER
Air Force Systems Command
Griffiss Air Force Base, New York 13441

This report has been reviewed by the RADC Information Office (OI) and is releasable to the National Technical Information Service (NTIS). At NTIS it will be releasable to the general public, including foreign nations.

RADC-TR-78-238 has been reviewed and is approved for publication.

APPROVED: Stuart H. Talbot

STUART H. TALBOT
Project Engineer

APPROVED: Fred I. Diamond

FRED I. DIAMOND, Technical Director
Communications and Control Division

FOR THE COMMANDER: John P. Huss

JOHN P. HUSS
Acting Chief, Plans Office

If your address has changed or if you wish to be removed from the RADC mailing list, or if the addressee is no longer employed by your organization, please notify RADC (DCCR), Griffiss AFB NY 13441. This will assist us in maintaining a current mailing list.

Do not return this copy. Retain or destroy.

UNCLASSIFIED
SECURITY CLASSIFICATION OF THIS PAGE (When Data Entered)

REPORT DOCUMENTATION PAGE

READ INSTRUCTIONS BEFORE COMPLETING FORM

1. REPORT NUMBER: RADC-TR-78-238
2. GOVT ACCESSION NO.: TR-78-238
3. RECIPIENT'S CATALOG NUMBER:
4. TITLE (and Subtitle): TDMA TIMING LOOPS FOR HIGH DATA RATE SYSTEMS
5. TYPE OF REPORT & PERIOD COVERED: Interim Report
6. PERFORMING ORG. REPORT NUMBER: 710300-1(ESL)
7. AUTHOR(s): W. G. Swarner, R. J. Huff, C. W. Chaung, H. S. Eilts
8. CONTRACT OR GRANT NUMBER(s): F30602-75-C-0061
9. PERFORMING ORGANIZATION NAME AND ADDRESS: The Ohio State University ElectroScience Laboratory, Department of Electrical Engineering, Columbus OH 43212
10. PROGRAM ELEMENT, PROJECT, TASK AREA & WORK UNIT NUMBERS: 65230907
11. CONTROLLING OFFICE NAME AND ADDRESS: Rome Air Development (DCCR), Griffiss AFB NY 13441
12. REPORT DATE: November 1978
13. NUMBER OF PAGES: 187
14. MONITORING AGENCY NAME & ADDRESS (if different from Controlling Office): Same
15. SECURITY CLASS. (of this report): UNCLASSIFIED
15a. DECLASSIFICATION DOWNGRADING SCHEDULE: N/A
16. DISTRIBUTION STATEMENT (of this Report): Approved for public release; distribution unlimited
17. DISTRIBUTION STATEMENT (of the abstract entered in Block 20, if different from Report): Same
18. SUPPLEMENTARY NOTES: RADC Project Engineer: Stuart H. Talbot (DCCR)
19. KEY WORDS (Continue on reverse side if necessary and identify by block number): TDMA system timing; Optimum filters; Kalman filters; Digital communications; Satellite communications; Synchronization
20. ABSTRACT (Continue on reverse side if necessary and identify by block number):

Optimum linear recursive filtering techniques are applied to achieve system synchronization for a high data rate bit synchronous TDMA satellite or relay communications system employing two sampled data delay lock loops at each terminal to establish receive clock and transmit timing relative to a system clock at the satellite or relay. It is shown that a system employing an optimum filter in the receive clock loop with open loop coupling to a separate ranging loop for transmit timing can provide synchronization adequate for a 40 Mbit/s system containing highly maneuverable airborne terminals or relays.

→ next page

DD FORM 1 JAN 73 1473

UNCLASSIFIED
SECURITY CLASSIFICATION OF THIS PAGE (When Data Entered)

267 360

Filter models for system timing are developed and analyzed, simulation data are presented to verify and augment the analytical results, and design curves and equations applicable to receive-only as well as transmit-receive synchronization for systems containing maneuvering terminals or maneuvering relays are given.

PREFACE

This report, OSURF Report No. 710300-1, was prepared by the Electro-Science Laboratory, Department of Electrical Engineering, The Ohio State University, Columbus, Ohio. The research reported was funded by Rome Air Development Center, Griffiss Air Force Base, New York, under Contract F30602-75-C-0061. Mr. Stuart Talbot is the RADC Program Monitor.

The model development and timing analyses of Section IV were performed by Dr. Chuang, the extended up-link analysis of Section V by Dr. Huff, and the simulation studies of Section VII by Mr. Eilts. The remaining sections were contributed by Dr. Swarner, who also served as task coordinator.

The many helpful suggestions and guidance provided by Dr. Huff, Mr. R. C. Taylor, and others of the OSU Satellite Communications Facility relative to the RADC/OSU TDMA system are acknowledged and greatly appreciated.

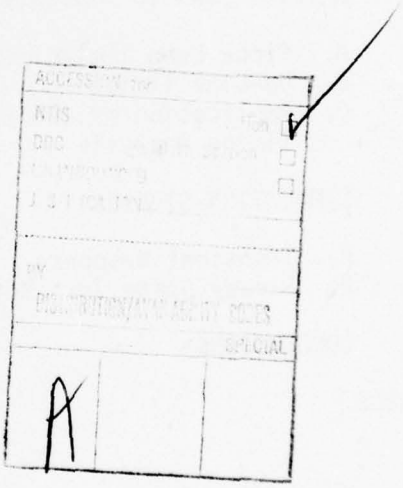

CONTENTS

SECTION I
INTRODUCTION

This report describes the application of linear optimum recursive filtering to upgrade system timing for a bit-synchronous time division multiple access (TDMA) relay communications system. This system was previously developed at The Ohio State University (OSU) ElectroScience Laboratory [1-6] under contracts with the Rome Air Development Center (RADC) of the United States Air Force. Greatly increased signaling rates and improved tracking of highly maneuverable airborne terminals or relays are thus achievable while retaining the advantages of efficiency, flexibility, and anti-jam protection capabilities inherent in this system.

In Section II background information relative to the RADC/OSU TDMA system is given, and in Section III a brief summary of the pertinent results of basic Kalman filter theory [7,8] are presented as a preface to the analyses of Sections IV and V.

In Section IV, a two-dimensional model for the clock loop timing filter is first developed and transient and steady state solutions are obtained following essentially the method employed by Friedland [9]. A three-dimensional augmented model is then developed employing an acceleration correlation coefficient similar to that used by Singer and Behnke [10] for whitening the maneuver noise. Closed-form steady state, as well as transient solutions, for this model are obtained. Transient response is then studied utilizing computer iteration techniques, and results of Monte Carlo simulation studies to check the validity of the models and analytical results are presented. Finally, the problem of up-link synchronization is studied using a method of open loop corrections from the clock loop to the ranging loop to augment the closed loop transmit timing corrections. Expressions for the clock loop and ranging loop timing errors are derived and closed-form steady-state solutions for the transmit timing error variances for a system containing a maneuvering relay and for a system containing maneuvering terminals are obtained and evaluated.

Section V presents a more complete "second generation" analysis of up-link timing utilizing a modified open loop feedback scheme to achieve somewhat lower error variance under receiver noise limited (as opposed to maneuver limited) conditions. This analysis also features retention of additional cross correlation terms, neglected in the previous analysis, which should lead to more accurate analytical results at a cost of increased complexity of the resulting expressions and a corresponding increase in computational effort required to obtain numerical data.

Applications of these results to system design are considered in Section VI. The form of the steady state solutions of Sections IV and V, although mathematically concise, are not particularly amenable to direct application in system design; hence alternative forms are

developed and a series of system design curves giving system parameters as a function of known, or specified, signal and vehicle maneuverability statistics and required timing accuracy are presented. Comparisons between the approximate solutions for up-link timing of Section IV and the more exact solutions of Section V are also given.

In Section VII, typical examples of computer simulation results are given showing system transient response and steady state performance for different signal and noise parameters, and a comparison of steady state error variance with analytical results is given. Conclusions and recommendations are summarized in Section VIII.

SECTION II
BACKGROUND

Techniques for implementing time division multiple access (TDMA) satellite communications systems, particularly those containing a large number of small non-stationary terminals, e.g., aircraft, have previously been developed and successfully demonstrated, both theoretically and experimentally, using prototype modems and a satellite simulator with adaptive spatial processor developed and constructed at this laboratory [1-6].

The signaling format for this system is shown in Figure 1 [5]. The time continuum is divided into non-overlapping intervals or slots, each of which is (normally) allocated for the relaying of signal from no more than one terminal at a time. The slots are defined with respect to the time base of the network clock signal (NCS) present on the satellite down-link once each subframe. At each user terminal the time-base of a locally-generated signal (clock) is aligned with the time base of the received NCS to establish a local receive clock. In turn, a transmit clock is timed so that pulses transmitted by the terminal occupy assigned time slots on arriving at the satellite. Proper transmit clock timing is obtained, during the link-range slots, by estimating the error in arrival time of pulses transmitted by the terminal as they are received on the down-link relative to the local receive clock.

The principal features of this system are:

(1) Only one signal is incident on the satellite at a time so that small terminals do not have to compete for down-link power with much larger ground based terminals which may also be using the system.

(2) A flexible demand assignment signaling format permits efficient use of channel capacity for a large number of both small and large terminals at various data rates compatible with their needs and capabilities.

(3) Differential detection is used (with 2ϕ or 4ϕ DPSK modulation) to minimize signal coherence requirements so that an adaptive spatial processor (adaptive array antenna) can be effectively used at the satellite for up-link protection from interference and jamming.

(4) Bit synchronous timing of both up-link and down-link signals relative to a system clock at the satellite, and the use of differential detection, essentially eliminate the need for preambles and guard space between data bursts thus permitting efficient signal switching and adaptive array operation for small as well as large data bursts.

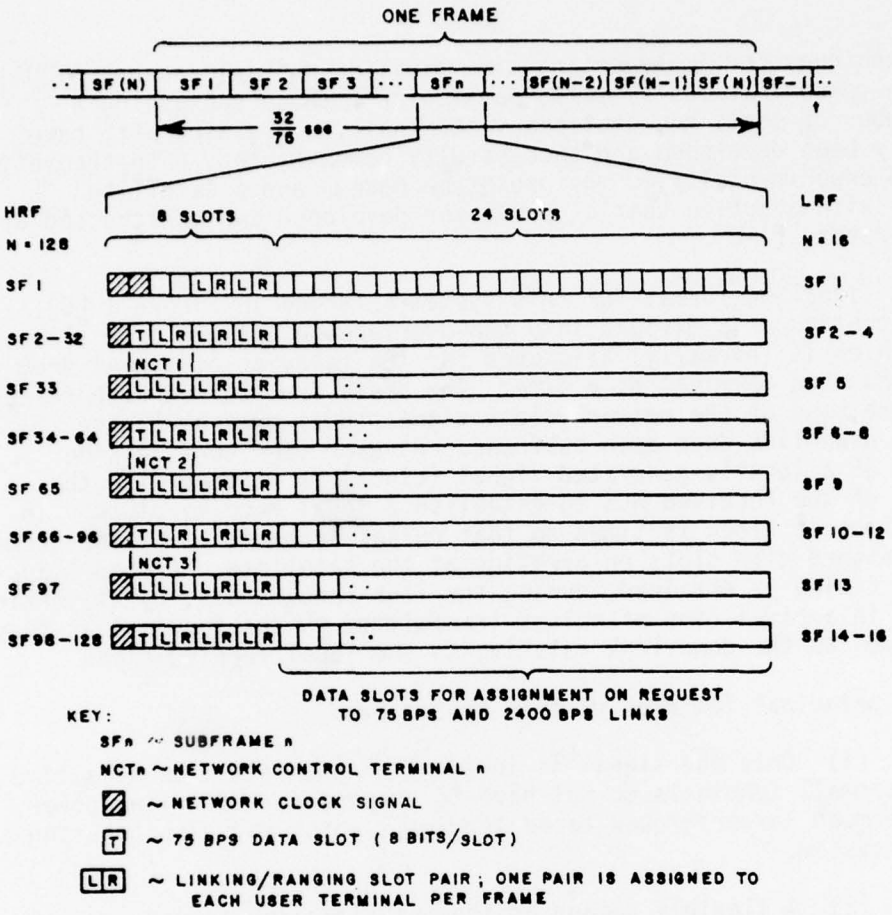

Figure 1. The TDMA modem signaling formats.

A moderate amount of spectrum spreading, via a suitable PN code, is used as a basis for identification of desired signals for spatial processing and also provides additional processing gain for interference reduction.

To obtain reliable operation the timing of all received signals relative to the receive clock must be accurately maintained at each terminal. Practical timing error limits are about 5 percent of the spectrum spreading code chip width to avoid a significant increase in error rate [1]. In the present system this requires accurate control of the transmit timing as well as the receive clock timing relative to the system clock at the satellite and is accomplished by means of two sampled data delay lock loops at each terminal. The first loop phase locks the local receive clock to timing pulses received on the down-link from the satellite once each subframe. These timing pulses may either originate at the satellite - which is especially advantageous when an adaptive array is employed at the satellite, or may be relayed by the satellite from a designated network control terminal. With the receive clock timing thus established the terminal is able to receive all properly-timed transmitted signals relayed by the satellite. The second loop then adjusts the terminal transmit clock so that a ranging pulse transmitted by the terminal once each frame is received on the down-link properly synchronized with the receive clock timing previously established. These delay lock loops operate linearly provided that the timing error does not exceed $\pm 1/2$ chip. Separate coarse ranging (search) circuits (not considered in this report) are used for initial acquisition, or after loss of lock, to bring the error within this operating range.

The prototype system, designed to demonstrate concepts and feasibility and to obtain experimental data compatible with the small terminal concept, employed a relatively low code chip rate of 175.2 Kbps for the lower rate format, and 1.4016 Mbps for the higher rate format. The required timing accuracy for this system, for both transmit and receive clock timing, was readily achieved using simple averaging filters (no memory) in the delay lock loops. As the data rate and/or the terminal maneuverability is increased, however, absolute timing accuracy must also increase in order to retain the same relative accuracy and corresponding error rate. The techniques developed in this report should provide timing accuracy sufficient for similar systems operating at 40 Mbit/s, or greater, with highly maneuverable terminals or relays having accelerations on the order of 5 g.

The method of improving timing accuracy developed in this report employs an optimum linear recursive (Kalman) filter in the terminal receive clock loop to derive an optimum estimate of the system timing, T, (time delay proportional to satellite range) from the noise-corrupted clock pulses received from the satellite by the maneuvering terminal. Optimum estimates of delay rate $\dot{T}$ (velocity) and $\ddot{T}$ (acceleration) are

also derived by this filter and are fed as open loop corrections to the transmit timing loop in a manner similar to that used, for T only, in the original system [1]. Thus the prediction capability of the clock loop filter is utilized in the ranging (transmit timing) loop as well. (Unfortunately, timing errors due to clock oscillator drift are essentially doubled when the open loop correction scheme is used.)

Note that to prevent instability, the rate at which new range estimates can be derived by the closed loop ranging loop is limited by the round trip path delay between the terminal and the relay (approximately 0.25 sec. for a synchronous satellite relay), while no such restriction applies to the system clock pulse rate and terminal clock loop. Hence for a satellite communications system these open loop corrections can be made at a much higher rate (several times per subframe) than can the closed loop range estimates derived by the ranging loop (once per frame).

In effect then, the clock loop provides the tracking capability for transmit timing as well as receive timing, except for a constant range offset. Only this constant offset, plus corrections for inaccuracies in the open loop inputs and for oscillator drift needs to be determined by the ranging loop, and this can be done effectively at a slower rate with a less sophisticated circuit. For this reason, in the present analysis, the original averaging filter is retained in the ranging loop. However, some improvement in transmit timing accuracy should be achievable by applying an optimum filter in this loop also to obtain a better estimate of the offset and drift parameters and this may be the subject of future studies.

SECTION III
THE BASIC OPTIMUM LINEAR RECURSIVE (KALMAN)FILTER

The basic theory of the discrete optimum linear recursive filter, often called the Kalman filter, is well known and adequately documented elsewhere (see, for example, Sage and Melsa [7] and Nahi [8]) and will not be repeated here. However, some pertinent results and implications of the basic analysis which are applicable to the model development and subsequent analytical solutions of Sections IV and V are summarized here for convenience.

A convenient form of the basic Kalman filter for application to the present problem is given in Figure 2. The purpose of this filter

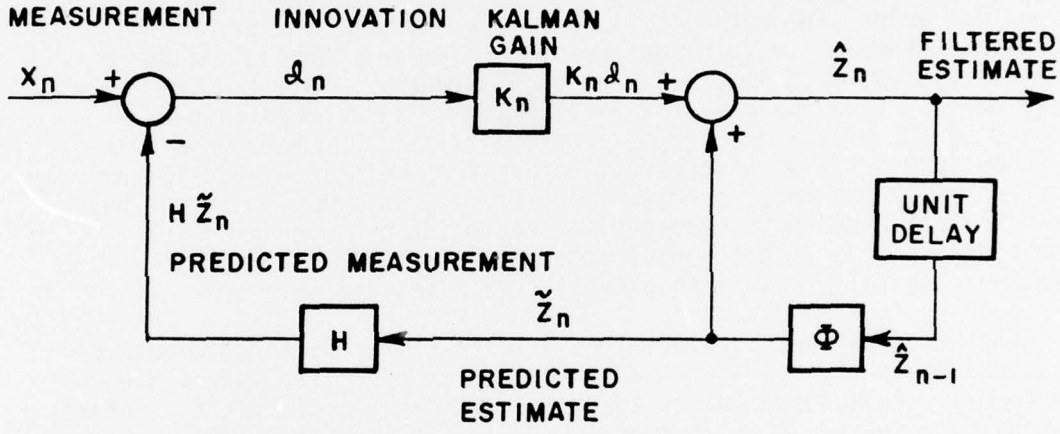

Figure 2. Basic Kalman filter.

is to derive an optimum filtered estimate $\hat{Z}_n$ of the system state vector Z_n following arrival of each noise-corrupted measured data point X_n. As shown in Figure 2, this is accomplished by summing two components: (1) the predicted estimate $\tilde{Z}_n$, and (2) the innovation $\mathcal{I}_n$ multiplied by the Kalman gain vector K_n.

The predicted estimate $\tilde{Z}_n$, which provides the memory of "learned" component of each new estimate, is derived from the previous filtered estimate $\hat{Z}_{n-1}$ via the transition matrix Φ. Thus the predicted estimate is up-dated and recycled with the receipt of every data point so that, at any given time, this estimate contains information, with optimum weighting, on all previous data points collected up to that time.

The innovation $\mathcal{I}_n$ contains the new information supplied by the current measured data point and is obtained by subtracting, from this measured data, the predicted measurement which is the best estimate of what the measurement should have been, based on all previous data collected to date. The predicted measurement is obtained from the predicted estimate $\hat{Z}_n$ via the H-matrix which allows for the fact that the measurement variables X_n may differ from the system state variables Z_n. The innovation therefore contains only the random part (white noise) of the measured data and consists of (for the present example) the random component of the effects of terminal maneuvers and the measurement noise.

The Kalman gain vector provides the optimum weighting between the innovation and the predicted estimate and normally varies (decreases) with each subsequent data point after initial turn-on or acquisition until steady state is reached asymptotically, at which time the adaptive Kalman filter is equivalent to the steady state Wiener filter. The Kalman gain vector is computed for each specific model (see Section IV), and its value, for each iteration n, depends upon the prior statistics assumed; i.e., the measurement noise and terminal maneuver noise statistics which must be supplied externally. Note that the gain in no way depends upon the measured data (a common misconception perpetrated by the often used term - adaptive filter) and hence can be pre-computed and stored if desired, rather than being computed iteratively concurrent with the measurements. However, if, in addition to the basic Kalman filter, a means is provided for measuring and upgrading the prior statistics as a function of time, these may be used in the iterative gain calculations to provide true adaptability.

The error variances, i.e., the variance of the difference between the actual value of each state variable and its estimated value, are also normally calculated (since these are used in calculating the gains) and provide a measure of filter performance. These calculated variances, however, like the gain calculations, are accurate and optimum only to the extent that the actual measurement noise and terminal maneuver statistics agree with the prior statistics assumed for the calculation and, of course, to the degree that the model accurately describes the actual physical process. Hence computer simulation or actual measurements are highly desirable in addition to the filter analysis to validate the results obtained.

As is evident from Figure 2, increasing the Kalman gain vector increases the relative input from the current measurement and hence increases the capability of the filter to track a maneuvering terminal. It also increases the contribution from measurement noise, however, and so it is not surprising that the optimum gain setting is found to depend upon the ratio σ_a/σ_ξ, where σ_a and σ_ξ are the standard deviations of the maneuver "noise" and measurement noise, respectively. Increasing this ratio increases the optimum gain setting, and conversely. In

particular, if we let the maneuver statistics (σ_a) approach zero (i.e., stationary terminals and relay) then the gain vector asymptotically approaches zero with increasing time (since the state vector becomes completely predictable, and hence the gain can be reduced to zero to reduce the input noise), and the filter becomes decoupled from the measurement. This situation must obviously be avoided since, if this happens, even the smallest error in the modeling and/or measurement process will lead to very large errors in the predictions even though the predicted error variance will approach zero along with the gain, a condition known as divergence. This problem is easily avoided by assuming a sufficiently large value of σ_a in the modelling process. Then if the actual maneuver statistics fall below this value the filter performance, although not truly optimum, will generally be adequate, and divergence will not occur.

The principal equations associated with the basic Kalman filter of Figure 2 are summarized below for convenience.

$$\hat{Z}_n = \tilde{Z}_n + K_n \mathscr{l}_n \qquad \text{(filtered estimate)} \qquad (1)$$

$$\tilde{Z}_n = \Phi \hat{Z}_{n-1} \qquad \text{(predicted estimate)} \qquad (2)$$

$$\mathscr{l}_n = X_n - H \tilde{Z}_n \qquad \text{(innovation)} \qquad (3)$$

where Z_n is the system state vector modeled recursively as

$$Z_{n+1} = \Phi Z_n + \Gamma \mu_n \qquad (4)$$

and the measurement is given by

$$X_n = H Z_n + \xi_n. \qquad (5)$$

In the above equations, μ_n and ξ_n are white maneuver noise and measurement noise, respectively. The state vector Z_n, state transition matrix Φ, and the matrices H and Γ are model dependent and are developed for two specific models in the following section, where expressions for the Kalman gain vector K_n and the associated error covariance matrices are also derived.

SECTION IV
MODELING OF A KALMAN FILTER IN TDMA TIMING SYSTEMS

A. Introduction

The terminal receive clock timing system of the TDMA modems developed at The Ohio State University ElectroScience Laboratory employs a sampled data delay lock loop (SDDLL) as shown in Figure 3a [1]. When in lock, the sampled error voltage versus timing error characteristic (E_S vs ε) is linear for $|\varepsilon| < \Delta/2$ where Δ is the chip length of the PN code. This sets an upper limit on the timing error for linear operation of the SDDLL at half the chip length. The discrete loop filter in the SDDLL is a simple averaging filter in which N=4 samples are currently averaged to obtain an output error voltage sample E_S which then is used to adjust the clock rate to reduce the error. A simplified model of the SDDLL including the averaging filter is given in Figure 3b.

Values of the chip length Δ and the timing correction period T_f (4/subframe rate) for the current system in which 4 pulses are averaged are 5.7 μs and 107 ms, respectively, for the lower rate format; and 0.71 μsec and 13.3 ms, respectively, for the higher rate format giving a ratio $T_f/\Delta = 1.9 \cdot 10^4$ for both data formats. If we allow a timing error of .05Δ for acceptable performance (to avoid a significant increase in error rate) then a range rate up to 2.6 μsec/sec (≈1800 mi/hr relative terminal velocity-assuming no oscillator drift or noise contributions) could be accommodated. In the ranging (transmit timing) loop, however, where the minimum correction time is limited by the round trip path delay, the correction time used is T_F = frame rate = 0.427 sec. yielding, for the same error criteria as above, a maximum range rate of 0.67 μsec/sec (450 mi/hr) for the lower rate format and 0.084 μsec/sec (56 mi/hr.) for the higher rate format. Thus the need for open loop corrections to the ranging loop from the receive clock loop (currently provided by the cross strap - see Section II) is clearly indicated when maneuvering terminals and high code chip rates are involved.

We now desire to increase the code chip rate to approximately 40 Mbps, or greater, from the current values of 175 Kbps and 1.4 Mbps for the lower and higher rate formats, respectively, and to allow for tracking of rapidly maneuvering terminals. For a relative timing error of 0.05Δ an absolute timing accuracy on the order of 1 nsec will now be required.

In the absence of measurement noise, the required tracking accuracy could be achieved simply by scaling the sampling interval by the same ratio as the chip length, i.e., retaining the same TDMA format as before, as measured in chips, since the relative timing error due to

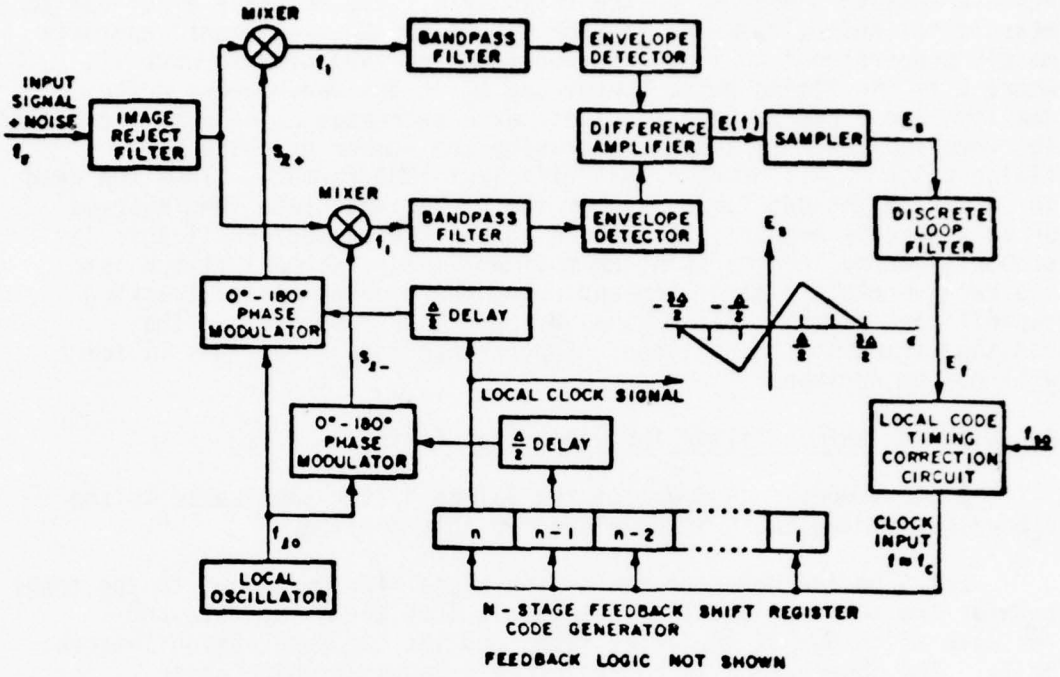

(a) BLOCK DIAGRAM

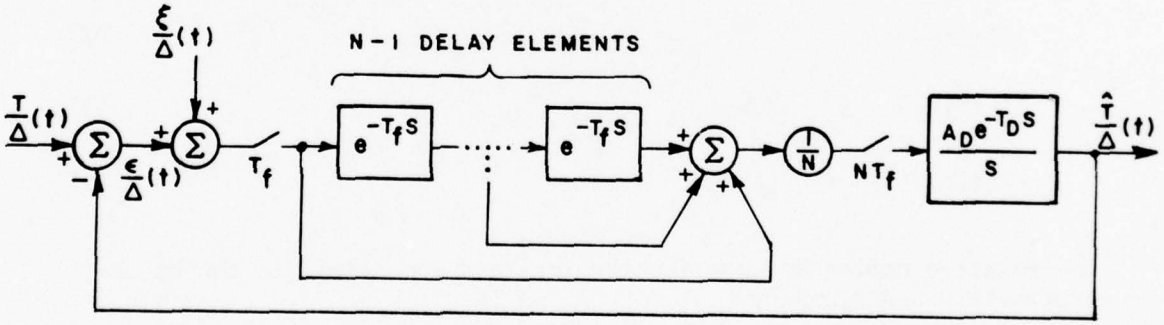

(b) MATHEMATICAL MODEL

Figure 3. The sampled data delay-lock loop (SDDLL).

vehicle maneuvers depends on the ratio T_f/Δ. The relative error due to measurement noise, however, is (for $E/N_0 > 10$, N_0 = constant) approximately proportional to $(1/E)^{1/2}$ (see Equation (48) of Reference 1), where E is the timing pulse energy and N_0 is the measurement noise density; and E can be held constant, with decreased Δ, only by increasing the received power P_r and/or increasing the number of chips M per timing pulse (i.e., using a less efficient TDMA format). Thus the need for a more efficient timing system for higher data rate TDMA systems of this type is evident. As mentioned earlier in Section II this is accomplished by incorporating an optimum linear (Kalman) filter into the receive clock timing loop and using the prediction and tracking capabilities of this filter also, by open loop coupling, in the ranging (transmit timing) loop. Appropriate models for this filter will now be derived.

B. Discrete Kalman Filter for Clock Loop Timing

A two-dimensional model of the Kalman filter applicable to the clock loop timing SDDLL is developed in this section.

Let T be the delay of the timing signal (proportional to the range between the terminal and the satellite), $\dot{T}$ be the delay rate and $\ddot{T}$ the rate of change of the delay rate, and let the observation interval be T_f. The observation is corrupted by a Gaussian white noise ξ, i.e.,

$$X(n) = T(n) + \xi(n) \tag{6}$$

where n represents the nth sample, and the expected values of the measurement noise are given by

$$E[\xi(n)] = 0 \tag{7}$$

$$E[\xi^2(n)] = \sigma_\xi^2 = \text{const.} \tag{8}$$

$$E[\xi(n)\xi(k)] = 0 \quad (n \neq k) \; . \tag{9}$$

The relative motion between the terminal and the satellite can be approximately described by

$$T(n+1) = T(n) + \dot{T}(n)T_f + \frac{1}{2}\ddot{T}(n)T_f^2 \tag{10}$$

$$\dot{T}(n+1) = \dot{T}(n) + \ddot{T}(n)\, T_f . \tag{11}$$

If $\ddot{T}(n)$ can be modeled by white noise, then

$$E[\ddot{T}(n)] = 0 \tag{12}$$

$$E[\ddot{T}^2(n)] = \sigma_a^2 = \text{const.} \tag{13}$$

$$E[\ddot{T}(n)\ddot{T}(k)] = 0 \ (n \neq k) \ . \tag{14}$$

Writing (10), (11) and (6) in matrix form, we have

$$Z(n+1) = \Phi \, Z(n) + \Gamma \ddot{T}(n) \tag{15}$$

where

$$Z(n) = \begin{bmatrix} T(n) \\ \dot{T}(n) \end{bmatrix} \tag{16}$$

$$\Phi \equiv \begin{bmatrix} 1 & T_f \\ 0 & 1 \end{bmatrix} \tag{17}$$

$$\Gamma = \begin{bmatrix} T_f^2/2 \\ T_f \end{bmatrix} \tag{18}$$

and

$$X(n) = H \, Z(n) + \xi(n) \tag{19}$$

where

$$H = [1 \ 0]. \tag{20}$$

For the specific application of the Kalman filter in the SDDLL, it is more convenient to write T, $\dot{T}$, $\ddot{T}$, σ_ξ and σ_a in units of the chip length Δ. The observation interval T_f, which is controlled by the local clock, is not constant because of the non-zero delay rate $\dot{T}$. However, as shown below, the observation interval T_f in (10) and (11) can be replaced by its constant nominal value with negligible error. Assume that the code frequency of the timing signal is 40 MHz. Then the chip length Δ is equal to 25 nsec. Also assume that $\dot{T}$ = 3 μsec/sec = 120 Δ/sec (about three times the speed of sound) and the nominal observation interval = .01 sec. The change in the observation interval from

one observation to the next is only 30 nsec. If this change in the observation interval is included in (10) and (11), it will only contribute $\dot{T} \times 30$ nsec $= 3.6 \times 10^{-6}$ Δ, which is negligible. Therefore, the observation interval T_f will be considered constant.

Following standard procedures for the Kalman filter (see Chapter III) we obtain the optimum estimate of Z(n),

$$\hat{Z}(n) = \tilde{Z}(n) + K(n)\,[X(n) - H\,\tilde{Z}(n)] \tag{21}$$

with

$$\tilde{Z}(n) = \Phi\,\hat{Z}(n-1) \tag{22}$$

where

$$\hat{Z}(n) = \begin{bmatrix} \hat{T}(n) \\ \hat{\dot{T}}(n) \end{bmatrix} \tag{23}$$

is the optimum estimate of Z(n) after the measurement X(n) is processed (i.e., the filtered estimate), and

$$\tilde{Z}(n) = \begin{bmatrix} \tilde{T}(n) \\ \tilde{\dot{T}}(n) \end{bmatrix} \tag{24}$$

is the optimum estimate of Z(n) before the measurement X(n) is processed (the predicted estimate). The gain matrix K(n) is given by

$$K(n) = \tilde{P}(n)\,H^T[H\,\tilde{P}(n)\,H^T + R]^{-1} \tag{25}$$

where

$$R = \sigma_\xi^2 \tag{26}$$

and

$$\tilde{P}(n) = E[(\tilde{Z}(n) - Z(n))(\tilde{Z}(n) - Z(n))^T] \tag{27}$$

is the covariance matrix of estimation error prior to processing X(n). The covariance matrix $\tilde{P}(n)$ is computed recursively using the variance equation

$$\tilde{P}(n+1) = \Phi\hat{P}(n)\Phi^T + \Gamma Q \Gamma^T \tag{28}$$

with

$$\hat{P}(n) = [I-K(n)\ H]\ \tilde{P}(n) \tag{29}$$

where

$$\hat{P}(n) = E[(\hat{Z}(n) - Z(n))(\hat{Z}(n) - Z(n))^T] \tag{30}$$

is the covariance matrix of estimation error after processing $X(n)$,

$$Q = \sigma_a^2 \tag{31}$$

is the variance of the random acceleration, and superscript T indicates the transpose of the matrix. Using the matrix inversion lemma [7], we obtain from (29),

$$\hat{P}^{-1}(n) = \tilde{P}^{-1}(n) + H^T R^{-1}\ H. \tag{32}$$

Multiplying (32) by $\hat{P}(n)$ and $\tilde{P}(n)$, we obtain

$$\tilde{P}(n) = \hat{P}(n) + \hat{P}(n) H^T R^{-1}\ H\ \tilde{P}(n). \tag{33}$$

By comparing the above equation with (29), we have

$$K(n) = \hat{P}(n)\ H^T\ R^{-1}\ . \tag{34}$$

The initial estimation of $\hat{Z}$ (after two data points have been received) is given by

$$\hat{Z}(2) = \begin{bmatrix} X(2) \\ \\ \frac{1}{T_f}\ (X(2)-X(1)) \end{bmatrix} \tag{35}$$

where the values of X(1) and X(2) are obtained implicitly (outside the SDDLL) from the 1st and 2nd range delay measurements, respectively. Then the initial value of the covariance matrix of estimation error is

$$\hat{P}(2) = \begin{bmatrix} \sigma_\xi^2 & \sigma_\xi^2/T_f \\ \\ \sigma_\xi^2/T_f & \frac{1}{4}\ \sigma_a^2\ T_f^2 + 2\sigma_\xi^2/T_f^2 \end{bmatrix}. \tag{36}$$

The transient behavior is best studied using numerical methods and will be given in section D. The steady-state behavior is given in the following.

In the steady state, (28) and (29), using (25) reduce to

$$\tilde{P} = \Phi \hat{P} \Phi^T + \Gamma Q \Gamma^T \tag{37}$$

and

$$\hat{P} = \tilde{P} - \tilde{P} H^T [H\tilde{P}H^T+R]^{-1} H \tilde{P} \quad . \tag{38}$$

Combining (37) and (38),

$$\Phi^{-1}(\tilde{P}-\Gamma Q\Gamma^T)(\Phi^{-1})^T = \tilde{P}-\tilde{P}H^T[H\tilde{P}H^T+R]^{-1}H\tilde{P}. \tag{39}$$

Let

$$\tilde{P} = \begin{bmatrix} \tilde{P}_1 & \tilde{P}_2 \\ \tilde{P}_2 & \tilde{P}_3 \end{bmatrix} \tag{40}$$

then

$$H\tilde{P}H^T+R=[1 \quad 0] \begin{bmatrix} \tilde{P}_1 & \tilde{P}_2 \\ \tilde{P}_2 & \tilde{P}_3 \end{bmatrix} \begin{bmatrix} 1 \\ 0 \end{bmatrix} + \sigma_\xi^2 = \tilde{P}_1 + \sigma_\xi^2 \tag{41}$$

$$\tilde{P}H^T[H\tilde{P}H^T+R]H\tilde{P} = \frac{1}{\tilde{P}_1+\sigma_\xi^2} \begin{bmatrix} \tilde{P}_1 & \tilde{P}_2 \\ \tilde{P}_2 & \tilde{P}_3 \end{bmatrix} \begin{bmatrix} 1 \\ 0 \end{bmatrix} [1 \quad 0] \begin{bmatrix} \tilde{P}_1 & \tilde{P}_2 \\ \tilde{P}_2 & \tilde{P}_3 \end{bmatrix} = \frac{1}{\tilde{P}_1+\sigma_\xi^2} \begin{bmatrix} \tilde{P}_1^2 & \tilde{P}_1\tilde{P}_2 \\ \tilde{P}_1\tilde{P}_2 & \tilde{P}_2^2 \end{bmatrix} \tag{42}$$

and

$$\tilde{P}-\tilde{P}H^T[H\tilde{P}H^T+R]^{-1}H\tilde{P} = \frac{1}{\tilde{P}_1+\sigma_\xi^2} \begin{bmatrix} \tilde{P}_1\sigma_\xi^2 & \tilde{P}_2\sigma_\xi^2 \\ \tilde{P}_2\sigma_\xi^2 & \tilde{P}_1\tilde{P}_3-\tilde{P}_2^2+\tilde{P}_3\sigma_\xi^2 \end{bmatrix} . \tag{43}$$

We also have

$$\Phi^{-1} = \begin{bmatrix} 1 & -T_f \\ 0 & 1 \end{bmatrix} \tag{44}$$

$$\Gamma Q \Gamma^T = \begin{bmatrix} T_f^2/2 \\ T_f \end{bmatrix} [T_f^2/2 \quad T_f] \sigma_a^2 = \sigma_a^2 \begin{bmatrix} T_f^4/4 & T_f^3/2 \\ T_f^3/2 & T_f^2 \end{bmatrix} \tag{45}$$

$$\tilde{P} - \Gamma Q \Gamma^T = \begin{bmatrix} \tilde{P}_1 - \frac{\sigma_a^2 T_f^4}{4} & \tilde{P}_2 - \frac{\sigma_a^2 T_f^3}{2} \\ \tilde{P}_2 - \frac{\sigma_a^2 T_f^3}{2} & \tilde{P}_3 - \sigma_a^2 T_f^2 \end{bmatrix} \tag{46}$$

and

$$\Phi^{-1}(\tilde{P} - \Gamma Q \Gamma^T)(\Phi^{-1})^T = \begin{bmatrix} \tilde{P}_1 - 2\tilde{P}_2 T_f + \tilde{P}_3 T_f^2 - \frac{\sigma_a^2 T_f^4}{4} & \tilde{P}_2 - \tilde{P}_3 T_f + \frac{\sigma_a^2 T_f^3}{2} \\ \tilde{P}_2 - \tilde{P}_3 T_f + \frac{\sigma_a^2 T_f^3}{2} & \tilde{P}_3 - \sigma_a^2 T_f^2 \end{bmatrix}. \tag{47}$$

On equating both sides of (39),

$$\tilde{P}_1 - 2\tilde{P}_2 T_f + \tilde{P}_3 T_f^2 - \sigma_a^2 T_f^4/4 = \tilde{P}_1 \sigma_\xi^2/(\tilde{P}_1 + \sigma_\xi^2) \tag{48}$$

$$\tilde{P}_2 - \tilde{P}_3 T_f + \sigma_a^2 T_f^3/2 = \tilde{P}_2 \sigma_\xi^2/(\tilde{P}_1 + \sigma_\xi^2) \tag{49}$$

and

$$\tilde{P}_3 - \sigma_a^2 T_f^2 = \tilde{P}_3 - \tilde{P}_2^2/(\tilde{P}_1 + \sigma_\xi^2) \quad . \tag{50}$$

The algebraic manipulations for determining $\tilde{P}_1$, $\tilde{P}_2$ and $\tilde{P}_3$ are as follows:

Define

$$A = \frac{\tilde{P}_1}{\sigma_\xi^2} \tag{51}$$

$$B = \frac{\tilde{P}_2}{\sigma_\xi \sigma_a T_f} \tag{52}$$

and

$$r = \frac{4\sigma_\xi}{\sigma_a T_f^2} \quad . \tag{53}$$

Then from (50):

$$A = B^2 - 1. \tag{54}$$

(48) $\times \frac{1}{\sigma_\xi^2}$ + (49) $\times \frac{T_f}{\sigma_\xi^2}$:

$$A - \frac{4}{r} B + \frac{4}{r^2} = \frac{A}{1+A} + \frac{B}{1+A} \cdot \frac{4}{r} \quad . \tag{55}$$

From (55):

$$B = \frac{r}{4} \left[\frac{A^2+4(1+A)/r^2}{2+A} \right] . \tag{56}$$

Substituting (56) into (54),

$$r^4A^4-8r^2A^3+(16-72r^2)A^2+(32-128r^2)A+(16-64r^2) = 0 \tag{57}$$

or

$$[r^2A^2-4(1+2r)A-4(1+2r)][r^2A^2-4(1-2r)A-4(1-2r)] = 0. \tag{58}$$

Therefore

$$A = \pm \frac{\sqrt{1+2r}\ (\sqrt{1+2r} \pm 1)^2}{r^2} \tag{59}$$

or

$$A = \pm \frac{\sqrt{1-2r}\ (\sqrt{1-2r} \pm 1)^2}{r^2} \quad . \tag{60}$$

The positive sign options must be chosen since $A \geq 0$ and, the second solution (60) must be discarded because it makes $\tilde{P}_1\tilde{P}_3 - \tilde{P}_2^2 < 0$. Therefore:

$$A = \frac{\sqrt{1+2r}\ (\sqrt{1+2r} + 1)^2}{r^2} \quad . \tag{61}$$

Finally we obtain

$$\frac{\tilde{P}_1}{\sigma_\xi^2} = \frac{\sqrt{1+2r}\ (\sqrt{1+2r} + 1)^2}{r^2} \tag{62}$$

$$\frac{\tilde{P}_2}{\sigma_\xi \sigma_a T_f} = \frac{(\sqrt{1+2r} + 1)^2}{2r} \tag{63}$$

$$\frac{\tilde{P}_3}{\sigma_a^2 T_f^2} = \frac{1}{2}\ (\sqrt{1+2r} + 1) \tag{64}$$

where

$$r = \frac{4\sigma_\xi}{\sigma_a T_f^2} \quad . \tag{65}$$

The ratio r is a dimensionless parameter which could be regarded as a form of noise to signal ratio.

From (38)

$$\hat{P} = \frac{1}{1+\tilde{P}_1/\sigma_\xi^2} \begin{bmatrix} \tilde{P}_1 & \tilde{P}_2 \\ \tilde{P}_2 & \tilde{P}_3 + \frac{D}{\sigma_\xi^2} \end{bmatrix} \equiv \begin{bmatrix} \hat{P}_1 & \hat{P}_2 \\ \hat{P}_2 & \hat{P}_3 \end{bmatrix} \tag{66}$$

where

$$D = \tilde{P}_1\tilde{P}_3 - \tilde{P}_2^2 \quad . \tag{67}$$

Therefore

$$\frac{\hat{P}_1}{\sigma_\xi^2} = \frac{\sqrt{1+2r}\ (\sqrt{1+2r} - 1)^2}{r^2} \tag{68}$$

$$\frac{\hat{P}_2}{\sigma_\xi \sigma_a T_f} = \frac{(\sqrt{1+2r} - 1)^2}{2r} \tag{69}$$

$$\frac{\hat{P}_3}{\sigma_a^2 T_f^2} = \frac{1}{2}(\sqrt{1+2r} - 1) \quad . \tag{70}$$

Then from (34)

$$K = \begin{bmatrix} K_T \\ \\ K_{\dot{T}} \end{bmatrix} = \hat{P}\, H^T R^{-1} = \begin{bmatrix} \hat{P}_1/\sigma_\xi^2 \\ \\ \hat{P}_2/\sigma_\xi^2 \end{bmatrix} \quad . \tag{71}$$

Therefore the steady state gain factors are given by

$$K_T = \frac{\sqrt{1+2r}\ (\sqrt{1+2r} - 1)^2}{r^2} \tag{72}$$

and

$$K_{\dot{T}} = \frac{2(\sqrt{1+2r} - 1)^2}{T_f r^2} \quad . \tag{73}$$

Graphs of $\hat{P}_1/\sigma_\xi^2 = K_T$, $\tilde{P}_1/\sigma_\xi^2$ and $K_{\dot{T}} T_f$ as functions of r are shown in Figure 4. It is seen that the normalized timing error variance just after processing a data point $\hat{P}_1/\sigma_\xi^2$ is always less than 1, while the normalized timing error variance just prior to processing a data point $\tilde{P}_1/\sigma_\xi^2$ can be larger or smaller than 1. The cross over point occurs at $r \approx 16$. Therefore if the observation interval is chosen to be

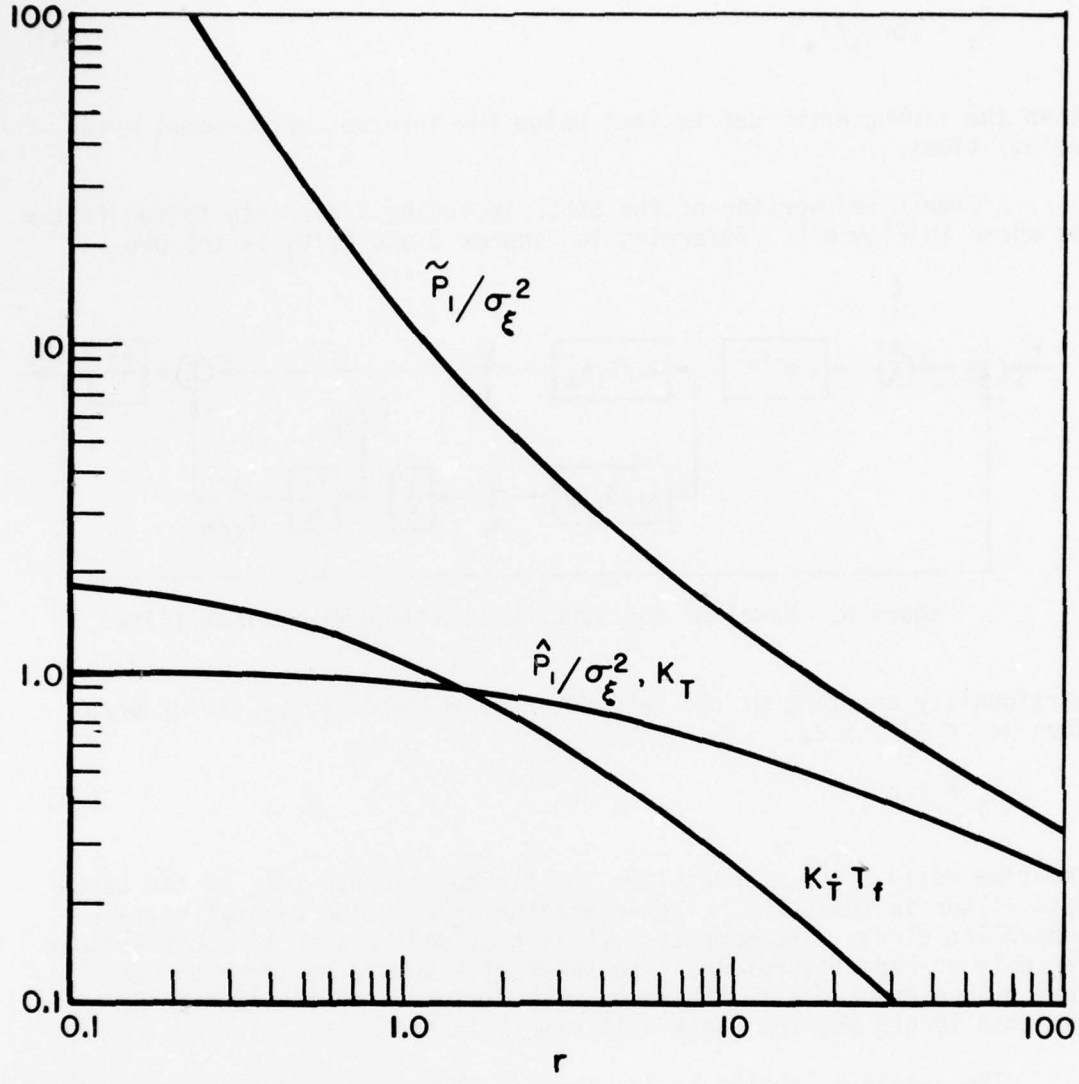

Figure 4. Steady-state gains and error variances versus r for the two-dimensional Kalman filter.

$$T_f < .5\sqrt{\sigma_\xi/\sigma_a} \ , \tag{74}$$

then the timing error can be kept below the inherent measurement error at all times.

A simplified version of the SDDLL including a discrete Kalman filter is shown in Figure 5. Referring to Figures 3 and 5, k_1 is the pro-

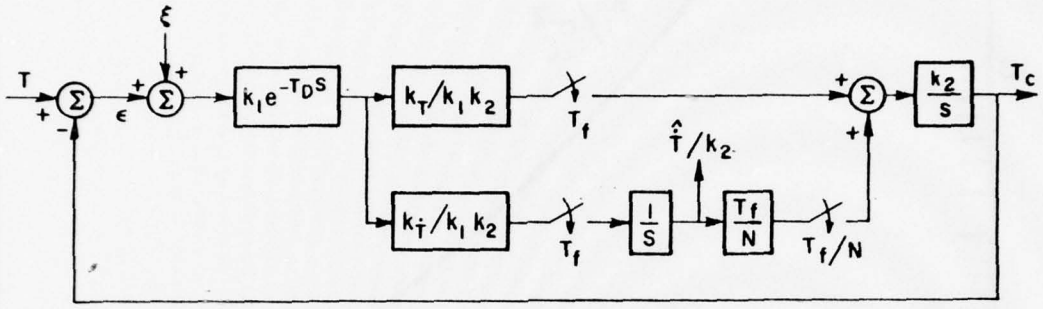

Figure 5. Model of the SDDLL with a discrete Kalman filter.

portionality constant of the sampled error voltage versus timing error when $|\varepsilon| < \Delta/2$, i.e.,

$$E_s = k_1\varepsilon \ . \tag{75}$$

The time delay $e^{-T_D S}$ accounts for the finite response time of the band-pass filter in the SDDLL. The integrator k_2/s is the digital voltage controlled clock. The sampler T_f/N is provided because time corrections can only be made discretely. The value of N should be large enough that timing error due to the range rate will be a small fraction of the chip length and the clock will remain locked.

The samplers labeled T_f in Figure 5 close momentarily once per sample period at times $t = nT_f+T_D$ where nT_f indicates the arrival times of the samples T, while the sampler labeled T_f/N closes N times per sample period (evenly spaced) with the initial closure occurring at $t = nT_f + T_D + T_f/2n$.

The filter output, T_C in Figure 5, provides an optimum timing estimate (within limits established by the discrete corrections T_f/N) at all times. This estimate varies from the predicted estimate $\check{T}_n$ (with variance $\check{P}_n$ - the worst case) just prior to processing the nth data point to the filtered estimate $\hat{T}_n$ (with variance P_n - the best case) just after the nth data point has been processed.

If the bandwidth of the band-pass filter is optimum [1], i.e.,

$$B_{IF_{opt}} = 1.37/M\Delta \tag{76}$$

where $M\Delta$ is the length of the PN code, then

$$\frac{\sigma_\xi}{\Delta} = \frac{1}{2}\left[\frac{1.215}{E/N_o} + C\,\frac{1.476}{(E/N_o)^2}\right]^{1/2} \tag{77}$$

where

$$C = \begin{cases} 2 \text{ for square-law detection} \\ 1 \text{ for linear detection} \end{cases} \tag{78}$$

$E = P_r M\Delta$ = input pulse energy (joules)

P_r = input power (watts)

and

N_o = one-sided input noise power spectral density (watts per Hertz).

To obtain the standard deviation of the maneuver noise σ_a, we assume that the probability density of $\ddot{T}$ is as shown in Figure 6 [10].

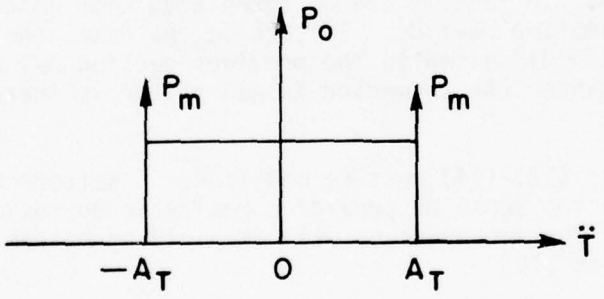

Figure 6. Probability density of $\ddot{T}$.

The quantity A_T in this figure might be considered as the maximum "path delay acceleration" given by

$$A_T = A/c \ (\text{sec/sec}^2) \tag{79}$$

where

A = terminal acceleration (m/sec^2) relative to the satellite, and

c = velocity of light (m/sec).

Therefore, since the mean value $E(\ddot{I})$ is zero by symmetry, the variance is given by

$$\sigma_a^2 = E(\ddot{I}^2) = \int_{-\infty}^{\infty} \ddot{I}^2 \, p(\ddot{I}) \, d\ddot{I} = \frac{A_T^2}{3} \ (1 + 4P_m - P_o) \ (\text{sec}^{-2}) \tag{80}$$

where $p(\ddot{I})$ is the probability density function of Figure 6. The value of σ_a thus obtained is taken to be a known constant in the modeling of the Kalman filter.

If σ_ξ or σ_a vary widely with time in a given application, separate measurements (or estimates) of σ_ξ/σ_a could be made periodically and used in place of the calculated constants to obtain improved filter performance.

C. Augmented Discrete Kalman Filter

In the previous section the maneuver noise $\ddot{I}$ is considered to be white. However, in a TDMA modem a typical sampling period T_f is only about .01 sec which is much shorter than the time required for executing a manuever, hence the maneuver at one sampling period will be correlated with the maneuver at the previous and at the next sampling period. In fact it can be correlated with maneuvers separated by many sampling periods. If such is the case, the simple discrete Kalman filter discussed in the previous section may not yield satisfactory performance. An augmented Kalman filter is therefore needed.

First, Equations (12)-(14) must be modified. A satisfactory correlation function in the sense of providing realistic approximations to the statistics of the maneuvers as well as yielding mathematically tractable solutions is [10]

$$E[\ddot{I}(n) \ \ddot{I}(k)] = \sigma_a^2 \rho^{|n-k|} \tag{81}$$

where σ_a^2 is obtained as before (Figure 6 and Equation (36)) and the correlation coefficient ρ is modeled by

$$\rho = \begin{cases} 1 - \lambda T_f & \text{if} \quad T_f \leq \frac{1}{\lambda} \\ 0 & \text{if} \quad T_f > \frac{1}{\lambda} \end{cases} \tag{82}$$

The quantity λ is essentially the inverse of the average manuever duration. With the correlation defined as above, the dynamics of the terminal are then described by

$$T(n+1) = T(n) + \dot{T}(n)\, T_f + \frac{1}{2} \ddot{T}(n)\, T_f^2 \tag{83}$$

$$\dot{T}(n+1) = \dot{T}(n) + \ddot{T}(n)\, T_f \tag{84}$$

$$\ddot{T}(n+1) = \rho\, \ddot{T}(n) + u(n) \tag{85}$$

where $u(n)$ is a white noise of zero-mean and variance $\sigma_a^2(1-\rho^2)$. In matrix notation, (83)-(85) becomes

$$Z(n+1) = \Phi Z(n) + \Gamma u(n) \tag{86}$$

where

$$Z(n) = \begin{bmatrix} T(n) \\ \dot{T}(n) \\ \ddot{T}(n) \end{bmatrix} \tag{87}$$

$$\Phi = \begin{bmatrix} 1 & T_f & T_f^2/2 \\ 0 & 1 & T_f \\ 0 & 0 & \rho \end{bmatrix} \tag{88}$$

and

$$\Gamma = \begin{bmatrix} 0 \\ 0 \\ 1 \end{bmatrix}. \tag{89}$$

The measurement is given by

$$X(n) = H\, Z(n) + \xi(n) \tag{90}$$

with

$$H = [1\ 0\ 0] \tag{91}$$

and the statistics of $\xi(n)$ as given previously in Equations (7)-(9).

Mathematical development of the augmented Kalman filter follows essentially the same path as in the previous section, with a few changes in the matrix contents (see Equations (28) through (36)),

$$Q = \sigma_a^2(1-\rho^2) \tag{92}$$

$$\hat{Z}(2) = \begin{bmatrix} \bar{X}(2) \\ \frac{1}{T_f}\,(X(2)-X(1)) \\ 0 \end{bmatrix} \tag{93}$$

and

$$\hat{P}(2) = \begin{bmatrix} \sigma_\xi^2 & \sigma_\xi^2/T_f & 0 \\ \sigma_\xi^2/T_f & \frac{\sigma_a^2 T_f^2}{4} + 2\sigma_\xi^2/T_f^2 & \frac{\rho\sigma_a^2 T_f}{2} \\ 0 & \frac{\rho\sigma_a^2 T_f}{2} & \sigma_a^2 \end{bmatrix} . \tag{94}$$

Again, the steady-state behavior is discussed first. In the steady state, let

$$\tilde{P} = \begin{bmatrix} \tilde{P}_1 & \tilde{P}_2 & \tilde{P}_4 \\ \tilde{P}_2 & \tilde{P}_3 & \tilde{P}_5 \\ \tilde{P}_4 & \tilde{P}_5 & \tilde{P}_6 \end{bmatrix} . \tag{95}$$

Then from (39), we obtain

$$A - \frac{8}{r} B + \frac{16}{r^2} C + \frac{4}{r} D - \frac{16}{r^2} E + \frac{4}{r^2} F = \frac{A}{1+A} - \frac{4}{r^2} \tag{96}$$

$$B - \frac{4}{r} C - D + \frac{6}{r} E - \frac{2}{r} F = \frac{B}{1+A} + \frac{2}{r} \tag{97}$$

$$C - 2E + F = C - \frac{B^2}{1+A} - 1 \tag{98}$$

$$D - \frac{4}{r} E + \frac{2}{r} F = \frac{\rho D}{1+A} - \frac{2}{r} \tag{99}$$

$$E - F = \rho E - \frac{\rho BD}{1+A} + 1 \tag{100}$$

$$F = \rho^2 F - \frac{\rho^2 D^2}{1+A} \tag{101}$$

where

$$r = 4\sigma_\xi / \sigma_a T_f^2 \tag{102}$$

$$A = \tilde{P}_1 / \sigma_\xi^2 \tag{103}$$

$$B = \tilde{P}_2 / \sigma_\xi \sigma_a T_f \tag{104}$$

$$C = \tilde{P}_3 / \sigma_a^2 T_f^2 \tag{105}$$

$$D = \tilde{P}_4 / \rho \sigma_\xi \sigma_a \tag{106}$$

$$E = \tilde{P}_5 / \rho \sigma_a^2 T_f \tag{107}$$

and

$$F = (\tilde{P}_6 - \sigma_a^2) / \rho^2 \sigma_a^2 \quad . \tag{108}$$

Manipulations for solving this system of equations are as follows:

(99) - $\frac{2}{r}$ x (98):

$$D = \frac{2}{r} B^2/(1+A-\rho) \quad . \tag{109}$$

Substituting (109) into (101):

$$F = - \frac{4\rho^2 B^4}{r^2(1+A-\rho)^2(1+A)(1-\rho^2)} \quad . \tag{110}$$

Substituting (110) into (98):

$$E = \frac{1}{2} + \frac{B^2}{2(1+A)} - \frac{2\rho^2 B^4}{r^2(1+A-\rho)^2(1+A)(1-\rho^2)} \quad . \tag{111}$$

Substituting (109), (110) and (111) into (100):

$$B^2 \left[1 + \frac{2\rho B}{r(1+A-\rho)(1-\rho)}\right]^2 = \frac{1+\rho}{1-\rho} (1+A) \tag{112}$$

or

$$B \left[1 + \frac{2\rho B}{r(1+A-\rho)(1-\rho)}\right] = \sqrt{\frac{1+\rho}{1-\rho}} \sqrt{1+A} \quad . \tag{113}$$

(96) + $\frac{4}{r}$ x (97) + $\frac{4}{r^2}$ x (98):

$$A - \frac{4}{r} B = (A + \frac{4}{r} B - \frac{4}{r^2} B^2)/(1+A) \tag{114}$$

or

$$B = \frac{r}{2} (\sqrt{1+A} \pm 1)^2 \quad . \tag{115}$$

Now let

$$A = (x \mp 1)^2 - 1 \tag{116}$$

and

$$r = r_\rho \left(\frac{1+\rho}{1-\rho}\right)^{1/2} \quad . \tag{117}$$

Then substituting (115), (116) and (117) into (113) gives

$$x^4 + 2(1-\rho)\left(\mp 1 - \frac{1}{r_\rho}\right)x^3 + (1-\rho)\left[(1-\rho) \pm \frac{6}{r_\rho}\right]x^2 - \frac{2(1-\rho)(3-\rho)}{r_\rho}\,x \pm \frac{2(1-\rho)^2}{r_\rho} = 0. \tag{118}$$

It can be shown (since $A = \hat{P}_1/\sigma_\xi^2$ must be real and non-negative) that the lower sign options of Equation (118) must be used, and in addition that this equation yields only one positive real root, which is the correct root.

The 4th order equation (118) may be solved by the standard (closed form) method as given in many mathematical handbooks [11-12] or by computer iteration techniques. Both methods have been used to generate results presented in this report. (The iteration techniques are easier to program while the closed form solutions are more efficient.)

If $r_\rho(1-\rho)^2 >> 1$, then an approximate solution for x is

$$x \approx \frac{1}{r_\rho} + \left(\frac{2}{r_\rho}\right)^{1/2}\left(1 + \frac{1}{4r_\rho} - \frac{1}{32r_\rho^2}\right) - \frac{\rho}{2(1-\rho)^2}\left(\frac{2}{r_\rho}\right)^{3/2}\left[1 - \frac{2\rho}{1-\rho}\left(\frac{2}{r_\rho}\right)^{1/2} + \frac{(15+3\rho+31\rho^2)}{16(1-\rho)^2}\left(\frac{2}{r_\rho}\right)\right]. \tag{119}$$

From (34) and (38) we obtain the steady-state gain matrix,

$$K = \begin{bmatrix} K_T \\ K_T^{\bullet} \\ K_T^{\bullet\bullet} \end{bmatrix} = \begin{bmatrix} \hat{P}_1/\sigma_\xi^2 \\ \hat{P}_2/\sigma_\xi^2 \\ \hat{P}_4/\sigma_\xi^2 \end{bmatrix} \tag{120}$$

where

$$K_T = \hat{P}_1/\sigma_\xi^2 = \frac{\tilde{P}_1/\sigma_\xi^2}{1 + \tilde{P}_1/\sigma_\xi^2} \tag{121}$$

$$K_{\dot{T}} = \hat{P}_2/\sigma_\xi^2 = \frac{4}{rT_f} \frac{\tilde{P}_2/\sigma_\xi\sigma_a T_f}{1+\tilde{P}_1/\sigma_\xi^2} \tag{122}$$

$$K_{\ddot{T}} = \hat{P}_4/\sigma_\xi^2 = \frac{4\rho}{rT_f^2} \frac{\tilde{P}_4/\rho\sigma_\xi\sigma_a}{1+\tilde{P}_1/\sigma_\xi^2} \quad . \tag{123}$$

Then we obtain from Equations (96) to (123)

$$A = (x+1)^2 - 1 = \frac{\tilde{P}_1}{\sigma_\xi^2} \tag{124}$$

$$B = \frac{r}{2}\left(\sqrt{1+A}-1\right)^2 = \frac{\tilde{P}_2}{\sigma_\xi\sigma_a T_f} \tag{125}$$

$$D = \frac{2B^2}{r(1+A-\rho)} = \frac{\tilde{P}_4}{\rho\sigma_\xi\sigma_a} \tag{126}$$

$$K_T = \frac{\hat{P}_1}{\sigma_\xi^2} = \frac{A}{1+A} \tag{127}$$

$$K_{\dot{T}}T_f = \frac{4}{r} \frac{B}{1+A} \tag{128}$$

$$K_{\ddot{T}}T_f^2 = \frac{4\rho}{r} \frac{D}{1+A} \quad . \tag{129}$$

Graphs of $\tilde{P}_1/\sigma_\xi^2$, $\hat{P}_1/\sigma_\xi^2 = K_T$, $K_{\dot{T}}T_f$, and $K_{\ddot{T}}T_f^2$ as functions of r_ρ for different values of ρ (obtained from the exact solution, Equation (118)) are shown in Figures 7 through 10. Note that for $\rho=0$ the augmented Kalman filter reduces to the two-dimensional filter analyzed earlier, and the corresponding curves are in agreement with those given previously in Figure 4.

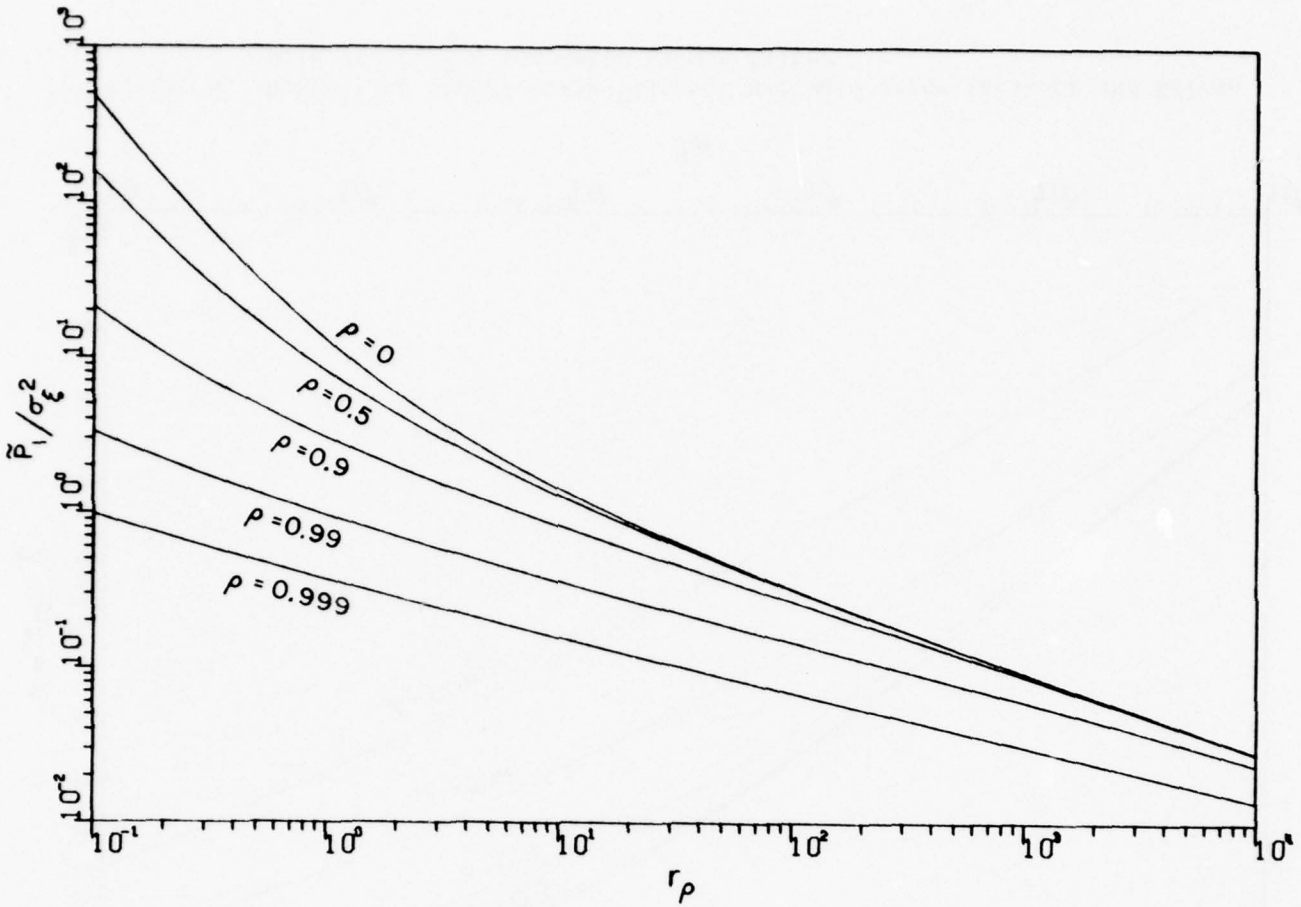

Figure 7. Normalized steady state predicted estimate error variance vs. r_ρ for augmented Kalman filter.

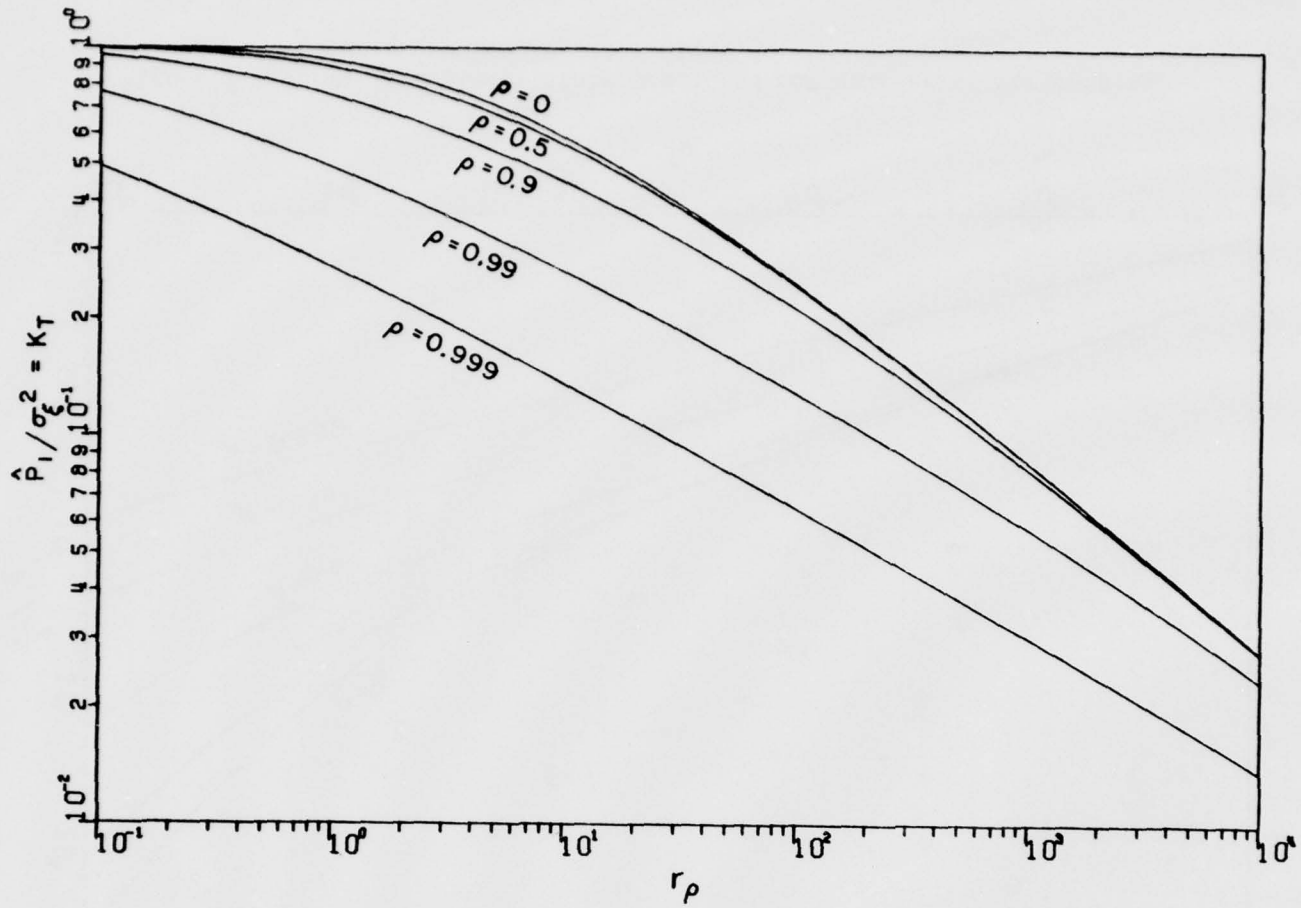

Figure 8. Normalized steady state filtered estimate error variance and Kalman gain vs. r_ρ for augmented Kalman filter

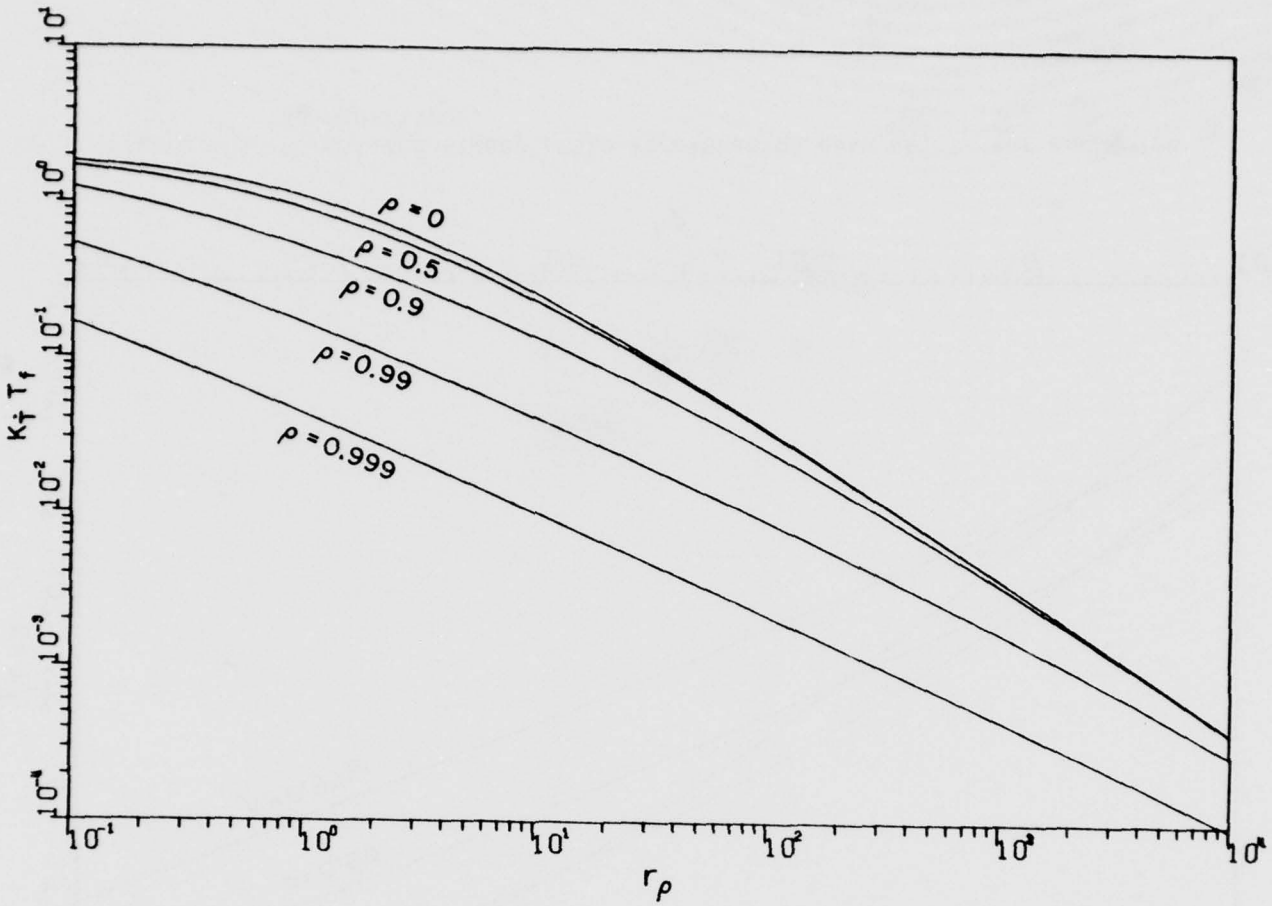

Figure 9. Normalized steady state velocity gain vs. r_ρ for augmented Kalman filter.

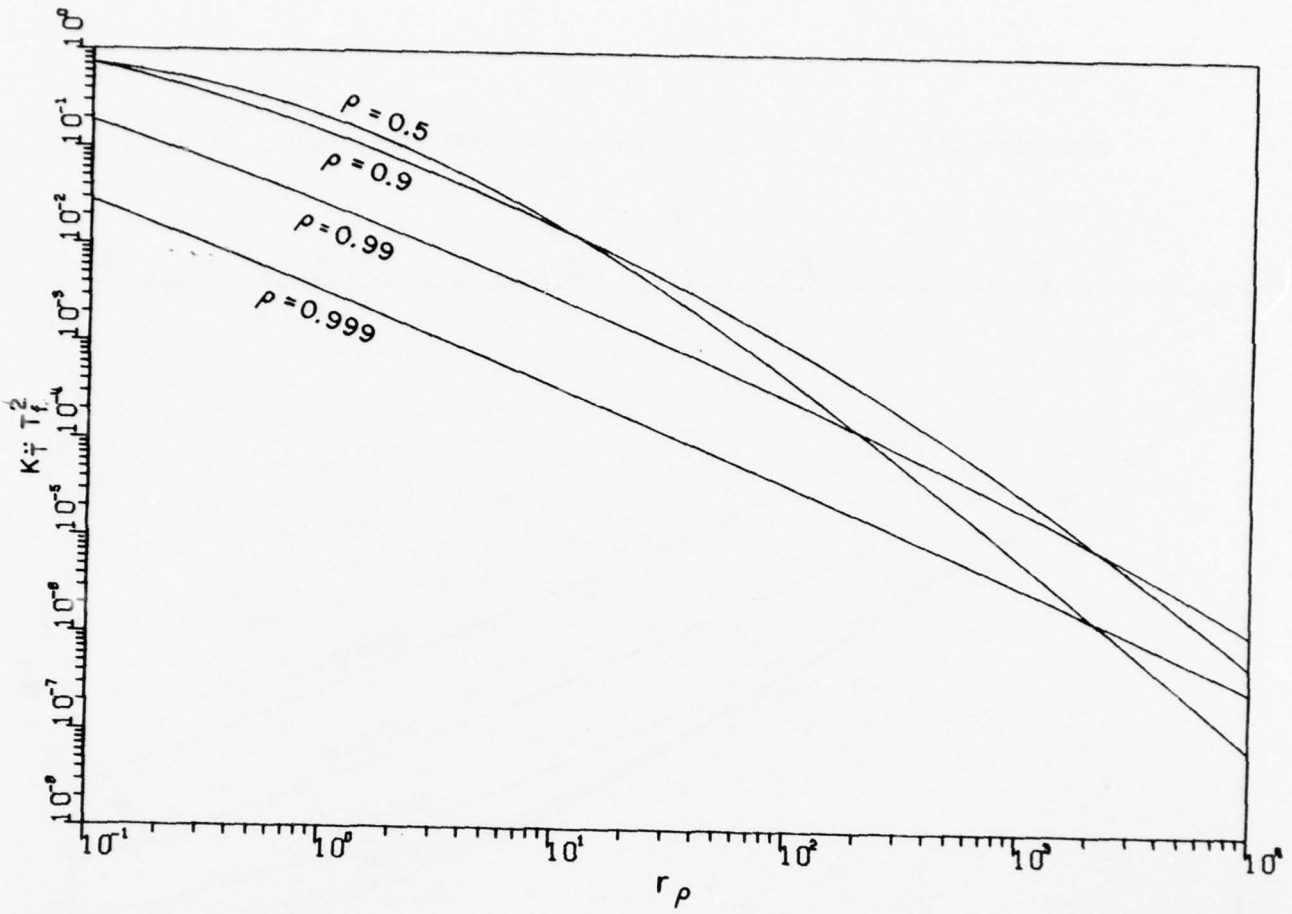

Figure 10. Normalized steady state acceleration gain vs. r_ρ for augmented Kalman filter.

A model of the resulting augmented Kalman filter incorporated into the receive clock sampled data delay lock loop is given in Figure 11. Sampling switch timing for this model and comments con-

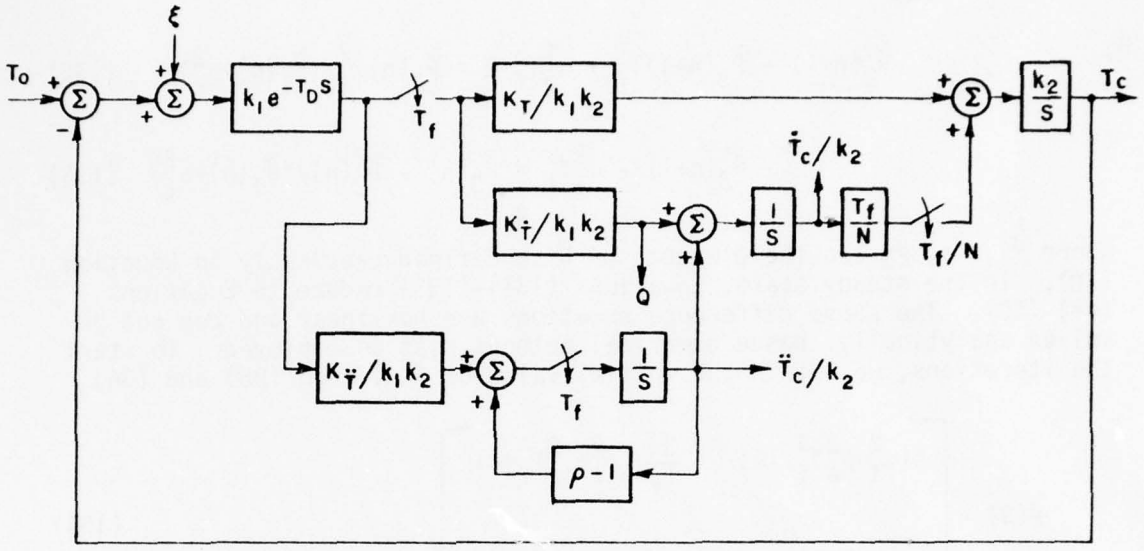

Figure 11. Model of the SDDLL with an augmented Kalman filter.

cerning the time delay and the output T_c are the same as that previously given for the two-dimensional model of Figure 5.

D. Transient Response of the Discrete Kalman Filter

The settling time is an important factor to consider when choosing a suitable filter for implementation in the SDDLL. A Kalman filter, though optimum in a sense, requires more computer storage and computer time than, for example, the (steady state) Wiener filter. If the settling time is sufficiently short, a corresponding Wiener filter can be used in place of the more sophisticated Kalman filter. In this section, the transient responses of the discrete Kalman filters discussed in previous sections will be studied and curves of the transient response and approximate expressions for the settling time will be obtained.

The transient response of the simple discrete Kalman filter is studied first. Combining Equations (28) and (29),

$$\Phi^{-1}[\tilde{P}(n+1)-\Gamma Q\Gamma^T]\Phi^{-1T} = \tilde{P}(n) - \tilde{P}(n)H^T[H\tilde{P}(n)H^T+R]^{-1}H\,\tilde{P}(n). \qquad (130)$$

Equating corresponding elements on both sides of (130), we obtain

$$\tilde{P}_1(n+1) - 2\tilde{P}_2(n+1)T_f + \tilde{P}_3(n+1)T_f^2 - \sigma_a^2 T_f^4/4 = \tilde{P}_1(n)\sigma_\xi^2/(\tilde{P}_1(n)+\sigma_\xi^2) \quad (131)$$

$$\tilde{P}_2(n+1) - \tilde{P}_3(n+1)T_f + \sigma_a^2 T_f^3/2 = \tilde{P}_2(n)\sigma_\xi^2/(\tilde{P}_1(n)+\sigma_\xi^2) \quad (132)$$

$$\tilde{P}_3(n+1) - \sigma_a^2 T_f^2 = \tilde{P}_3(n) - \tilde{P}_2^2(n)/(\tilde{P}_1(n)+\sigma_\xi^2) \quad (133)$$

where $\tilde{P}_1$, $\tilde{P}_2$, $\tilde{P}_3$ are the elements of $\tilde{P}$ as defined previously in Equation (40). In the steady state, Equations (131)-(133) reduce to Equations (48)-(50). The above difference equations are nonlinear and can not be solved analytically, hence numerical methods must be employed. To start the iterations, we obtain the initial value of $\tilde{P}(n)$ from (28) and (36)

$$\tilde{P}(3) = \begin{bmatrix} 5(\sigma_\xi^2+\sigma_a^2 T_f^4/10) & \frac{3}{T_f}(\sigma_\xi^2+\sigma_a^2 T_f^4/4) \\ \frac{3}{T_f}(\sigma_\xi^2+\sigma_a^2 T_f^4/4) & \frac{2}{T_f^2}(\sigma_\xi^2+5\sigma_a^2 T_f^4/8) \end{bmatrix} . \quad (134)$$

It is convenient to define the following variables:

$$r = 4\sigma_\xi/\sigma_a T_f^2 \quad (135)$$

$$A(n) = \tilde{P}_1(n)/\sigma_\xi^2 \quad (136)$$

$$B(n) = \tilde{P}_2(n)/\sigma_\xi \sigma_a T_f \quad (137)$$

$$C(n) = \tilde{P}_3(n)/\sigma_a^2 T_f^2 . \quad (138)$$

Then (131) through (134) become

$$A(n+1) = \frac{8}{r}B(n+1) - \frac{16}{r^2}C(n+1) + \frac{A(n)}{1+A(n)} + \frac{4}{r^2} \quad (139)$$

$$B(n+1) = \frac{4}{r}C(n+1) + \frac{B(n)}{1+A(n)} - \frac{2}{r} \quad (140)$$

$$C(n+1) = C(n) - \frac{B^2(n)}{1+A(n)} + 1 \tag{141}$$

and

$$\tilde{P}(3) = \begin{bmatrix} 5\left(1 + \frac{8}{5r^2}\right)\sigma_\xi^2 & \frac{3}{4} r\left(1 + \frac{4}{r^2}\right)\sigma_\xi\sigma_a T_f \\ \frac{3}{4} r\left(1 + \frac{4}{r^2}\right)\sigma_\xi\sigma_a T_f & \frac{1}{8} r^2\left(1 + \frac{10}{r^2}\right)\sigma_a^2 T_f^2 \end{bmatrix} . \tag{142}$$

The filtered covariance elements are related to A(n), B(n) and C(n) by

$$\hat{P}_1(n)/\sigma_\xi^2 = A(n)/(1+A(n)) \tag{143}$$

$$\hat{P}_2(n)/\sigma_\xi\sigma_a T_f = B(n)/(1+A(n)) \tag{144}$$

$$\hat{P}_3(n)/\sigma_a^2 T_f^2 = C(n) - B^2(n)/(1+A(n)) \tag{145}$$

and the gain factors are

$$K_T(n) = \hat{P}_1(n)/\sigma_\xi^2 \tag{146}$$

$$K_{\dot{T}}(n) = \frac{4}{rT_f} \cdot \hat{P}_2(n)/\sigma_\xi\sigma_a T_f . \tag{147}$$

Graphs of $\tilde{P}_1(n)/\sigma_\xi^2$, $K_T(n)$ and $K_{\dot{T}}(n)T_f$ for different values of r are given by the ρ=0 curves in Figures 12, 13 and 14. From these figures, we obtain a fairly good approximation for the settling time,

$$\Delta\tau \approx 2.5\ r^{1/2}\ T_f . \tag{148}$$

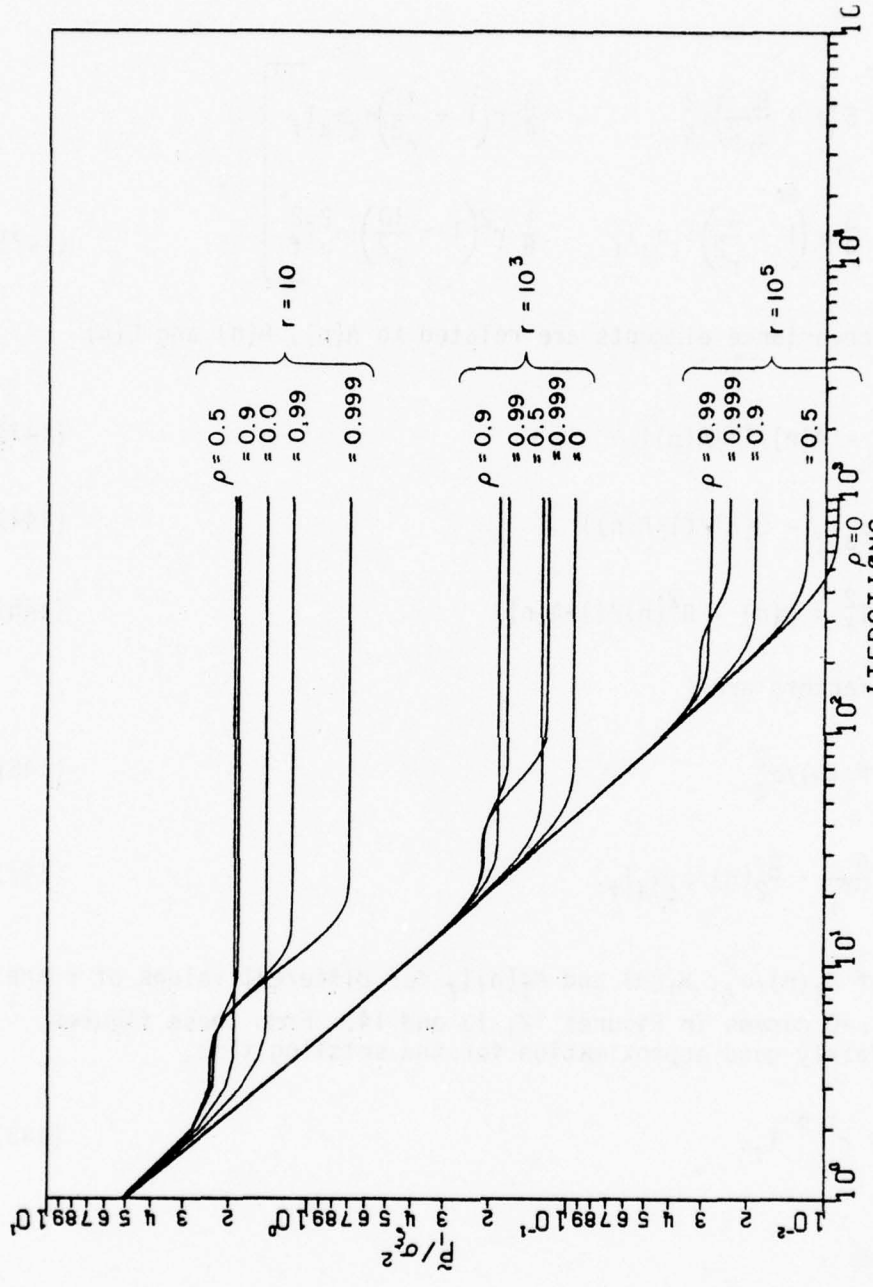

Figure 12. Normalized predicted estimate error variance transient behavior for the Kalman filter.

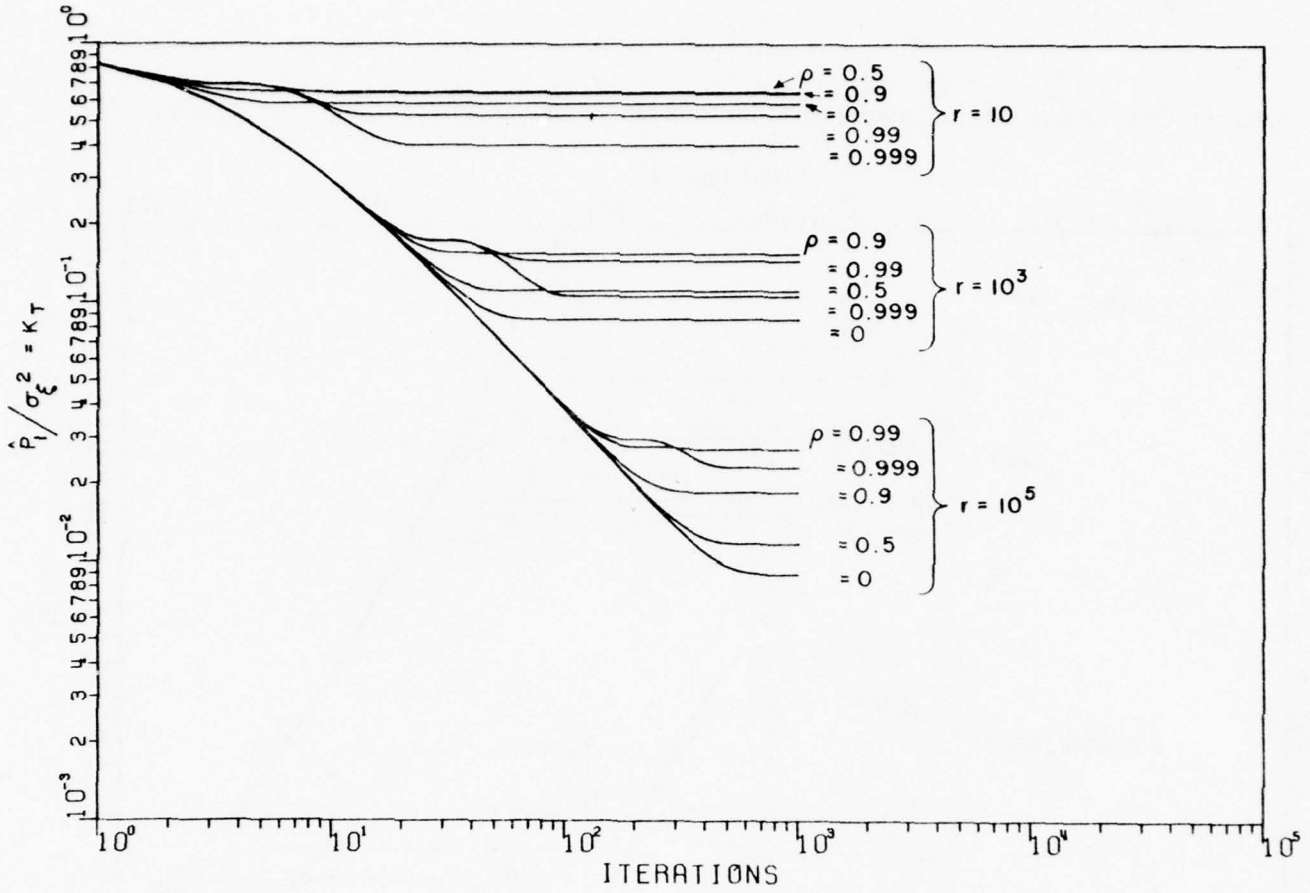

Figure 13. Normalized filtered estimate error variance and Kalman gain transient behavior for the Kalman filter.

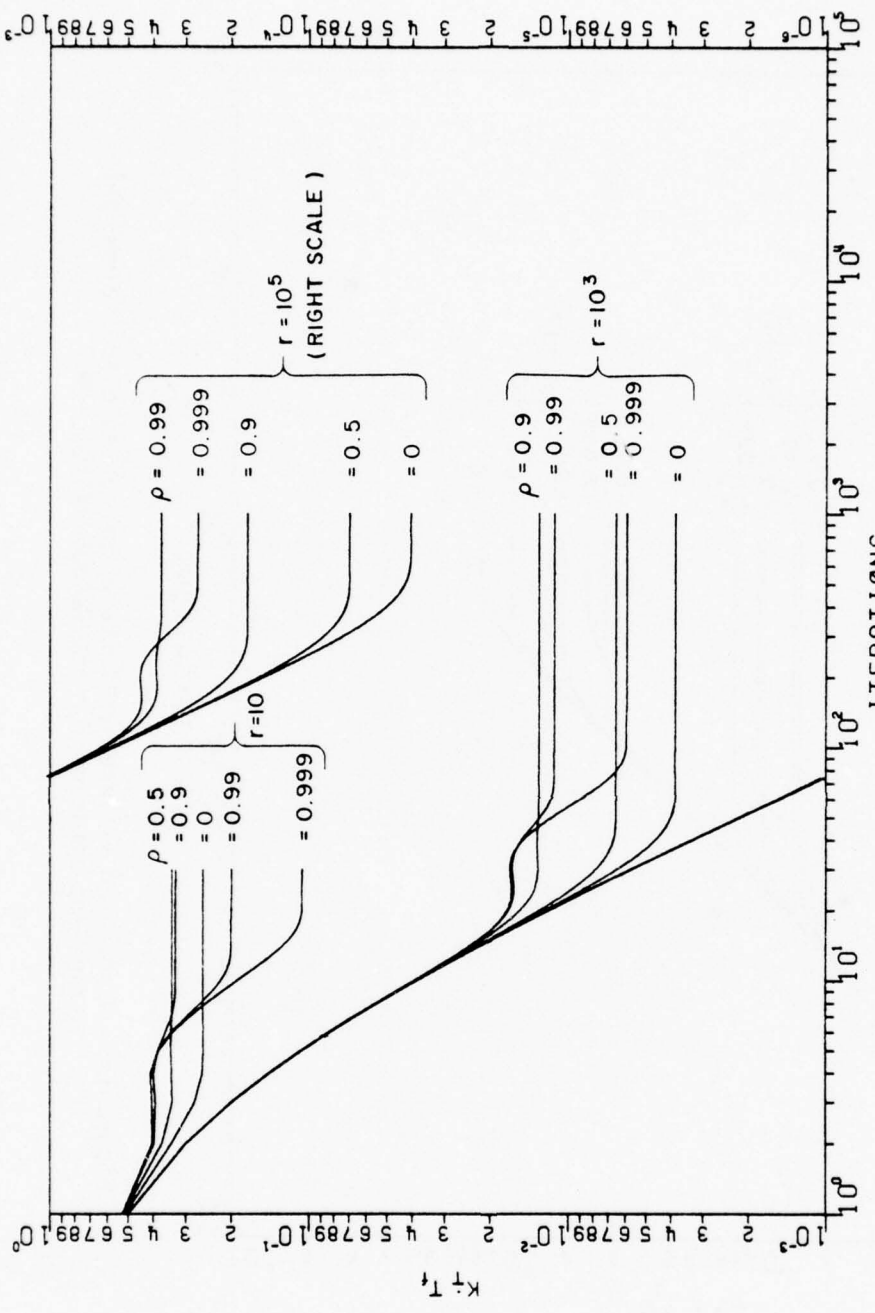

Figure 14. Normalized velocity gain transient behavior for the Kalman filter.

For example, using a typical value of $T_f \approx .01$ sec

$$\Delta\tau \approx \begin{cases} .08 \text{ sec} , & r=10 \\ .8 \text{ sec} , & r=10^3 \\ 8 \text{ sec} , & r=10^5 \end{cases} . \tag{149}$$

From the definition of r (Equation (135)), Equation (148) indicates that the settling time depends only on the ratio σ_ξ/σ_a, irrespective of the sampling period T_f. However, we have neglected correlation in the maneuver noise when deriving (148). As the sampling period becomes shorter, the effect of correlation in the maneuver noise can not be overlooked. We expect that the settling time will also depend on the sampling period when correlation is included.

Now consider the transient response of the augmented discrete Kalman filter. Following the same reasoning as above, we obtain the recursive covariance equations as follows:

$$A(n+1) = \frac{8}{r} B(n+1) - \frac{16}{r^2} C(n+1) - \frac{4}{r} D(n+1) + \frac{16}{r^2} E(n+1) - \frac{4}{r^2} F(n+1)$$

$$+ \frac{A(n)}{1+A(n)} - \frac{4}{r^2} \tag{150}$$

$$B(n+1) = \frac{4}{r} C(n+1) + D(n+1) - \frac{6}{r} E(n+1) + \frac{2}{r} F(n+1)$$

$$+ \frac{B(n)}{1+A(n)} + \frac{2}{r} \tag{151}$$

$$C(n+1) = 2E(n+1)-F(n+1)+C(n) - \frac{B^2(n)}{1+A(n)} - 1 \tag{152}$$

$$D(n+1) = \frac{4}{r} E(n+1) - \frac{2}{r} F(n+1) + \frac{\rho D(n)}{1+A(n)} - \frac{2}{r} \tag{153}$$

$$E(n+1) = F(n+1) + \rho E(n) - \frac{\rho B(n) D(n)}{1+A(n)} + 1 \tag{154}$$

$$F(n+1) = \rho^2 F(n) - \frac{\rho^2 D^2(n)}{1+A(n)} \tag{155}$$

where r, A(n), B(n) and C(n) are defined as before and

$$D(n) = \tilde{P}_4(n)/\rho\sigma_\xi\sigma_a \tag{156}$$

$$E(n) = \tilde{P}_5(n)/\rho\sigma_a^2 T_f \tag{157}$$

$$F(n) = (\tilde{P}_6(n)-\sigma_a^2)/\rho^2\sigma_a^2 \quad . \tag{158}$$

In the steady state (150)-(155) reduce to (96)-(101). The initial covariance matrix is obtained from (94) and (28)

$$\tilde{P}(3) = \begin{bmatrix} 5\left(1 + \frac{8(1+\rho)}{5r^2}\right)\sigma_\xi^2 & \frac{3}{4}r\left(1 + \frac{4(1+\rho)}{r^2}\right)\sigma_\xi\sigma_a T_f & \frac{2(1+\rho)}{r}\rho\sigma_\xi\sigma_a \\ \frac{3}{4}r\left(1 + \frac{4(1+\rho)}{r^2}\right)\sigma_\xi\sigma_a T_f & \frac{1}{8}r^2\left(1 + \frac{10+8\rho}{r^2}\right)\sigma_a^2 T_f^2 & \left(1+\frac{1}{2}\rho\right)\rho\sigma_a^2 T_f \\ \frac{2(1+\rho)}{r}\rho\sigma_\xi\sigma_a & \left(1+\frac{1}{2}\rho\right)\rho\sigma_a^2 T_f & \sigma_a^2 \end{bmatrix} . \tag{159}$$

The filtered covariance matrix elements are then given by

$$\hat{P}_1(n)/\sigma_\xi^2 = A(n)/(1+A(n)) \tag{160}$$

$$\hat{P}_2(n)/\sigma_\xi\sigma_a T_f = B(n)/(1+A(n)) \tag{161}$$

$$\hat{P}_3(n)/\sigma_a^2 T_f^2 = C(n)-B^2(n)/(1+A(n)) \tag{162}$$

$$\hat{P}_4(n)/\rho\sigma_\xi\sigma_a = D(n)/(1+A(n)) \tag{163}$$

$$\hat{P}_5(n)/\rho\sigma_a^2 T_f = E(n) - B(n)D(n)/(1+A(n)) \tag{164}$$

$$\hat{P}_6(n)/\rho^2\sigma_a^2 = F(n) - D^2(n)/(1+A(n)) + 1/\rho^2 \tag{165}$$

and the gain factors are

$$K_T(n) = \hat{P}_1(n)/\sigma_\xi^2 \tag{166}$$

$$K_{\dot{T}}(n) = \frac{4}{rT_f}\ \hat{P}_2(n)/\sigma_\xi\sigma_a T_f \tag{167}$$

$$K_{\ddot{T}}(n) = \frac{4\rho}{rT_f^2}\ \hat{P}_4(n)/\rho\sigma_\xi\sigma_a \quad . \tag{168}$$

Graphs of $\hat{P}_1(n)/\sigma_\xi^2$, $K_T(n)$, $K_{\dot{T}}(n)T_f$ and $K_{\ddot{T}}(n)T_f^2$ for different values of r and ρ are shown in Figures 12 through 15. From these figures we obtain an approximation for the settling time

$$\Delta\tau \approx 2.5r^{1/2}\left(\frac{1-\rho}{1+\rho}\right)^{1/4} T_f \approx 2.5\ r_\rho^{1/2}T_f, \text{ if } r^{1/2}(1-\rho)>1. \tag{169}$$

The condition $r^{1/2}(1-\rho)>1$ is essentially the same one under which (119) is obtained. For fixed r, the settling time decreases as ρ increases until the condition $r^{1/2}(1-\rho)>1$ is no longer satisfied. Then the settling time increases as ρ increases further. The dependence of $\Delta\tau$ on the sampling period is implicitly contained in ρ ($\rho=1-\lambda T_f$). For $r<10^5$, $\rho<.999$ and $T_f=.01$ sec, the settling time falls approximately in the range of one-tenth to ten seconds.

E. Monte Carlo Simulation

Performance of the discrete Kalman filter described in the previous sections can be investigated using a Monte Carlo simulation method. In this method, the receiver noise and the maneuver noise are generated by a computer using arithmetical random number formulas. The results of several simulation studies are summarized here.

In the first case, the simulation method was used to obtain a comparison between the performances of the discrete Kalman filter and its corresponding Wiener filter. Correct statistics of the receiver noise and the maneuver noise were assumed. Values of ρ, σ_a and σ_ξ were chosen as

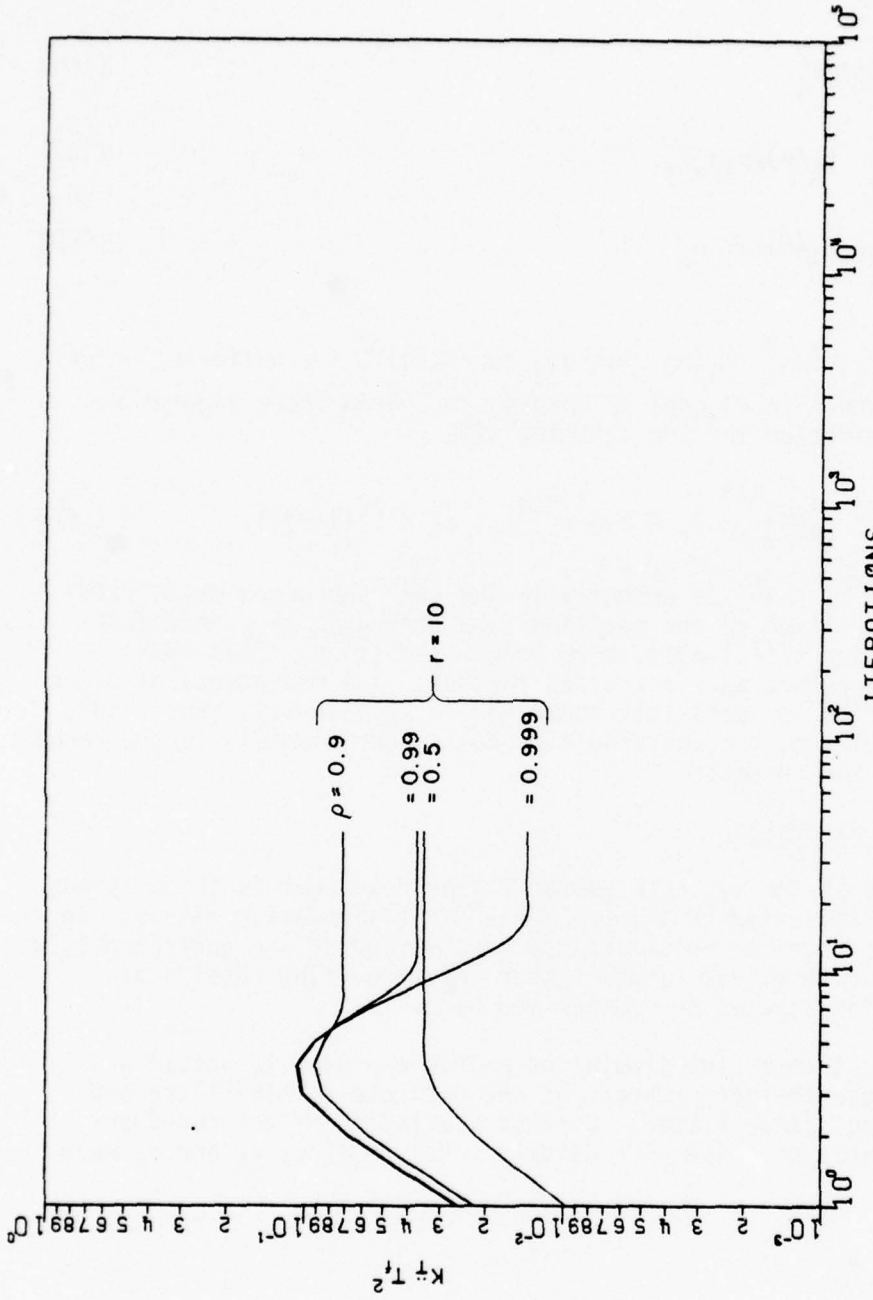

Figure 15a. Normalized acceleration gain transient behavior for the Kalman filter (r=10).

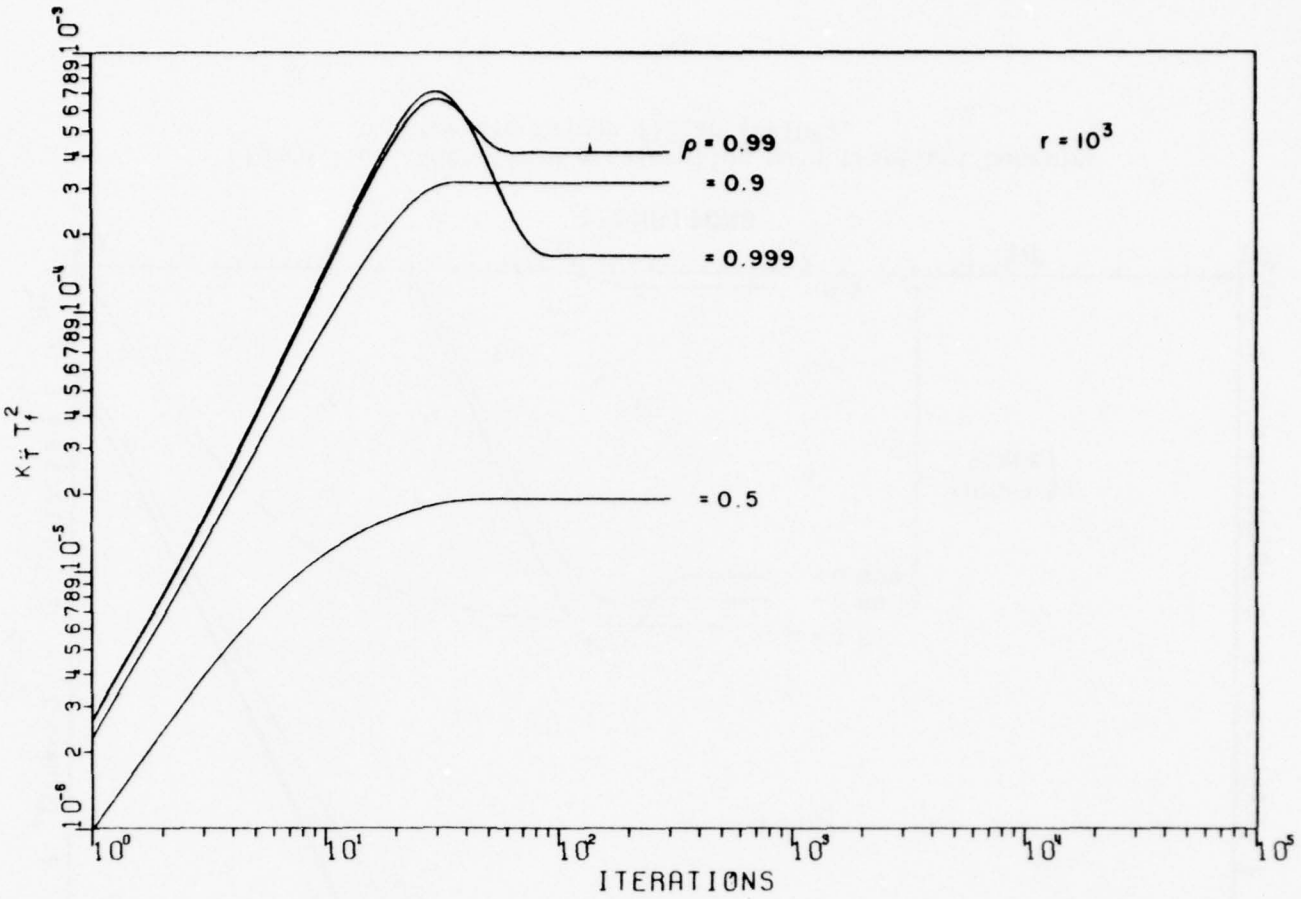

Figure 15b. Normalized acceleration gain transient behavior for the Kalman filter ($r=10^3$).

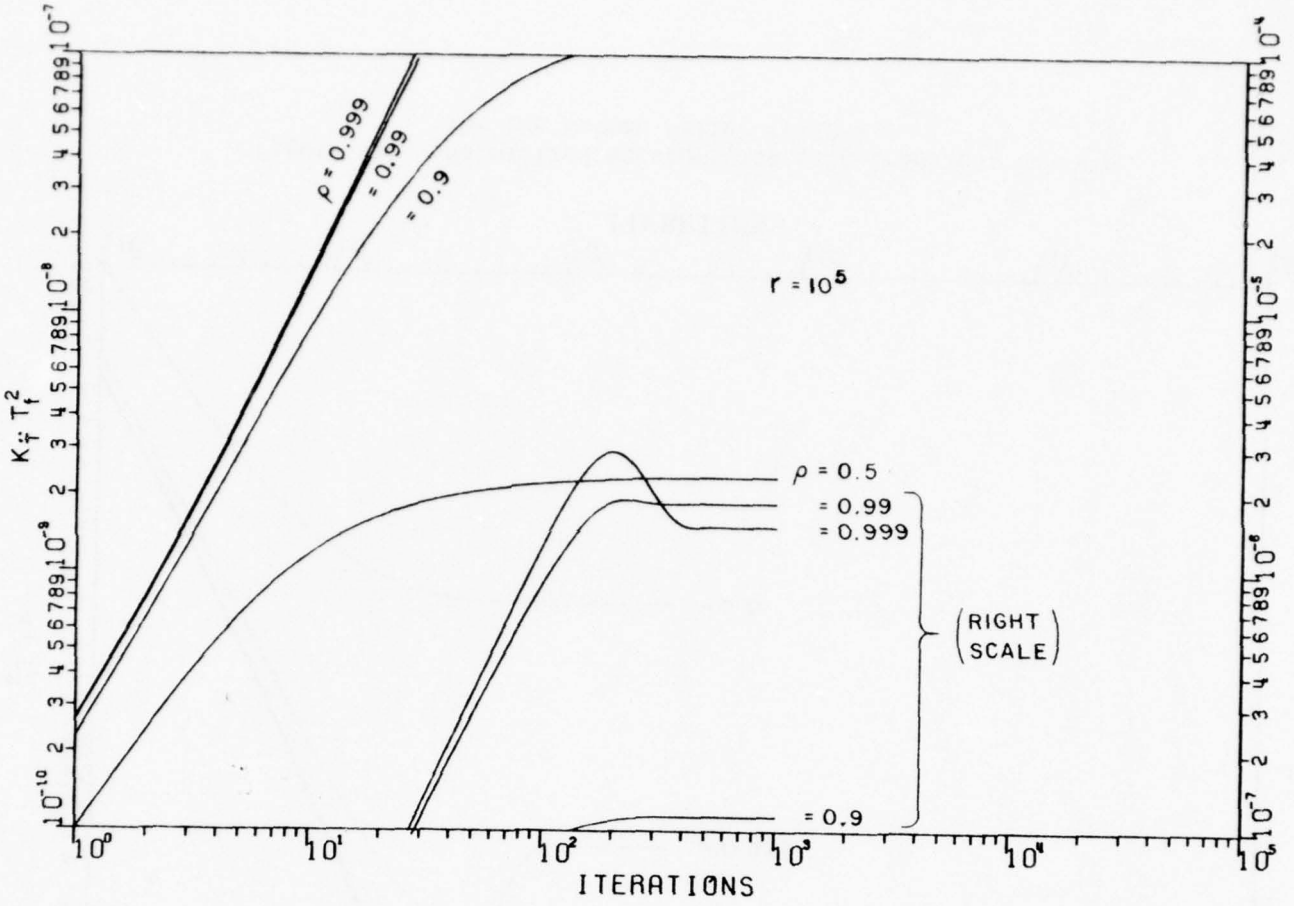

Figure 15c. Normalized acceleration gain transient behavior for the Kalman filter ($r=10^5$).

$$\rho = 0, .5, .9, .99, .999 \tag{170}$$

$$\sigma_a = .5\Delta/\text{sec}^2, 15\Delta/\text{sec}^2 \tag{171}$$

and

$$\sigma_\xi = .01\Delta, .1\Delta. \tag{172}$$

For a code chip rate of 40 Mbit/s, Δ = 25 nsec. Then $\sigma_a = 15\Delta/\text{sec}^2$ represents an acceleration of 11g which is probably the highest for aircraft. For σ_a equal to $15\Delta/\text{sec}^2$, the sampling period T_f should not be greater than .02 sec. in order to keep the transient timing error below 0.5Δ and thus avoid loss of lock. In this simulation study T_f was chosen to be .01 sec.

In the steady state, the standard deviation of the one-step-prediction timing error $\sqrt{P}$, was found to agree in general to within 10% of the analytical results of Section C, except for $\sigma_a = .5\Delta/\text{sec}^2$, $\sigma_\xi = .1\Delta$, in which case the simulation results were 30% lower than the analytical results.

The settling time of the discrete Kalman filter agrees with Equation (169). For the corresponding Wiener filter, the settling time is about twice as long. For $\sigma_\xi = .1\Delta$ the timing error of the Wiener filter in the transient state can become greater than $.5\Delta$ which could unlock the local clock of the SDDLL. This is also true for the Kalman filter if $\sigma_\xi > .2\Delta$. It appears that a better initial estimate than that given by Equations (93) and (94) is needed if $\sigma_\xi > .2\Delta$. The crucial points are the initial estimates of $T(n)$ and of $\dot{T}(n)$. Error in the initial estimate of $\ddot{T}(n)$ is rather unimportant because of the short sampling period.

In the second simulation study, the performance of the simple discrete Kalman filter was compared to that of the augmented Kalman filter of the previous study. If a simple discrete Kalman filter is implemented irrespective of the correlation coefficient, the performance will not be optimum. The higher the value of ρ, the poorer the performance will be.

Assuming correct values of σ_a and σ_ξ in implementing the simple Kalman filter, the performance was degraded by 3% for ρ = .5, 40% for ρ = .9 and 60% for ρ = .99. However, the analysis of previous sections indicates that the maneuver noise standard deviation σ_a should be replaced by $\sigma_a[(1+\rho)/(1-\rho)]^{1/2}$ if a simple discrete Kalman filter is to be implemented for $\rho \neq 0$ (i.e., this is equivalent to replacing the parameter r by r_ρ - see Equations (102) and (117). Improvements in performance can then be obtained. This was verified in the simulation study except

for the case $\rho = .99$, $\sigma_a = 15\Delta/sec^2$, $\sigma_\xi = .01\Delta$. For other parametric values the degradation in the performance was only 1% for $\rho = .5$, 10% for $\rho = .9$ and 30% for $\rho = .99$. Thus it appears that with ρ less than .99 and with proper substitution of the maneuver noise variance, the simple discrete Kalman filter can be implemented to save computation time and storage cost while still providing satisfactory performance. For ρ equal to .99 and higher, the augmented discrete Kalman filter should be used.

One potential major disadvantage of implementing the discrete Kalman filter is that it may require accurate estimation of the value $r = 4\sigma_\xi/\sigma_a T_f^2$. Therefore in the third simulation study the effect of the accuracy of r on the performance of the discrete Kalman filter was studied. First, for $\rho = .99$ and .999, it was found that the performance of the augmented filter is degraded by only 10% if the estimation of r is off by a factor of 2, and by 80% if the estimation of r is off by a factor of 5. Testing values of σ_a and σ_ξ are the same as in the first two studies. The small percentage of degradation can be attributed to the small slopes of the curves shown in Figure 7. The same study was then repeated for $\rho = 0$, .5 and .9 using the simple discrete Kalman filter with proper substitution of the manuever noise. Results were essentially the same as for the augmented filter with only a slight increase in the percentage degradation of performance.

The tracking capability of the discrete Kalman filter (worst case) was then considered. The terminal was initially stationary and the discrete Kalman filter with assumed values of ρ, σ_a and σ_ξ was in the steady state. Then an instantaneous velocity was suddenly imparted to the terminal as when a frequency offset occurs. Typical response of the discrete Kalman filter is shown in Figure 16. Following an initial over-shoot the filter settles down quickly. It was found that the maximum instantaneous velocity which can be imparted to the terminal without risk of unlocking the local clock of the SDDLL is approximately given by

$$\dot{\Delta T}_{max} \approx 1.80\ r^{-1/2}\ \Delta/T_f \quad . \tag{173}$$

Results of additional simulation studies of the discrete Kalman filter, including transient response, noise performance for stationary terminals, and comparisons of analytical values of error variance with simulation results are given in Section VII.

F. Up-Link Synchronization

Closed-loop synchronization of the TDMA system is achieved by adjusting the timing of up-link transmissions to maintain a prescribed timing relationship between the received down link signals and a

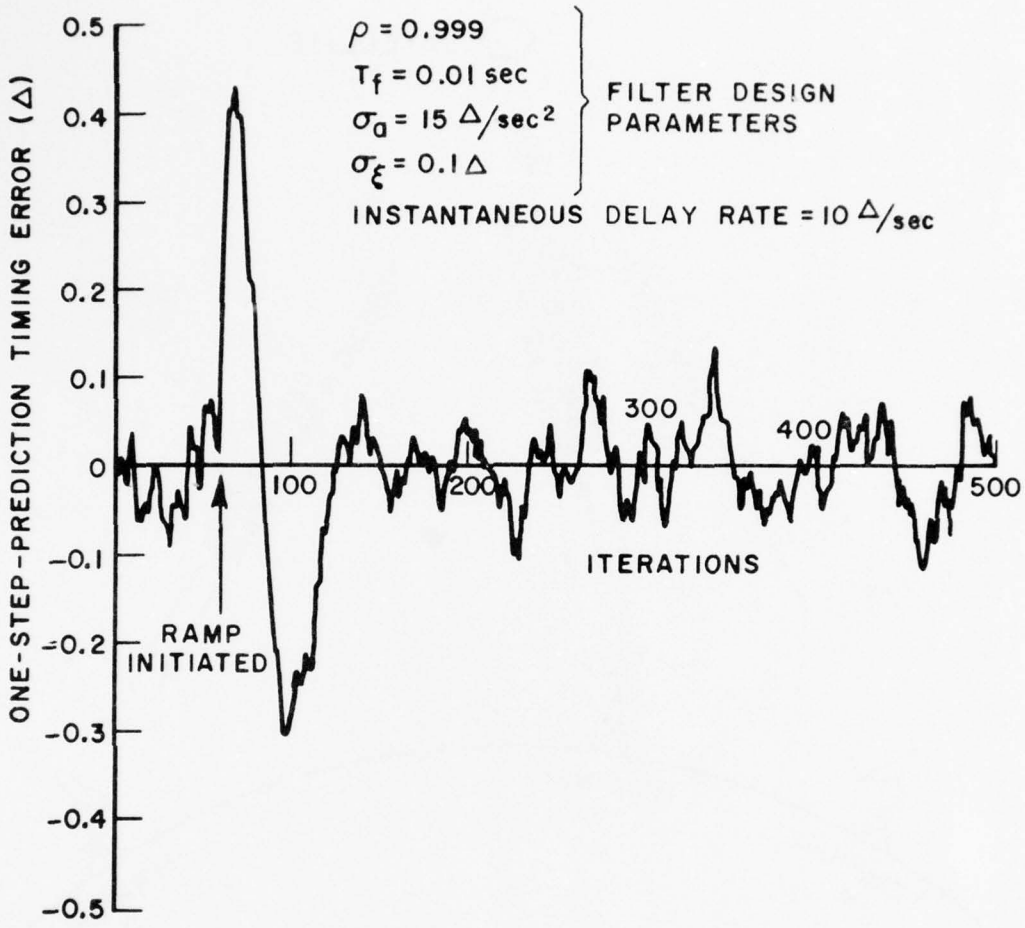

Figure 16. Ramp response of a discrete Kalman filter.

network clock signal. The synchronization of the single one way link illustrated in Figure 17 [1] will be considered in this section.

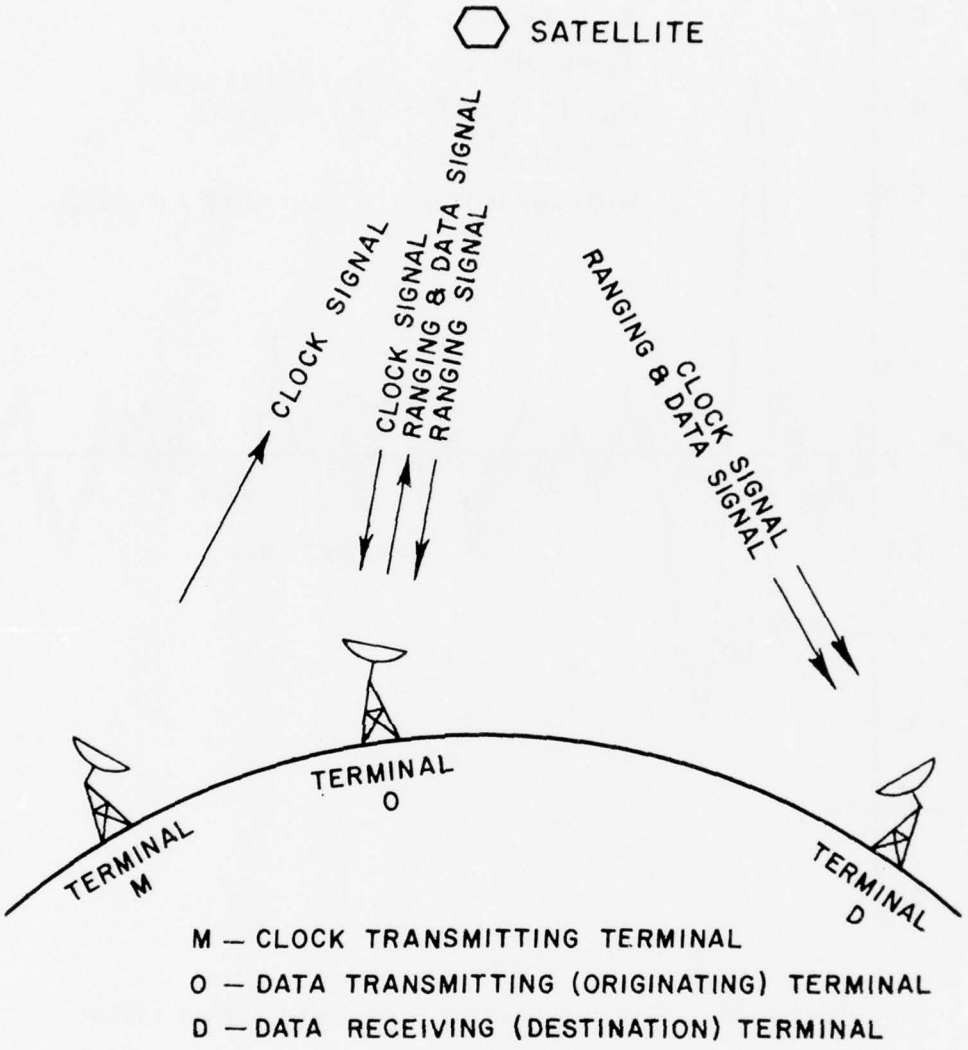

Figure 17. A single (one-way) TDMA link.

As previously stated, the terminals need not be ground-based. Fast moving terminals can be included. Following [1], it will be assumed that a portion of the time allocated to each terminal is devoted exclusively to transmission of a pulsed envelope ranging signal from which timing error information is extracted. Strict preservation of the TDMA concept requires that the network clock signal also have a pulsed envelope waveform.

The TDMA synchronizing receiver employs two sampled-data delay-lock loops (SDDLL's) to maintain proper signal timing. In one SDDLL, the time base of a locally generated clock signal is aligned with the time base of the received network-clock signal. This SDDLL with a discrete Kalman filter has been analyzed in previous sections. The second SDDLL estimates the timing error of the received ranging signal relative to the locked local clock and appropriately corrects the timing of the up-link transmissions. The performance of the second SDDLL will be discussed in this section. Both the network clock and ranging signal waveforms are bi-phase modulated by suitable PN codes. An abbreviated block diagram of the synchronizing receiver is shown in Figure 18 [1]. (Identical codes for the clock and ranging loops are assumed here for simplicity, although different codes are actually used for signal identification.) Note that the averaging loop filter in the clock loop of the original TDMA modem has been replaced by a discrete Kalman filter. However, as stated previously in Section II, within the spectral range of the timing signal and the dynamic range of the terminal motion, the discrete Kalman filter in the clock loop can provide the tracking function for both loops. Therefore, in the ranging loop the simple averaging loop filter will be retained.

Closed-loop timing corrections in the ranging loop must be separated by an interval larger than the propagation delay of the ranging signal (about 250 msec when a synchronous satellite relay is used) in order to maintain ranging loop stability. However, if fast moving terminals and a high code chip rate are employed, timing error in the ranging loop accumulated in such a time interval can be larger than $\Delta/2$ if only closed-loop corrections are made. Therefore, estimates of the down-link delay rate and acceleration derived in the clock loop are employed as open-loop corrections in the ranging loop. The modified two-loop TDMA synchronizer used previously [1], with certain changes as shown in Figure 19, will serve this purpose. In this figure, ΔT_{cf} and ΔT_{rf} are the sampling period offsets (errors) in the clock loop and the ranging loop, respectively (i.e., $\Delta T_{c,rf} = T_{c,rf} - T_f$ where $T_{c,rf}$ are the nominal subframe lengths and T_f is the actual subframe length at the satellite). The formula for determining the quantity A_0 will be given later. Details of the clock loop Kalman filter were given previously in Figure 11.

Relationships between the sampling instants of the samplers are shown in Figure 20, where T_a is the PN code period. It will be assumed that the N_r ranging signal pulses are sampled every T_f seconds where $T_f = KT_a$. Neglecting circuit delays, the sampling instants (A) represent the times when system clock samples are received and corrections in local clock timing are made as a result of measured timing errors. At times (B) additional corrections are made, as predicted by the Kalman filter, to compensate for the effects of terminal or satellite maneuvers (velocity and acceleration). Times (C) indicate when ranging pulses are received on the down-link. Note that the N_r ranging pulses of each burst are spaced by the subframe time, T_f, as are the system clock pulses but

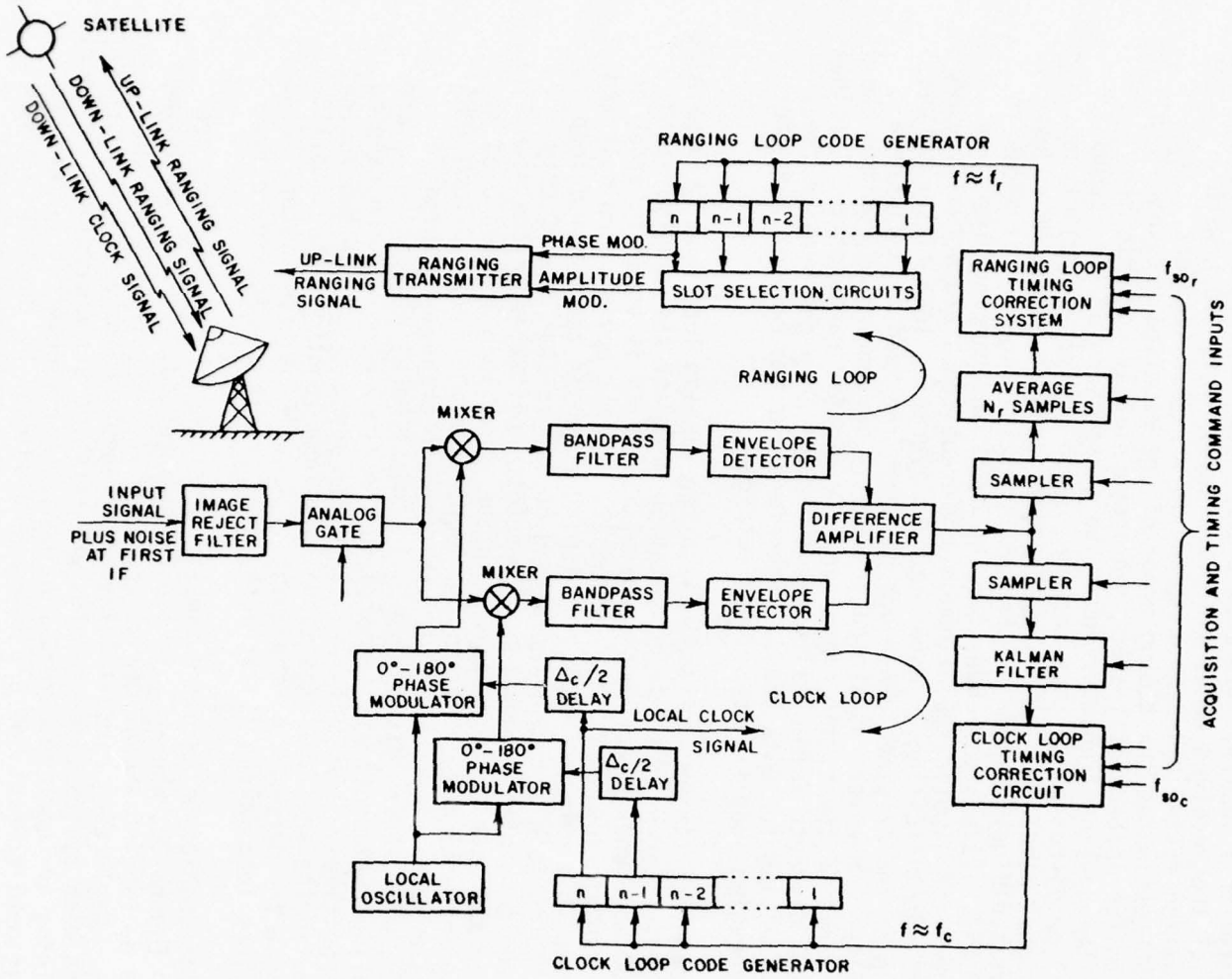

Figure 18. The basic two-loop TDMA synchronizer.

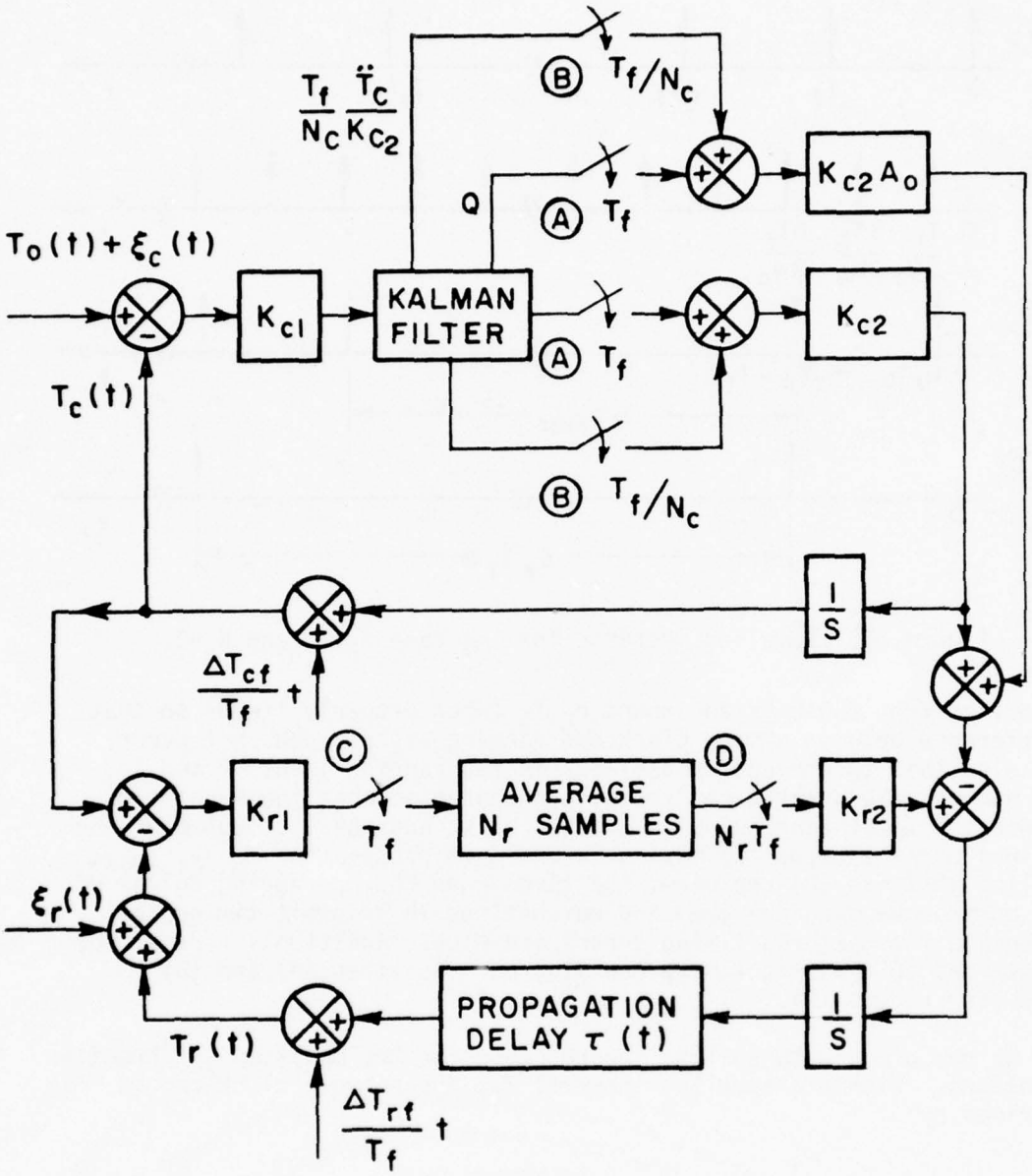

Figure 19. A model of the modified two-loop TDMA synchronizer.

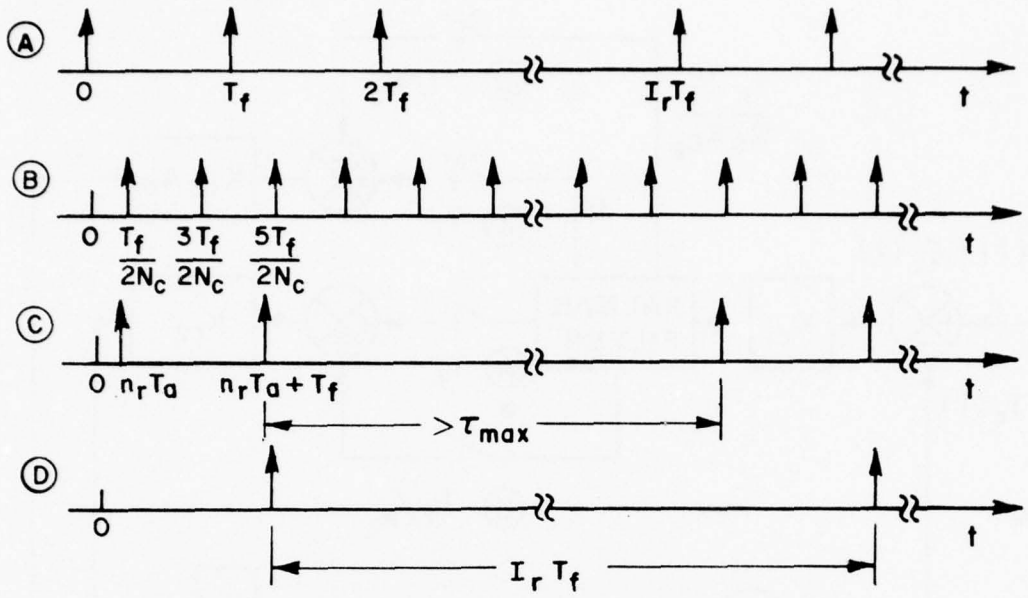

Figure 20. Sampling instants for the case N_r=2, and N_c=2.

are offset from these by an amount $n_r T_a$ (when properly timed) so that interference between system clock and ranging signals does not occur. Note also that to prevent instability in the ranging loop, T_f and I_r (the number of subframes per frame) are chosen so that the separation between the first ranging pulse of each burst and the last pulse of the previous burst exceeds the maximum round-trip propagation delay, τ_{max}. Sampling instants (D) represent the times when the N_r ranging pulses of each burst have been averaged and corrections in transmit timing to compensate for measured timing errors are made. Additional (open-loop) corrections to transmit timing are also made at times (A) and (B) above (see Figure 19).

We now proceed to analyze the responses of the modified synchronizer as follows. Within a sampling interval T_f, the network clock can be described by

$$T_o(nT_f+\delta) = T_o(nT_f) + \dot{T}_o(nT_f)\delta + \ddot{T}_o(nT_f)\delta^2/2, \quad 0 \leq \delta \leq T_f. \tag{174}$$

In the steady-state, the discrete Kalman filter can track non-random delay accurately. Therefore, in the steady-state

$$E[T_c(nT_f+\delta)] = E[T_o(nT_f)] + E[\dot{T}_o(nT_f)]\delta + E[\ddot{T}_o(nT_f)]\delta^2/2. \qquad (175)$$

where E[ ] indicates the expected value. However, this equation is true only when the corrections from samplers (B) of Figure 19 can be made continuously. To account for the discrete nature of these corrections, (175) is modified:

$$E[T_c(nT_f+m\frac{T_f}{N_c}+\theta)] = E[T_o(nT_f)] + E[\dot{T}_o(nT_f)]\, m\frac{T_f}{N_c}$$

$$+ E[\ddot{T}_o(nT_f)]m^2\frac{T_f^2}{2N_c^2} + \frac{\Delta T_{cf}}{T_f}\theta. \qquad (176)$$

where

$$-\frac{T_f}{2N_c} < \theta < \frac{T_f}{2N_c},\ 0 \le m \le N_c \quad \text{and} \quad 0 \le m\frac{T_f}{N_c} + \theta \le T_f. \qquad (177)$$

Thus the expected value of the clock-loop timing error is

$$\varepsilon_{cs}(nT_f+m\frac{T_f}{N_c}+\theta) = E[T_o(nT_f+m\frac{T_f}{N_c}+\theta) - T_c(nT_f+m\frac{T_f}{N_c}+\theta)]$$

$$= \left\{E[\dot{T}_o(nT_f)] - \frac{\Delta T_{cf}}{T_f} + E[\ddot{T}_o(nT_f)]\left(\frac{\theta}{2}+m\frac{T_f}{N_c}\right)\right\}\theta\,. \qquad (178)$$

The subscript s denotes the expected value. From the previous sections we obtain the variance of the clock-loop timing error,

$$\sigma^2_{\varepsilon_c}(nT_f+\delta) = \hat{P}_1 + 2\hat{P}_2\delta + \hat{P}_3\delta^2 + \hat{P}_4\delta^2 + \hat{P}_5\delta^3 + \hat{P}_6\delta^4/4,\ \delta = m\frac{T_f}{N_c} \qquad (179)$$

and

$$\sigma^2_{\varepsilon_c}(nT_f+T_f-0)=\tilde{P}_1 \qquad (180)$$

where the $\hat{P}_i$'s and $\tilde{P}_i$'s are elements of the covariance matrices $\hat{P}$ and $\tilde{P}$, respectively, as defined in (95). The variance $\sigma^2_{\varepsilon_c}(nT_f+\delta)$ is a monotonically increasing function of δ.

Next, consider the ranging-loop response. We shall first derive some additional formulas related to the steady-state Kalman filter which are essential to the calculation of the ranging-loop timing error. From (86),

$$Z(n+\ell) = \Phi^{\ell} Z(n) + \sum_{k=1}^{\ell} \Phi^{\ell-k} \Gamma u(n+k-1) \tag{181}$$

where

$$\Phi = \begin{bmatrix} 1 & T_f & T_f^2/2 \\ 0 & 1 & T_f \\ 0 & 0 & \rho \end{bmatrix} \tag{182}$$

and

$$\Phi^{\ell} = \begin{bmatrix} 1 & \ell T_f & \frac{T_f^2}{2}\sum_{k=1}^{\ell}\rho^{k-1}(2\ell-2k+1) \\ 0 & 1 & T_f\sum_{k=1}^{\ell}\rho^{k-1} \\ 0 & 0 & \rho^{\ell} \end{bmatrix} = \begin{bmatrix} 1 & \ell T_f & \frac{T_f^2}{2}[2\ell(1-\rho)-(1+\rho)(1-\rho^{\ell})/(1-\rho)^2] \\ 0 & 1 & T_f(1-\rho^{\ell})/(1-\rho) \\ 0 & 0 & \rho^{\ell} \end{bmatrix}. \tag{183}$$

Thus

$$\ddot{T}_o(n+\ell) = \rho^{\ell}\ddot{T}_o(n) + \sum_{k=1}^{\ell}\rho^{\ell-k}u(n+k-1) \tag{184}$$

$$\dot{T}_o(n+\ell) = \dot{T}_o(n) + T_f\left\{\frac{1-\rho^{\ell}}{1-\rho}\ddot{T}_o(n) + \sum_{k=1}^{\ell}\frac{1-\rho^{\ell-k}}{1-\rho}u(n+k-1)\right\} \tag{185}$$

$$T_o(n+\ell) = T_o(n)+\ell T_f \dot{T}_o(n) + \frac{T_f^2}{2}\left\{\frac{2\ell(1-\rho)-(1+\rho)(1-\rho^{\ell})}{(1-\rho)^2}\ \ddot{T}_o(n)\right.$$

$$\left. + \sum_{k=1}^{\ell}\left[\frac{2(\ell-k)(1-\rho)-(1+\rho)(1-\rho^{\ell-k})}{(1-\rho)^2}\right.\right. \qquad (186)$$

$$\left.\left. \cdot\ u(n+k-1)\right]\right\} \quad .$$

Also from (19), (21), (22) and (86),

$$Z_\varepsilon(n+1) = Z(n+1)-\hat{Z}(n+1)=(I-KH)[\Phi Z_\varepsilon(n)+\Gamma u(n)]-K\xi_c(n+1) \qquad (187)$$

and

$$Z_\varepsilon(n+\ell) = [(I-KH)\Phi]^{\ell}Z_\varepsilon(n) + \sum_{k=1}^{\ell}[(I-KH)\Phi]^{\ell-k}[(I-KH)\Gamma u(n+k-1)-K\xi_c(n+k)]$$

$$(\text{for} \quad \ell > 0). \qquad (188)$$

Thus

$$\hat{P}(\ell) \equiv E[Z_\varepsilon(n+\ell)Z_\varepsilon^T(n)] = [(I-KH)\Phi]^{\ell}\hat{P} \qquad (189)$$

$$\sigma_\xi(\ell) \equiv E[Z_\varepsilon(n+\ell)\xi_c(n)] = -[(I-KH)\phi]^{\ell}K\sigma^2_{\xi_c} \qquad (190)$$

$$\sigma_a(\ell) \equiv E[Z_\varepsilon(n+\ell)u(n)] = [(I-KH)\Phi]^{\ell-1}(I-KH)\Gamma\sigma_a^2(1-\rho^2). \qquad (191)$$

Note that $\sigma_\xi(\ell)$ and $\sigma_a(\ell)$ are vector quantities, i.e.,

$$\sigma_a(\ell) = \begin{bmatrix} \sigma_{aT}(\ell) \\ \sigma_{a\dot{T}}(\ell) \\ \sigma_{a\ddot{T}}(\ell) \end{bmatrix} \qquad (192)$$

and similarly, for $\sigma_\xi(\ell)$.

Now refer to Figure 19. The ranging-loop clock at $I_r T_f + \ell T_f + n_r T_a$ (i.e., the time at which a ranging pulse is received) is related to that same clock at $\ell T_f + n_r T_a$ (one frame earlier) by the expression

$$T_r(I_r T_f + \ell T_f + n_r T_a) = T_r(\ell T_f + n_r T_a) + \frac{\Delta T_{rf}}{T_f} I_r T_f + C_\tau(\ell, I_r + \ell) + C_o(\ell, I_r + \ell) + C_c \quad (193)$$

where C_τ, C_o and C_c are due to the propagation delay change, the open-loop correction and the closed-loop correction, respectively.

Because of the propagation delay, any change in satellite motion is not known at the terminal until after the (one-way) propagation delay has elapsed, while a change in terminal motion is known immediately. Hence the effects of the propagation delay change C_τ differ depending upon whether the satellite or the terminal is maneuvering. The case of a stationary terminal and maneuvering satellite (worst case) will be considered first. In this case C_τ is given by

$$C_\tau(\ell, I_r + \ell) = 2[T_o(I_r T_f + \ell T_f + n_r T_a) - T_o(\ell T_f + n_r T_a)]. \quad (194)$$

Expressions for the open-loop and the closed-loop corrections involve the propagation delay τ and the ranging-loop sampling instant $n_r T_a$. Let

$$\tau - n_r T_a = N_\tau T_f - m_\tau \frac{T_f}{N_c} - \theta_\tau \quad (195)$$

i.e., the time period from transmission of the ranging pulse to the nearest subframe boundary (and received system clock pulse) preceeding reception of this pulse is expressed as an integer number (N_τ) of subframes (T_f) minus an integer number (m_τ) of clock loop correction intervals (T_f/N_c) minus the remaining offset (θ_τ),

where

$$-\frac{T_f}{2N_c} < \theta_\tau < \frac{T_f}{2N_c}, \quad 0 \leq m_\tau \leq N_c \text{ and } 0 \leq m_\tau \frac{T_f}{N_c} + \theta_\tau \leq T_f. \quad (196)$$

Then

$$C_o(\ell, I_r+\ell) = -\left[T_c(I_rT_f+\ell T_f-N_\tau T_f)-T_c(\ell T_f-N_\tau T_f) - \frac{\Delta T_{cf}}{T_f} I_rT_f\right]$$

$$-\left[\dot{T}_c(I_rT_f+\ell T_f-N_\tau T_f)-\dot{T}_c(\ell T_f-N_\tau T_f)\right]\left(\frac{m_\tau T_f}{N_c} + A_o\right)$$

$$-\left[\ddot{T}_c(I_rT_f+\ell T_f-N_\tau T_f)-\ddot{T}_c(\ell T_f-N_\tau T_f)\right]\left(\frac{m_\tau T_f}{2N_c} + A_o\right)\frac{m_\tau T_f}{N_c} \tag{197}$$

and

$$C_c = \frac{A_r}{N_r}\sum_{n=0}^{N_r-1}\left\{T_c(nT_f+n_rT_a)-\xi_r(nT_f+n_rT_a)-T_r(nT_f+n_rT_a)\right\} \tag{198}$$

if

$$\tau+(N_r-1)T_f-I_rT_f < \ell\ T_f < \tau + (N_r-1)T_f \tag{199}$$

where

$$A_r = k_{r1}k_{r2}. \tag{200}$$

In (198) it can be shown that

$$T_r(nT_f+n_rT_a) = T_r(\ell T_f+n_rT_a) + \frac{\Delta T_{rf}}{T_f}(n-\ell)T_f-C_\tau(n,\ell)-C_o(n,\ell). \tag{201}$$

Using (194) and (201), we obtain from (198)

$$C_c = A_r\left[T_o(\ell T_f+n_rT_a)-T_r(\ell T_f+n_rT_a)\right] - A_r\left(\frac{N_r-1}{2} - \ell\right)T_f\ \frac{\Delta T_{rf}}{T_f}$$

$$+\frac{A_r}{N_r}\sum_{n=0}^{N_r-1}\left\{T_o(\ell T_f+n_rT_a)-2T_o(nT_f+n_rT_a)+T_c(nT_f+n_rT_a)-\xi_r(nT_f+n_rT_a)+C_o(n,\ell)\right\}. \tag{202}$$

Using (194) and (202) in (193)

$$T_o(I_rT_f+\ell T_f+n_rT_a)-T_r(I_rT_f+\ell T_f+n_rT_a) = (1-A_r)[T_o(\ell T_f+n_rT_a) - T_r(\ell T_f+n_rT_a)]+W_1+W_2 \tag{203}$$

where

$$W_1 = T_o(\ell T_f+n_rT_a)-T_o(I_rT_f+\ell T_f+n_rT_a)-C_o(\ell, I_r+\ell) - \left[I_rT_f - A_r\left(\frac{N_r-1}{2}-\ell\right)\right]\frac{\Delta T_{rf}}{T_f} + \frac{A_r}{N_r}\sum_{n=0}^{N_r-1}\left\{T_o(nT_f+n_rT_a)-T_o(\ell T_f+n_rT_a)-C_o(n,\ell)\right\} \tag{204}$$

and

$$W_2 = \frac{A_r}{N_r}\sum_{n=0}^{N_r-1}\left\{T_o(nT_f+n_rT_a)-T_c(nT_f+n_rT_a)+\xi_r(nT_f+n_rT_a)\right\}. \tag{205}$$

We shall assume that the clock loop is in the steady state. Then making use of (178) and (184)-(186) we obtain the expected values of (204) and (205),

$$E[W_1] = E[\ddot{T}_o(-N_\tau T_f)]T_f^2\left[\frac{\rho^\ell(\rho^{I_r}-1)}{1-\rho} + \frac{A_r}{N_r}\sum_{n=0}^{N_r-1}\frac{\rho^\ell-\rho^n}{1-\rho}\right] \cdot\left[\frac{(1+\rho)(1-\rho^{N_\tau})}{2(1-\rho)} + \rho^{N_\tau}\cdot\frac{n_rT_a}{T_f} - \rho^{N_\tau}(1-\rho)\frac{n_r^2T_a^2}{2T_f^2} - \left(\frac{m_\tau}{N_c}+\frac{A_o}{T_f}\right) + (1-\rho)\frac{m_\tau}{N_c}\left(\frac{m_\tau}{2N_c}+\frac{A_o}{T_f}\right)\right] - \left[I_r-A_r\left(\frac{N_r-1}{2}-\ell\right)\left(\frac{\Delta T_{cf}}{T_f}+\frac{\Delta T_{rf}}{T_f}\right)T_f\right] \tag{206}$$

and

$$E[W_2] = A_r\varepsilon_{cs}(n_rT_a) = A_r\varepsilon_{cs}(\ell T_f+n_rT_a). \tag{207}$$

Equation (206) can be made independent of $E[\ddot{T}_o(-N_\tau T_f)]$ if A_o is chosen according to the expression

$$A_o = \left\{ \frac{(1+\rho)(1-\rho^{N_\tau})}{2(1-\rho)} - \frac{m_\tau}{N_c} + (1-\rho)\left[\frac{m_\tau^2}{2N_c^2} + \rho^{N_\tau}\left[\frac{n_rT_a}{T_f} - (1-\rho)\frac{n_r^2T_a^2}{2T_f^2} \right] \right] \right\} \frac{T_f}{1-(1-\rho)\frac{m_\tau}{N_c}} \quad . \tag{208}$$

For $\rho \approx 1$, (208) reduces to

$$A_o = \left(N_\tau - \frac{m_\tau}{N_c} + \frac{n_rT_a}{T_f} \right) T_f \approx \tau \quad . \tag{209}$$

Then from (203), (206), (207) and (208) we obtain

$$\varepsilon_{rs}(I_rT_f+\ell T_f+n_rT_a) - (1-A_r)\varepsilon_{rs}(\ell T_f+n_rT_a)$$

$$= -\left[I_r - A_r\left(\frac{N_r-1}{2} - \ell \right) \right]\left(\frac{\Delta T_{cf}}{T_f} + \frac{\Delta T_{rf}}{T_f} \right) T_f + A_r\varepsilon_{cs}(\ell T_f+n_rT_a) \tag{210}$$

where

$$\varepsilon_{rs}(nT_f+n_rT_a) = E[T_o(nT_f+n_rT_a)-T_r(nT_f+n_rT_a)] \tag{211}$$

and

$$\tau + (N_r-1)T_f - I_rT_f < \ell T_f < \tau + (N_r-1)T_f \ . \tag{212}$$

From (210), we obtain the solution for the mean ranging loop timing error $\varepsilon_{rs}(nI_rT_f+\ell T_f+n_rT_a)$ as

$$\varepsilon_{rs}(nI_rT_f+\ell T_f+n_rT_a) = \varepsilon_{rs}(\ell T_f+n_rT_a)(1-A_r)^n-[1-(1-A_r)^n]$$

$$\cdot\left\{\left(\frac{I_r}{A_r}-\frac{N_r-1}{2}+\ell\right)\left(\frac{\Delta T_{cf}}{T_f}+\frac{\Delta T_{rf}}{T_f}\right)T_f-\varepsilon_{cs}(\ell T_f+n_rT_a)\right\}\ . \tag{213}$$

For the system to be stable,

$$\lim_{n\to\infty}(1-A_r)^n=0. \tag{214}$$

Thus we must set

$$0 < A_r < 2. \tag{215}$$

In the steady-state, the mean ranging loop timing error is given by

$$\varepsilon_{rs}(nI_rT_f+\ell T_f+n_rT_a) = -\left(\frac{I_r}{A_r}-\frac{N_r-1}{2}+\ell\right)\left(\frac{\Delta T_{cf}}{T_f}+\frac{\Delta T_{rf}}{T_f}\right)T_f+\varepsilon_{cs}(\ell T_f+n_rT_a)\ , \tag{216}$$

The relationships between $E[T_o]$, $E[T_c]$, and $E[T_r]$ for $E[\ddot{T}_o]=0$, $N_r=2$, and $N_c=1$ are shown in Figure 21. This figure will be examined in detail later (in Section VI-B) when applications to system design are considered.

To calculate the variance of the ranging-loop timing error, we assume that all the random processes of (203) are zero-mean. This is permissible since the control system is approximately linear in the sampled-data sense over the range of operation for which the model is applicable. Using (184)-(186), (208) and the following relations

$$T_c(nT_f) = T_o(nT_f)-T_\varepsilon(nT_f), \qquad \dot{T}_c(nT_f) = \dot{T}_o(nT_f)-\dot{T}_\varepsilon(nT_f) \tag{217}$$

$$\ddot{T}_c(nT_f) = \ddot{T}_o(nT_f) - \ddot{T}_\varepsilon(nT_f) \tag{218}$$

we can rewrite (204) and (205) as

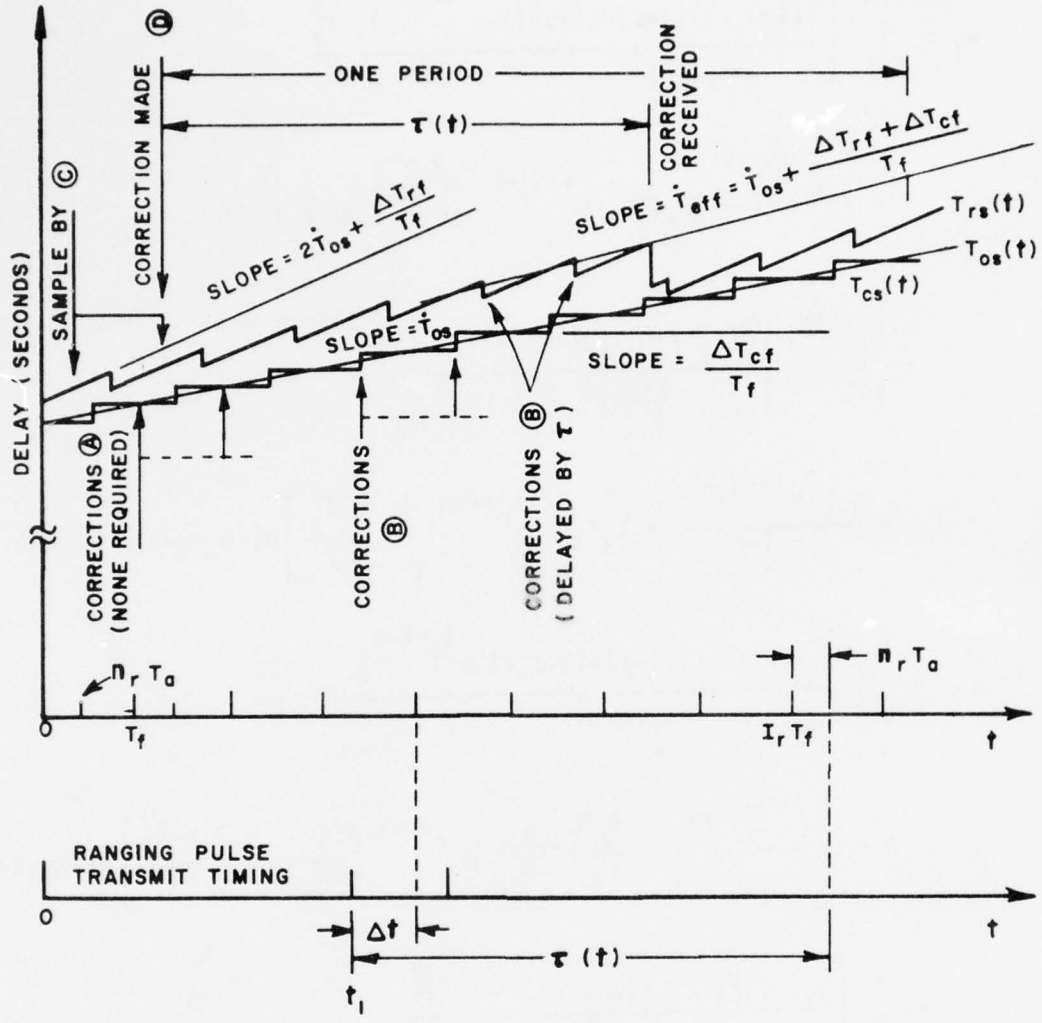

Figure 21. The steady-state delay-function responses of the modified synchronizer for the case $N_r=2$, $N_c=1$.

$$W_1 = \sum_{k=1}^{\ell+N_\tau} \left[\frac{2(\ell+N_\tau-k)(1-\rho)-(1+\rho)(1-\rho^{\ell+N_\tau-k})}{(1-\rho)^2} \frac{T_f^2}{2} \right.$$

$$\left. + \frac{1-\rho^{\ell+N_\tau-k}}{1-\rho} n_r T_a T_f + \rho^{\ell+N_\tau-k} \frac{n_r^2 T_a^2}{2} \right] u(-N_\tau+k-1)$$

$$- \sum_{k=1}^{I_r+\ell+N_\tau} \left[\frac{2(I_r+\ell+N_\tau-k)(1-\rho)-(1+\rho)(1-\rho^{I_r+\ell+N_\tau-k})}{(1-\rho)^2} \frac{T_f^2}{2} \right.$$

$$\left. + \frac{1-\rho^{I_r+\ell+N_\tau-k}}{1-\rho} n_r T_a T_f + \rho^{I_r+\ell+N_\tau-k} \frac{n_r^2 T_a^2}{2} \right] u(-N_\tau+k-1)$$

$$+ \sum_{k=1}^{I_r+\ell} \left[\frac{2(I_r+\ell-k)(1-\rho)-(1+\rho)(1-\rho^{I_r+\ell-k})}{(1-\rho)^2} \frac{T_f^2}{2} \right.$$

$$\left. + \frac{1-\rho^{I_r+\ell-k}}{1-\rho} \left(\frac{m_\tau}{N_c} + \frac{A_o}{T_f} \right) T_f^2 + \rho^{I_r+\ell-k} \left(\frac{m_\tau}{2N_c} + \frac{A_o}{T_f} \right) \frac{m_\tau T_f^2}{N_c} \right] u(-N_\tau+k-1)$$

$$- \sum_{k=1}^{\ell} \left[\frac{2(\ell-k)(1-\rho)-(1+\rho)(1-\rho^{\ell-k})}{(1-\rho)^2} \frac{T_f^2}{2} \right.$$

$$\left. + \frac{1-\rho^{\ell-k}}{1-\rho} \left(\frac{m_\tau}{N_c} + \frac{A_o}{T_f} \right) T_f^2 + \rho^{\ell-k} \left(\frac{m_\tau}{2N_c} + \frac{A_o}{T_f} \right) \frac{m_\tau T_f^2}{N_c} \right] u(-N_\tau+k-1)$$

(219)

(cont. next page)

$$-[T_\varepsilon(I_r T_f+\ell T_f-N_\tau T_f)-T_\varepsilon(\ell T_f-N_\tau T_f)]$$

$$-[\dot{T}_\varepsilon(I_r T_f+\ell T_f-N_\tau T_f)-\dot{T}_\varepsilon(\ell T_f-N_\tau T_f)]\left(\frac{m_\tau}{N_c}+\frac{A_o}{T_f}\right)T_f$$

$$-[\ddot{T}_\varepsilon(I_r T_f+\ell T_f-N_\tau T_f)-\ddot{T}_\varepsilon(\ell T_f-N_\tau T_f)]\left(\frac{m_\tau}{2N_c}+\frac{A_o}{T_f}\right)\frac{m_\tau}{N_c}T_f^2$$

$$+\frac{A_r}{N_r}\sum_{n=0}^{N_r-1}\cdot$$

$$\left\{\sum_{k=1}^{n+N_\tau}\left[\frac{2(n+N_\tau-k)(1-\rho)-(1+\rho)(1-\rho^{n+N_\tau-k})}{(1-\rho)^2}\,\frac{T_f^2}{2}+\frac{1-\rho^{n+N_\tau-k}}{1-\rho}\right.\right.$$

$$\left.n_r T_a T_f+\rho^{n+N_\tau-k}\,\frac{n_r^2T_a^2}{2}\right]u(-N_\tau+k-1)$$

$$-\sum_{k=1}^{\ell+N_\tau}\left[\frac{2(\ell+N_\tau-k)(1-\rho)-(1+\rho)(1-\rho^{\ell+N_\tau-k})}{(1-\rho)^2}\,\frac{T_f^2}{2}+\frac{1-\rho^{\ell+N_\tau-k}}{1-\rho}\right.$$

$$\left.n_r T_a T_f+\rho^{\ell+N_\tau-k}\,\frac{n_r^2T_a^2}{2}\right]u(-N_\tau+k-1)$$

$$+\sum_{k=1}^{\ell}\left[\frac{2(\ell-k)(1-\rho)-(1+\rho)(1-\rho^{\ell-k})}{(1-\rho)^2}\,\frac{T_f^2}{2}+\frac{1-\rho^{\ell-k}}{1-\rho}\left(\frac{m_\tau}{N_c}+\frac{A_o}{T_f}\right)\right.$$

$$\left.T_f^2+\rho^{\ell-k}\left(\frac{m_\tau}{2N_c}+\frac{A_o}{T_f}\right)\frac{m_\tau T_f^2}{N_c}\right]u(-N_\tau+k-1) \qquad (219)$$

(cont. next page)

$$- \sum_{k=1}^{n} \left[\frac{2(n-k)(1-\rho)-(1+\rho)(1-\rho^{n-k})}{(1-\rho)^2} \frac{T_f^2}{2} + \frac{1-\rho^{n-k}}{1-\rho}\left(\frac{m_\tau}{N_c} + \frac{A_o}{T_f}\right) T_f^2 + \rho^{n-k}\left(\frac{m_\tau}{2N_c} + \frac{A_o}{T_f}\right)\frac{m_\tau T_f^2}{N_c}\right] u(-N_\tau+k-1)$$

$$- [T_\varepsilon(\ell T_f - N_\tau T_f) - T_\varepsilon(nT_f - N_\tau T_f)]$$

$$- [\dot{T}_\varepsilon(\ell T_f - N_\tau T_f) - \dot{T}_\varepsilon(nT_f - N_\tau T_f)]\left(\frac{m_\tau}{N_c} + \frac{A_o}{T_f}\right) T_f$$

$$- [\ddot{T}_\varepsilon(\ell T_f - N_\tau T_f) - \ddot{T}_\varepsilon(nT_f - N_\tau T_f)]\left(\frac{m_\tau}{2N_c} + \frac{A_o}{T_f}\right)\frac{m_\tau}{N_c} T_f^2 \Bigg\} \tag{219}$$

and

$$W_2 = \frac{A_r}{N_r} \sum_{n=2}^{N_r-1} \left\{ T_\varepsilon(nT_f) + \dot{T}_\varepsilon(nT_f) n_r T_a + \ddot{T}_\varepsilon(nT_f) \frac{n_r^2 T_a^2}{2} + \xi_r(nT_f + n_r T_a) \right\} . \tag{220}$$

Due to the complexity of the expression, we shall consider two cases only. For the first case let the clock loop and ranging loop measurement noise variances be identical and assume no maneuver noise, i.e.,

$$\sigma_{\xi r} = \sigma_{\xi c} = \sigma_\xi, \ \sigma_a = 0 \tag{221}$$

and periodically-stationary.

In this case, all the random variables, u and T_ε, $\dot{T}_\varepsilon$, $\ddot{T}_\varepsilon$ are zero. Thus (203) reduces to

$$\varepsilon_r(I_rT_f+\ell T_f+n_rT_a) = T_o(I_rT_f+\ell T_f+n_rT_a)-T_r(I_rT_f+\ell T_f+n_rT_a)$$

$$= (1-A_r)\varepsilon_r(\ell T_f+n_rT_a) + \frac{A_r}{N_r}\sum_{n=0}^{N_r-1}\varepsilon_r(nT_f+n_rT_a) \quad (222)$$

and the variance of ε_r is

$$\sigma^2_{\varepsilon r}(I_rT_f+\ell T_f+n_rT_a) = \sigma^2_{\varepsilon r}(\ell T_f+n_rT_a) = \frac{A_r}{N_r(2-A_r)}\sigma^2_\xi . \quad (223)$$

For the second case we assume

$$n_r = m_\tau = 0, \quad A_r = N_r = 1, \quad \rho \geq .99, \quad \ell = N_\tau = I_r >> 1. \quad (224)$$

Because the largest variance occurs at $\ell=N_\tau$, this is the most important case to investigate. In this case, because the value of ρ is close to unity,

$$A_o \approx N_\tau T_f \quad (225)$$

and (203) reduces to

$$\varepsilon_r(I_rT_f+\ell T_f+n_rT_a) \approx -\sum_{k=1}^{I_r+\ell+N_\tau}(I_r+\ell+N_\tau-k)^2\,\frac{T_f^2}{2}\,u(-N_\tau+k-1)$$

$$+\sum_{k=1}^{I_r+\ell}\left[(I_r+\ell-k)^2\,\frac{T_f^2}{2}+(I_r+\ell-k)N_\tau T_f^2\right]u(-N_\tau+k-1)$$

$$-T_\varepsilon(I_rT_f+\ell T_f-N_\tau T_f)-\dot{T}_\varepsilon(I_rT_f+\ell T_f-N_\tau T_f)N_\tau T_f$$

$$+\sum_{k=1}^{N_\tau}(N_\tau-k)^2\,\frac{T_f^2}{2}\,u(-N_\tau+k-1)$$

$$+T_\varepsilon(-N_\tau T_f)+\dot{T}_\varepsilon(-N_\tau T_f)N_\tau T_f+T_\varepsilon(0)+\xi_r(n_rT_a)$$

$$=-\sum_{k=I_r+\ell+1}^{I_r+\ell+N_\tau}(I_r+\ell+N_\tau-k)^2\,\frac{T_f^2}{2}\,u(-N_\tau+k-1)$$

$$-\sum_{k=1}^{I_r+\ell}\frac{N_\tau^2T_f^2}{2}\,u(-N_\tau+k-1)+\sum_{k=1}^{N_\tau}(N_\tau-k)^2\,\frac{T_f^2}{2}\,u(-N_\tau+k-1)$$

$$-T_\varepsilon(I_rT_f+\ell T_f-N_\tau T_f)-\dot{T}_\varepsilon(I_rT_f+\ell T_f-N_\tau T_f)\,N_\tau T_f$$

$$+T_\varepsilon(-N_\tau T_f)+\dot{T}_\varepsilon(-N_\tau T_f)N_\tau T_f+T_\varepsilon(0)+\xi_r(n_rT_a)\quad.$$

(226)

Then substituting $\ell = N_\tau$ into (226),

$$\varepsilon_r(I_rT_f+N_\tau T_f+n_rT_a) \approx -\sum_{k=1}^{N_\tau}[(N_\tau-k)^2u(I_r+k-1)+N_\tau^2u(k-1)+k(2N_\tau-k)$$

$$u(-N_\tau+k-1)]\frac{T_f^2}{2}$$

$$-T_\varepsilon(I_rT_f) - \dot{T}_\varepsilon(I_rT_f)N_\tau T_f$$

$$+T_\varepsilon(-N_\tau T_f) + \dot{T}_\varepsilon(-N_\tau T_f)N_\tau T_f + T_\varepsilon(0) + \xi_r(n_rT_a) \qquad (227)$$

and substituting $N_\tau=I_r$ into the right-hand side of (227) and taking the expected value of ε_r^2, we obtain

$$\sigma_{\varepsilon r}^2(I_rT_f+N_\tau T_f+n_rT_a) \approx \sum_{k=1}^{I_r}[(I_r-k)^4+I_r^4+k^2(2I_r-k)^2]\frac{T_f^4}{4}(1-\rho^2)\sigma_a^2$$

$$+3\hat{P}_1+4\hat{P}_2I_rT_f+2\hat{P}_3I_r^2T_f^2+\sigma_{\xi r}^2$$

$$+\sum_{k=1}^{I_r}E\Big\{u(k-1)[(I_r-k)^2T_\varepsilon(I_rT_f)$$

$$+I_r^2\dot{T}_\varepsilon(I_rT_f)I_rT_f]\,T_f^2\Big\} \qquad (228)$$

or

$$\sigma^2_{\varepsilon r}(I_r T_f + N_\tau T_f + n_r T_a) \approx \sum_{k=1}^{I_r} [(I_r-k)^4 + I_r^4 + k^2(2I_r-k)^2] \frac{T_f^4}{4}(1-\rho^2)\sigma_a^2$$

$$+3\hat{P}_1 + 4\hat{P}_2 I_r T_f + 2\hat{P}_3 I_r^2 T_f^2 + \sigma^2_{\xi r}$$

$$+ \sum_{k=1}^{I_r} [(I_r-k)^2 \sigma_{a_T}(I_r-k+1)T_f^2 + I_r^2 \sigma_{a_f}(I_r-k+1) I_r T_f^3] \qquad (229)$$

where use has been made of (191) and (192). In applying Equation (191), terms are neglected if $\ell > I_r$.

Graphs of the ranging loop error variance, Equation (229) are shown in Figures 22 and 23. If the propagation delay is assumed to be .25 sec. then Figure 22 applies for T_f = .01 sec. and Figure 23 for T_f = .001 sec.

From the two cases considered, we can obtain an approximation for $\sigma^2_{\varepsilon r}(I_r T_f + N_\tau T_f + n_r T_a)$ when $N_r > 1$ by replacing $\sigma^2_{\xi r}$ with $\sigma^2_{\xi r}/N_r$ in Equation (229).

For the case of a maneuvering terminal and stationary satellite, derivation of the ranging loop timing error follows essentially the same procedure as described above with the following changes: The equation for the effects of a propagation delay change C_τ, (Equation (194)) is replaced by

$$C_\tau(\ell, I_r+\ell) = T_o(I_r T_f + \ell T_f + n_r T_a) - T_o(\ell T_f + n_r T_a)$$

$$+ T_o(I_r T_f + \ell T_f + n_r T_a - \tau) - T_o(\ell T_f + n_r T_a - \tau) \qquad (230)$$

and the gain factor A_o (Equation (209)) becomes

$$A_o = 0 \qquad (231)$$

i.e., no open loop (predicted) velocity or acceleration corrections are needed since any change in range for the case of the stationary satellite is immediately evident at the terminal.

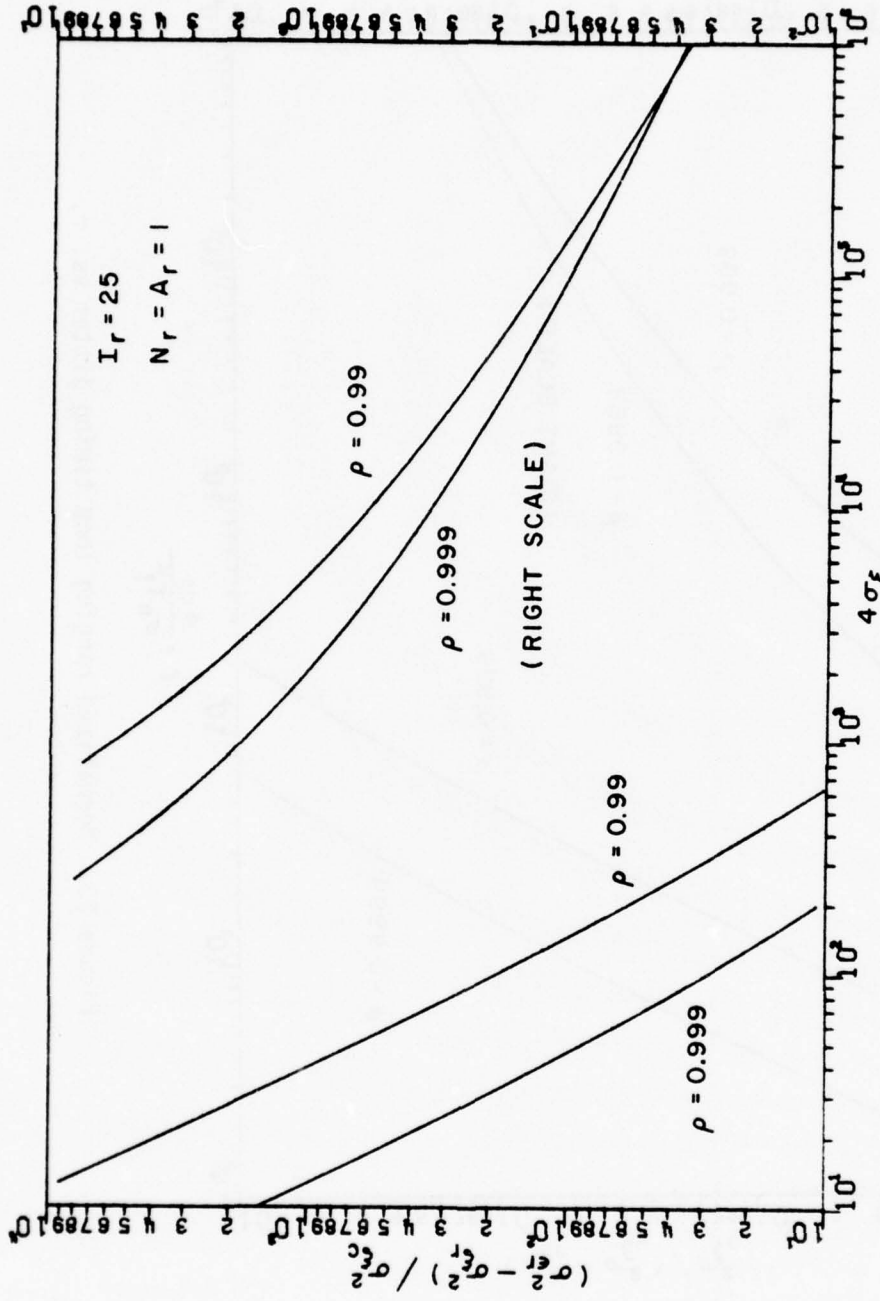

Figure 22. Normalized ranging loop timing jitter vs. r.

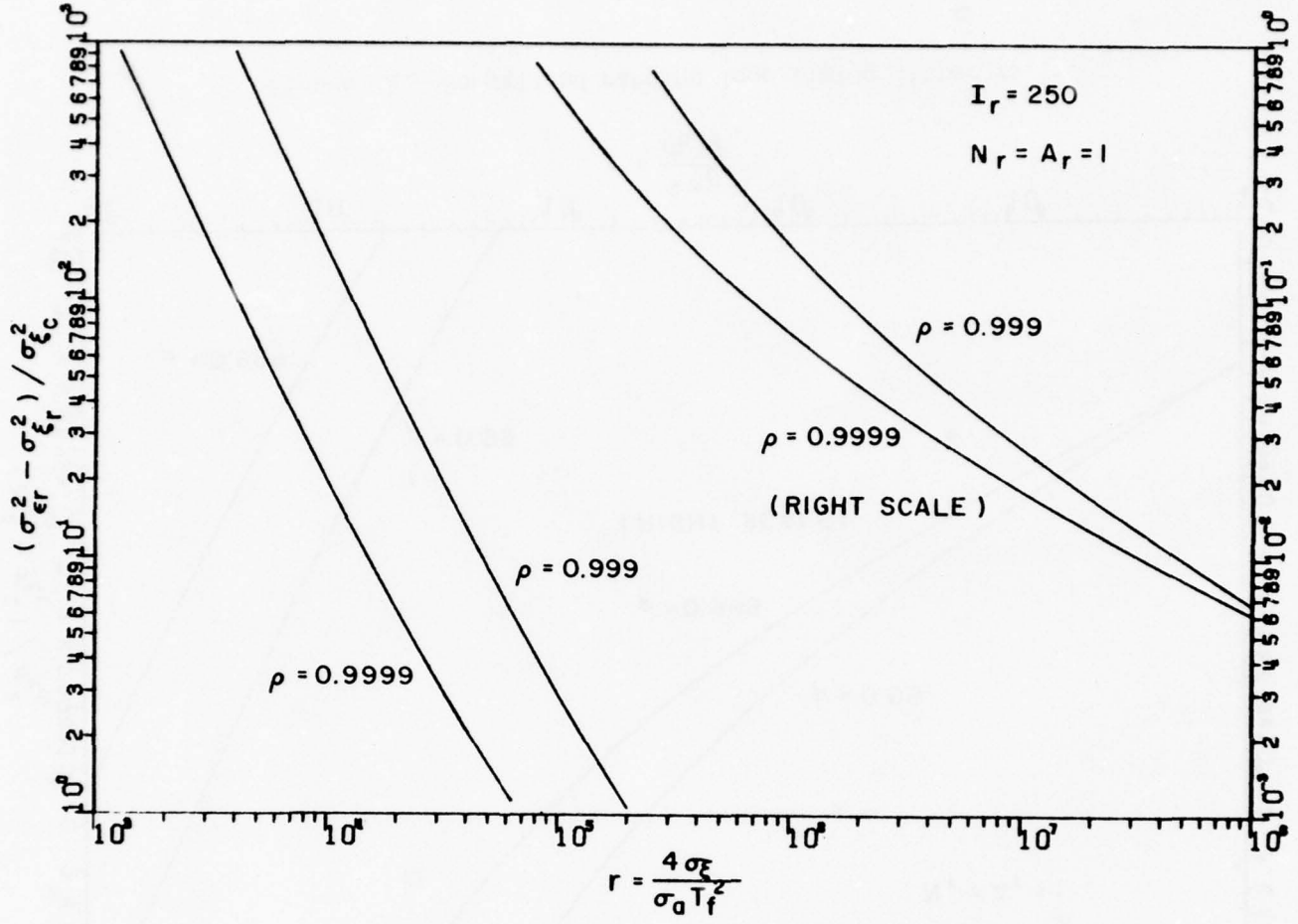

Figure 23. Normalized ranging loop timing jitter vs. r.

In the steady-state, the expected ranging loop timing error ε_{rs} is still given by Equation (216). However, the equation for calculating the variance of the ranging loop timing error becomes

$$\begin{aligned}
\varepsilon_r(I_rT_f+\ell T_f+n_rT_a) &= (1-A_r)\varepsilon_r(\ell T_f+n_rT_a) \\
&+ (1-A_r)\left[T_\varepsilon(\ell T_f-N_\tau T_f)+\dot{T}_\varepsilon(\ell T_f-N_\tau T_f)\frac{m_\tau T_f}{N_c}\right. \\
&\left.+ \ddot{T}_\varepsilon(\ell T_f-N_\tau T_f)\frac{m_\tau^2}{2N_c^2}T_f^2\right] \\
&- \left[T_\varepsilon(I_rT_f+\ell T_f-N_\tau T_f)+\dot{T}_\varepsilon(I_rT_f+\ell T_f-N_\tau T_f)\frac{m_\tau T_f}{N_c}\right. \\
&\left.+ \ddot{T}_\varepsilon(I_rT_f+\ell T_f-N_\tau T_f)\frac{m_\tau^2}{2N_c^2}T_f^2\right] \\
&+ \frac{A_r}{N_r}\sum_{n=0}^{N_r-1}\left[T_\varepsilon(nT_f-N_\tau T_f)+\dot{T}_\varepsilon(nT_f-N_\tau T_f)\frac{m_\tau T_f}{N_c}\right. \\
&\left.+ \ddot{T}_\varepsilon(n-N_\tau)\frac{m_\tau^2}{2N_c^2}T_f^2\right] \\
&+ \frac{A_r}{N_r}\sum_{n=0}^{N_r-1}\left[T_\varepsilon(nT_f)+\dot{T}_\varepsilon(nT_f)n_rT_a+\ddot{T}_\varepsilon(nT_f)\frac{n_r^2T_a^2}{2}\right. \\
&\left.+ \xi_r(nT_f+n_rT_a)\right] \quad . \qquad (232)
\end{aligned}$$

For the case

$$\ell = N_\tau = I_r, \quad A_r = N_r = 1, \quad n_r = m_\tau = 0 \tag{233}$$

the variance is

$$\sigma^2_{\varepsilon r}(I_r T_f + \ell T_f + n_r T_a) \approx 3\hat{P}_1 + \sigma^2_{\xi r} \tag{234}$$

which corresponds to Equation (229) of the stationary terminal case. Curves of $\hat{P}_1/\sigma^2_\xi$ vs. r_ρ were given previously in Section C (see Figure 8).

SECTION V
UP-LINK TIMING - EXTENDED ANALYSIS

A. Introduction and General Analysis

This section presents a more complete analysis of up-link timing error including development of a model applicable to both the stationary-satellite moving-terminal case and the stationary-terminal moving-satellite case. An optimum form of augmented open loop coupling from the clock loop to the ranging loop is developed (needed only in the case of the moving satellite) which differs from that utilized in Section IV-F in that only an acceleration term ($\ddot{T}_0$) is used rather than a combination of acceleration and velocity ($\dot{T}_0$). This is possible since a constant satellite velocity (zero-acceleration) produces a constant offset in receive clock and up-link timing which is compensated for by the coarse ranging system during initial lock-up. Thus no tracking is required to compensate for the presence of a velocity term and only the acceleration term is needed. Elimination of the velocity term should reduce the noise coupled from the clock loop to the ranging loop and hence result in reduced error variance under noise-limited operating conditions. The analysis of this section also retains additional cross correlation terms not included in the previous analysis and consequently should produce more accurate results. Typical data and comparisons with data from the analysis of Section IV-F are given in Section VI. Additional notation used in the subsequent analysis is:

$R(t)$ ∿ distance between the relay and a user terminal

$D(t)$ ∿ a delay function defined as $D(t) \triangleq R(t)/c$ where c is the speed of light

$d_d(t)$ ∿ down-link delay
$d_t(t)$ ∿ round-trip (total) delay = τ
$d_u(t)$ ∿ up-link delay referenced to the receive time base: $d_u(t) \triangleq d_t(t) - d_d(t)$

$t_{rp}(n)$ ∿ time of occurrence (receipt) of the n-th ranging pulse in a burst of N_r successive ranging pulses

T_{Dr} ∿ ranging loop processing delay

T_F ∿ frame duration = $N_F T_f$ where T_f is the subframe duration, and

$N_F \equiv I_r$ ∿ Number of subframes per frame.

Also we have

$$\varepsilon_c(t) \triangleq T_o(t)-T_c(t) \tag{235}$$

$$\varepsilon_r(t) \triangleq T_o(t)-T_r(t) \tag{236}$$

and

$$\varepsilon_{rc}(t) \triangleq T_c(t)-T_r(t)=T_o(t)-\varepsilon_c(t)-T_r(t)=\varepsilon_r(t)-\varepsilon_c(t) \quad . \tag{237}$$

It is assumed that the clock frequencies in various parts of the system are related by

$$f_r=f_c=f_o=f_a+\Delta f_o \tag{238}$$

and

$$f_s=f_a \tag{239}$$

where

f_r ∿ ranging loop code generator clocking frequency
f_c ∿ clock loop code generator clocking frequency
f_a ∿ assigned code generator clocking frequency
f_s ∿ effective code generator clocking frequency associated with the network clock signal radiated by the satellite (relay)

A model of the two-loop terminal synchronization system with simple cross strapping applicable to the stationary satellite case is given in Figure 24 and an illustration of the delay function vs. time for a typical terminal maneuver is given in Figure 25. From these figures we obtain

$$d_d(t) = D(t) \tag{240}$$

$$d_t(t) = d_d(t)+"d_u(t)" \triangleq D(t)+D(t-2D(t))+\dot{D}_o(t-2D(t))[D(t)-D(t-2D(t))] \tag{241}$$

$$T_o(t) = D(t) \tag{242}$$

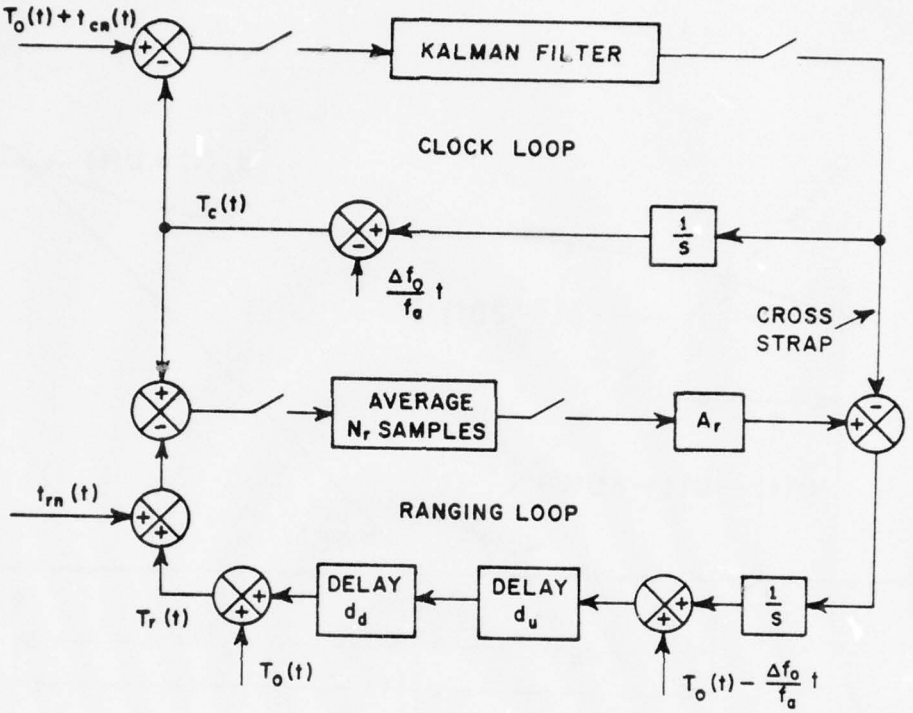

Figure 24. Model of the TDMA synchronizer for the stationary satellite case.

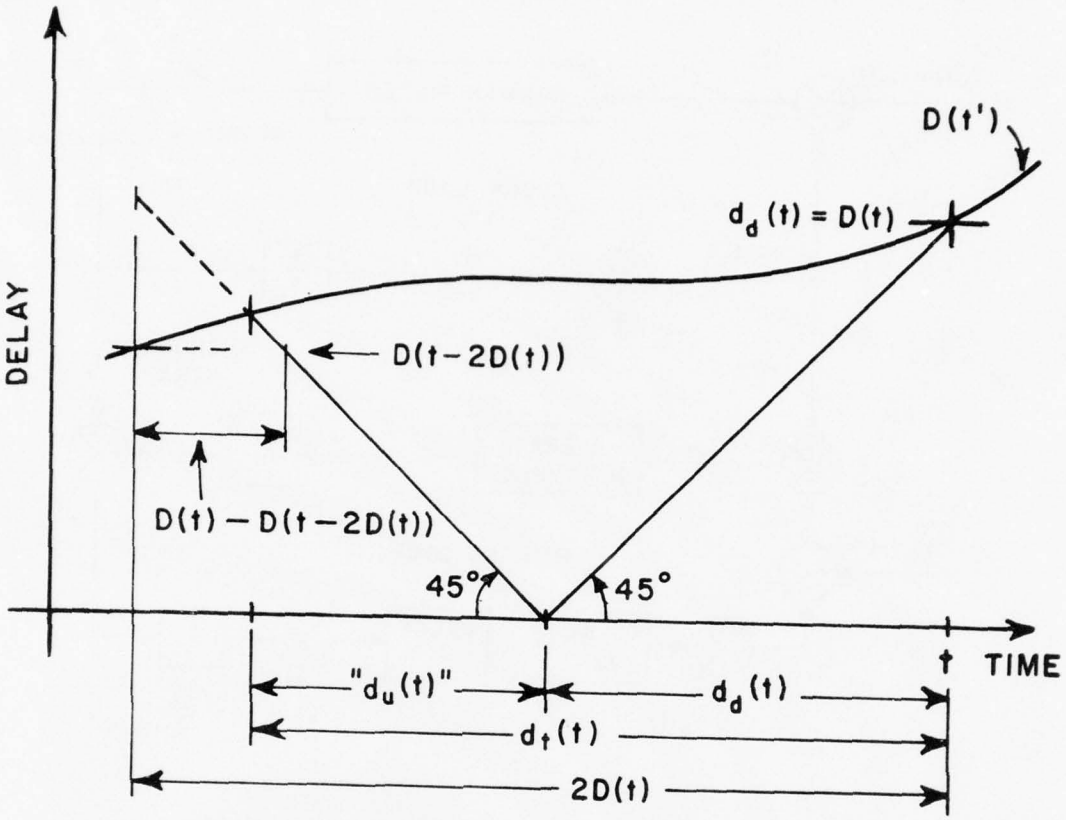

Figure 25. Delay functions for the stationary satellite case.

and

$$T_r(t_o+T_F) = T_r(t_o) + T_o(t_o+T_F) - T_o(t_o)$$

$$+ T_o(t_o+T_F-d_t(t_o+T_F)) - T_o(t_o-d_t(t_o)) - \frac{\Delta f_o}{f_a} T_F$$

$$- [T_c(t_o+T_F-d_t(t_o+T_F)) - T_c(t_o-d_t(t_o)) + \frac{\Delta f_o}{f_a} T_F]$$

$$+ \frac{A_r}{N_r} \sum_{n=1}^{N_r} [T_c(t_{rp}(n)) - T_r(t_{rp}(n)) - t_{rn}(t_{rp}(n))] \qquad (243)$$

where

$$t_o < [t_{cr} + \delta_t(t_{cr})] < t_o + T_F \qquad (244)$$

$$t_{cr} \doteq t_{rp}(N_r) + T_{Dr} \qquad (245)$$

and

$$\delta_t(t) \doteq D(t) + D(t+2D(t)) + D(t+2D(t))\,[D(t+2D(t))-D(t)]. \qquad (246)$$

It follows that

$$\varepsilon_r(t_o+T_F) = \varepsilon_r(t_o) - \varepsilon_c(t_o+T_F-d_t(t_o+T_F)) + \varepsilon_c(t_o-d_t(t_o))$$

$$+ 2\,\frac{\Delta f_o}{f_a} T_F - \frac{A_r}{N_r} \sum_{n=1}^{N_r} [\varepsilon_r(t_{rp}(n)) - \varepsilon_c(t_{rp}(n)) - t_{rn}(t_{rp}(n))].$$

(247)

Similarly, from Figures 26 and 27, for the stationary terminal case there results

$$d_d(t) \doteq D(t-D(t)) + \dot{D}(t-D(t))\,[D(t)-D(t-D(t))]\,, \tag{248}$$

$$d_t(t) = 2d_d(t), \tag{249}$$

$$T_o(t) \triangleq D(t-d_d(t)), \tag{250}$$

and

$$T_r(t_o+T_F) = T_r(t_o) + 2[D(t_o+T_F-d_d(t_o+T_F)) - D(t_o-d_d(t_o))] - \frac{\Delta f_o}{f_a} T_F$$

$$- [T_c(t_o+T_F-d_t(t_o+T_F)) - T_c(t_o-d_t(t_o)) + \frac{\Delta f_o}{f_a} T_F]$$

$$+ \frac{A_r}{N_r} \sum_{n=1}^{N_r} [T_c(t_{rp}(n)) - T_r(t_{rp}(n)) - t_{rn}(t_{rp}(n))] \tag{251}$$

where

$$t_o < [t_{cr} + \delta_t(t_{cr})] < t_o+T_F \tag{252}$$

$$r \doteq t_{rp}(N_r) + T_{Dr} \tag{253}$$

and

$$\delta_t(t) \doteq 2[D(t+D(t)) + \dot{D}(t+D(t))[D(t+D(t)) - D(t)]] \quad . \tag{254}$$

Since

$$T_o(t) \triangleq D(t-d_d(t)) \tag{255}$$

it follows that

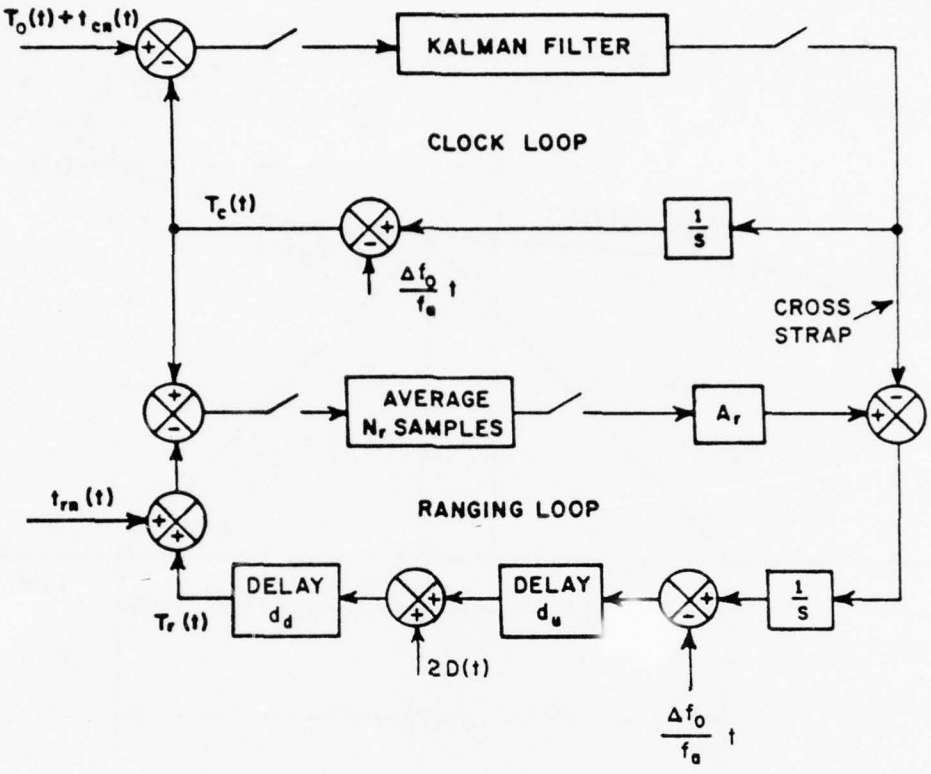

Figure 26. Model of the TDMA synchronizer for the stationary terminal case.

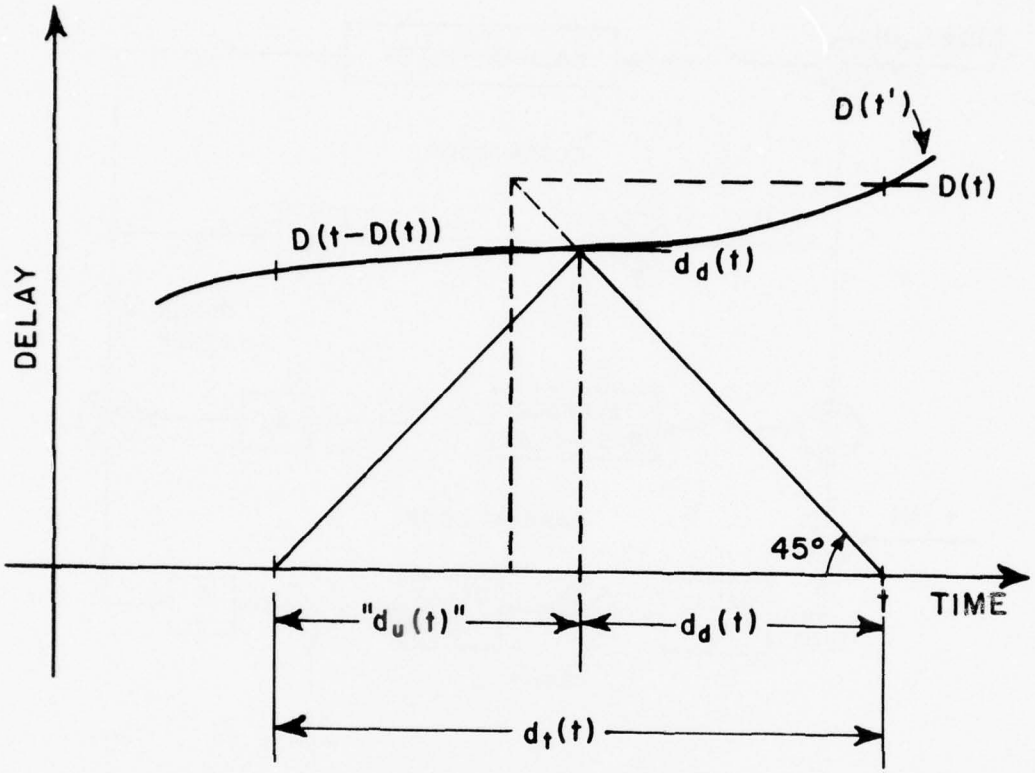

Figure 27. Delay functions for the stationary terminal case.

$$\varepsilon_r(t_o+T_F) = \varepsilon_r(t_o) - \varepsilon_c(t_o+T_F-d_t(t_o+T_F)) + \varepsilon_c(t_o-d_t(t_o))$$

$$+ 2\,\frac{\Delta f_o}{f_a}\,T_F - \frac{A_r}{N_r}\sum_{n=1}^{N_r}\left[\varepsilon_r(t_{rp}(n)) - \varepsilon_c(t_{rp}(n)) - t_{rn}(t_{rp}(n))\right]$$

$$- \Delta_o(t_o+T_F) + \Delta_o(t_o) \qquad (256)$$

where

$$\Delta_o(t) \triangleq T_o(t) - T_o(t-d_t(t)) \quad . \qquad (257)$$

Then by noting that

$$\Delta_o'(t) \triangleq \Delta_o(t+\delta_t(t)) \qquad (258)$$

$$\Delta_o'(t-d_t(t)) = \Delta_o(t-d_t(t)) + \delta_t(t-d_t(t)) = \Delta_o(t) \qquad (259)$$

where the prime indicates an equivalent term shifted to the opposite end of the delay blocks ($d_t(t) = d_d(t) + d_u(t)$) the equivalent model of Figure 28 is obtained.

The effect of the term $\Delta_o(t+\delta_t(t))$ in the preceding model (Figure 28) can be minimized via additional open loop corrections. Assume that such corrections are made every T_f/N_a seconds and that t_a represents a correction instant. Ideally, the open-loop correction at $t=t_a+T_f/N_a^-$ would equal $O_a(t_a+t_f/N_a^-)$ where

$$O_a(t_a+T_f/N_a^-) = -\left\{\Delta_o[(t_a+T_f/N_a^-) + \delta_t(t_a+T_f/N_a^-)] - \Delta_o[t_a+\delta_t(t_a)]\right\}$$

$$\doteq -\ddot{T}_o(t_a+T_f/N_a^-)\cdot\delta_t(t_a+T_f/N_a^-)\cdot\frac{T_f}{N_a} \quad . \qquad (260)$$

Since $\ddot{T}_o$ is not known exactly, the added open loop corrections can, at best, be estimates, $\hat{O}_a$, where

$$\hat{O}_a \doteq -\hat{\ddot{T}}_o\cdot\delta_t\cdot\frac{T_f}{N_a} \quad . \qquad (261)$$

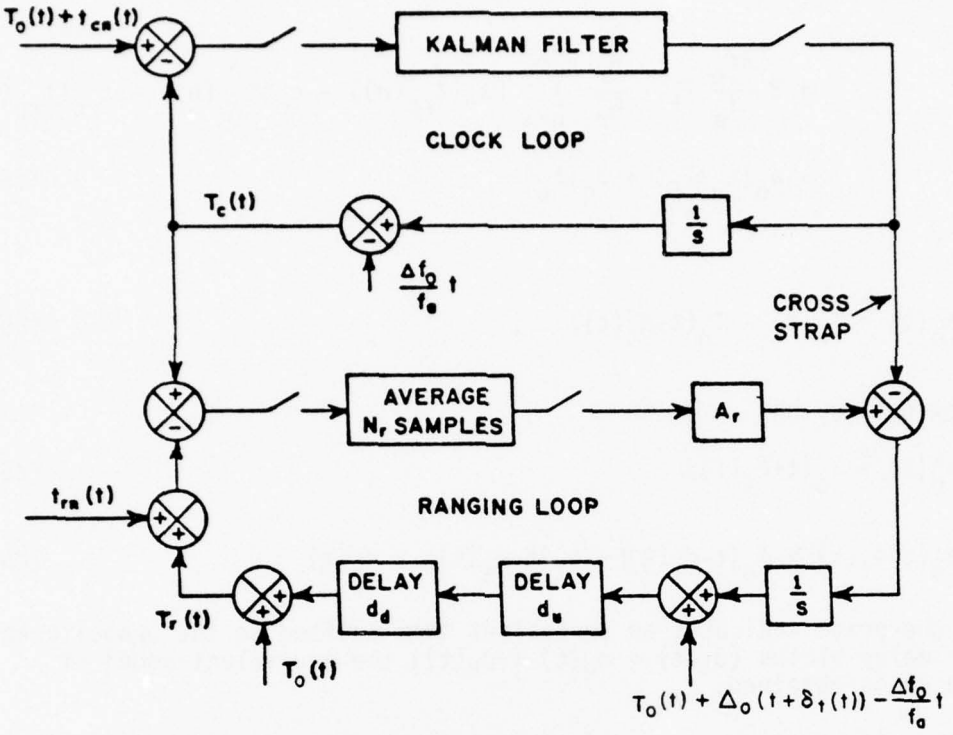

Figure 28. Equivalent model of the TDMA synchronizer for the stationary terminal case.

The addition of this term via an augmented cross strap from the clock loop to the ranging loop is shown in the augmented model of Figure 29.

An equivalent model for the TDMA synchronizer with augmented cross strap is given in Figure 30. Although appearing somewhat more complex than that of Figure 29 in that there is a certain amount of redundancy in the arrangement of signal inputs and function blocks, it is more amenable to the analysis to follow and is applicable (by setting appropriate terms to zero) to the stationary satellite case as well as to the stationary terminal case. From Figure 30 we obtain

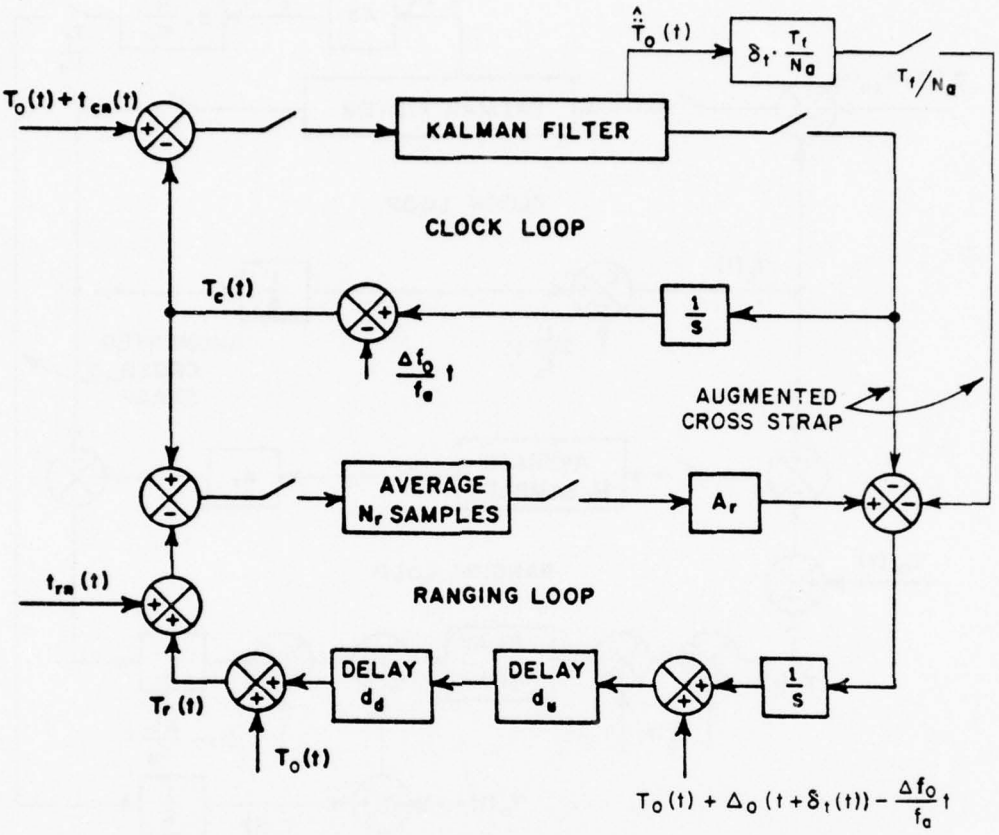

Figure 29. Augmented cross strap model of the TDMA Synchronizer for the stationary terminal case.

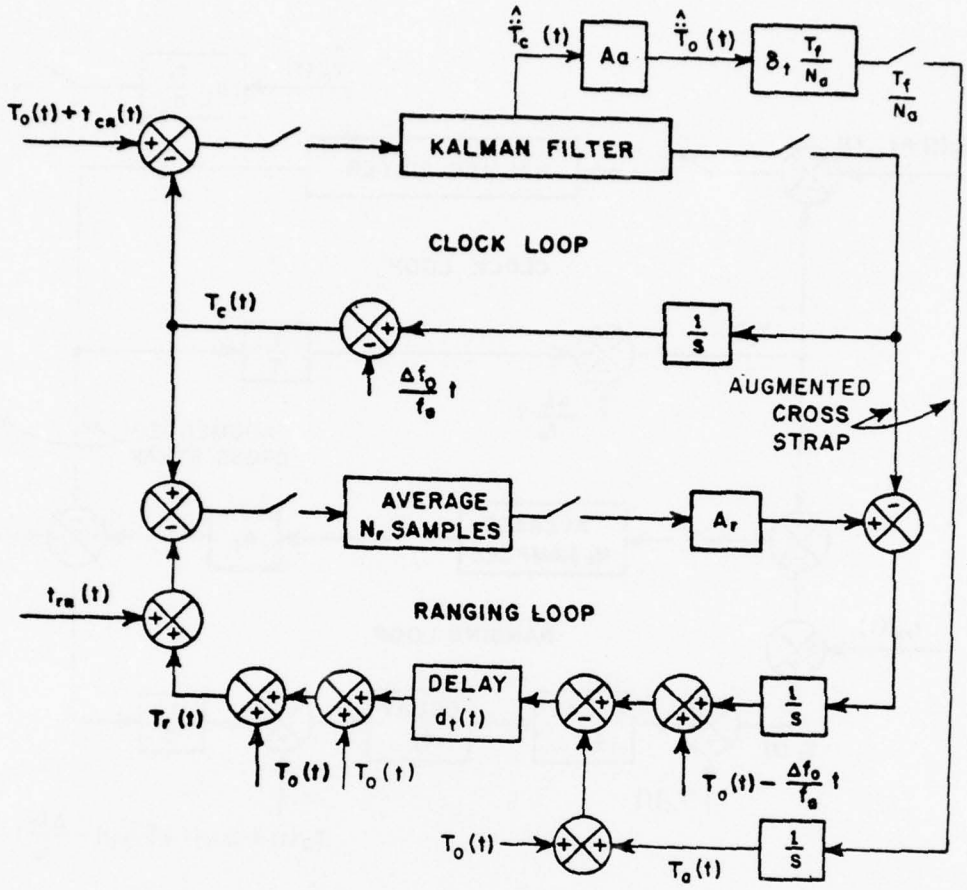

Figure 30. Equivalent augmented cross strap model of the TDMA syncrhonizer.

$$T_r(t_o+T_F) = T_r(t_o) + T_o(t_o+T_F) - T_o(t_o)$$

$$+ T_o(t_o+T_F-d_t(t_o+T_F)) - T_o(t_o-d_t(t_o)) - \frac{\Delta f_o}{f_a} T_F$$

$$- [T_c(t_o+T_F-d_t(t_o+T_F)) - T_c(t_o-d_t(t_o)) + \frac{\Delta f_o}{f_a} T_F]$$

$$+ \frac{A_r}{N_r} \sum_{n=1}^{N_r} [T_c(t_{rp}(n)) - T_r(t_{rp}(n)) - t_{rn}(t_{rp}(n))]$$

$$+ Q(t_o+T_F) - Q(t_o) \qquad (262)$$

where

$$t_{cr} + \delta_t(t_{cr}) - T_F < t_o < t_{cr} + \delta_t(t_{cr}) \qquad (263)$$

$$\bar{t}_{cr} = t_{rp}(N_r) + T_{Dr} \qquad (264)$$

$$\delta_t(t) \doteq 2\left\{D(t+D(t)) + \dot{D}(t+D(t))\,[D(t+D(t)) - D(t)]\right\} \qquad (265)$$

$$T_F > d_t + (N_r-1)\,T_f + T_{Dr} \qquad (266)$$

$$Q(t) \triangleq T_o(t) - T_o(t-d_t(t)) - T_a(t-d_t(t)) \qquad (267)$$

and $T_a(t)$ is defined in the equivalent model of the augmented cross strap synchronizer, Figure 30. Similarly,

$$T_r(t_{rp}(n)) = T_r(t_o)+T_o(t_{rp}(n)) - T_o(t_o)$$

$$+ T_o(t_{rp}(n)-d_t(t_{rp}(n))) - T_o(t_o-d_t(t_o)) - \frac{\Delta f_o}{f_a}[t_{rp}(n)-t_o]$$

$$- \left\{ T_c(t_{rp}(n)-d_t(t_{rp}(n))) - T_c(t_o-d_t(t_o)) + \frac{\Delta f_o}{f_a}[t_{rp}(n)-t_o] \right\}$$

$$+ Q(t_{rp}(n)) - Q(t_o). \qquad (268)$$

Using this expression and the defining equations for ε_c and ε_r, Equations (235) and (236), it can be shown that

$$\frac{A_r}{N_r} \sum_{n=1}^{N_r} [T_c(t_{rp}(n)) - T_r(t_{rp}(n))] = A_r[\varepsilon_r(t_o)+\varepsilon_c(t_o-d_t(t_o))+Q(t_o)]$$

$$- \frac{A_r}{N_r} \sum_{n=1}^{N_r} [\varepsilon_c(t_{rp}(n))+\varepsilon_c(t_{rp}(n)-d_t(t_{rp}(n))+Q(t_{rp}(n))]$$

$$- A_r \left[(t_o-t_{rp}(1)) - \frac{(N_r-1)}{2} T_f\right] \frac{2\Delta f_o}{f_a} \quad . \qquad (269)$$

Incorporating this result in the expression for $T_r(t_o+T_F)$, Equation (262), and solving for $\varepsilon_r(t_o+T_F)$ gives

$$\varepsilon_r(t_o+T_F) = (1-A_r)[\varepsilon_r(t_o)+\varepsilon_c(t_o-d_t(t_o))+Q(t_o)]$$

$$- \varepsilon_c(t_o+T_F-d_t(t_o+T_F)) - Q(t_o+T_F)$$

$$+ \frac{A_r}{N_r} \sum_{n=1}^{N_r} [\varepsilon_c(t_{rp}(n))+\varepsilon_c(t_{rp}(n)-d_t(t_{rp}(n)))+Q(t_{rp}(n))+t_{rn}(t_{rp}(n))]$$

$$+ \left\{ A_r\left[(t_o-t_{rp}(1)) - \frac{(N_r-1)}{2} T_f\right] + T_F \right\} \frac{2\Delta f_o}{f_a} \quad . \qquad (270)$$

From this expression it is evident that

$$\varepsilon_r(t_o+2T_F)=(1-A_r)[\varepsilon_r(t_o+T_F)+\varepsilon_c(t_o+T_F-d_t(t_o+T_F))+Q(t_o+T_F)]$$

$$- \varepsilon_c(t_o+2T_F-d_t(t_o+2T_F))-Q(t_o+2T_F)$$

$$+ \frac{A_r}{N_r} \sum_{n=1}^{N_r} [\varepsilon_c(t_{rp}(n)+T_F)+\varepsilon_c(t_{rp}(n)+T_F-d_t(t_{rp}(n)+T_F))$$

$$+ Q(t_{rp}(n)+T_F)+t_{rn}(t_{rp}(n)+T_F)]$$

$$+ \left\{A_r[(t_o+T_F-(t_{rp}(1)+T_F)) - \frac{(N_r-1)}{2} T_F]+T_F\right\} \frac{2\Delta f_o}{f_a} \quad . \qquad (271)$$

Substituting the expression for $\varepsilon_r(t_o+T_F)$, Equation (270), into Equation (271) gives

$$\varepsilon_r(t_o+2T_F) = (1-A_r)^2[\varepsilon_r(t_o)+\varepsilon_c(t_o-d_t(t_o))+Q(t_o)]$$

$$- \varepsilon_c(t_o+2T_F-d_t(t_o+2T_F)) - Q(t_o+2T_F)$$

$$+ \sum_{\ell=0}^{1} (1-A_r)^{\ell} \frac{A_r}{N_r} \sum_{n=1}^{N_r} [\varepsilon_c(t_{rp}(n)+(1-\ell)T_F)$$

$$+\varepsilon_c(t_{rp}(n)+(1-\ell)T_F-d_t(t_{rp}(n)+(1-\ell)T_F))$$

$$+Q(t_{rp}(n)+(1-\ell)T_F)+t_{rn}(t_{rp}(n)+(1-\ell)T_F)]$$

$$+\left\{A_r[(t_o-t_{rp}(1)) - \frac{(N_r-1)}{2} T_f]+T_F\right\} \frac{2\Delta f_o}{f_a} \sum_{\ell=0}^{1} (1-A_r)^{\ell} \quad .$$

(272)

Continuing in this manner it can be shown that

$$\varepsilon_r(t_o+mT_F) = (1-A_r)^m[\varepsilon_r(t_o)+\varepsilon_c(t_o-d_t(t_o))+Q(t_o)]$$

$$- \varepsilon_c(t_o+mT_F-d_t(t_o+mT_F))-Q(t_o+mT_F)$$

$$+ \sum_{\ell=0}^{m-1}(1-A_r)^{\ell}\frac{A_r}{N_r}\sum_{n=1}^{N_r}[\varepsilon_c(t_{rp}(n)+(m-1-\ell)T_F)$$

$$+ \varepsilon_c(t_{rp}(n)+m-1-\ell)T_F-d_t(t_{rp}(n)+(m-1-\ell)T_F))$$

$$+ Q(t_{rp}(n)+(m-1-\ell)T_F)+t_{rn}(t_{rp}(n)+(m-1-\ell)T_F)]$$

$$+ \left\{A_r[(t_o-t_{rp}(1))-\frac{(N_r-1)}{2}T_f]+T_F\right\}\frac{2\Delta f_o}{f_a}\sum_{\ell=0}^{m-1}(1-A_r)^{\ell}. \quad (273)$$

Clearly, $(1-A_r)^m$ must diminish to zero as m is increased to a large value if the transmit timing loop is to respond in an acceptable manner. Consequently, a necessary condition for a "stable" response is that A_r assume a value between zero and two:

$$0 < A_r < 2 \quad . \quad (274)$$

Assume that this condition is satisfied and that m equals a (any) number M for which

$$(1-A_r)^M <<< 1. \quad (275)$$

It follows that

AD-A062 992 OHIO STATE UNIV RESEARCH FOUNDATION COLUMBUS F/G 17/2
TDMA TIMING LOOPS FOR HIGH DATA RATE SYSTEMS.(U)
NOV 78 W G SWARNER, C W CHUANG, R J HUFF F30602-75-C-0061
UNCLASSIFIED OSURF-710300-1(ESL) RADC-TR-78-238 NL

2 OF 3
AD
A062992

$$\varepsilon_r(t_o+MT_F) \doteq \left\{(t_o-t_{rp}(1)) + \left[\frac{N_F}{A_r} - \frac{(N_r-1)}{2}\right]T_f\right\}\frac{2\Delta f_o}{f_a}$$

$$-\varepsilon_c(t_o+MT_F-d_t(t_o+MT_F))$$

$$+\sum_{\ell=0}^{M-1}(1-A_r)^{\ell}[S(\varepsilon_c,t_{rp},M-1-\ell) + S(\varepsilon_c,t_{rp}-d_t,M-1-\ell)$$

$$+ S(t_{rn},t_{rp},M-1-\ell)] - q(t_o,t_{rp},M) \qquad (276)$$

where

$$N_F \triangleq T_F/T_f = I_r \qquad (277)$$

$$S(x,t_{rp},k) \triangleq \frac{A_r}{N_r}\sum_{n=1}^{N_r} x(t_{rp}(n) + kT_F) \qquad (278)$$

$$S(x,t_{rp}-d_t,k) \triangleq \frac{A_r}{N_r}\sum_{n=1}^{N_r} x(t_{rp}(n)+kT_F-d_t(t_{rp}(n)+kT_F)) \qquad (279)$$

and

$$q(t_o,t_{rp},M) \triangleq Q(t_o+MT_F) - \sum_{\ell=0}^{M-1}(1-A_r)^{\ell}S(Q,t_{rp},M-1-\ell)\ . \qquad (280)$$

Equation (276) above is applicable to the stationary terminal (maneuvering satellite) case, and, by setting $q(t_o,t_{rp},M)$ equal to zero, is also applicable to the stationary satellite (maneuvering terminal) case.

B. Stationary-Satellite Maneuvering-Terminal Case

Assume that $q(t_o,t_{rp},M)$ equals zero and that the mean value of $\varepsilon_c(t)$, $E\{\varepsilon_c(t)\}$, is negligibly small for sufficiently large values of t. Then

$$\varepsilon_{rs}(t_o+MT_F) \triangleq E\left\{\varepsilon_r(t_o+MT_F)\right\} \doteq \left\{(t_o-t_{rp}(1))+\left[\frac{N_F}{A_r} - \frac{(N_r-1)}{2}\right]T_f\right\}\frac{2\Delta f_o}{f_a} \qquad (281)$$

and

$$\varepsilon_{rn}(t_o+MT_F) \triangleq \varepsilon_r(t_o+MT_F) - \varepsilon_{rs}(t_o+MT_F)$$

$$\doteq - \varepsilon_{cn}(t_o+MT_F-d_t(t_o+MT_F))$$

$$+ \sum_{\ell=0}^{M-1} (1-A_r)^{\ell}[S(\varepsilon_{cn},t_{rp},M-1-\ell) + S(\varepsilon_{cn},t_{rp},M-1-\ell)$$

$$+ S(t_{rn},t_{rp},M-1-\ell)] \tag{282}$$

where

$$\varepsilon_{cn}(t) \triangleq \varepsilon_c(t) - E\{\varepsilon_c(t)\} \quad . \tag{283}$$

It follows that

$$\sigma_{\varepsilon_{rn}}^2(t_o+MT_F) \triangleq E\left\{\varepsilon_{rn}^2(t_o+MT_F)\right\} = \sigma_{\varepsilon_{cn}}^2(t_o+MT_F-d_t) \quad .$$

$$+ \sum_{\ell_1=0}^{M-1} \sum_{\ell_2=0}^{M-1} (1-A_r)^{(\ell_1+\ell_2)} \Bigg\{ E\left\{S(\varepsilon_{cn},t_{rp},M-1-\ell_1)S(\varepsilon_{cn},t_{rp},M-1-\ell_2)\right\}$$

$$+ E\left\{S(\varepsilon_{cn},t_{rp}-d_t,M-1-\ell_1)S(\varepsilon_{cn},t_{rp}-d_t,M-1-\ell_2)\right\}$$

$$+ E\left\{S(t_{rn},t_{rp},M-1-\ell_1)S(t_{rn},t_{rp},M-1-\ell_2)\right\}$$

$$+ 2E\left\{S(\varepsilon_{cn},t_{rp},M-1-\ell_1)S(\varepsilon_{cn},t_{rp}-d_t,M-1-\ell_2)\right\}\Bigg\}$$

$$- 2 \sum_{\ell=0}^{M-1} (1-A_r)^{\ell} \Bigg\{ E\left\{\varepsilon_{cn}(t_o+MT_F-d_t)S(\varepsilon_{cn},t_{rp},M-1-\ell)\right\}$$

$$+ E\left\{\varepsilon_{cn}(t_o+MT_F-d_t)S(\varepsilon_{cn},t_{rp}-d_t,M-1-\ell)\right\}\Bigg\} \quad . \tag{284}$$

It follows from the defining equation for $S(x,t_{rp},k)$ (Equation (278)) that

$$E\left\{S(t_{rn},t_{rp},M-1-\ell_1)\ S(t_{rn},t_{rp},M-1-\ell_2)\right\} =$$

$$\left(\frac{A_r}{N_r}\right)^2 \sum_{n_1=1}^{N_r} \sum_{n_2=1}^{N_T} E\left\{t_{rn}(t_{rp}(n_1)+(M-1-\ell_1)T_F)t_{rn}(t_{rp}(n_2)+(M-1-\ell_2)T_F)\right\}$$

$$= \begin{cases} \frac{A_r^2}{N_r}\ \sigma^2_{t_{rn}} & \ell_2=\ell_1 \\ 0 & \ell_2\neq\ell_1 \end{cases} . \qquad (285)$$

Thus

$$\sum_{\ell_1=0}^{M-1} \sum_{\ell_2=0}^{M-1} (1-A_r)^{(\ell_1+\ell_2)} E\left\{S(t_{rn},t_{rp},M-1-\ell_1)S(t_{rn},t_{rp},M-1-\ell_2)\right\} =$$

$$\frac{A_r^2}{N_r}\ \sigma^2_{t_{rn}} \sum_{\ell=0}^{M-1} (1-A_r)^{2\ell} \doteq \frac{A_r}{(2-A_r)N_r}\ \sigma^2_{t_{rn}} . \qquad (286)$$

Neither $\varepsilon_{cn}(t)$ nor $\varepsilon_{rn}(t)$ are stationary in the strict sense; consequently, $\sigma^2_{\varepsilon_{rn}}(t_o+MT_F)$ depends on (t_o-d_t), $t_{rp}(1)$, and $t_{rp}(1)-d_t)$ in addition to other parameters. However, the expression for the variance of $\varepsilon_{rn}(t_o+MT_F)$ is reasonably tractable when

$$t_{rp}(1) = (N_1+\alpha_1)T_f \qquad (287)$$

$$d_t = N_dT_f \qquad (288)$$

and

$$t_o = [N_o+(N_1+\alpha_1)+N_r+N_d-N_F]T_f \qquad (289)$$

where

$$0 < \alpha_1 < 1 \tag{290}$$

N_1 and N_d represent constant integers, N_o is any integer for which

$$0 \leq N_o \leq N_F - 1 \tag{291}$$

and

$$0 < T_{D_r} < T_f. \tag{292}$$

Designate the variance of $\varepsilon_{rn}(t_o+MT_F)$ when these constraints apply by $\sigma^2_{\varepsilon_{rn}}(N_o,\alpha_1)$ and assume that the clock loop has been operating over an indefinitely-long interval of time so that

$$E\left\{\varepsilon_{cn}(t_1+K_1T_f)\varepsilon_{cn}(t_2+K_2T_f)\right\} = E\left\{\varepsilon_{cn}(t_1+(K_1+K)T_f)\varepsilon_{cn}(t_2+(K_2+K)T_f)\right\} \tag{293}$$

where t_1 and t_2 represent arbitrary instants in time and K_1, K_2, and K are arbitrary integers. Finally, define $R_{\varepsilon_{cn}}(K,\alpha)$ where K is an integer as

$$R_{\varepsilon_{cn}}(K,\alpha) \triangleq E\left\{\varepsilon_{cn}((K+\alpha)T_f)\varepsilon_{cn}(\alpha T_f)\right\} \quad . \tag{294}$$

Incorporating the notation and constraints presented in the preceding paragraph into the expression for $\sigma^2_{\varepsilon_{rn}}(t_o+MT_F)$ (Equation (284)) gives

$$\sigma_{\varepsilon_{rn}}^2(N_o,\alpha_1) \doteq \sigma_{\varepsilon_{cn}}^2(\alpha_1 T_f) + \frac{A_r}{(2-A_r)N_r}\,\sigma_{t_{rn}}^2$$

$$+ 2\left(\frac{A_r}{N_r}\right)^2 \sum_{\ell_1=0}^{M-1} \sum_{\ell_2=0}^{M-1} (1-A_r)^{(\ell_1+\ell_2)} \sum_{n_1=1}^{N_r} \sum_{n_2=1}^{N_r} [R_{\varepsilon_{cn}}((\ell_1-\ell_2)N_F-(n_1-n_2),\alpha_1)$$

$$+ R_{\varepsilon_{cn}}((\ell_1-\ell_2)N_F-N_d-(n_1-n_2),\alpha_1)]$$

$$- 2\,\frac{A_r}{N_r} \sum_{\ell=0}^{M-1} (1-A_r)^{\ell} \sum_{n=1}^{N_r} [R_{\varepsilon_{cn}}(\ell N_F+N_o+N_r-(n-1),\alpha_1)$$

$$+ R_{\varepsilon_{cn}}(\ell N_F+N_d+N_c+N_r-(n-1),\alpha_1)]. \quad (295)$$

Using this equation, it can be shown that

$$\sigma_{\varepsilon_{rn}}^2(N_o,\alpha_1) \doteq \sigma_{\varepsilon_{cn}}^2(\alpha_1 T_f) + \frac{A_r}{(2-A_r)N_r}\,\sigma_{t_{rn}}^2$$

$$+ \frac{2A_r}{(2-A_r)N_r^2} \left\{ \sum_{n=-(N_r-1)}^{N_r-1} (N_r-|n|)[R_{\varepsilon_{cn}}(|n|,\alpha_1)+R_{\varepsilon_{cn}}(|N_d+n|,\alpha_1)] \right.$$

$$+ \sum_{\ell=1}^{\infty} (1-A_r)^{\ell} \sum_{n=-(N_r-1)}^{N_r-1} (N_r-|n|)[2R_{\varepsilon_{cn}}(\ell N_F+n,\alpha_1)$$

$$\left. + R_{\varepsilon_{cn}}(|\ell N_F-N_d+n|,\alpha_1)+R_{\varepsilon_{cn}}(\ell N_F+N_d+n,\alpha_1)] \right\}$$

$$- \frac{2A_r}{N_r} \sum_{\ell=0}^{\infty} (1-A_r)^{\ell} \sum_{n=1}^{N_r} [R_{\varepsilon_{cn}}(\ell N_F+N_o+n,\alpha_1)+R_{\varepsilon_{cn}}(\ell N_F+N_d+N_o+n,\alpha_1)].$$

(296)

When

$$\alpha_1 << 1 \text{ and } \alpha_1 < \frac{1}{2N_c} \tag{297}$$

$\sigma^2_{\varepsilon_{rn}}(N_o,\alpha_1)$ is designated as $\hat{\sigma}^2_{\varepsilon_{rn}}(N_o)$ and is given by

$$\begin{aligned}\hat{\sigma}^2_{\varepsilon_{rn}}(N_o) \cong\ & \hat{P}_1 + \frac{A_r}{(2-A_r)N_r}\sigma^2_{t_{rn}} \\ & + \frac{2A_r}{(2-A_r)N_r^2}\left\{\sum_{n=-(N_r-1)}^{N_r-1}(N_r-|n|)[\hat{P}_1(|n|)+\hat{P}_1(|N_d+n|)]\right. \\ & \qquad + \sum_{\ell=1}^{\infty}(1-A_r)^{\ell}\sum_{n=-(N_r-1)}^{N_r-1}(N_r-|n|)[2\hat{P}_1(\ell N_F+n) \\ & \qquad\qquad \left. + \hat{P}_1(|\ell N_F-N_d+n|)+\hat{P}_1(\ell N_F+N_d+n)]\right\} \\ & - \frac{2A_r}{N_r}\sum_{\ell=0}^{\infty}(1-A_r)^{\ell}\sum_{n=1}^{N_r}[\hat{P}_1(\ell N_F+N_o+n)+\hat{P}_1(\ell N_F+N_d+N_o+n)].\end{aligned} \tag{298}$$

Similarly, when

$$(1-\alpha_1) << 1 \text{ and } (1-\alpha_1) < \frac{1}{2N_c} \tag{299}$$

$\sigma^2_{\varepsilon_{rn}}(N_o,\alpha_1)$ is designated as $\tilde{\sigma}^2_{\varepsilon_{rn}}(N_o)$ and is given by Equation (298) on replacing $\hat{P}_1(k)$ by $\tilde{P}_1(k)$.

C. Stationary-Terminal Maneuvering-Satellite Case

Now consider the case where the terminal is stationary and both normal and auxiliary cross-straps are implemented. Computational difficulties are minimized by presuming that

$$A_r=N_r=N_a=1 \tag{300}$$

$$t_{rp}(1)=(N_1+\alpha_1)T_f \tag{301}$$

$$d_t=\delta_t=N_dT_f \tag{302}$$

and

$$t_o=[N_o+(N_1+\alpha_1)+N_d+1-N_F]T_f \tag{303}$$

where

$$0<(1-\alpha_1) << 1 \tag{304}$$

$$(1-\alpha_1) < \frac{1}{2N_c} \tag{305}$$

N_1 and N_d are constant integers, N_o is any integer for which

$$0 \leq N_o \leq (N_F-1) \tag{306}$$

and

$$0 < T_{D_r} < T_f \ . \tag{307}$$

The sampler associated with the auxiliary cross strap is presumed to be actuated at instants

$$t_a(K) = KT_f+T_D+\alpha_aT_f \tag{308}$$

where K is any integer, T_D represents the clock loop processing delay, and α_aT_f is a positive lag introduced to avoid the simultaneous closure of two series-connected samplers. It is presumed that

$$T_D << T_f \tag{309}$$

and that

$$0 < \alpha_a << 1 \ . \tag{310}$$

When the constraints delineated in the preceding paragraph apply, $q(t_o,t_{rp},M)$ (Equation (280)) is designated as $\tilde{q}_1(N_o,N_1,M)$ and is given by

$$\tilde{q}_1(N_o,N_1,M) = Q[(N_o+N_d+1+N_1+\alpha_1+(M-1)N_F)T_f]-Q[(N_1+\alpha_1+(M-1)N_F)T_f]. \tag{311}$$

Using the defining equation for Q(t) (Equation (267)), it can be shown that

$$\begin{aligned} Q[(N_o+N_d+1+N_1+\alpha_1+(M-1)N_F)T_f] &\doteq Q[(N_1+\alpha_1+(M-1)N_F)T_f] \\ &+ T_o[(N_o+1+N_d+N_1+1+(M-1)N_F)T_f]-T_o[(N_1+1+(M-1)N_F)T_f] \\ &- \left\{T_o[(N_o+1+N_1+1+(M-1)N_F)T_f]-T_o[(N_1+1-N_d+(M-1)N_F)T_f]\right\} \\ &- \sum_{k=1}^{N_o+1+N_d} A_a N_d T_f^{2\cdot\cdot} T_c[t_a(N_1-N_d+k+(M-1)N_F)] \end{aligned} \tag{312}$$

since

$$T_o[(K+\alpha_1)T_f] \doteq T_o[(K+1)T_f] \tag{313}$$

when

$$0 < (1-\alpha_1) << 1 \quad . \tag{314}$$

Using the foregoing expressions, it can be shown that

$$T_o[(N_o+1+N_d+N_1+1+(M-1)N_F)T_f] = T_o[(N_o+1+N_1+1+(M-1)N_F)T_f]$$

$$+ N_d T_f \dot{T}_o[(N_o+1+N_1+1+(M-1)N_F)T_f]$$

$$+ \frac{T_f^2}{2} S_\rho(N_d) \ddot{T}_o[(N_o+1+N_1+1+(M-1)N_F)T_f]$$

$$+ \frac{T_f^2}{2} \sum_{k=1}^{N_d} S_\rho(N_d-k) u[N_o+1+N_1+1+k-1+(M-1)N_F] \qquad (315)$$

where

$$S_\rho(K) \triangleq \begin{cases} \dfrac{2K(1-\rho)-(1+\rho)(1-\rho^K)}{(1-\rho)^2} , & K \geq 0 \\ 0 , & K = -1 . \end{cases} \qquad (216)$$

The latter definition makes the analysis applicable when N_d equals zero. Similarly,

$$T_o[(N_1+1+(M-1)N_F)T_f] = T_o[(N_1+1-N_d+(M-1)N_F)T_f]$$

$$+ N_d T_f \dot{T}_o[(N_1+1-N_d+(M-1)N_F)T_f]$$

$$+ \frac{T_f^2}{2} S_\rho(N_d) \ddot{T}_o[(N_1+1-N_d+(M-1)N_F)T_f]$$

$$+ \frac{T_f^2}{2} \sum_{k=1}^{N_d} S_\rho(N_d-k) u[N_1+1-N_d+k-1+(M-1)N_F] . \qquad (317)$$

Combining the above expressions in an appropriate manner gives

$$\tilde{q}_1(N_o,N_1,M) \doteq N_d T_f \left\{ \dot{T}_o[(N_o+1+N_1+1+(M-1)N_F)T_f] - \dot{T}_o[(N_1+1-N_d+(m-1)N_F)T_f] \right\}$$

$$+ \frac{T_f^2}{2} S_\rho(N_d) \left\{ \ddot{T}_o[(N_o+1+N_1+1+(M-1)N_F)T_f] - \ddot{T}_o[(N_1+1-N_d+(M-1)N_F)T_f] \right\}$$

$$+ \frac{T_f^2}{2} \sum_{k=1}^{N_d} S_\rho(N_d-k) \left\{ u[N_o+1+N_1+1+k-1+(M-1)N_F] \right.$$

$$\left. - u[N_1+1-N_d+k-1+(M-1)N_F] \right\}$$

$$- A_a N_d T_f^2 \sum_{k=1}^{N_o+1+N_d} \left\{ \ddot{T}_o[(N_1-N_d+k+(M-1)N_F)T_f] \right.$$

$$\left. - \ddot{T}_\varepsilon[t_a(N_1-N_d+k+(M-1)N_F)] \right\} \qquad (318)$$

whenever

$$\ddot{T}_c[t_a(K)] \doteq \ddot{T}_o(KT_f) - \ddot{T}_\varepsilon[t_a(K)] \quad . \qquad (319)$$

Now,

$$\dot{T}_o[(N_o+1+N_1+1+(M-1)N_F)T_f] = \dot{T}_o[(N_1+1-N_d+(M-1)N_F)T_f]$$

$$+ T_f \left\{ \left(\frac{1-\rho^{(N_o+1+N_d)}}{1-\rho} \right) \ddot{T}_o[(N_1+1-N_d+(M-1)N_F)T_f] \right.$$

$$\left. + \sum_{k=1}^{N_o+1+N_d} \left(\frac{1-\rho^{(N_o+1+N_d-k)}}{1-\rho} \right) u[N_1+1-N_d+k-1+(M-1)N_F] \right\} \qquad (320)$$

and

$$\ddot{T}_o[(N_o+1+N_1+1+(M-1)N_F)T_f] = \rho^{(N_o+1+N_d)}\,\ddot{T}_o[(N_1+1-N_d+(M-1)N_F)T_f]$$

$$+\sum_{k=1}^{N_o+1+N_d}\rho^{(N_o+1+N_d-k)}\,u[N_1+1-N_d+k-1+(M-1)N_F]\quad . \tag{321}$$

Since

$$\dot{T}_o[(n+1)T_f] = \dot{T}_o(nT_f)+T_f\cdot\ddot{T}_o(nT_f) \tag{322}$$

it follows that

$$\dot{T}_o[(n+\ell)T_f] = \dot{T}_o(nT_f) + T_f\sum_{k_1=0}^{\ell-1}\ddot{T}_o[(n+k_1)T_f]\quad ,\quad \ell \geq 1. \tag{323}$$

It was previously shown that

$$\dot{T}_o[(n+\ell)T_f] = \dot{T}_o(nT_f)+T_f\left\{\left(\frac{1-\rho^{\ell}}{1-\rho}\right)\ddot{T}_o(nT_f) + \sum_{k=1}^{\ell}\left(\frac{1-\rho^{(\ell-k)}}{1-\rho}\right)u(n+k-1)\right\},$$

$$\ell \geq 1\quad . \tag{324}$$

Thus

$$\sum_{k_1=0}^{\ell-1}\ddot{T}_o[(n+k_1)T_f] = \left(\frac{1-\rho^{\ell}}{1-\rho}\right)\ddot{T}_o(nT_f) + \sum_{k=1}^{\ell}\left(\frac{1-\rho^{(\ell-k)}}{1-\rho}\right)u(n+k-1)\ ,$$

$$\ell \geq 1\quad . \tag{325}$$

Combining the last few equations gives

$$\tilde{q}_1(N_o,N_1,M) \doteq N_d T_f^2 \left\{ \left(\frac{1-\rho^{(N_o+1+N_d)}}{1-\rho} \right) \ddot{T}_o[(N_1+1-N_d+(M-1)N_F)T_f] \right.$$

$$\left. + \sum_{k=1}^{N_o+1+N_d} \left(\frac{1-\rho^{(N_o+1+N_d-k)}}{1-\rho} \right) u[N_1+1-N_d+k-1+(M-1)N_F] \right\}$$

$$+ \frac{T_f^2}{2} S_\rho(N_d) \left\{ (\rho^{(N_o+1+N_d)}-1) \ddot{T}_o[(N_1+1-N_d+(M-1)N_F)T_f] \right.$$

$$\left. + \sum_{k=1}^{N_o+1+N_d} \rho^{(N_o+1+N_d-k)} u[N_1+1-N_d+k-1+(M-1)N_F] \right\}$$

$$+ \frac{T_f^2}{2} \sum_{k=1}^{N_d} S_\rho(N_d-k) \left\{ u[N_o+1+N_1+1+k-1+(M-1)N_F] \right.$$

$$\left. - u[N_1+1-N_d+k-1+(M-1)N_F] \right\}$$

$$- A_a N_d T_f^2 \left\{ \left(\frac{1-\rho^{(N_o+1+N_d)}}{1-\rho} \right) \ddot{T}_o[(N_1+1-N_d+(M-1)N_F)T_f] \right.$$

$$\left. + \sum_{k=1}^{N_o+1+N_d} \left(\frac{1-\rho^{(N_o+1+N_d-k)}}{1-\rho} \right) u[N_1+1-N_d+(M-1)N_F] \right\}$$

$$+ A_a N_d T_f^2 \sum_{k=1}^{N_o+1+N_d} \ddot{T}_\varepsilon[t_a(N_1-N_d+k+(M-1)N_F)] \quad . \qquad (326)$$

Equivalently,

$$\tilde{q}_1(N_o,N_1,M) \doteq T_f^2\left[\left(\frac{1+\rho}{2}\right)\left(\frac{1-\rho^{N_d}}{1-\rho}\right) - A_a N_d\right]$$
$$\cdot\left\{\left(\frac{1-\rho^{(N_o+1+N_d)}}{1-\rho}\right)\ddot{T}_o[(N_1+1-N_d+(M-1)N_F)T_f]\right.$$
$$\left. + \sum_{k=1}^{N_o+1+N_d}\left(\frac{1-\rho^{(N_o+1+N_d-k)}}{1-\rho}\right)u[N_1-N_d+k+(M-1)N_F]\right\}$$
$$+ \frac{T_f^2}{2}S_\rho(N_d)\sum_{k=1}^{N_o+1+N_d}u[N_1-N_d+k+(M-1)N_F]$$
$$+ \frac{T_f^2}{2}\sum_{k=1}^{N_d}S_\rho(N_d-k)\left\{u[N_o+1+N_1+k+(M-1)N_F]\right.$$
$$\left. - u[N_1-N_d+k+(M-1)N_F]\right\}$$
$$+ T_f^2 A_a N_d \sum_{k=1}^{N_o+1+N_d}\ddot{T}_\varepsilon[t_a(N_1-N_d+k+(m-1)N_F)] \quad . \qquad (327)$$

Now, constrain A_a to the value

$$A_a = \frac{1}{N_d}\left(\frac{1+\rho}{2}\right)\left(\frac{1-\rho^{N_d}}{1-\rho}\right) \qquad (328)$$

as further analysis for arbitrary values of A_a is extremely unwieldy. Designate $\tilde{q}_1(N_o,N_1,M)$ when A_a equals the particular value just specified by $\tilde{q}_{1p}(N_o,N_1,M)$. Then from Equation (327), it follows that

$$\tilde{q}_{1p}(N_o,N_1,M) \doteq \frac{T_f^2}{2}\left\{\sum_{k=1}^{N_d}[S_\rho(N_d)-S_\rho(N_d-k)]u[N_1-N_d+k+(M-1)N_F]\right.$$

$$+ S_\rho(N_d)\sum_{k=1+N_d}^{N_o+1+N_d} u[N_1-N_d+k+(M-1)N_F]$$

$$+ \sum_{k=1}^{N_d} S_\rho(N_d-k)u[N_o+1+N_1+k+(M-1)N_F]$$

$$\left.+ (1+\rho)\left(\frac{1-\rho^{N_d}}{1-\rho}\right)\sum_{k=1}^{N_o+1+N_d} \ddot{T}_\varepsilon[t_a(N_1-N_d+k+(M-1)N_F)]\right\} . \tag{329}$$

For the model under consideration,

$$E\{u(K)\} = 0 \tag{330}$$

and

$$E\{\ddot{T}_\varepsilon(KT_f)\} = 0 \quad . \tag{331}$$

As a result,

$$E\left\{\tilde{q}_{1p}(N_o,N_1,M)\right\} = 0 \quad . \tag{332}$$

Designate the variance of $\tilde{q}_{1p}(N_o,N_1,M)$ by $\sigma^2_{\tilde{q}_{1p}}(N_o)$. Using the expressions

$$E\left\{u(K_1)u(K_2)\right\} = \begin{cases}\sigma_u^2 & , \quad K_1 = K_2 \\ 0 & , \quad K_1 \neq K_2\end{cases} \tag{333}$$

and

$$E\left\{\ddot{T}_\varepsilon[t_a(K_1T_f)]\ u(K_2)\right\} = 0 \quad , \qquad K_2 > K_1 \tag{334}$$

and the foregoing equation for $\tilde{q}_{1p}(N_o,N_1,M)$, it can be shown that

$$\sigma^2_{\tilde{q}_{1p}}(N_o) \triangleq E\left\{\tilde{q}^2_{1p}(N_o,N_1,M)\right\}$$

$$\doteq \frac{T_f^4}{4}\left\{\left\{\sum_{k=1}^{N_d}[(S_\rho(N_d)-S_\rho(N_d-k))^2+S_\rho^2(N_d-k)]+(N_o+1)S_\rho^2(N_d)\right\}\sigma_u^2\right.$$

$$+ (1+\rho)^2\left(\frac{1-\rho^{N_d}}{1-\rho}\right)^2 \sum_{k_1=1}^{N_o+1+N_d}\sum_{k_2=1}^{N_o+1+N_d}\left\{E\,\ddot{T}_\varepsilon[t_a(N_1-N_d+k_1+(M-1)N_F)]\right.$$

$$\left.\cdot\,\ddot{T}_\varepsilon[t_a(N_1-N_d+k_2+(M-1)N_F)]\right\}$$

$$+ 2(1+\rho)\left(\frac{1-\rho^{N_d}}{1-\rho}\right)\left\{S_\rho(N_d)\sum_{k_1=1}^{N_o+1+N_d}\sum_{k_2=1}^{k_1}E\left\{\ddot{T}_\varepsilon[t_a(N_1-N_d+k_1+(M-1)N_F)]\right.\right.$$

$$\left.\left.\cdot\,u[N_1-N_d+k_2+(M-1)N_F]\right\}\right.$$

$$\left.-\sum_{k_1=1}^{N_o+1+N_d}\sum_{k_2=1}^{N_d}S_\rho(N_d-k_2)E\left\{\ddot{T}_\varepsilon[t_a(N_1-N_d+k_1+(M-1)N_F)]\right.\right.$$

$$\left.\left.\left.\cdot\,u[N_1-N_d+k_2+(M-1)N_F]\right\}\right\}\right\}. \qquad (335)$$

Equivalently,

$$\sigma^2_{\tilde{q}_{1p}}(N_o) \doteq \frac{T_f^4}{4}\left\{\left\{\left\{\left\{(N_o+1+N_d)S_\rho^2(N_d)-2\sum_{k=0}^{N_d-1}S_\rho(k)[S_\rho(N_d)-S_\rho(k)]\right\}\sigma_u^2\right.\right.\right.$$

$$+(1+\rho)^2\left(\frac{1-\rho^{N_d}}{1-\rho}\right)^2\left\{(N_o+1+N_d)R^{\cdot\cdot}_{T_\varepsilon}(0,\alpha_a+\frac{T_D}{T_f})\right.$$

$$\left.+2\sum_{\ell=1}^{N_o+N_d}(N_o+1+N_d-\ell)R^{\cdot\cdot}_{T_\varepsilon}(\ell,\alpha_a+\frac{T_D}{T_f})\right\}$$

$$+2(1+\rho)\left(\frac{1-\rho^{N_d}}{1-\rho}\right)\sum_{\ell=0}^{N_o+N_d}R^{\cdot\cdot}_{T_\varepsilon u}(\ell,\alpha_a+\frac{T_D}{T_f})$$

$$\left.\left.\left.\cdot[S_\rho(N_d)(N_o+1+N_d-\ell)-F_s(\ell)]\right\}\right\}\right\} \tag{336}$$

where

$$R^{\cdot\cdot}_{T_\varepsilon}(K,\alpha) \triangleq E\left\{\ddot{T}_\varepsilon[(K+K_1+\alpha)T_f]\,\ddot{T}_\varepsilon[(K_1+\alpha)T_f]\right\} \tag{337}$$

$$R^{\cdot\cdot}_{T_\varepsilon u}(K,\alpha) \triangleq E\left\{\ddot{T}_\varepsilon[(K+K_1+\alpha)T_f]\,u(K_1)\right\}\quad,\quad 0<\alpha<1 \tag{338}$$

K_1 and K_2 are arbitrary integers, and

$$F_s(\ell) \triangleq \begin{cases} \sum_{k_2=1}^{N_d} S_\rho(N_d-k_2) = \sum_{k=0}^{N_d-1} S_\rho(k) & ,\quad \ell \leq N_o+1 \\ \sum_{k_2=1}^{N_d-[\ell-(N_o+1)]} S_\rho(N_d-k_2) = \sum_{k=\ell-(N_o+1)}^{N_d-1} S_\rho(k) & ,\quad \ell \geq N_o+1. \end{cases} \tag{339}$$

The random component of the ranging loop timing error for the particular case under consideration is designated as $\tilde{\varepsilon}_{rn_{1p}}(t)$. From earlier expressions, it can be shown that

$$\begin{aligned}\tilde{\varepsilon}_{rn_{1p}}(t_o+MT_F) = &- \varepsilon_{cn}[(N_o+1+N_1+\alpha_1+(M-1)N_F)T_f] \\ &+ \varepsilon_{cn}[(N_1+\alpha_1+(M-1)N_F)T_f] \\ &+ \varepsilon_{cn}[(N_1+\alpha_1-N_d+(M-1)N_F)T_f] \\ &- \tilde{q}_{1p}(N_o,N_1,M) \end{aligned} \tag{340}$$

provided

$$0 < (1-\alpha_1) << 1. \tag{341}$$

It follows that

$$\sigma^2_{\tilde{\varepsilon}_{rn_{1p}}}(N_o) \doteq \sigma^2_{\tilde{\varepsilon}_{rn}}(N_o)\Big|_{A_r=N_r=1} + \sigma^2_{\tilde{q}_{1p}}(N_o) - 2R_{\tilde{q}_{1p}\tilde{\varepsilon}_{rn}}(N_o)_0 \tag{342}$$

where

$$\begin{aligned}R_{\tilde{q}_{1p}\tilde{\varepsilon}_{rn}}(N_o)_0 = - E\Big\{\tilde{q}_{1p}(N_o,N_1,M)\Big[&\varepsilon_{cn}[(N_o+1+N_1+\alpha_1+(M-1)N_F)T_f] \\ &- \varepsilon_{cn}[(N_1+\alpha_1+(M-1)N_F)T_f] \\ &- \varepsilon_{cn}[(N_1+\alpha_1-N_d+(M-1)N_F)T_f]\Big]\Big\}. \end{aligned} \tag{343}$$

Using the foregoing equation for $\tilde{q}_{1p}(N_o,N_1,M)$, Equation (329)), it can be shown that

$$-2R_{\tilde{q}_{1p}\tilde{\varepsilon}_{rn}}(N_o)_0 \doteq T_f^2 \Bigg\{ S_\rho(N_d) \sum_{k=1}^{N_o+1+N_d} E\Big\{\varepsilon_{cn}[(N_o+1+N_1+\alpha_1+(M-1)N_F)T_f] \cdot u[N_1-N_d+k+(M-1)N_F]\Big\}$$

$$- \sum_{k=1}^{N_d} S_\rho(N_d-k) E\Big\{\varepsilon_{cn}[(N_o+1+N_1+\alpha_1+(M-1)N_F)T_f] \cdot u[N_1-N_d+k+(M-1)N_F]\Big\}$$

$$- S_\rho(N_d) \sum_{k=1}^{N_d} E\Big\{\varepsilon_{cn}[(N_1+\alpha_1+(M-1)N_F)T_f] \cdot u[N_1-N_d+k+(M-1)N_F]\Big\}$$

$$+ \sum_{k=1}^{N_d} S_\rho(N_d-k) E\Big\{\varepsilon_{cn}[(N_1+\alpha_1+(M-1)N_F)T_f] \cdot u[N_1-N_d+k+(M-1)N_F]\Big\}$$

$$+(1+\rho)\left(\frac{1-\rho^{N_d}}{1-\rho}\right) \sum_{k=1}^{N_o+1+N_d} E\Big\{\ddot{T}_\varepsilon[t_a(N_1-N_d+k+(M-1)N_F)] \cdot \Big[\varepsilon_{cn}[(N_o+1+N_1+\alpha_1+(M-1)N_F)T_f] - \varepsilon_{cn}[(N_1+\alpha_1+(M-1)N_F)T_f] - \varepsilon_{cn}[(N_1+\alpha_1-N_d+(M-1)N_F)T_f]\Big]\Big\}\Bigg\} . \quad (344)$$

Equivalently,

$$-2R_{\tilde{q}_{1p}\tilde{\varepsilon}_{rn}}(N_o)_0 \doteq T_f^2\Bigg\{S_\rho(N_d)\sum_{\ell=N_d}^{N_o+N_d} R_{\tilde{\varepsilon}_{cn}u}(\ell) + \sum_{\ell=0}^{N_d-1} S_\rho(\ell)\, R_{\tilde{\varepsilon}_{cn}u}(\ell) - R_{\tilde{\varepsilon}_{cn}u}(\ell+N_o+1)\Big] + (1+\rho)\left(\frac{1-\rho^{N_d}}{1-\rho}\right)\Bigg[\sum_{\ell=N_d}^{N_o+N_d} R_{\tilde{\varepsilon}_{cn}\ddot{\hat{T}}_\varepsilon}(\ell) - 2\sum_{\ell=1}^{N_o+1} R_{\ddot{\hat{T}}_\varepsilon\tilde{\varepsilon}_{cn}}(\ell) - \sum_{\ell=N_o+2}^{N_o+1+N_d} R_{\ddot{\hat{T}}_\varepsilon\tilde{\varepsilon}_{cn}}(\ell)\Bigg]\Bigg\} \tag{345}$$

where

$$R_{\tilde{\varepsilon}_{cn}u}(K) \triangleq E\Big\{\varepsilon_{cn}[(K+K_1+\alpha_1)T_f]\; u[K_1]\Big\} \tag{346}$$

$$R_{\tilde{\varepsilon}_{cm}\ddot{\hat{T}}_\varepsilon}(K) \triangleq E\Big\{\varepsilon_{cn}[(K+K_1+\alpha_1)T_f]\;\ddot{T}_\varepsilon[(K_1+\alpha_2)T_f]\Big\} \tag{347}$$

$$R_{\ddot{\hat{T}}_\varepsilon\tilde{\varepsilon}_{cn}}(K) \triangleq E\Big\{\ddot{T}_\varepsilon[(K+K_1+\alpha_2)T_f]\;\varepsilon_{cn}[(K_1+\alpha_1)T_f]\Big\} \tag{348}$$

$$0 < (1-\alpha_1) << 1 \tag{349}$$

$$0 < \alpha_2 << 1 \tag{350}$$

and K and K_1 are arbitrary integers. Note that

$$R_{\tilde{\varepsilon}_{cn}\ddot{\hat{T}}_\varepsilon}(-K) = R_{\ddot{\hat{T}}_\varepsilon\tilde{\varepsilon}_{cn}}(K). \tag{351}$$

The equations developed in this section are applied in Section VI-C to calculate typical data applicable to up-link synchronization for a high data rate bit-synchronous TDMA satellite (relay) communications system.

SECTION VI
APPLICATIONS TO SYSTEM DESIGN

In this section the steady state solutions for the clock and ranging loop timing error variances derived in Sections IV and V are applied to determine system specifications and performance as a function of known, or chosen, system parameters. Since the form of the solutions obtained earlier is not particularly convenient for this use, different forms are derived, and design curves are given which permit optimum system design with minimum effort.

In Section VI-A only the clock loop timing required to receive properly timed signals on the down-link is considered, while in Section VI-B the ranging loop timing error limits adequate for transmission are considered. Because of the coupling between the clock and ranging loops, as discussed earlier, an adequate design for transmission timing normally results in more than adequate receive clock loop performance. Hence for terminals involving both transmission and reception the results of Section VI-B are applicable, while the results of Section VI-A yield considerably less critical specifications for receive only terminals.

A. Clock Loop Timing

A typical design problem would be to determine the system parameters required to establish communications at a given chip rate and specified maximum error rate with a terminal whose maneuver parameters are known or can be estimated. A method for system design utilizing the steady state results of Section IV-C for a receive-only terminal employing an augmented Kalman filter will now be illustrated by example.

Example 1

Given:

Chip Rate $(\frac{1}{\Delta})$ = 40 Mbit/s

Maximum Bit Error Probability = 10^{-4}

Maximum Terminal Acceleration (A) = 49 m/sec^2 (5g.)

Probability That Terminal will not Accelerate (P_o) = .5

Average Maneuver Duration ($1/\lambda$) = 5 sec.

Find:

Suitable System Parameters:

$T_f = KM\Delta$ = subframe time (i.e., time between system clock samples)

$M\Delta$ = clock pulse length

E/N_o = clock pulse energy to noise density ratio

P/N_o = received power to noise density ratio

The Kalman Gain Constants (Steady State):

K_T = range gain

$K_{\dot{T}}$ = velocity gain

$K_{\ddot{T}}$ = acceleration gain

Other Related Parameters:

σ_ξ = receiver (measurement) noise standard deviation

σ_a = maneuver noise standard deviation

ρ = correlation coefficient

$\hat{P}_1$ = filtered estimate (minimum) timing error variance

$\tilde{P}_1$ = predicted estimate (maximum) timing error variance

From a previous study [1] the maximum timing jitter resulting in no significant increase in error rate is approximately $.05\Delta$. Hence we choose the predicted estimate (worst case) error variance as

$$\tilde{P}_1 = (.05\Delta)^2 = 1.5625 \cdot 10^{-18} \ (\text{sec}^2). \tag{352}$$

From comparisons of typical values of the error variances $\hat{P}_1$ and $\tilde{P}_1$ vs. the measurement noise variance σ_ξ^2 in Section III, we choose as a reasonable value for σ_ξ

$$\sigma_\xi = .05\Delta = 1.25 \cdot 10^{-9} \text{ sec.} \tag{353}$$

Then:

$$\frac{\tilde{P}_1}{\sigma_\xi^2} = \frac{(.05\Delta)^2}{(.05\Delta)^2} = 1.0 \ . \tag{354}$$

Using the maneuver model of Figure 6 and Equation (80), with the probability of maximum acceleration, P_m, set equal to zero* yields the maneuver standard deviation

$$\sigma_a = \left[\frac{A_T^2}{3}(1 - P_o)\right]^{1/2} = \frac{A_T}{\sqrt{6}} = \frac{A}{c\sqrt{6}} = 6.67 \cdot 10^{-8} \text{ sec/sec}^2 \qquad (355)$$

where c is the velocity of light.

Now from the functional relationship relating $\tilde{P}_1/\sigma_\xi^2$ vs. $r\rho$ for various values of ρ, Figure 7, and the defining relations (from Section IV)

$$r_\rho = r\left(\frac{1-\rho}{1+\rho}\right)^{1/2} = \frac{4\sigma_\xi}{\sigma_a T_f^2}\left(\frac{1-\rho}{1+\rho}\right)^{1/2} \qquad (356)$$

and

$$\rho = 1 - \lambda T_f \quad \left(T_f \leq \frac{1}{\lambda}\right) \quad . \qquad (357)$$

The value of the subframe time T_f can be determined (by iteration) in the following manner; From the intersections of the curves of Figure 7 with the coordinate $\tilde{P}_1/\sigma_\xi^2 = 1.0$ (from Equation (354)) the values for columns (1) and (2) of Table 1 are obtained.

Table 1
System Parameters for the Solution of Example 1

(1) ρ	(2) r_ρ	(3) T_f (sec)	(4) r	(5) σ_a (sec/sec^2)
.99	0.94	.05	13.26	$1.51 \cdot 10^{-7}$
.9	6.8	.5	29.64	$6.75 \cdot 10^{-10}$
.5	14.5	2.5	25.11	$3.19 \cdot 10^{-11}$
0	16.2	5.0	16.2	$1.23 \cdot 10^{-11}$

*Since the relative acceleration between vehicle and satellite is dependent upon direction as well as magnitude, there is no reason to believe the maximum values are more probable than other values.

Corresponding values for column (3) and for columns (4) and (5) are then obtained via Equations (357) and (356), respectively. Then from Table 1 and the value $\sigma_a = 6.67 \cdot 10^{-8}$ sec/sec^2 obtained in Equation (355) we see that the solution must be somewhere in the range $.05 < T_f < .5$ and $.99 > \rho > .9$. Accurate interpolation directly from Figure 7, however, would be very difficult because of the few (4) applicable data points available and the non-linear spacing of the curves. To obtain additional accuracy it is noted that the data of columns (1) and (2) of Table 1 yield a smooth curve which can be readily interpolated if plotted in the form r_ρ vs. $(1-\rho)$ on a log-log plot as shown in Figure 31. Additional values for Table 1 are then computed for values of ρ and r_ρ obtained from this curve, converging on the required value of σ_a until the desired accuracy is obtained. The result is found to be

$$\rho = .9861$$
$$r_\rho = 1.29$$
$$T_f = .0695 \text{ sec}$$
$$r = 15.42$$
$$\sigma_a = 6.7 \cdot 10^{-8} \text{ sec/sec}^2 = 2.68\Delta \text{ (sec}^{-2}\text{)} \tag{358}$$

Then from Equation (77):

$$\frac{E}{N_o} = \frac{1.215^2}{8\left(\frac{\sigma_\xi}{\Delta}\right)} + \left[\left(\frac{1.215^2}{8\left(\frac{\sigma_\xi}{\Delta}\right)}\right)^2 + \frac{1.476C^2}{4\left(\frac{\sigma_\xi}{\Delta}\right)}\right]^{1/2} \tag{359}$$

$$\text{where} \quad C = \begin{cases} 2 \text{ for square law detection} \\ 1 \text{ for linear detection} \end{cases} \tag{360}$$

and substituting the values obtained above (with C=1)

$$\frac{E}{N_o} = 122.7 \sim 20.89 \text{ dB.} \tag{361}$$

If we now choose the number of slots per subframe

$$K = 32 \quad \text{(as in the present system)} \tag{362}$$

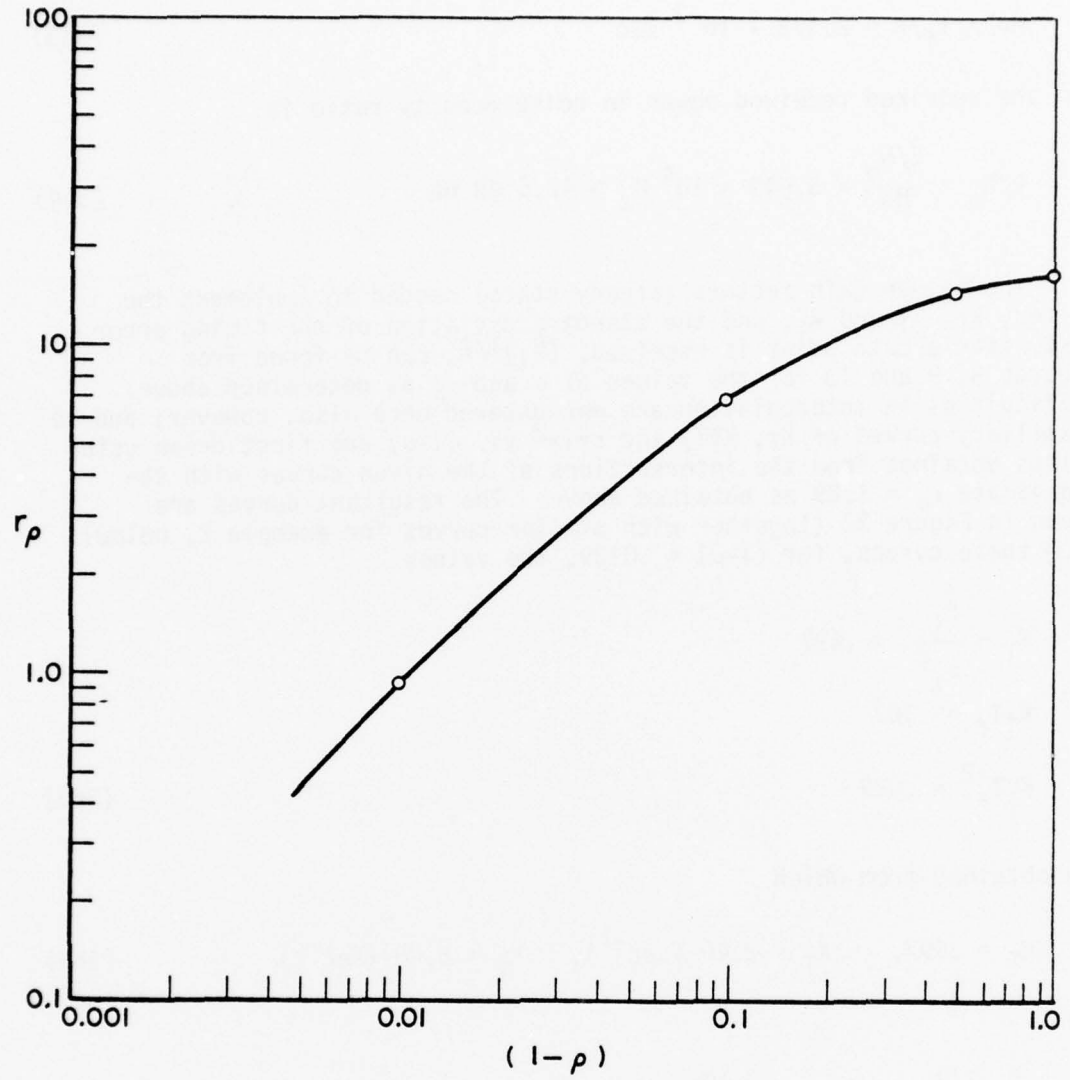

Figure 31. Filter parameters, r_ρ vs. $(1-\rho)$, for $\tilde{P}_1/\sigma_\xi^2 = 1.0$.

Then the timing pulse (slot) length becomes

$$M\Delta = T_f/K = 2.172 \cdot 10^{-3} \text{ sec} \tag{363}$$

and the required received power to noise density ratio is

$$P/N_o = \frac{E/N_o}{M\Delta} = 5.649 \cdot 10^4 \text{ Hz} \sim 47.5 \text{ dB Hz} . \tag{364}$$

The Kalman gain factors (steady state) needed to implement the filter, K_T, $K_{\dot{T}}$ and $K_{\ddot{T}}$, and the standard deviation of the timing error just after a data point is received, $(\hat{P}_1)^{1/2}$, can be found from Figures 8, 9 and 10 for the values of ρ and r_ρ as determined above. Difficulties in interpolation are encountered here also, however; and so auxilliary curves of K_T, $K_{\dot{T}}T_f$ and $K_{\ddot{T}}T_f^2$ vs. $(1-\rho)$ are first drawn using points obtained from the intersections of the given curves with the coordinate $r_\rho = 1.29$ as obtained above. The resultant curves are given in Figure 32 (together with similar curves for example 2, below). From these curves, for $(1-\rho) = .0139$, the values

$$K_T = \frac{\hat{P}_1}{\sigma_\xi^2} = .497$$

$$K_{\dot{T}}T_f = .167$$

$$K_{\ddot{T}}T_f^2 = .029 \tag{365}$$

are obtained from which

$$K_T = .497, \quad K_{\dot{T}} = 2.40 \ (\text{sec}^{-1}), \quad K_{\ddot{T}} = 6.00 \ (\text{sec}^{-2}) \tag{366}$$

and

$$(\hat{P}_1)^{1/2} = 8.812 \cdot 10^{-10} \text{ sec} = .035\Delta . \tag{367}$$

Example 2

This example is the same as Example 1 except the Bit Rate has been increased to 80 Mbps. Results are obtained as for Example 1 utilizing the auxilliary curves of Figures 31 and 32. Parameters for this example are compared to those of Example 1 in Table 2. It is

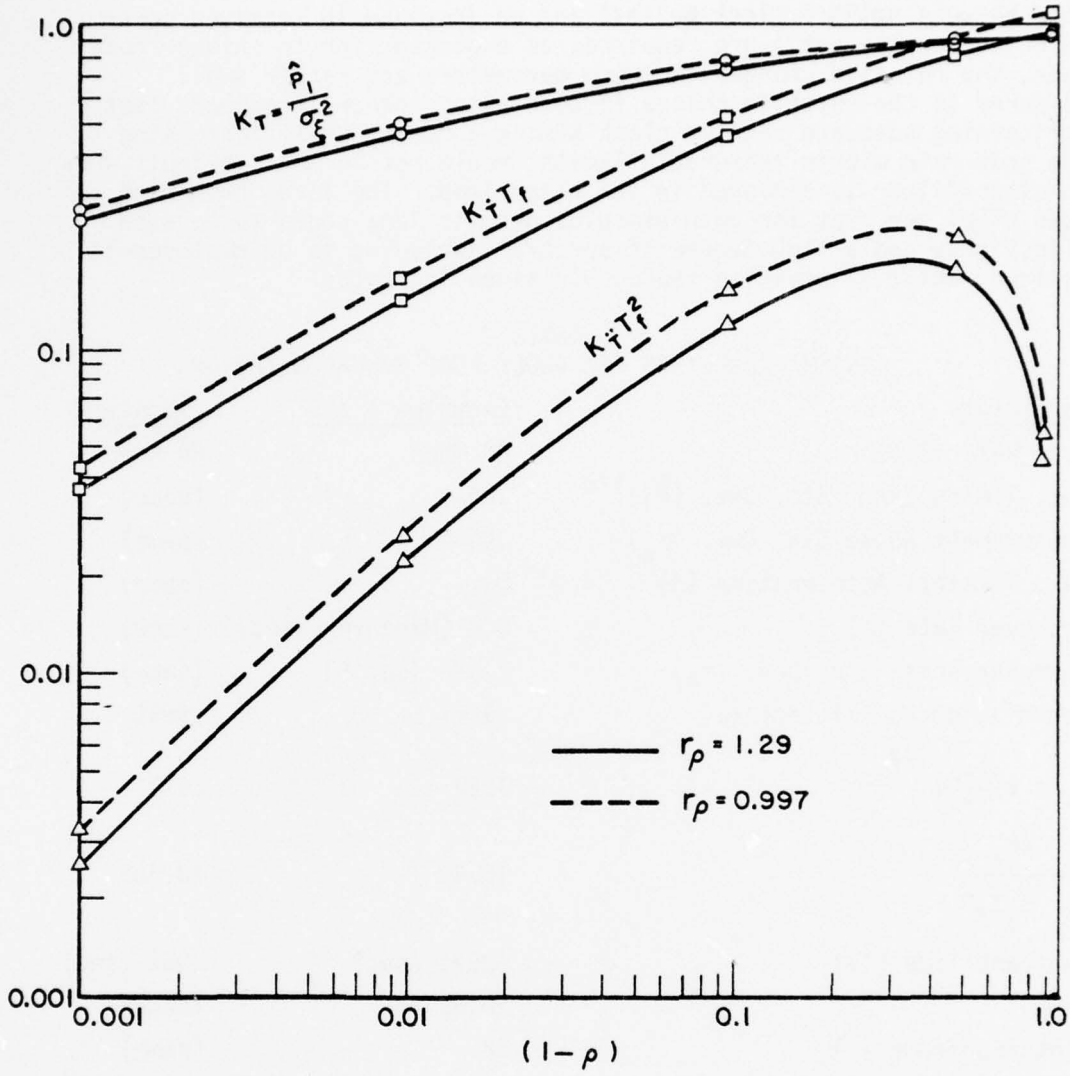

Figure 32. Kalman gain factors vs. (1-ρ) for examples 1 and 2.

interesting to note that while a decrease in subframe time (i.e., the time between network clock pulses) and an increase in received power to noise density ratio are required, as expected, for the higher code rate, the relative changes in these parameters are rather small compared to the relative change in code rate. Hence it appears that maintaining adequate receive clock timing accuracy while increasing the code rate within reasonable limits should not be too difficult when a Kalman filter is employed in the clock loop. The large number of code chips per slot for both examples permits long codes to be used effectively and a high degree of spectrum spreading to be employed if desired, while maintaining reasonable signaling rates.

Table 2
SYSTEM PARAMETERS FOR CLOCK LOOP SYNCHRONIZATION

Parameter	Examples 1 & 3	Example 2
Code Rate ($1/\Delta$)	40 Mbps	80 Mbps
Max. Timing Error Std. Dev. $(\tilde{P}_1)^{1/2}$	$.05\Delta$	(same)
Measurement Noise Stn. Dev. (σ_ξ)	$.05\Delta$	(same)
Max. Terminal Acceleration (A)	5g.	(same)
Maneuver Rate (λ)	0.2 (Maneuvers/sec)	(same)
Maneuver Noise Std. Dev. (σ_a)	2.68Δ (sec^{-2})	(same)
Correlation Coefficient (ρ)	.9861	.9896
$r_\rho = r(\frac{1-\rho}{1+\rho})^{1/2}$	1.29	.997
$r = \frac{4\sigma_\xi}{\sigma_a T_f^2}$	15.42	13.789
Subframe Time (T_f)	.0695 (sec)	.052 (sec)
E/N_0	20.89 dB	(same)
Slots/Subframe (K)	32	(same)
Timing Pulse Length ($M\Delta$)	$2.172 \cdot 10^{-3}$ (sec)	$1.625 \cdot 10^{-3}$ (sec)
Code Chips/Slot (M)	86,880	130,000
P/N_0	47.5 dB (Hz)	48.78 dB (Hz)
Min. Timing Error Std. Dev. $(\hat{P}_1)^{1/2}$	$.035\Delta$	$.0351\Delta$
K_T(range gain)	.497	.493
$K_{\dot{T}}$ (velocity gain)	2.40 (sec^{-1})	3.26 (sec^{-1})
$K_{\ddot{T}}$ (acceleration gain)	6.00 (sec^{-2})	10.17 (sec^{-2})

An iterative procedure is required in solving the above examples because the principal unknown, T_f, appears implicitly in both the parameter r_ρ (see Equation (356)), the abscissa of Figure 7, and in ρ(see Equation (357)) which identifies a particular curve of the family. This difficulty can be avoided by calculating and plotting the Kalman gains and error variances as a function of a new variable r_s which contains only known parameters

$$r_s \equiv \frac{\sigma_\xi \lambda^2}{\sigma_a} \quad . \tag{368}$$

Also it is convenient to specify each curve of the family by the parameter

$$\lambda T_f = 1-\rho \qquad \text{(from Equation (357))} \tag{369}$$

since this leads to more uniform curve spacing and facilitates interpolation as noted earlier.

Since the original solution (Equation (118)) was obtained as a function of the variables ρ and r_ρ, to obtain the desired curves an expression relating the new variable r_s to r_ρ and ρ is needed. This is obtained by combining Equations (356), (368) and (369) resulting in

$$r_s = \frac{(1-\rho)^2}{4} r = \frac{(1-\rho)^2}{4} \left(\frac{1+\rho}{1-\rho}\right)^{1/2} r_\rho \quad . \tag{370}$$

Curves of the Kalman gains and error variances vs. r_s are given in Figures 33 through 36. Example 3 below illustrates use of these curves in solving the system design problem of Example 1.

Example 3

From Example 1:

$$\sigma_\xi = .05\Delta = 1.25 \cdot 10^{-9} \text{ sec} \tag{371}$$

$$\sigma_a = 6.67 \cdot 10^{-8} \text{ sec/sec}^2 \tag{372}$$

$$\lambda = .2 \text{ maneuvers/sec} \tag{373}$$

and

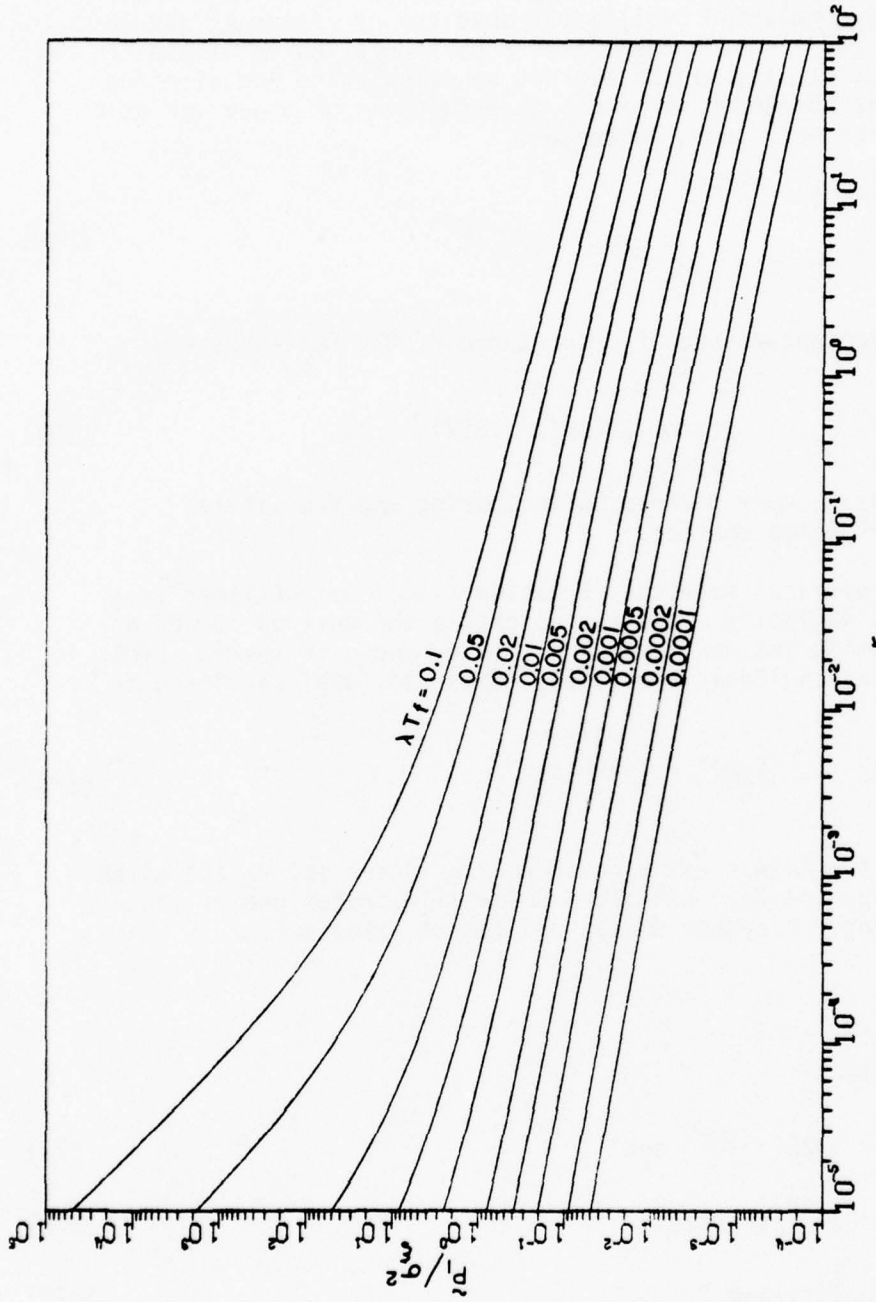

Figure 33. Predicted estimate error variance vs. r_s.

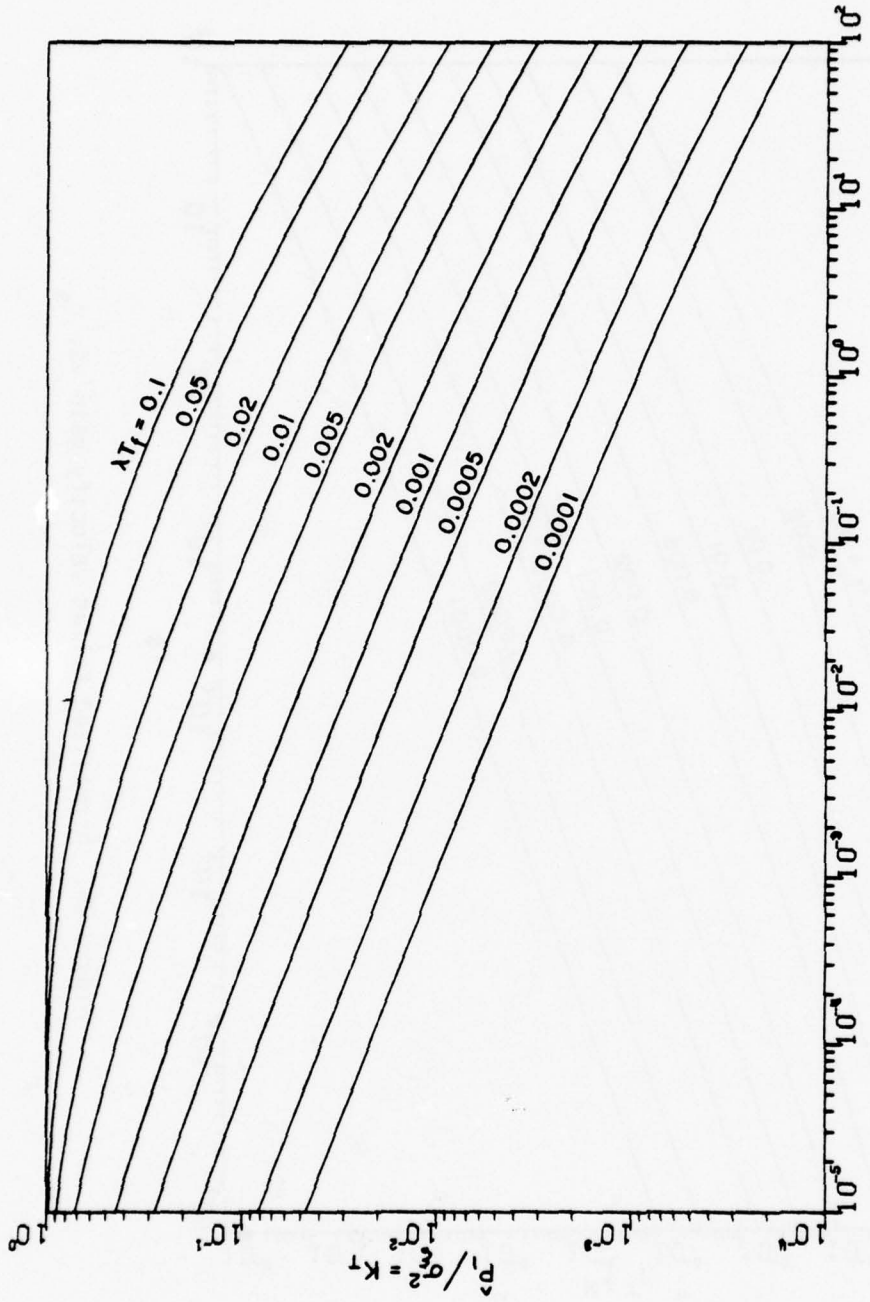

Figure 34. Kalman gain and filtered estimate error variance vs. r_s.

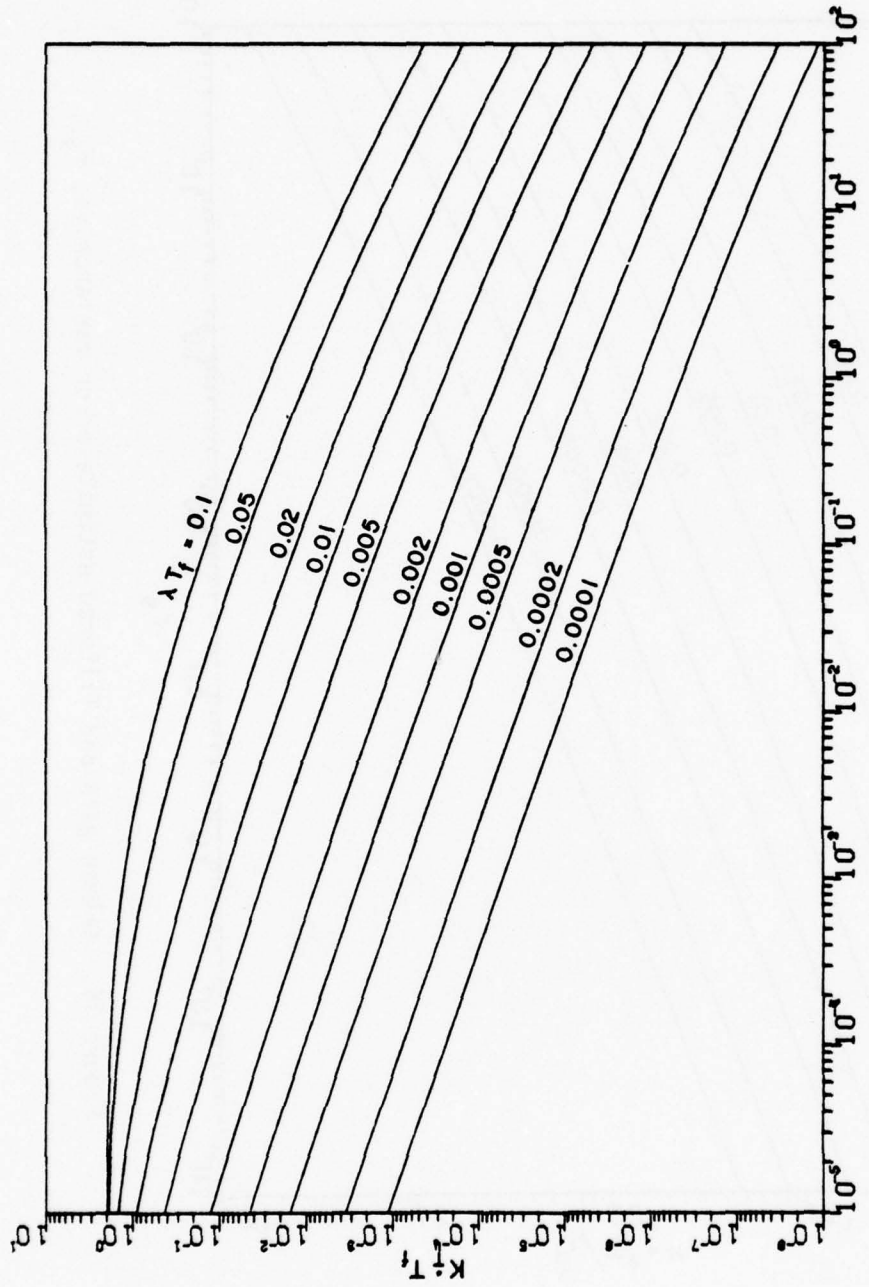

Figure 35. Normalized Kalman velocity gain vs. r_s.

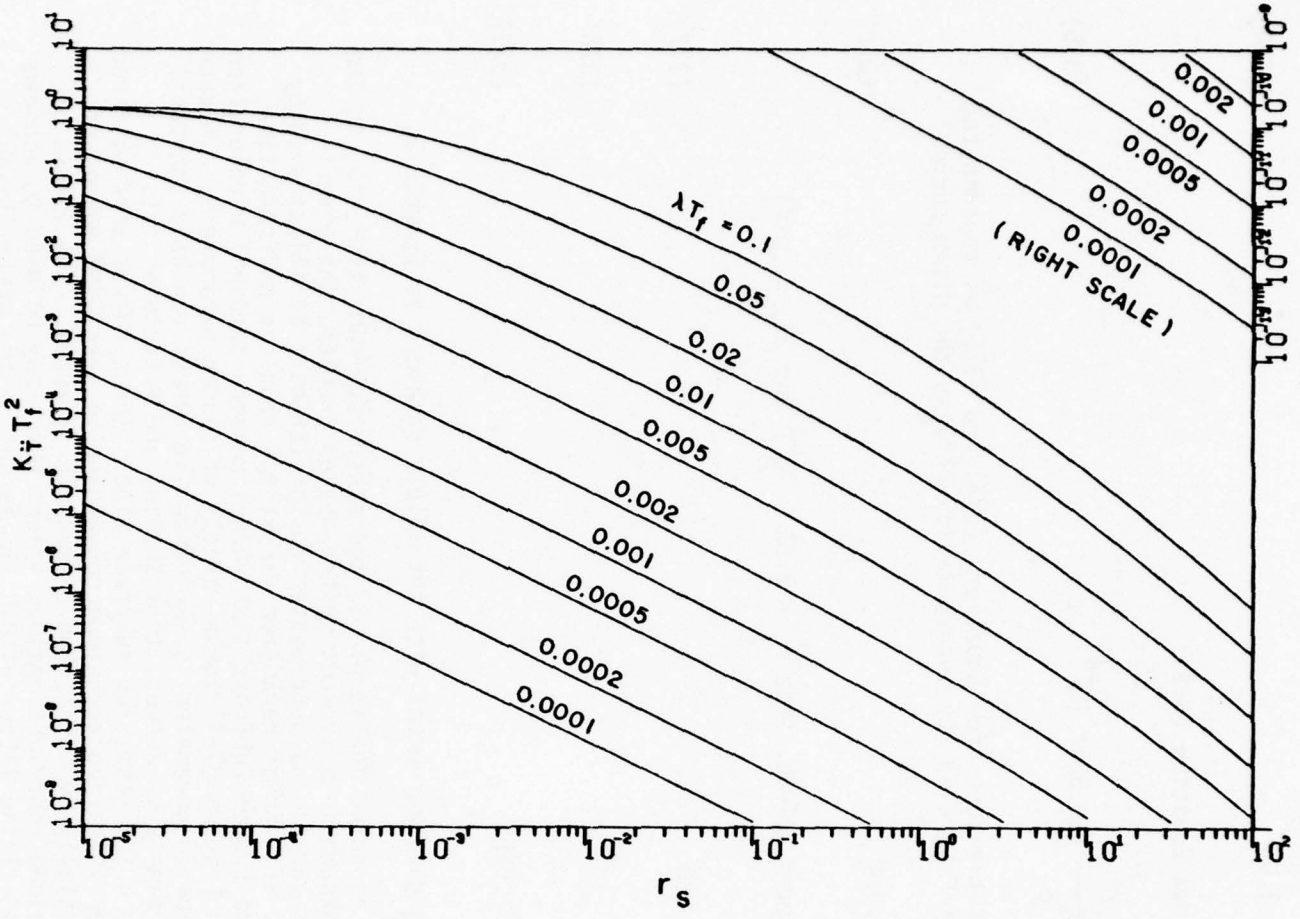

Figure 36. Normalized Kalman acceleration gain vs. r_s.

$$\frac{\hat{P}_1}{\sigma_\xi^2} = 1.00 \quad . \tag{374}$$

Then from Equation (368):

$$r_s = \frac{\sigma_\xi \lambda^2}{\sigma_a} = 7.50 \cdot 10^{-4} \quad . \tag{375}$$

Using the values from Equations (374) and (375) as coordinates, we find from Figure 33 (by interpolation between the given curves)

$$\lambda T_f \approx .014 \tag{376}$$

and from Figures 34-36, (for $r_s = 7.50 \cdot 10^{-4}$ and $\lambda T_f = .014$)

$$\frac{\hat{P}_1}{\sigma_\xi^2} \approx .50 \tag{377}$$

$$K_1^{\cdot} T_f \approx .17 \tag{378}$$

$$K_1^{\cdot\cdot} T_f^2 \approx .028 \tag{379}$$

which are in good agreement with the values obtained in Example 1.

Since, as noted in Example 1, the system subframe time, T_f, is the principal unknown in a typical system design problem, the effects of parameter variations upon system design can best be illustrated by studying the effects of parameter variations upon the subframe time. Curves of the system subframe time versus maximum terminal acceleration are given in Figures 37-41 for a variety of system parameters. In each figure a specific parameter is varied (while others are held constant) to obtain a family of curves, thus showing the effects of this parameter upon the resulting subframe time. These curves were obtained by a computer iteration technique converging to specified values of $\hat{P}_1/\sigma_{\xi 2}$ essentially by the method of Example 3, above. The values of T_f thus obtained represent maximum values which may be used to achieve the specified timing jitter within limits set by the other (fixed) parameters.

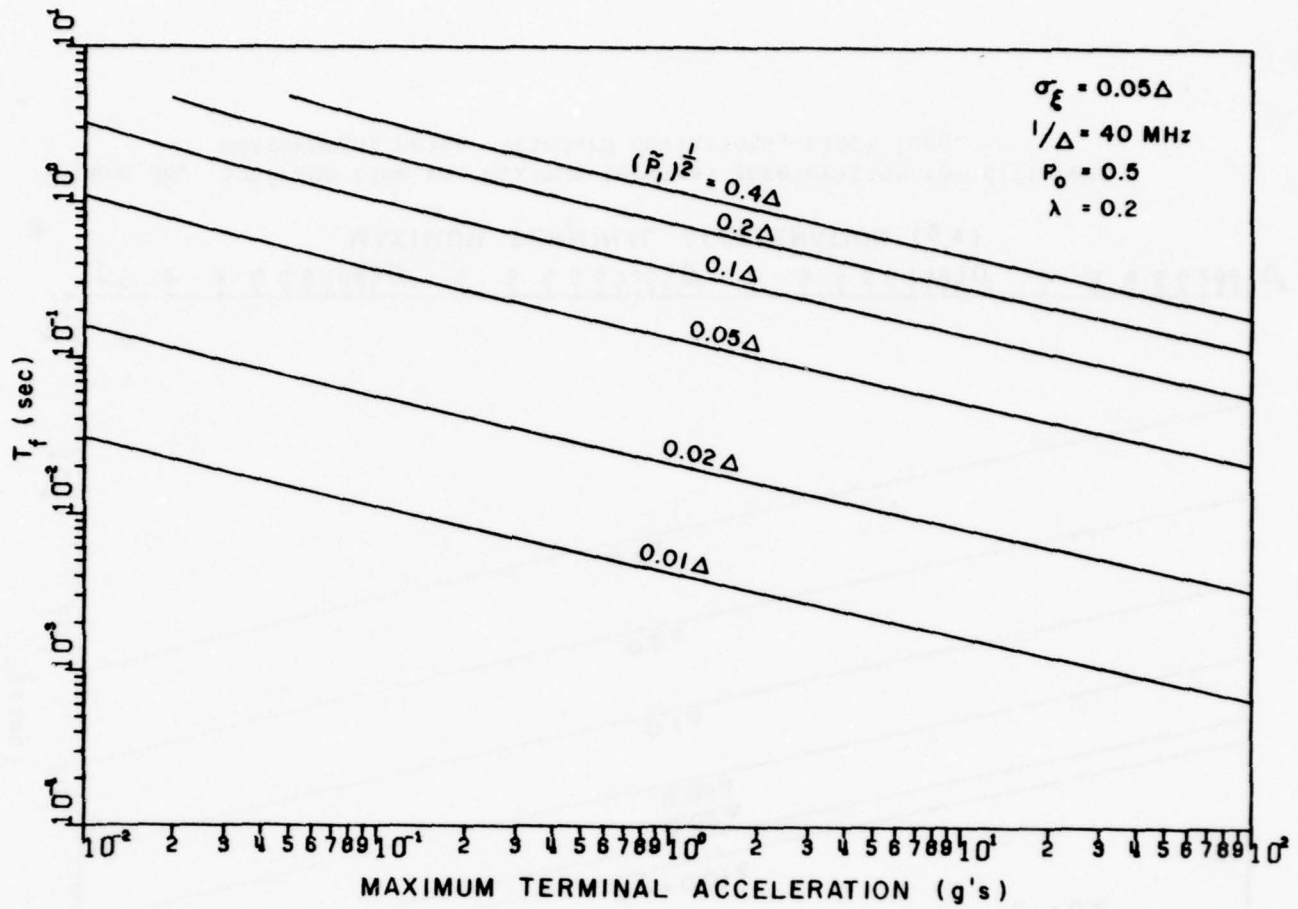

Figure 37. Subframe time vs. maximum terminal acceleration for different values of clock loop timing jitter.

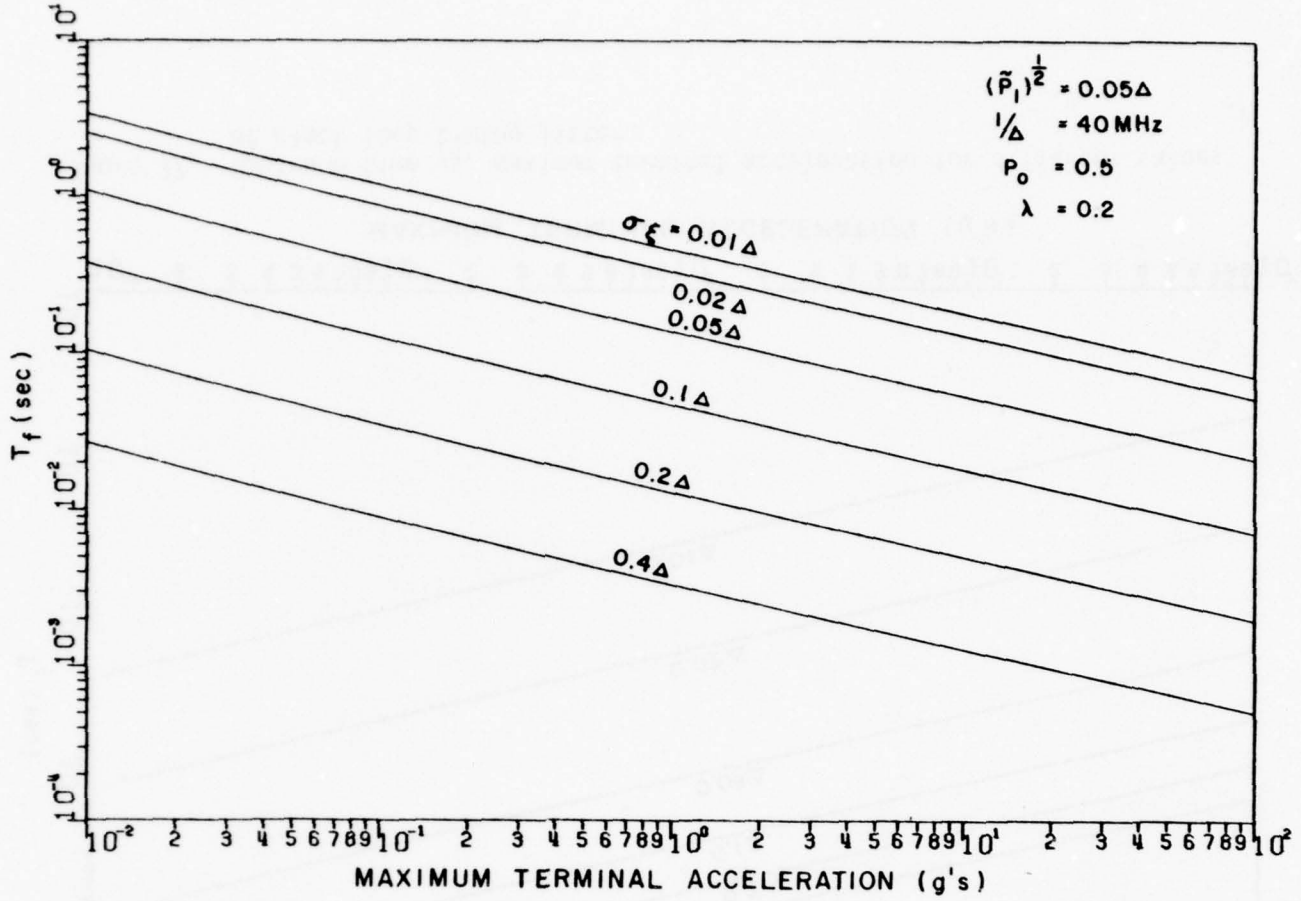

Figure 38. Subframe time vs. maximum terminal acceleration for different measurement noise standard deviations, clock loop.

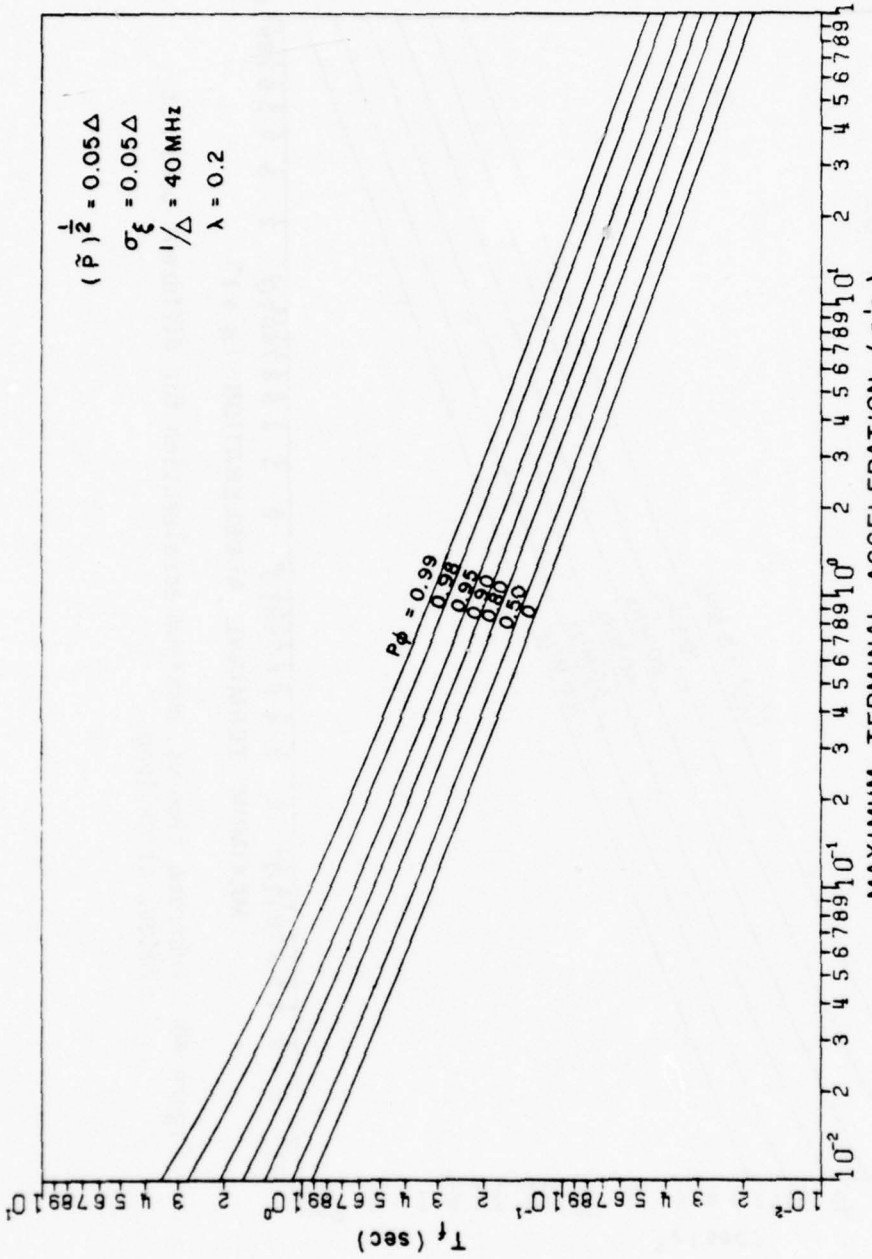

Figure 39. Subframe time vs. maximum terminal acceleration for different probabilities of zero acceleration, clock loop.

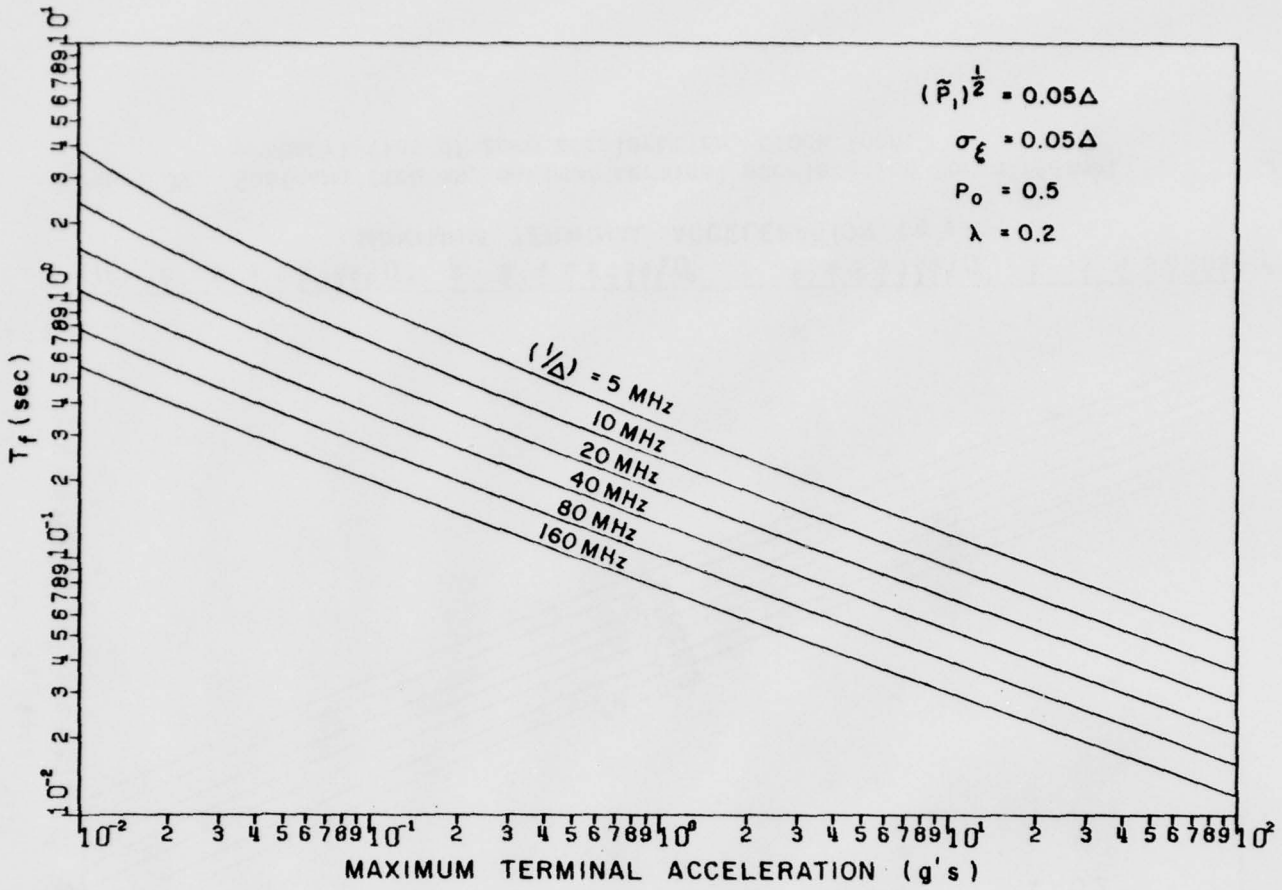

Figure 40. Subframe time vs. maximum acceleration for different code bit rates, clock loop.

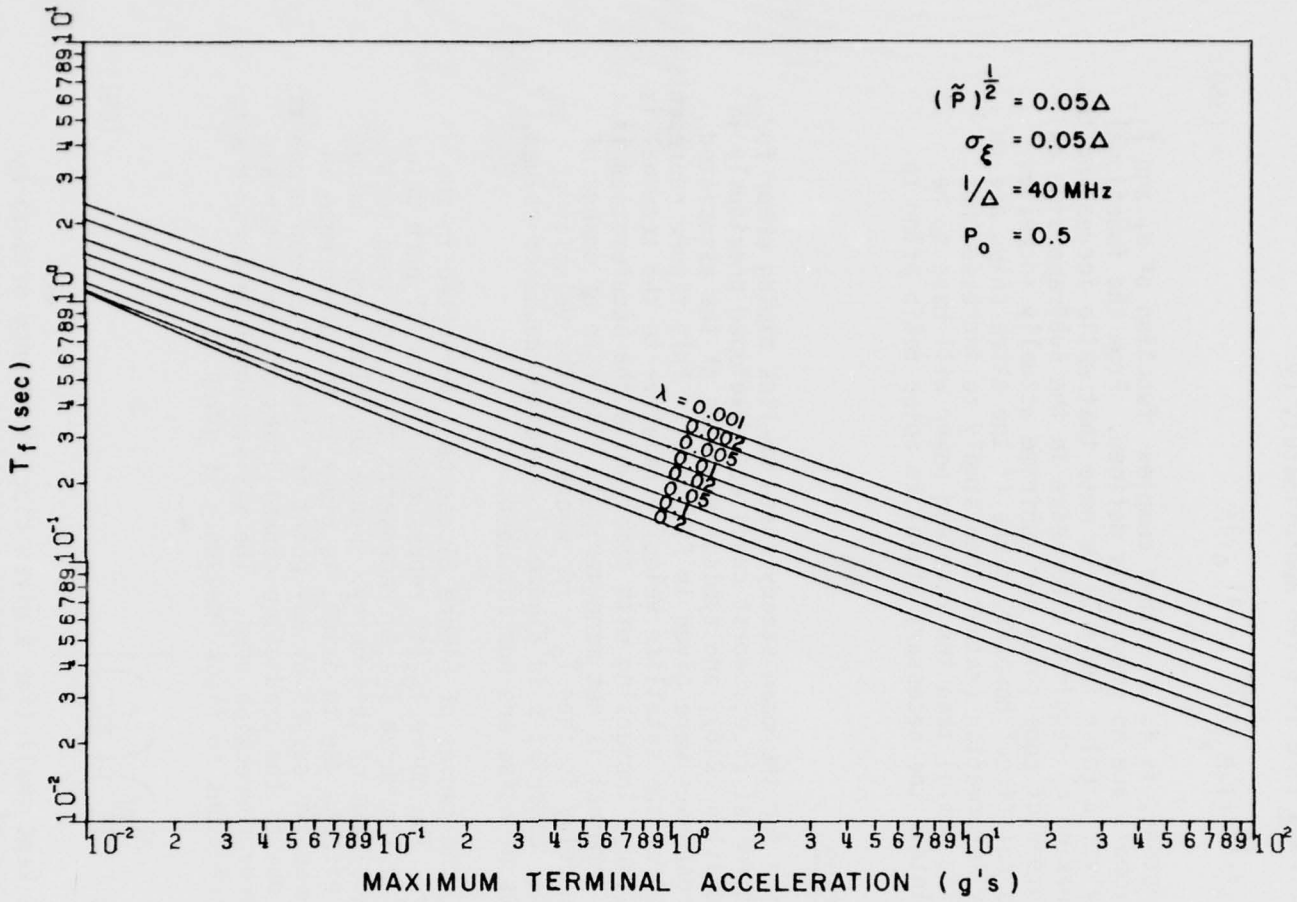

Figure 41. Subframe time vs. maximum acceleration for different terminal maneuver rates, clock loop.

From the data of Figures 37-41, in the range of parameters considered, the subframe time is given approximately by

$$T_f \approx k\, f_1\, \lambda^{-.19}\, (1-P_o)^{-.21}\, A^{-.41}\, \Delta^{.42} \tag{380}$$

where k is a constant, f_1 is a rather complex function of σ_ξ and $\tilde{P}_1$, and the other symbols are as previously defined. From the functional dependence of T_f vs. Δ (also Table 2) we note that while increasing the code rate (decreasing Δ) requires a decrease in the subframe time as expected, the number of code chips per subframe actually increases. This increase is not "free" however, since if the extra chips are to be used to carry information (rather than simply to increase the spectrum spreading ratio) then the received power will have to be increased to maintain the necessary signal to noise ratio prior to detection.

B. Up-Link Timing

An expression for the mean steady state up-link timing error for the stationary terminal (i.e., worst case) was developed previously in Section IV-F, Equation (216), and typical examples of the associated delay function responses were given in Figure 21. This figure represents conditions for which the satellite velocity relative to the terminal is a constant, $\dot{r}$, (range increasing with time) while the acceleration is zero (i.e., the terminal is not maneuvering). The rate of change of propagation path delay is then $\dot{\tau}_o = \dot{r}/c$ where c is the velocity of propagation. The subscript s in Figure 21 indicates expected values, i.e., the effects of noise are not included.

Physically, the curves of Figure 21 can be interpreted in the following manner. The curve $\tau_{os}(t)$ represents the actual path delay versus time, while the curve $\tau_{cs}(t)$ represents the clock loop (with Kalman filter) estimate of this delay. Hence the clock loop timing error, less the effects due to noise, is given by the difference in delay between these two curves at any point in time. The mean error is seen to be zero due to the prediction capabilities of the filter and the method of error correction used. The maximum absolute error due to the discrete corrections in clock frequency is given by

$$\varepsilon_{cs} = \left| \left(\dot{\tau}_{os} - \frac{\Delta T_{cf}}{T_f} \right) \left(\frac{T_f}{2N_c} \right) \right| \tag{381}$$

and hence can be kept small (for a given clock frequency offset) by choosing the number of clock frequency corrections per sampling interval, N_c, sufficiently large.

By analogy to the above we would like to consider the curve $T_{rs}(t)$ of Figure 21 as the ranging loop estimate of the propagation delay but, unfortunately, this is not the case since an actual delay estimate is not derived in the current ranging loop implementation. The curve $T_{rs}(t)$, which represents the timing function (sampling due to discrete ranging pulses neglected) at the point $T_r(t)$ in Figure 19, is simply related to such a delay estimate however, and will serve as well. By considering the model of Figure 19 relative to the physical situation, it can be seen that a ranging loop estimate of the propagation time delay could be obtained as

$$T_{pd}(t) = T_{os}(t) - (T_{rs}(t) - T_{os}(t)) = 2\,T_{os}(t) - T_{rs}(t) \qquad (382)$$

i.e., each point on the curve $T_{pd}(t)$ is the vertical reflection of the corresponding point on $T_{rs}(t)$ (same value of t for both points) about the curve $T_{os}(t)$. Hence the ranging loop timing error is (except for a sign reversal) given by the difference in time delay for the curves $T_{rs}(t)$ and $T_{os}(t)$ at any time t, analogous to that of the clock loop.

As indicated in Figure 21, measurements made of the ranging loop timing error (relative to the clock loop estimate $T_{cs}(t)$ since the actual value $T_{os}(t)$ is not available) at C and D are averaged and a correction made at D which would, in the absence of propagation delay, superimpose the curves $T_{rs}(t)$ and $T_{cs}(t)$ at that point (within limits set by the average value relative to the value at D). However, because of the round trip propagation delay, τ, this correction is not seen in the curve $T_{rs}(t)$ until τ seconds later, at which time, due to clock oscillator offsets, the correction will not, in general, be the required amount to superimpose the delay functions. Thus the mean ranging loop timing error is, in general, non-zero because of (1) the effects of discrete clock loop corrections and corresponding open loop corrections to the ranging loop upon ranging loop error measurements (i.e., the small steps in $T_{cs}(t)$ and $T_{rs}(t)$ of Figure 21) and (2) the effects of propagation delay and clock oscillator offsets upon the subsequent closed loop error corrections (the large saw tooth waveform in $T_{rs}(t)$).

Note that the open loop corrections to the ranging loop are delayed in the response $T_{rs}(t)$ relative to the clock loop by τ seconds, as is the closed loop correction. Thus the alignment of the offsets in $T_{rs}(t)$ relative to those of $T_{cs}(t)$ is τ dependent and could take on any value as the terminal-satellite range is varied. If we assume the error measurements are made near the times nT_f (n an integer) in Figure 21 so that the error between $T_{cs}(t)$ and $T_{os}(t)$ may be neglected (in the present system error measurements are made for $(n + 1/16)T_f < t < (n + 1/4)T_f$, depending upon the link range slots assigned to that particular terminal), then the maximum error due to the

discrete open loop corrections (for a non-maneuvering terminal) would be given by Equation (381). For non-optimum sampling times the maximum error could be twice this amount.

From Figure 21, the maximum ranging loop timing error due to the effects of propagation delay and clock oscillator offsets on the closed loop corrections is found to be

$$\varepsilon_{rM} = \left(\frac{\Delta T_{rf} + \Delta T_{cf}}{T_f} \right) \quad (I_r T_f + \tau) \tag{383}$$

and the mean error due to this cause is

$$\varepsilon_{rm} = \left(\frac{\Delta T_{rf} + \Delta T_{cf}}{T_f} \right) \left(\frac{I_r T_f}{2} + \tau \right) . \tag{384}$$

Thus to reduce this error (since we normally have no control over the propagation delay τ), we must minimize the clock oscillator offsets (i.e., use adequately stable clocks in both satellite and terminals) and keep the frame length $I_r T_f$ short, consistent with other requirements.

Expressions for the ranging loop timing error variance, including the effects of measurement noise and terminal maneuver statistics, were developed previously: Equations (229) and (234) of Section IV and Equations (298) and (342) of Section V. Assuming the mean error can be kept sufficiently small by appropriate choice of parameters as discussed above, the error variance becomes the crucial design criteria as for the clock loop timing of Section A (the mean error for the clock loop is zero, as noted above), hence application of these variance equations to system design will now be investigated. The development essentially parallels that for the clock loop (down-link) timing of section A, except that an additional parameter, I_r, the number of subframes per frame (which together with the subframe length T_f determines the frame length, $I_r T_f$) must be considered. Also, N_r, the number of ranging pulses per burst to be averaged in determining each closed loop correction, is assumed equal to one in the basic analysis with corrections for other values of N_r to be made by replacing $\sigma_{\xi r}^2$ with $\sigma_{\xi r}^2 / N_r$ as noted previously in Section IV-F.

Curves of normalized ranging loop timing jitter versus r for the stationary terminal case (from Equation (229)) were given in Figures 22 and 23 of Section IV. However, direct application of these curves to system design is not convenient because of the implicit dependence upon T_f of both r and ρ as noted previously for the case of clock loop

timing, Section A. Hence curves of normalized ranging loop timing jitter vs. r_s (see Equations (368)-(370)), which are more directly applicable, are given in Figures 42 through 44 for different values of I_r. Application of these curves to system design will be illustrated by an example.

Example 4

Given: Bit Rate $(\frac{1}{\Delta})$ = 40 Mbps
Maximum up-link timing jitter $(\sigma_{\varepsilon r})$ = .05Δ
Measurement noise standard deviation $(\sigma_{\xi r} = \sigma_{\xi c})$ = .0375Δ
Ranging pulses per burst (N_r) = 1
Probability that terminal will not accelerate (P_o) = .5
Maneuver rate (λ) = .1 maneuvers/sec
Maximum terminal acceleration (A) = 9.8 m/sec^2 (1 g.)
Number of subframes/frame (I_r) = 32 (or greater).

Then the normalized timing jitter is:

$$(\sigma_{\varepsilon r}^2 - \sigma_{\xi r}^2)/\sigma_{\xi c}^2 = \frac{(.05\Delta)^2 - (.0375\Delta)^2}{(.0375\Delta)^2} = .7778 \qquad (385)$$

from Equation (355)

$$\sigma_a = \frac{A}{c\sqrt{6}} = \frac{9.8}{3.10^8\sqrt{6}} = 1.334 \cdot 10^{-8} \text{ sec/sec}^2 \qquad (386)$$

and from Equation (368)

$$r_s = \frac{\sigma_\xi \lambda^2}{\sigma_a} = \frac{.0375}{40 \cdot 10^6} \cdot \frac{.1^2}{1.334 \cdot 10^{-8}} = 7.02 \cdot 10^{-4} \ . \qquad (387)$$

Then from Figure 42 (for I_r=32), using the coordinate values from Equations (385) and (387) we obtain (by interpolation between the given curves)

$$\lambda T_f \tilde{\simeq} .00084 \qquad (388)$$

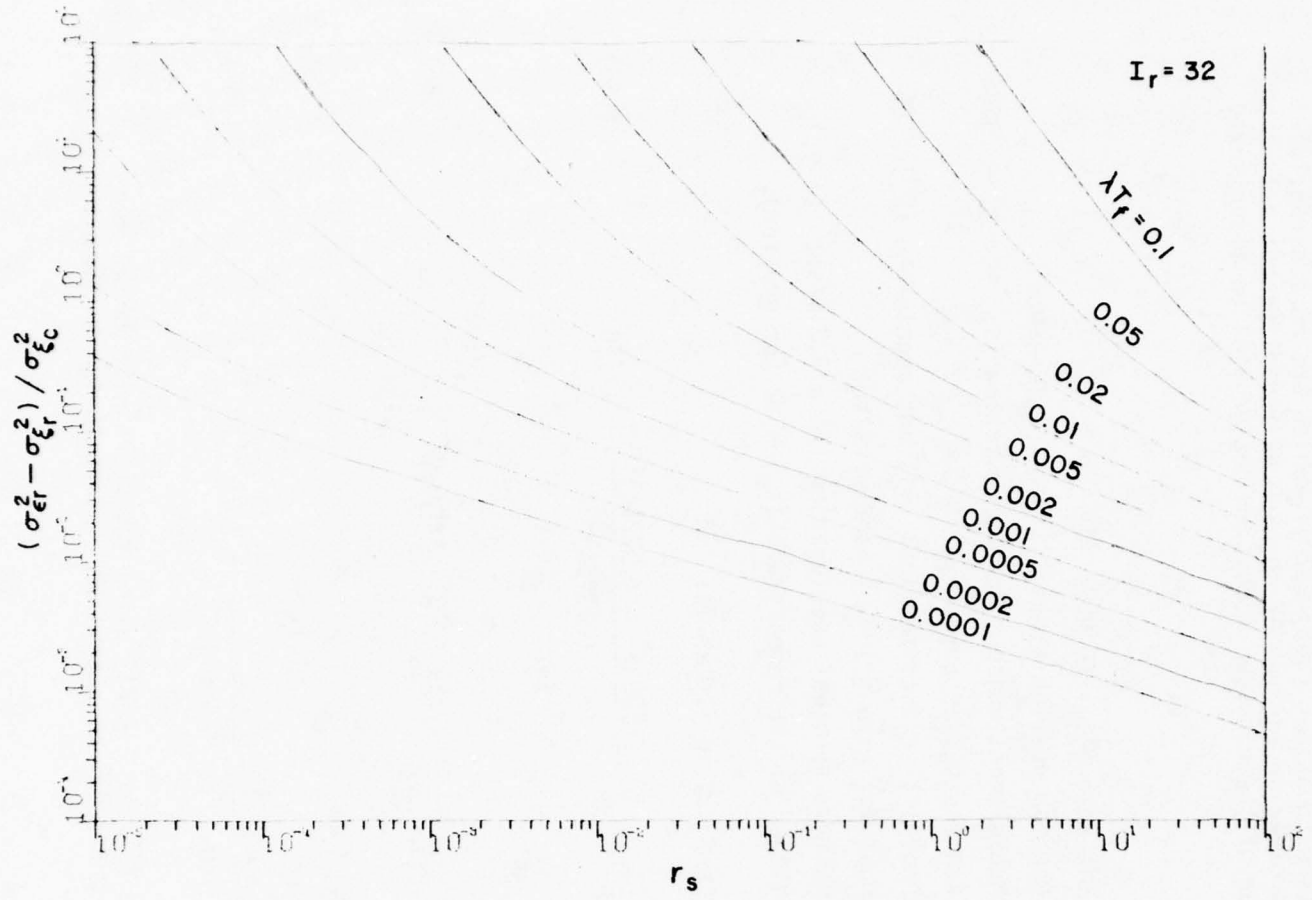

Figure 42. Normalized ranging loop timing jitter vs. r_s, stationary terminal, preliminary analysis.

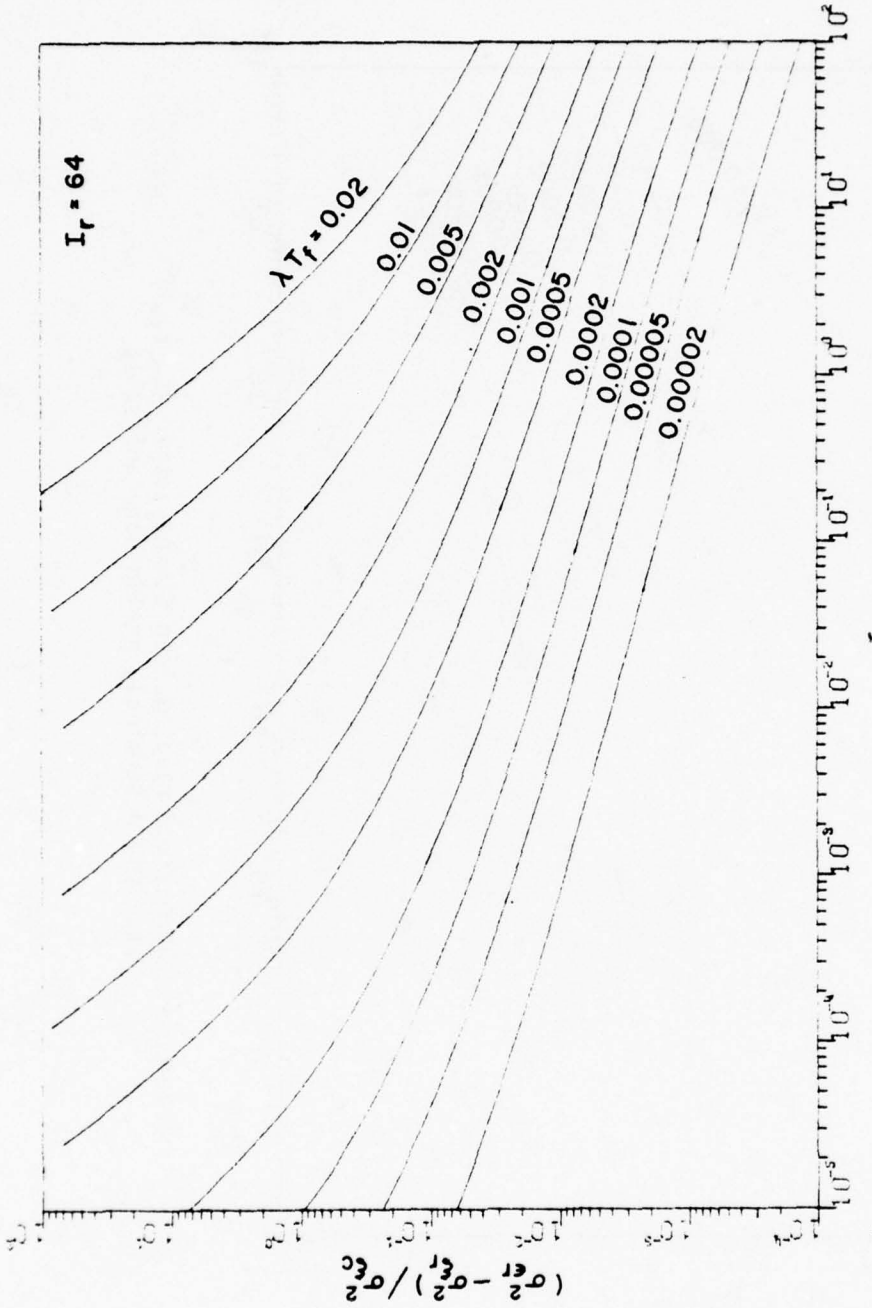

Figure 43. Normalized ranging loop timing jitter vs. r_s, stationary terminal, preliminary analysis.

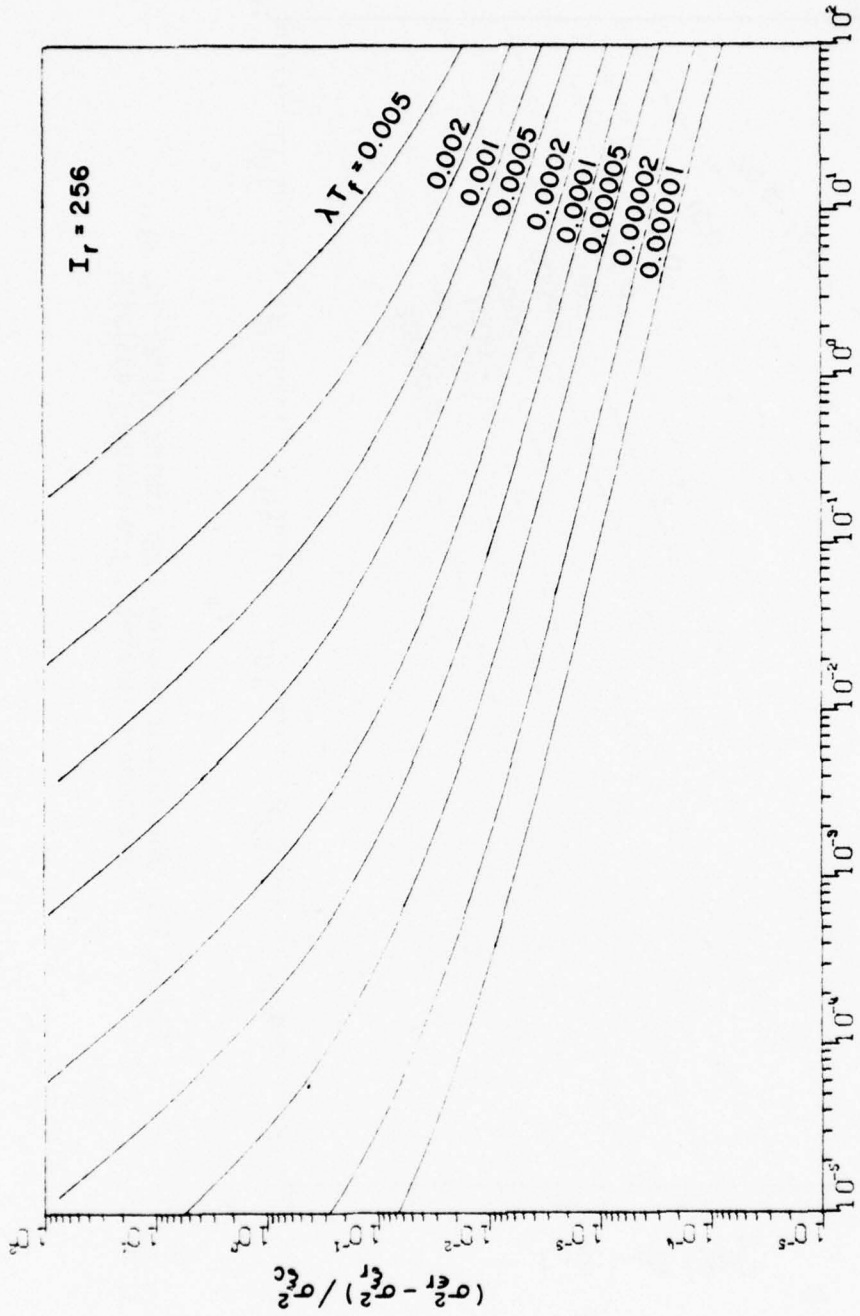

Figure 44. Normalized ranging loop timing jitter vs. r_s, stationary terminal, preliminary analysis.

Then

$$T_f = \frac{.00084}{\lambda} = 8.4 \text{ msec.} \tag{389}$$

The frame length is then

$$I_r T_f = 32 \cdot 8.4 \cdot 10^{-3} = .269 \text{ sec.} \tag{390}$$

From Section IV (see Figure 20) we note that, for stability, the frame length must exceed the round trip path delay which, for a synchronous satellite, varies from about .239 to .279 sec. as the terminal moves from the sub-satellite point to the horizon. Consequently the above value might be considered marginal.

We note, from Figure 43, that if we allow $I_r = 64$, rather than the original value of 32 as given above, the result is

$$\lambda T_f = .00051 \tag{391}$$

$$T_f = 5.1 \text{ msec} \tag{392}$$

and

$$I_r T_f = .326 \text{ sec} \tag{393}$$

which is adequate for all cases. Hence we choose these values.

The received ranging bit energy to noise density ratio may be found, if desired, from Equation (359) and the given value $\sigma_\xi = .0375$, as

$$E/N_o = 23.37 \text{ dB} \tag{394}$$

and if we choose the number of slots per subframe K=32 then the ranging pulse (slot) length is

$$M\Delta = T_f/K = 1.59 \cdot 10^{-4} \text{ sec} \qquad (6375 \text{ chips}) \tag{395}$$

and the received power to noise density ratio is

$$P/N_o = \frac{E/N_o}{M\Delta} = 61.3 \text{ dB Hz.} \tag{396}$$

The maximum clock loop error variance and the Kalman gain factors may be obtained from Figures 33 through 36, as in the previous section, using the values of λT_f and r_s as obtained above. The results are

$$\tilde{P}_1/\sigma_\xi^2 = 4.6 \cdot 10^{-2} \tag{397}$$

$$K_T = \hat{P}_1/\sigma_\xi^2 = 4.4 \cdot 10^{-2} \tag{398}$$

$$K_{\dot{T}}\, T_f = 9.8 \cdot 10^{-4} \tag{399}$$

$$K_{\ddot{T}}\, T_f^2 = 1.1 \cdot 10^{-5} \tag{400}$$

from which

$$K_{\dot{T}} = 9.8 \cdot 10^{-4}/5.1 \cdot 10^{-3} = .192 \qquad (\text{sec}^{-1}) \tag{401}$$

$$K_{\ddot{T}} = 1.1 \cdot 10^{-5}/(5.1 \cdot 10^{-3})^2 = .423 \quad (\text{sec}^{-2}) \tag{402}$$

and the standard deviation of the clock loop timing error (maximum) is

$$(\tilde{P}_1)^{1/2} = [4.6 \cdot 10^{-2}(.0375\Delta)^2]^{1/2} = .0080\Delta \ . \tag{403}$$

Alternatively, we might have decided to retain the value $I_r=32$ in the above example and increase the permissible subframe time T_f by choosing $N_r=2$ (i.e., by averaging 2 ranging pulses per frame). In this case by replacing $\sigma_{\xi r}^2$ with $\sigma_{\xi r}^2/N_r$ in Equation (385) we obtain

$$(\sigma_{\varepsilon r}^2 - \sigma_{\xi r}^2/N_r)/\sigma_{\xi c}^2 = 1.278 \ . \tag{404}$$

Using this value as the ordinate, together with $r_s=7.02 \cdot 10^{-4}$ (from Equation (387)), we find from Figure 42

$$\lambda T_f \approx .0011 \tag{405}$$

then

$$T_f = .0011/\lambda = 11 \text{ ms} \tag{406}$$

and the frame length becomes

$$I_r T_f = 32 \cdot 11 \cdot 10^{-3} = .352 \text{ sec.} \tag{407}$$

Now, if the 2 ranging pulses are spaced a subframe (T_f) apart as indicated by Figure 20 (Section IV-F), then we must have

$$I_r T_f > \tau_{max} + T_f \tag{408}$$

where

$$\tau_{max} + T_f = .279 + .011 = .290 \text{ sec} \quad . \tag{409}$$

Hence this alternative is also satisfactory. The remaining quantities of interest may then be found, if desired, as in the above example.

It can be seen, from Equation (229) and Figures 42-44, and similarly for Equations (234), (298) and (342) that there is a definite limit on the value of measurement noise permissible to obtain a given maximum ranging loop timing jitter. To obtain a solution we must have

$$(\sigma_{\varepsilon r}^2 - \sigma_{\xi r}^2/N_r)/\sigma_{\xi c}^2 > 0 \tag{410}$$

from which

$$\sigma_{\xi r} < \sigma_{\varepsilon r} \sqrt{N_r} \quad . \tag{411}$$

This definite limit did not exist in the clock loop since the Kalman filter used in that loop essentially provides optimum averaging over all previous samples rather than the discrete number of samples, N_r, used here. To obtain reasonable solutions we would expect to find the normalized timing jitter to be near unity, and almost certainly in the range

$$10^{-2} < (\sigma_{\varepsilon r}^2 - \sigma_{\xi r}^2/N_r)/\sigma_{\xi c}^2 < 10^2 \quad . \tag{412}$$

A similar solution could be obtained for the stationary satellite case from Equation (234) and the curves of Figure 8 using essentially the method of Example 1. However, this solution will be obtained as one term in the solution for the more exact expression, Equation (298) hence this equation will now be evaluated.

C. Application of The Extended Up-Link Timing Analysis

1. Stationary satellite, maneuvering terminals

If we let

$$A_r = N_r = 1 \tag{413}$$

(unity ranging loop gain constant, and a single ranging pulse per measurement)

and

$$N_o = N_d = N_F - 1 \tag{414}$$

(variance computed just prior to receipt of another ranging pulse, and path delay $\approx$ frame length)

where $N_F \equiv I_r$ = the number of subframes per frame

analogous to the special case (essentially worst case) considered in the preliminary analysis for uplink-timing, stationary satellite case; then, with appropriate changes in notation to facilitate comparison with the previous analysis, Equation (298) reduces to

$$\frac{\sigma_{\varepsilon r}^2 - \sigma_{\xi r}^2}{\sigma_{\xi_c}^2} = \frac{3\hat{P}_1}{\sigma_{\xi_c}^2} + 2\left\{\frac{\hat{P}_1(I_r-1)}{\sigma_{\xi_c}^2} - \frac{\hat{P}_1(I_r)}{\sigma_{\xi_c}^2}\right\} - 2\,\frac{\hat{P}_1(2I_r-1)}{\sigma_{\xi_c}^2} \tag{415}$$

(where the subscripts r and c on the σ_ξ's refer to the ranging loop and clock loop, respectively) while the normalized form of Equation (234) from the preliminary analysis is

$$\frac{\sigma_{\varepsilon r}^2 - \sigma_{\xi r}^2}{\sigma_{\xi_c}^2} \approx \frac{3\hat{P}_1}{\sigma_{\xi_c}^2} = 3K_T \quad . \tag{416}$$

The first term on the right hand side of Equation (415) (and the only term of Equation (416)) is simply 3 times the normalized clock loop timing filtered error variance, or from Equations (121) and (127), 3 times the Kalman gain factor K_T.

The second and third terms of Equation (415) may be evaluated using Equation (189) from which

$$\hat{P}(\ell) = [(I-KH)\Phi]^{\ell}\ \hat{P} \tag{417}$$

where (from Equations (88), (91) and (120))

$$[(I-KH)\Phi] = \begin{bmatrix} 1-K_T & (1-K_T)T_f & (1-K_T)\dfrac{T_f^2}{2} \\ -K_{\dot{T}} & 1-K_{\dot{T}}T_f & T_f-K_{\dot{T}}\dfrac{T_f^2}{2} \\ -K_{\ddot{T}} & -K_{\ddot{T}}T_f & \rho-K_{\ddot{T}}\dfrac{T_f^2}{2} \end{bmatrix} \tag{418}$$

the filtered error covariance matrix for the clock loop, $\hat{P}$, is defined as

$$\hat{P} \equiv \begin{bmatrix} \hat{P}_1 & \hat{P}_2 & \hat{P}_4 \\ \hat{P}_2 & \hat{P}_3 & \hat{P}_5 \\ \hat{P}_4 & \hat{P}_5 & \hat{P}_6 \end{bmatrix} \tag{419}$$

and

$$\hat{P}(\ell) \equiv \begin{bmatrix} \hat{P}_1(\ell) & \hat{P}_2(\ell) & \hat{P}_4(\ell) \\ \underline{\hat{P}}_2(\ell) & \hat{P}_3(\ell) & \hat{P}_5(\ell) \\ \underline{\hat{P}}_4(\ell) & \underline{\hat{P}}_5(\ell) & \hat{P}_6(\ell) \end{bmatrix} . \tag{420}$$

Note that while $\hat{P}$ (Equation (419)) is symmetric, $\hat{P}(\ell)$ (Equation (420)), in general, is not. This is indicated by the underscore notation in Equation (420) which permits retaining the original subscripts to avoid confusion, i.e.,

$$\hat{P}_i(\ell) \neq \underline{\hat{P}}_i(\ell), \text{ in general.} \tag{421}$$

From Equations (418), (419) and (420) there results

$$\hat{P}_1(\ell) = a_{11}\,\hat{P}_1 + a_{12}\,\hat{P}_2 + a_{13}\,\hat{P}_4 \tag{422}$$

where the a_{ij} are elements of the matrix

$$[a] \equiv \begin{bmatrix} a_{11} & a_{12} & a_{13} \\ a_{21} & a_{22} & a_{23} \\ a_{31} & a_{32} & a_{33} \end{bmatrix} = [(I-kH)\Phi]^{\ell} \tag{423}$$

Unfortunately, the above equations are not convenient for calculation since the matrix $[(I-kH)\Phi]$ is an explicit function of T_f (see Equation (418)). It can be shown that the normalized error variance (Equation (415)) is, in fact, independent of T_f; hence we desire an alternate formulation in which this pseudo dependence upon T_f does not appear. One way to do this is to redefine the system state variables and the resultant functions in dimensionless (normalized) form; i.e., Equations (83)-(91), etc. are replaced by

$$Z'_{(n+1)} = \Phi'\,Z'_{(n)} + \Gamma'\,u'_{(n)} \tag{424}$$

and

$$X'_{(n)} = H'\,Z'_{(n)} + \xi'_{(n)} \tag{425}$$

where

$$Z'_{(n)} = \begin{bmatrix} T_n \\ \dot{T}_n T_f \\ \ddot{T}_n \dot{T}_f^2 \end{bmatrix} \tag{426}$$

$$\Phi' = \begin{bmatrix} 1 & 1 & \frac{1}{2} \\ 0 & 1 & 1 \\ 0 & 0 & \rho \end{bmatrix} \tag{427}$$

$$K' = \begin{bmatrix} K_T \\ K_T^{\cdot} T_f \\ K_T^{\cdot\cdot} T_f^2 \end{bmatrix} \tag{428}$$

$$H' = H = [1 \quad 0 \quad 0] \tag{429}$$

$$\Gamma' = \Gamma = \begin{bmatrix} 0 \\ 0 \\ 1 \end{bmatrix} \tag{430}$$

$$\xi'(n) = \xi(n) \tag{431}$$

and

$$u'(n) = u(n)\, T_f^2 \quad . \tag{432}$$

In terms of this new set of dimensionless variables we can obtain

$$\frac{\hat{P}_1(\ell)}{\sigma_\xi^2} = b_{11} \frac{\hat{P}_1}{\sigma_\xi^2} + b_{12} \frac{\hat{P}_2 T_f}{\sigma_\xi^2} + b_{13} \frac{\hat{P}_4 T_f^2}{\sigma_\xi^2} \tag{433}$$

where the b_{ij} are elements of the dimensionless matrix

$$[b] \equiv \begin{bmatrix} b_{11} & b_{12} & b_{13} \\ b_{21} & b_{22} & b_{23} \\ b_{31} & b_{32} & b_{33} \end{bmatrix} = [(I-K'H)\Phi']^{\ell} \tag{434}$$

and

$$[(I-K'H)\Phi'] = \begin{bmatrix} 1-K_T & 1-K_T & \frac{1-K_T}{2} \\ -\dot{K}_T T_f & 1-\dot{K}_T T_f & 1-\frac{\dot{K}_T T_f}{2} \\ -\ddot{K}_T T_f^2 & -\ddot{K}_T T_f^2 & \rho-\ddot{K}_T \frac{T_f^2}{2} \end{bmatrix} . \quad (435)$$

Then from Equations (120) and (433)

$$\frac{\hat{P}_1(\ell)}{\sigma_\xi^2} = b_{11} K_T + b_{12} \dot{K}_T T_f + b_{13} \ddot{K}_T T_f^2 . \quad (436)$$

The normalized gains K_T, $\dot{K}_T T_f$, and $\ddot{K}_T T_f^2$ appearing in Equations (435) and (436) are directly obtained from the solution of the clock loop filter, Equations (120) to (129).

Curves of the normalized transmit timing error variance for the stationary satellite-moving terminal case versus the parameter r_s as obtained from Equation (415) are given in Figures 45-48 for different values of I_r, and a comparison of this solution with the approximate solution (Equation (416)) is given in Figure 49. It is seen that the approximation is good for higher values of λT_f (lower maneuver correlation) and for lower values of r_s (lower measurement noise to maneuver noise ratio) with some deterioration elsewhere. Over the range of parameters investigated (as shown by the curves) the contribution from the second term of Equation (415) was found to be at least an order of magnitude less than that from the 1st term and hence could generally be neglected with little error. The third term, however, becomes significant for higher values of r_s and/or lower values of λT_f. Both the second and third terms alternate in sign thus producing the "ripples" evident in the curves of Figures 46-49.

Example 5

Given the system parameters of Example 4 we have from Equation (385)

$$\frac{\sigma_{\varepsilon_r}^2 - \sigma_{\xi_r}^2}{\sigma_{\xi_c}^2} = .7778 \quad (437)$$

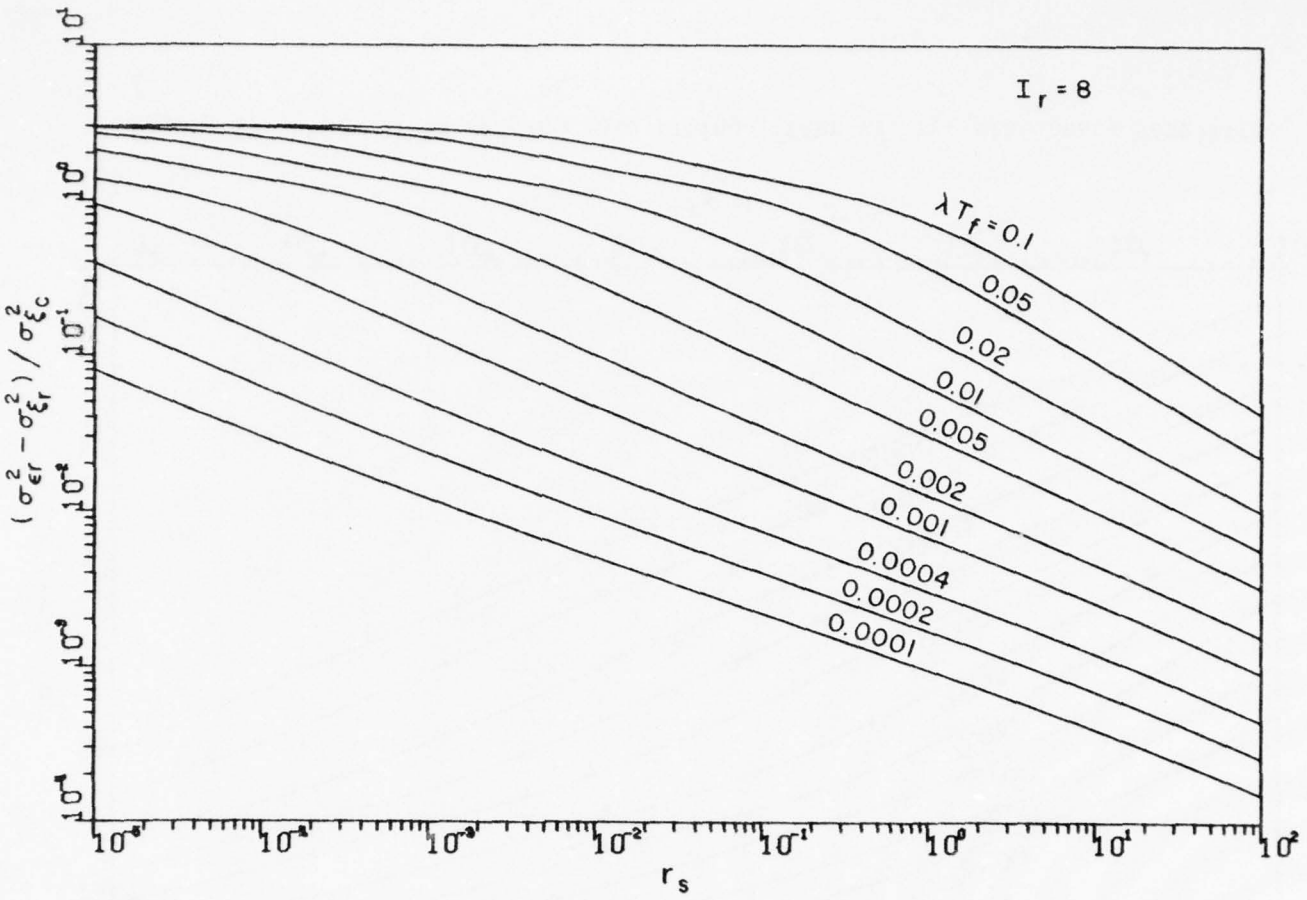

Figure 45. Normalized ranging loop timing jitter vs. r_s, stationary satellite.

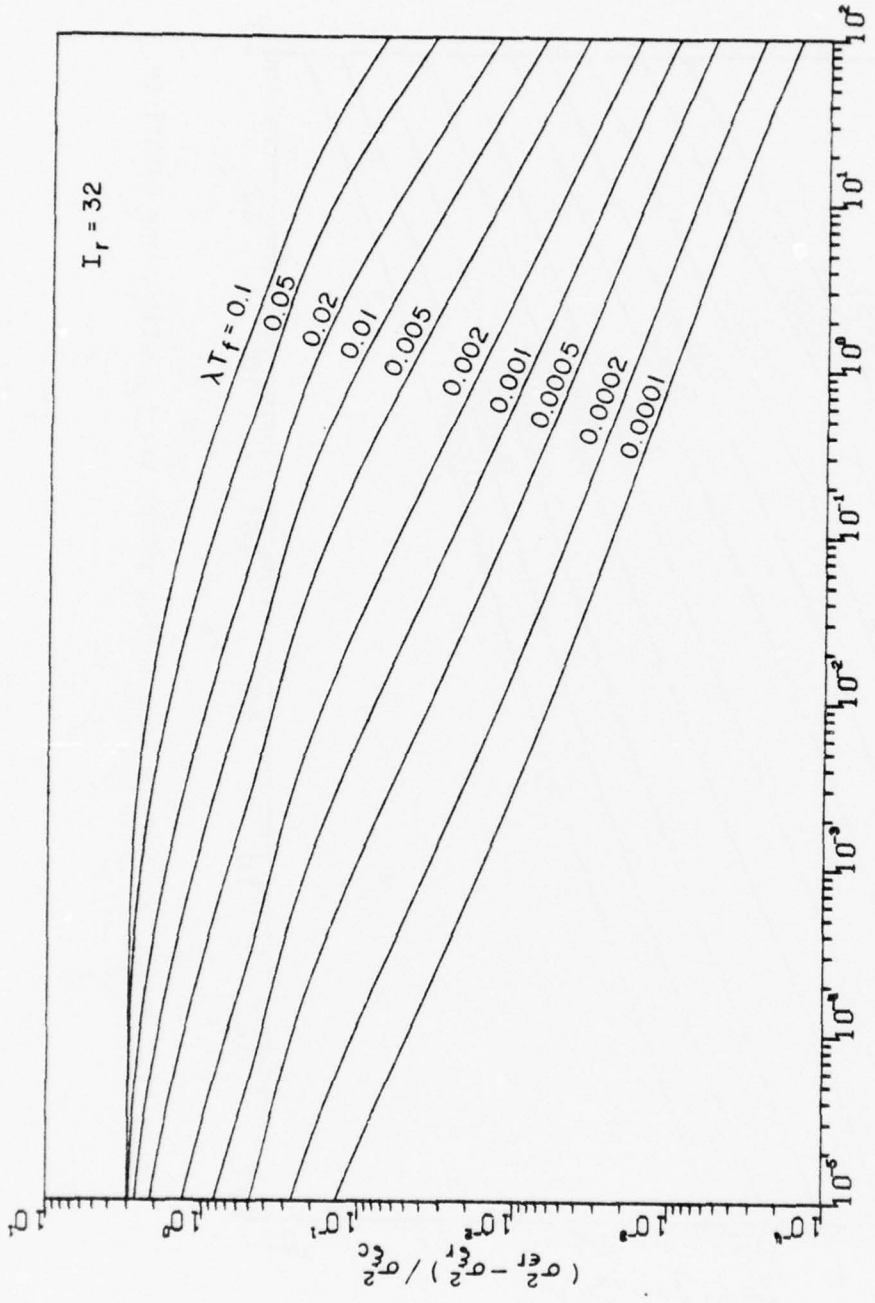

Figure 46. Normalized ranging loop timing jitter vs. r_s, stationary satellite.

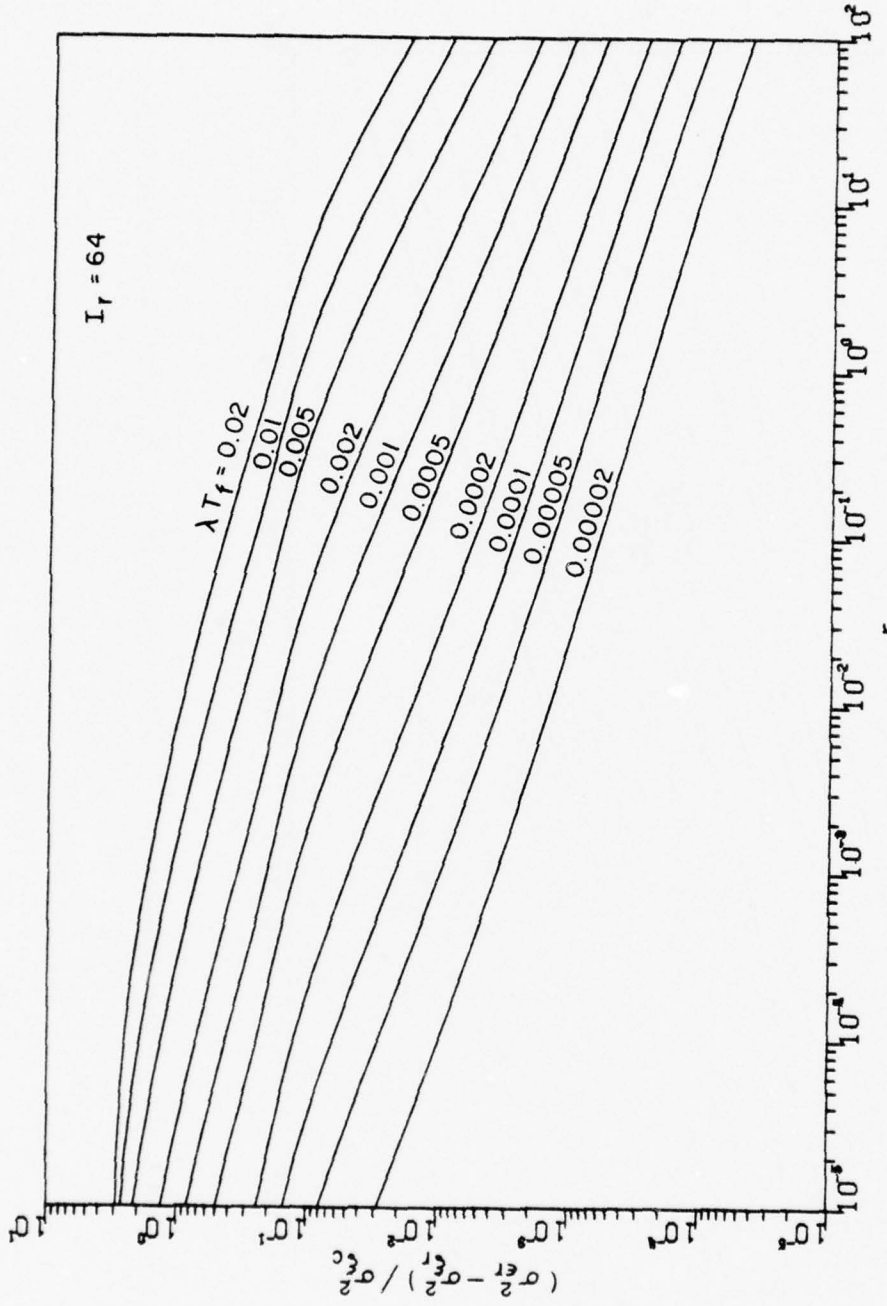

Figure 47. Normalized ranging loop timing jitter vs. r_s, stationary satellite.

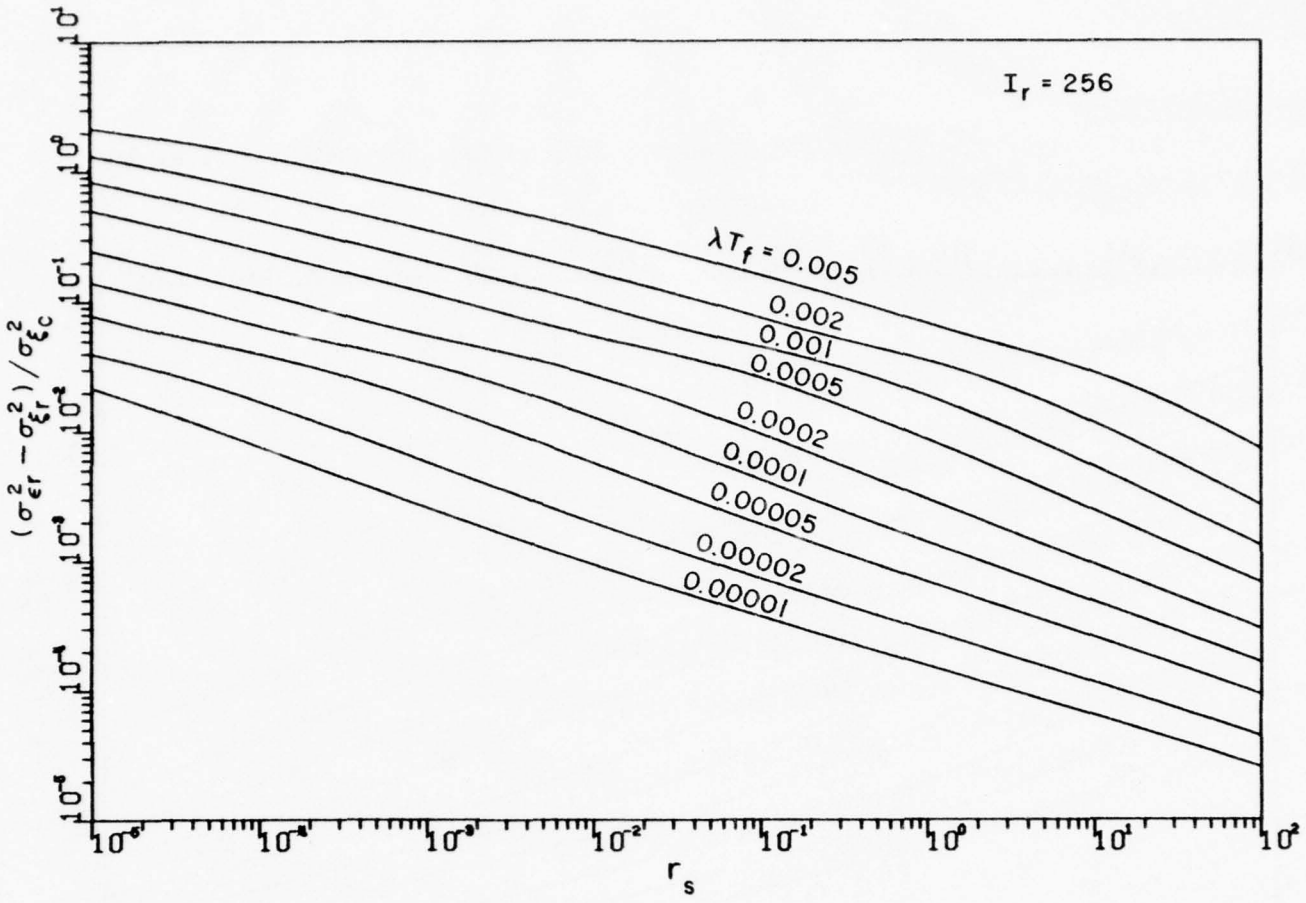

Figure 48. Normalized ranging loop timing jitter vs. r_s, stationary satellite.

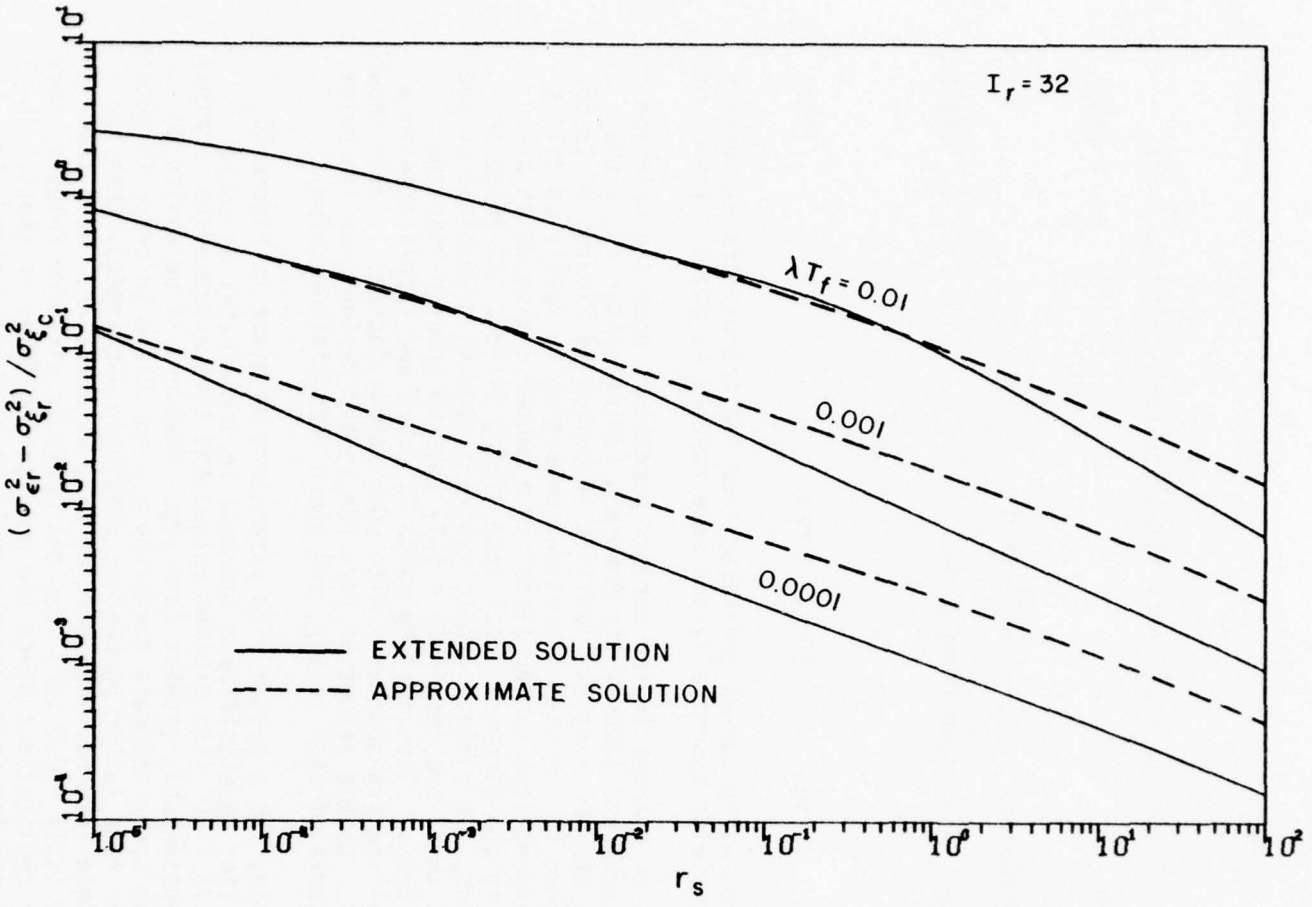

Figure 49. Comparison of extended and approximate solutions for the ranging loop timing jitter, stationary satellite.

and from Equation (387)

$$r_s = 7.02 \cdot 10^{-4} \tag{438}$$

Then from Figure 46 for the stationary satellite case (with $I_r = 32$)

$$\lambda T_f = .00500 \tag{439}$$

and using the parameters $\lambda = .1$ (sec^{-1}) and $I_r = 32$:

$$T_f = 50.0 \text{ ms} \qquad \text{(subframe time)} \tag{440}$$

and

$$T_F = I_r T_f = 1.60 \text{ sec} \qquad \text{(frame time).} \tag{441}$$

A similar solution using curves generated from the approximate expression (Equation (416)) yields essentially the same results as above (T_f=49.9 ms).

The effects of changes in the various parameters upon the solution for the maximum subframe time T_f (to insure a timing jitter $\sigma_{\varepsilon r} \leq$ the specified value) are shown by the families of curves in Figures 50 to 55. These were obtained by computer iteration converging to specified values of normalized ranging loop timing jitter in a manner analogous to that used previously in the study of clock loop timing jitter. As noted in the above examples, the minimum usable subframe time is determined by the requirement that the frame length $T_F = I_r T_f$ must be greater than the round trip path delay. The limiting value $T_F = 0.3$ sec (applicable to a synchronous satellite transponder - with some safety factor) is also shown in these figures. Usable values of T_f/Δ for system design then lie below the applicable curve of each family, and above this minimum value.

As an example, for a system with parameters as given in Figure 50, with $\sigma_{\varepsilon r} \leq .05\Delta$ (for no significant increase in error rate) we could choose $T_f/\Delta = 3.75 \cdot 10^5$ (the minimum value) and thus accommodate terminal accelerations considerably greater than 10g. However, if we desire to limit the maximum error standard deviation $\sigma_{\varepsilon r}$ to $.0425\Delta$ in order to obtain an improved error rate (other parameters remaining unchanged), then the maximum permissible terminal acceleration will be about 2g. Note that this lower limit ($I_r T_f = 0.3$ sec) does not apply to airborne relay systems or other similar applications where the propagation delay is short. In such cases, much shorter frame lengths could be used, if desired, to permit higher values of terminal acceleration and/or lower error rates, or to compensate for desired changes in other system parameters. As is evident from these figures the path length delay limitation ($T_f \geq .3$ sec) is generally not of great significance over the range of values studied for case of the stationary satellite relay.

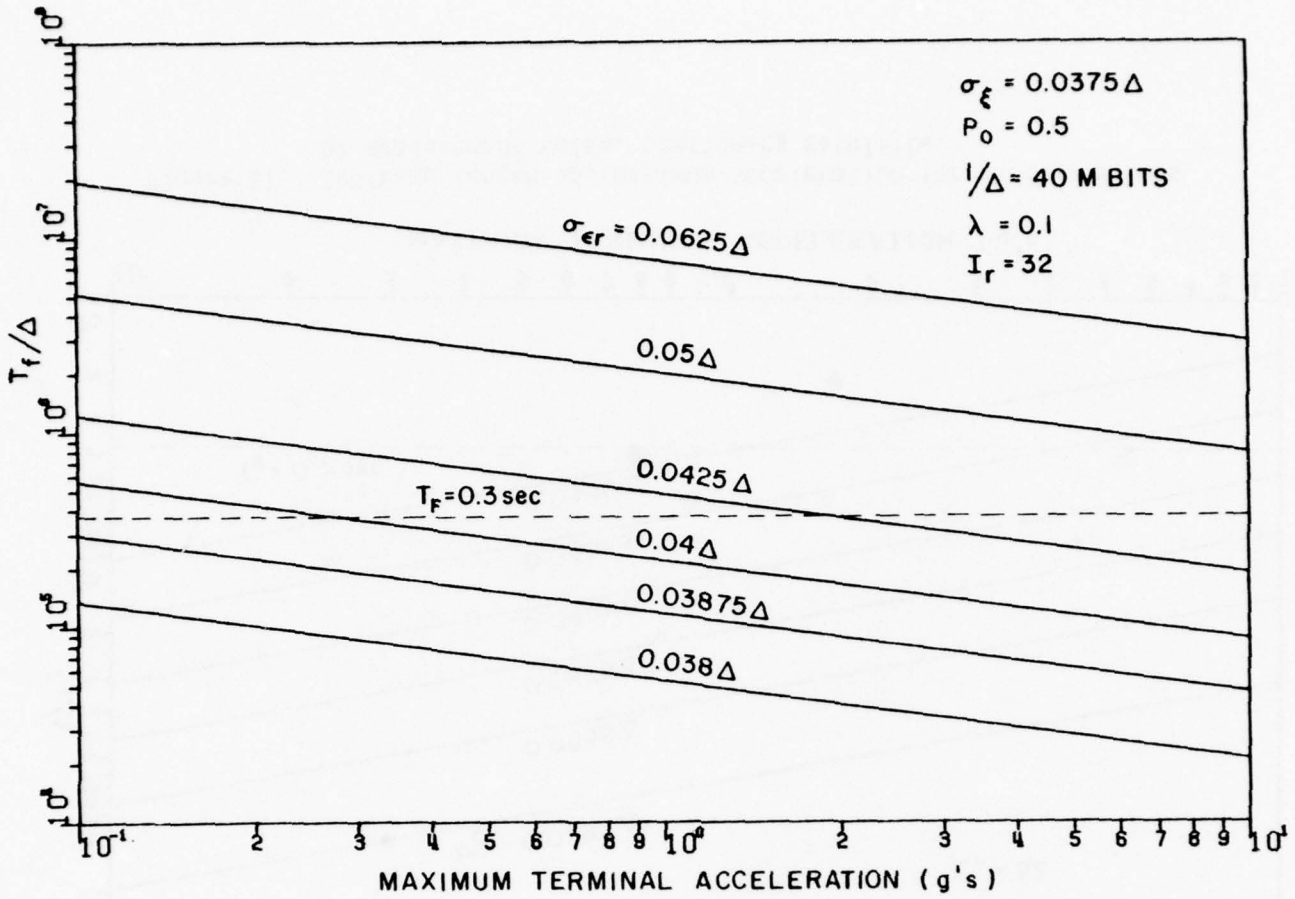

Figure 50. Subframe length vs. maximum acceleration for various values of transmit timing jitter, stationary satellite.

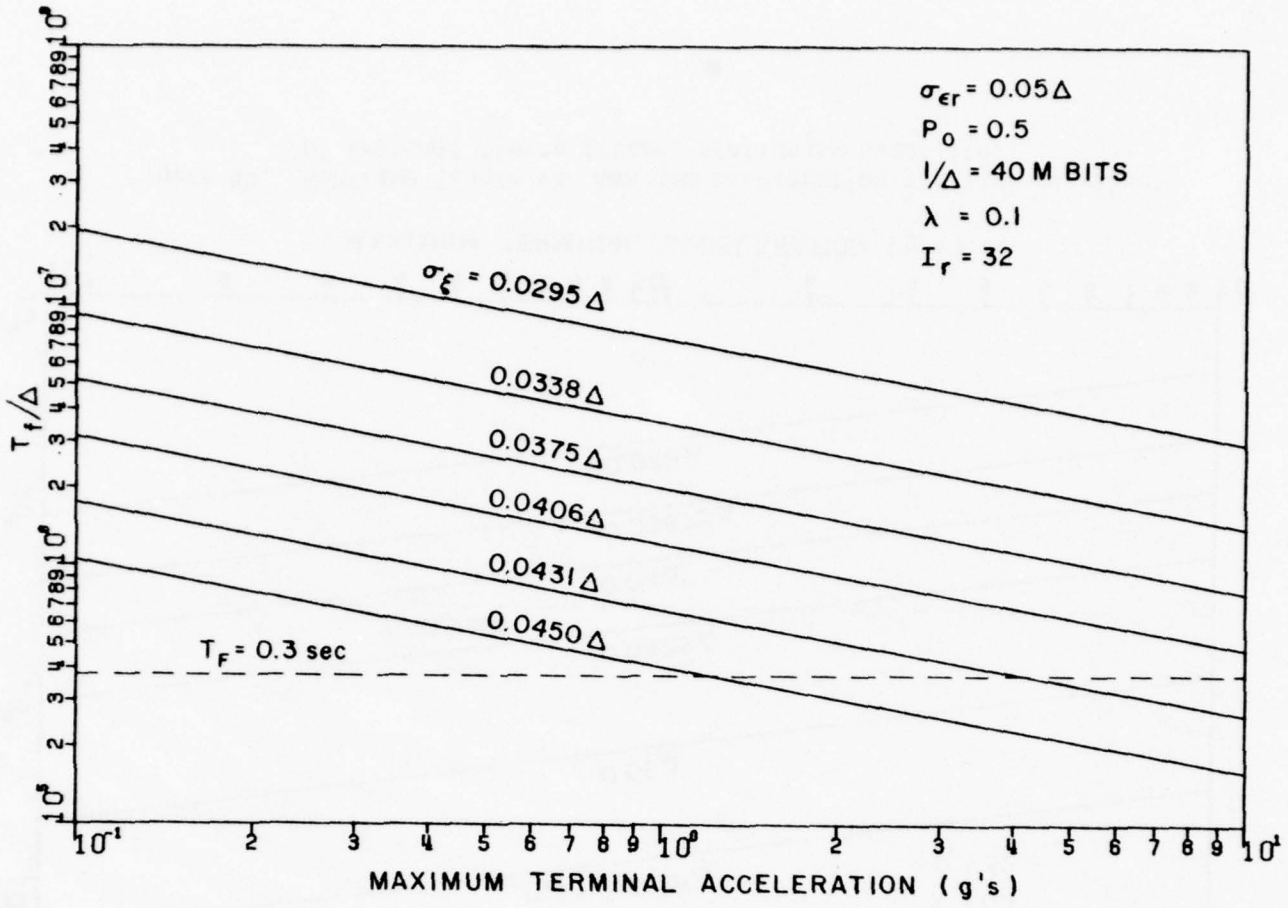

Figure 51. Subframe length vs. maximum acceleration for various values of measurement noise, stationary satellite.

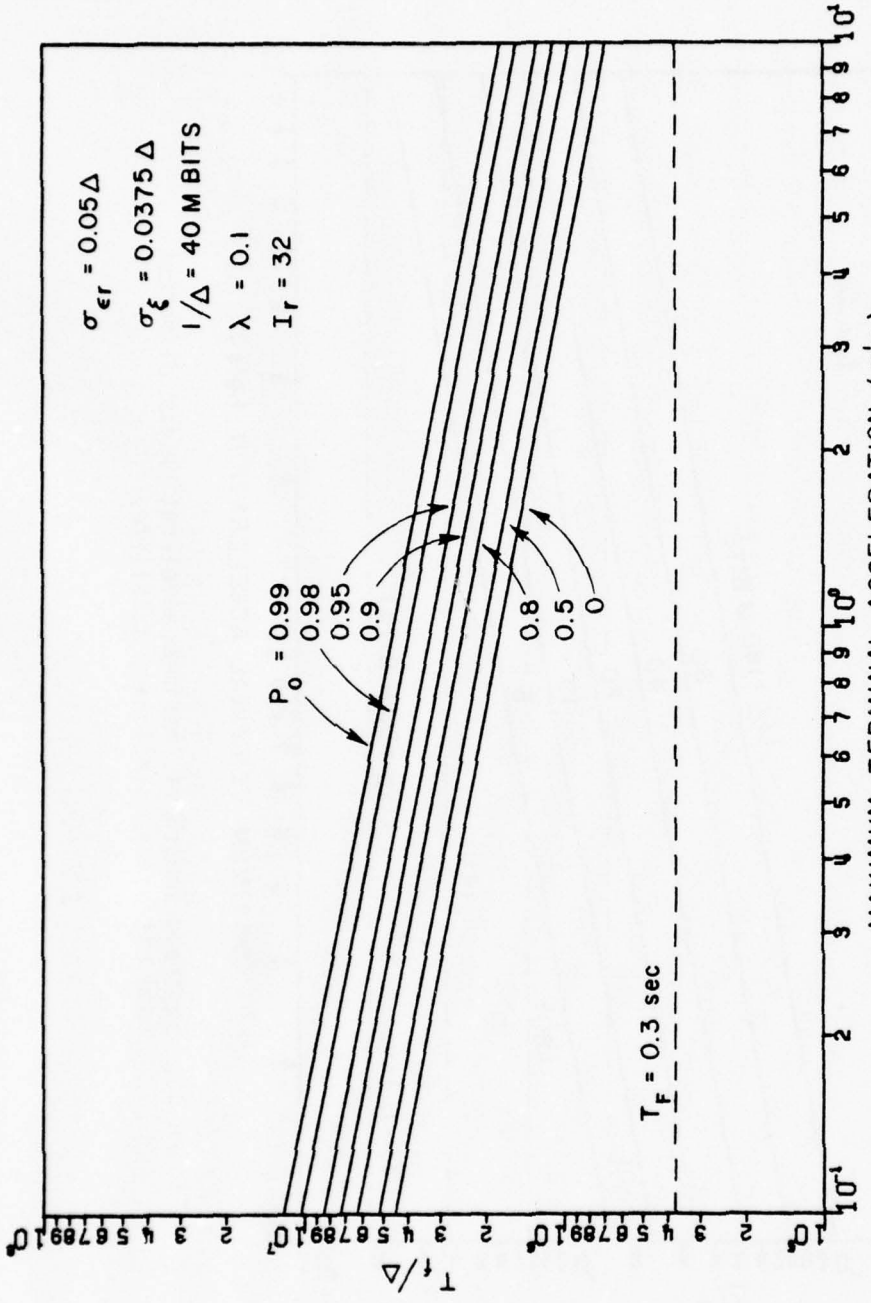

Figure 52. Subframe length vs. maximum acceleration for different maneuver probabilities, stationary satellite.

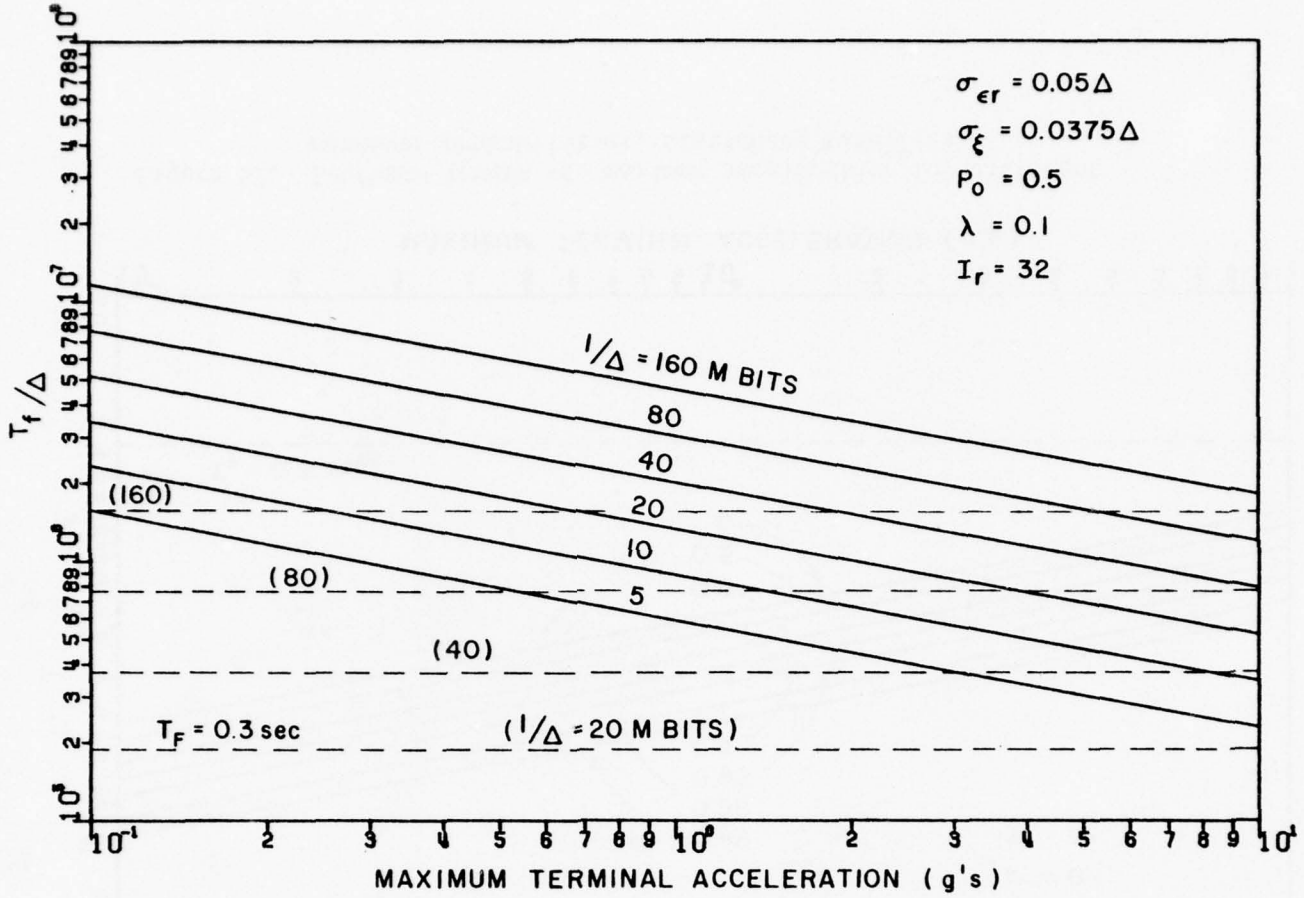

Figure 53. Subframe length vs. maximum acceleration for different code bit rates, stationary satellite.

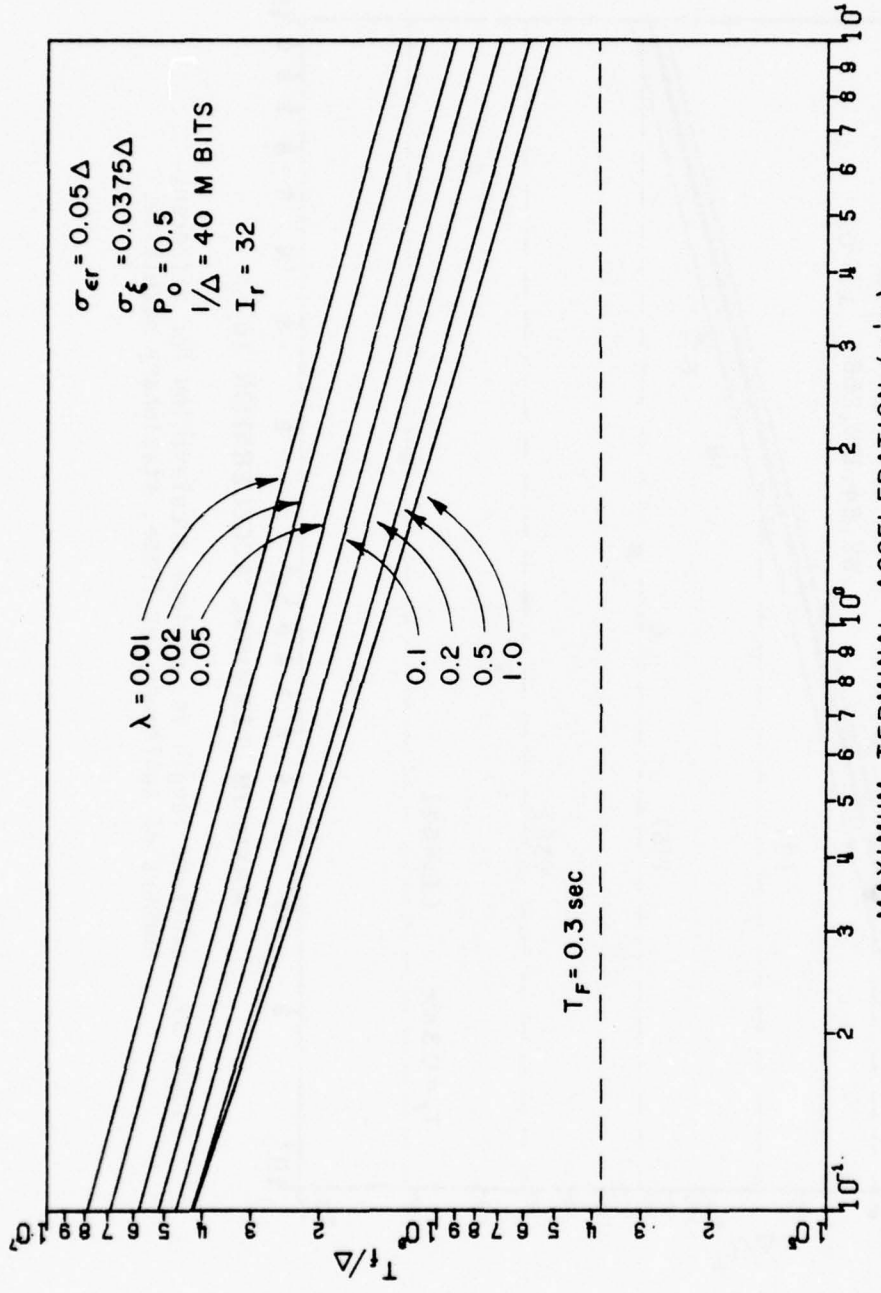

Figure 54. Subframe length vs. maximum acceleration for different maneuver rates, stationary satellite.

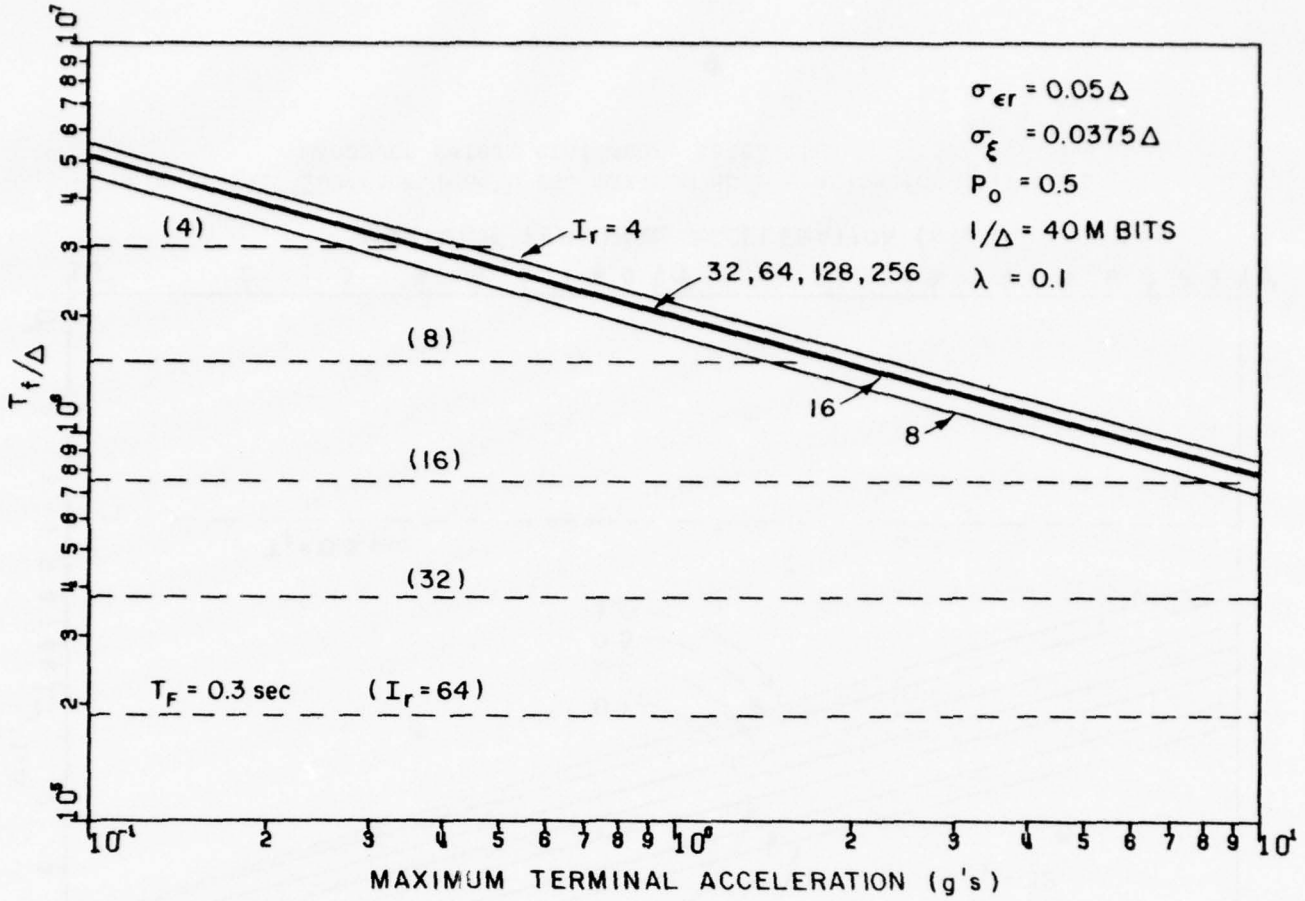

Figure 55. Subframe length vs. maximum acceleration for different numbers of subframes per frame, stationary satellite.

2. Stationary terminal, maneuvering satellite

We will again consider essentially the "worst case" condition analogous to that used in the previous analyses by choosing

$$N_o = N_d = N_{F-1} \tag{442}$$

where $N_F \equiv I_r$.

Also let

$$\alpha_a T_f + T_o << T_f \quad . \tag{443}$$

Then, with appropriate change of notation as used in the previous section, the normalized ranging loop timing error variance (from Equation (342)) can be written as

$$\frac{\sigma_{\varepsilon_{rt}}^2 - \sigma_{\xi_r}^2}{\sigma_{\xi_c}^2} = \frac{\sigma_{\varepsilon_r}^2 - \sigma_{\xi_r}^2}{\sigma_{\xi_c}^2} + \frac{\sigma_{\tilde{q}_{1p}}^2(N_o)}{\sigma_{\xi_c}^2} - \frac{2 R_{\tilde{q}_{1p}\tilde{\varepsilon}_{rn}}(N_o)_o}{\sigma_{\xi_c}^2} \tag{444}$$

where the subscript t denotes the stationary terminal case.

The 1st term on the right hand side of Equation (444) is simply the normalized timing error variance previously obtained for the case of the stationary satellite (Equation (415)), while the remaining terms are obtained from Equations (336) and (345), respectively (utilizing Equations (442) and (443) as:

$$\begin{aligned}\frac{\sigma_{\tilde{q}_{1p}}^2(N_o)}{\sigma_{\xi_c}^2} = \frac{4(1-\rho^2)}{r^2} &\left\{(2I_r-1)S_\rho^2(I_r-1) - 2\sum_{k=0}^{I_r-2} S_\rho(k)[S_\rho(I_r-1)-S_\rho(k)]\right\} \\ &+ C_\rho^2\left\{(2I_r-1)\frac{R_T^{\cdot\cdot}(0)T_f^4}{\sigma_{\xi_c}^2} + 2\sum_{\ell=1}^{2I_r-2}(2I_r-1-\ell)\frac{R_T^{\cdot\cdot}(\ell)T_f^4}{\sigma_{\xi_c}^2}\right\} \\ &+ C_\rho\left\{\sum_{\ell=0}^{2I_r-2}\frac{R_{Tu}^{\cdot\cdot}(\ell)T_f^4}{\sigma_{\xi_c}^2}[S_\rho(I_r-1)(2I_r-1-\ell)-F_s(\ell)]\right\}\end{aligned} \tag{445}$$

and

$$\frac{-2\,\tilde{R}_{q_{lp}\varepsilon_{rn}}(N_o)_o}{\sigma^2_{\xi_c}} = S_\rho(I_r-1)\sum_{\ell=I_r-1}^{2I_r-2}\frac{\tilde{R}_{\varepsilon_{cn}u}(\ell)T_f^2}{\sigma^2_{\xi_c}}$$

$$+\sum_{\ell=0}^{I_r-2}S_\rho(\ell)\left[\frac{\tilde{R}_{\varepsilon_{cn}u}(\ell)T_f^2}{\sigma^2_{\xi_c}}-\frac{\tilde{R}_{\varepsilon_{cn}u}(I_r+\ell)T_f^2}{\sigma^2_{\xi_c}}\right]$$

$$+2C_\rho\left[\sum_{\ell=I_r-1}^{2I_r-2}\frac{\tilde{R}_{\varepsilon_{cn}\ddot{\hat{T}}_e}(\ell)T_f^2}{\sigma^2_{\xi_c}}-2\sum_{\ell=1}^{I_r}\frac{\tilde{R}_{\ddot{\hat{T}}_e\varepsilon_{cn}}(\ell)T_f^2}{\sigma^2_{\xi_c}}\right.$$

$$\left.-\sum_{\ell=I_r+1}^{2I_r-1}\frac{\tilde{R}_{\ddot{\hat{T}}_e\varepsilon_{cn}}(\ell)T_f^2}{\sigma^2_{\xi_c}}\right] \tag{446}$$

where

$$C_\rho \equiv \frac{(1+\rho)(1-\rho^{I_r-1})}{2(1-\rho)} \tag{447}$$

$$r \equiv \frac{4\sigma_{\xi_c}}{\sigma_a T_f^2} \tag{448}$$

and $S_\rho(k)$ and $F_S(\ell)$ are as previously defined by Equations (316) and (339), respectively.

To evaluate Equations (445) and (446) we need expressions for the correlation functions $R_{\ddot{T}_\varepsilon}(\ell)$, $R_{\ddot{T}_\varepsilon u}(\ell)$, $R_{\tilde{\varepsilon}_{cn} u}(\ell)$, $R_{\tilde{\varepsilon}_{cn} \hat{\ddot{T}}_\varepsilon}(\ell)$, and $R_{\hat{\ddot{T}}_\varepsilon \tilde{\varepsilon}_{cn}}(\ell)$. From the defining equations (Equations (337), (338), (346), (347), and (348)) and Equations (189)-(191) we obtain:

$$R_{\ddot{T}_\varepsilon}(\ell) = \hat{P}_6(\ell) \tag{449}$$

$$R_{\ddot{T}_\varepsilon u}(\ell) = \sigma_{a\ddot{T}}(\ell) \tag{450}$$

$$R_{\tilde{\varepsilon}_{cn} u}(\ell) = \sigma_{aT}(\ell) \tag{451}$$

$$R_{\tilde{\varepsilon}_{cn} \hat{\ddot{T}}_\varepsilon}(\ell) = \hat{P}_4(\ell) \tag{452}$$

and

$$R_{\hat{\ddot{T}}_\varepsilon \tilde{\varepsilon}_{cn}}(\ell) = \hat{P}_4(\ell) \tag{453}$$

where $\sigma_{aT}(\ell)$ and $\sigma_{a\ddot{T}}(\ell)$ were previously defined by Equation (192) and the $\hat{P}_i(\ell)$ were defined by Equation (420).

Finally, using methods analogous to those of the previous section there results

$$\frac{R_{\ddot{T}_\varepsilon}(\ell) T_f^4}{\sigma_{\xi_c}^2} = b_{31} \frac{\hat{P}_4 T_f^2}{\sigma_{\xi_c}^2} + b_{32} \frac{\hat{P}_5 T_f^3}{\sigma_{\xi_c}^2} + b_{33} \frac{\hat{P}_6 T_f^4}{\sigma_{\xi_c}^2} \tag{454}$$

$$\frac{R_{\ddot{T}_\varepsilon u}(\ell) T_f^4}{\sigma_{\xi_c}^2} = \begin{cases} b_{33} \left(\frac{4}{r}\right)^2 (1-\rho^2) & , \ \ell \geq 1 \\ 0 \ , & \ell \leq 0 \end{cases} \tag{455}$$

$$\frac{R_{\tilde{\varepsilon}_{cn}u}(\ell)T_f^2}{\sigma_{\xi_c}^2} = \begin{cases} \underline{b}_{13}\left(\frac{4}{r}\right)^2(1-\rho^2) , & \ell \geq 1 \\ 0 , & \ell \leq 0 \end{cases} \tag{456}$$

$$\frac{R_{\tilde{\varepsilon}_{cn}\ddot{\tilde{T}}_\varepsilon}(\ell)T_f^2}{\sigma_{\xi_c}^2} = b_{11}\frac{\hat{P}_4T_f^2}{\sigma_{\xi_c}^2} + b_{12}\frac{\hat{P}_5T_f^3}{\sigma_{\xi_c}^2} + b_{13}\frac{\hat{P}_6T_f^4}{\sigma_{\xi_c}^2} \tag{457}$$

and

$$\frac{R_{\ddot{\hat{T}}_\varepsilon\tilde{\varepsilon}_{cn}}(\ell)T_f^2}{\sigma_{\xi_c}^2} = b_{31}\frac{\hat{P}_1}{\sigma_{\xi_c}^2} + b_{32}\frac{\hat{P}_2T_f}{\sigma_{\xi_c}^2} + b_{33}\frac{\hat{P}_4T_f^2}{\sigma_{\xi_c}^2} \tag{458}$$

where the b_{ij} are as defined in Equation (434), the $\underline{b}_{ij}$ are defined as the corresponding elements of the dimensionless matrix

$$[\underline{b}] \equiv \begin{bmatrix} \underline{b}_{11} & \underline{b}_{12} & \underline{b}_{13} \\ \underline{b}_{21} & \underline{b}_{22} & \underline{b}_{23} \\ \underline{b}_{31} & \underline{b}_{32} & \underline{b}_{33} \end{bmatrix} = [(I-K'H)\Phi']^{\ell-1} . \tag{459}$$

The normalized clock loop filtered error covariance terms are obtained from Equations (120)-(129), (160)-(165), and (448) as

$$\frac{\hat{P}_1}{\sigma_{\xi_c}^2} = K_T = \frac{A}{1+A} \tag{460}$$

$$\frac{\hat{P}_2T_f}{\sigma_{\xi_c}^2} = K_{\dot{T}}T_f = \frac{4}{r}\,\frac{B}{1+A} \tag{461}$$

$$\frac{\hat{P}_4 T_f^2}{\sigma_{\xi_c}^2} = K_T'' T_f^2 = \frac{4\rho}{r} \frac{D}{1+A} \tag{462}$$

$$\frac{\hat{P}_3 T_f^2}{\sigma_{\xi_c}^2} = \left(\frac{4}{r}\right)^2 \left[C - \frac{B^2}{1+A}\right] \tag{463}$$

$$\frac{\hat{P}_5 T_f^3}{\sigma_{\xi_c}^2} = \left(\frac{4}{r}\right)^2 \rho \left[E - \frac{BD}{1+A}\right] \tag{464}$$

and

$$\frac{\hat{P}_6 T_f^4}{\sigma_{\xi_c}^2} = \left(\frac{4\rho}{r}\right)^2 \left[F - \frac{D^2}{1+A} + \frac{1}{\rho^2}\right] \tag{465}$$

where A, B, and D are given by Equations (124)-(126) and, via Equations (101), (100) and (97),

$$F = -\frac{\rho^2}{1-\rho^2} \frac{D^2}{1+A} \tag{466}$$

$$E = \frac{F+1}{1-\rho} - \frac{\rho BD}{(1-\rho)(1+A)} \tag{467}$$

and

$$C = \frac{r}{4}\left(\frac{AB}{1+A} - D\right) + \frac{1}{2}(3E-F-1) \quad . \tag{468}$$

Curves of the normalized transmit timing error variance for the stationary-terminal maneuvering-satellite case versus the parameter r_s as obtained from Equation (444) are given in Figures 56 and 57 for values of I_r equal to 32 and 64 subframes/frame, respectively. The 1st term of the variance expression (Equation (444)) is dominant throughout most of the range of the curves. The second term is dominant, however, for small values of r_s, but decreases rapidly with increasing r_s thus producing the "breaks" in slope of the curves which are evident for larger values of λT_f. The third term is of alternating sign thus contributing to the ripples evident in these curves for lower values of r_s. This term also decreases with increasing r_s becoming generally negligible for $r_s \geq .01$.

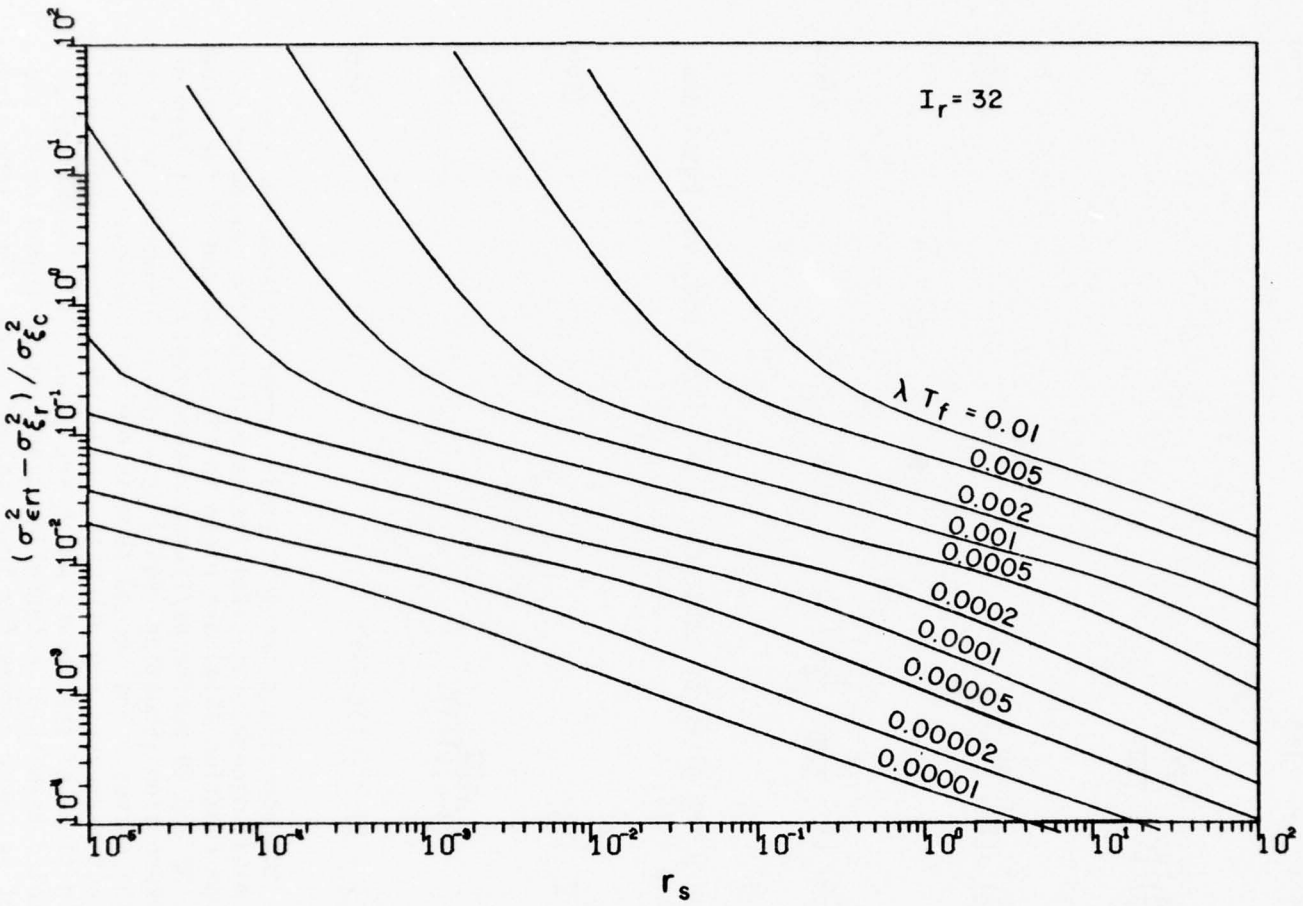

Figure 56. Normalized ranging loop timing jitter vs. r_s, stationary terminal.

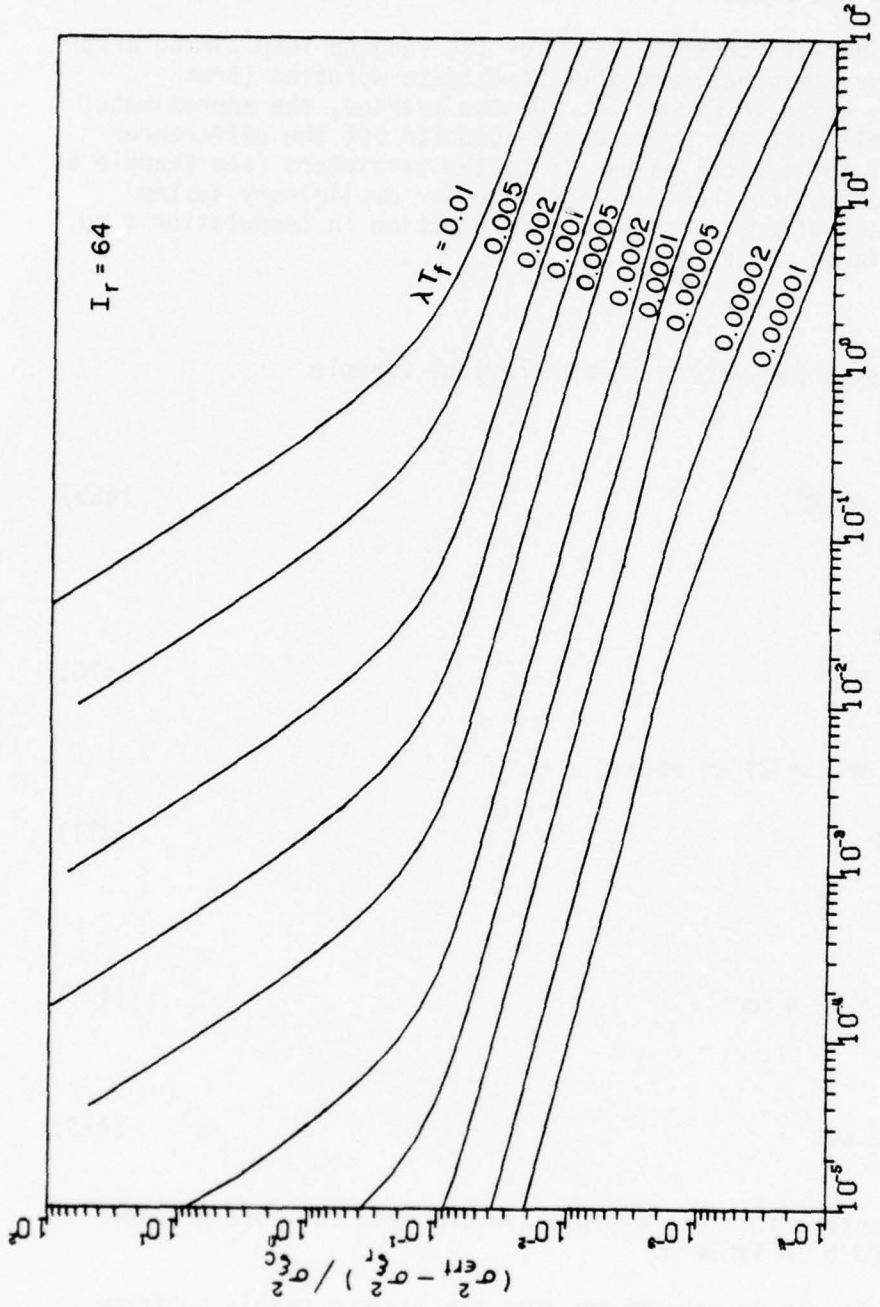

Figure 57. Normalized ranging loop timing jitter vs. r_s, stationary terminal.

The ripple for higher values of r_s is present in the first term (see Equation (415) and the associated discussion of sub-section 1. above).

A comparison between this solution for the ranging loop timing error variance (stationary terminal) and the approximate solution (from Equation (229)) is given in Figure 58. On the average, the approximate solution agrees well with the more exact solution but the differences may be significant for typical values of system parameters (see Example 6 below). The approximation should be adequate for preliminary system design, however, and offers a considerable reduction in computation time, particularly for large values of I_r.

Example 6

Using the system parameters of the previous example

$$\frac{\sigma^2_{\varepsilon_{rt}} - \sigma^2_{\xi_r}}{\sigma^2_{\xi_c}} = .7778 \tag{469}$$

and

$$r_s = 7.02 \cdot 10^{-4} \tag{470}$$

from Figure 56 (for I_r=32) we obtain

$$\lambda T_f = .00124 \quad . \tag{471}$$

Then

$$T_f = \frac{.00124}{.1} = 12.4 \text{ ms} \tag{472}$$

and

$$I_r T_f = 0.397 \text{ sec} \tag{473}$$

System parameters for this example are compared to those obtained for Examples 4 and 5 in Table 3.

Effects of changes in parameters upon the maximum usable subframe time for the case of a stationary-terminal maneuvering-satellite relay are shown by the families of curves, Figures 59 to 64. These curves were

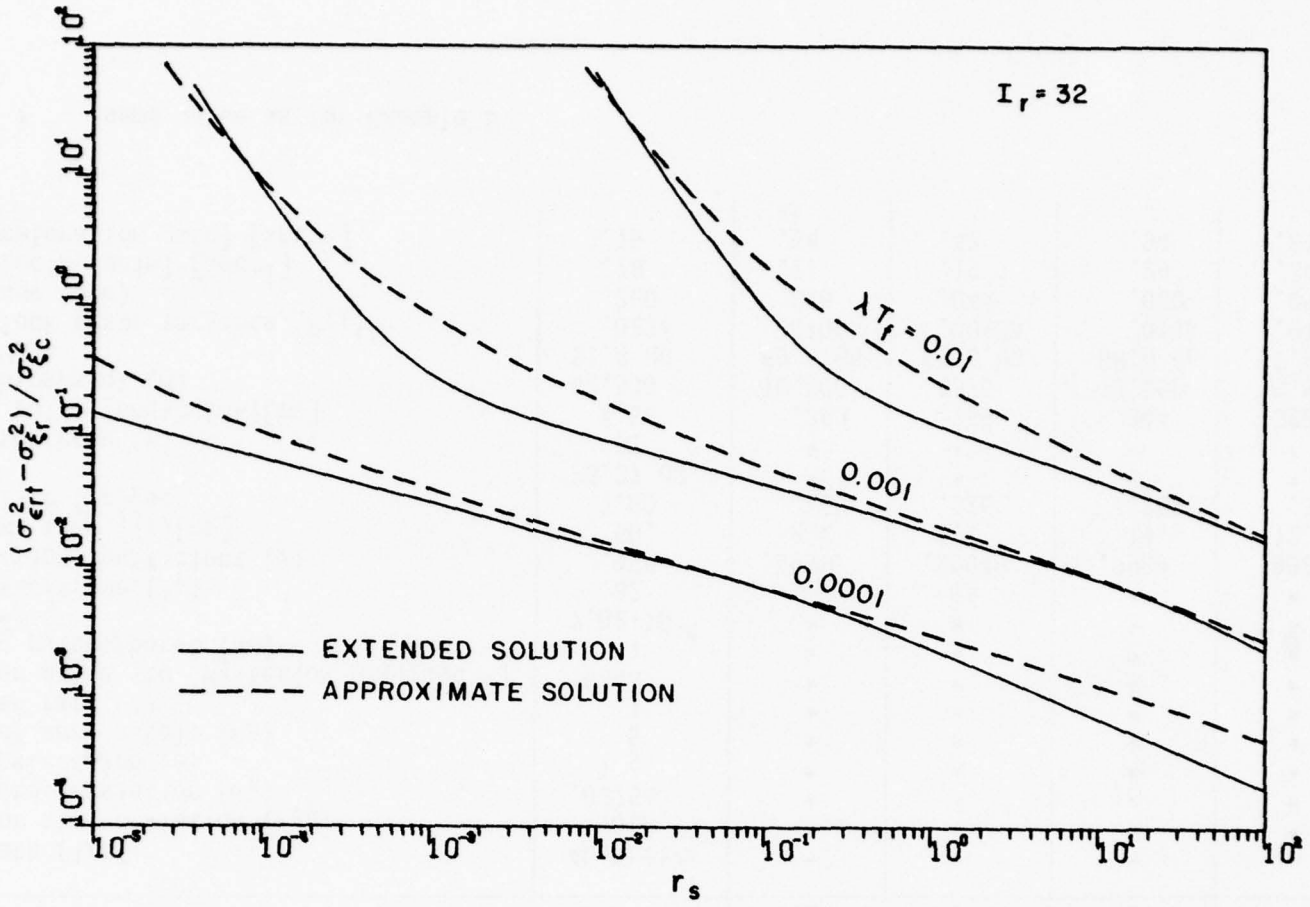

Figure 58. Comparison of extended and approximate solutions for the ranging loop timing jitter, stationary terminal.

Table 3
SYSTEM PARAMETERS FOR RANGING LOOP SYNCHRONIZATION

Parameter	STATIONARY SATELLITE	STATIONARY TERMINAL			
	Example 5	Example 4 (Approximations) a	b	c	Example 6
Code rate ($1/\Delta$)	40 Mbit/s	*	*	*	*
Tx error std. deviation (σ_{ε_r})	$.05\Delta$	*	*	*	*
Noise std. deviation (σ_ξ)	$.0375\Delta$	*	*	*	*
Max acceleration (A)	1 g.	*	*	*	*
Prob. of zero accel. (P_0)	.5	*	*	*	*
Maneuver rate (λ)	.1	*	*	*	*
Maneuver noise std. deviation (σ_a)[sec^{-2}]	$.534\Delta$	*	*	*	*
Ranging pulses/burst (N_r)	1	*	*	2	*
$r_s=\sigma_\xi\lambda^2/\sigma_a$	$7.02\cdot10^{-4}$	*	*	*	*
Subframes/frame (I_r)	32	*	64	*	*
Correlation coefficient (ρ)	.995	.99916	.99949	.9989	.99876
Subframe time (T_f)[ms]	50.	8.4	5.1	11.	12.4
Frame time (T_F)[sec]	1.60	.269	.326	.352	.397
E/N_0	23.37 dB	*	*	*	*
Slots/subframe (K)	32	*	*	*	*
Timing pulse length ($M\Delta$)[ms]	1.56	.263	.159	.344	.388
Code chips/slot (M)	62,500	10,500	6375	13,750	15,500
P/N_0 [Hz]	51.4 dB	59.2 dB	61.3 dB	58.0 dB	57.5 dB
Max. clock error variance $(\hat{P}_1)^{1/2}$	$.022\Delta$	$.0100\Delta$	$.0080\Delta$	$.011\Delta$	$.0118\Delta$
K_T (range gain)	.260	.066	.044	.080	.090
$K_{\dot{T}}$ (velocity gain) [sec^{-1}]	.78	.27	.19	.29	.34
$K_{\ddot{T}}$ (acceleration gain) [sec^{-2}]	1.15	.54	.42	.54	.64

* - same value as for Example 5

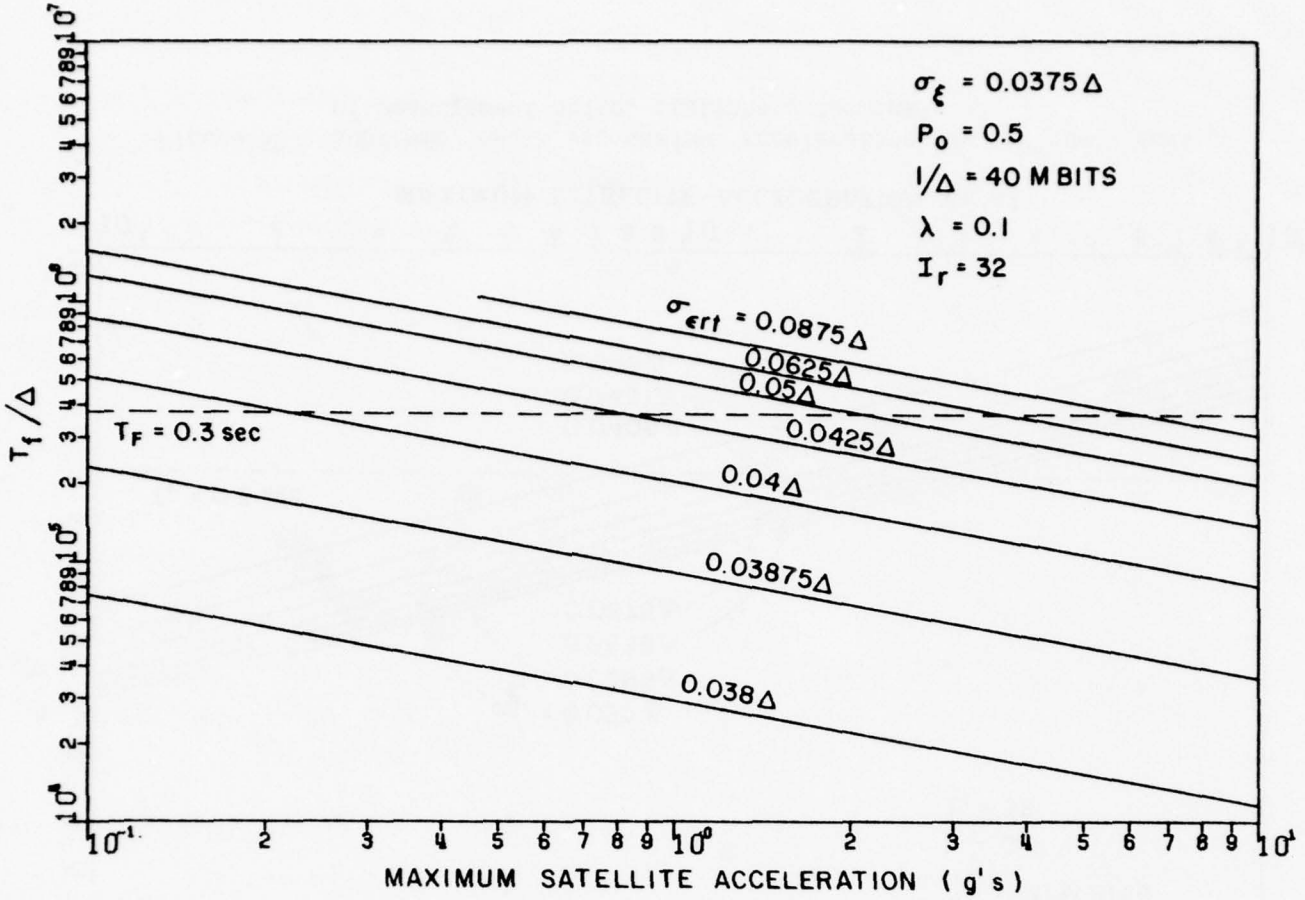

Figure 59. Subframe length vs. maximum acceleration for various values of transmit timing jitter, stationary terminal.

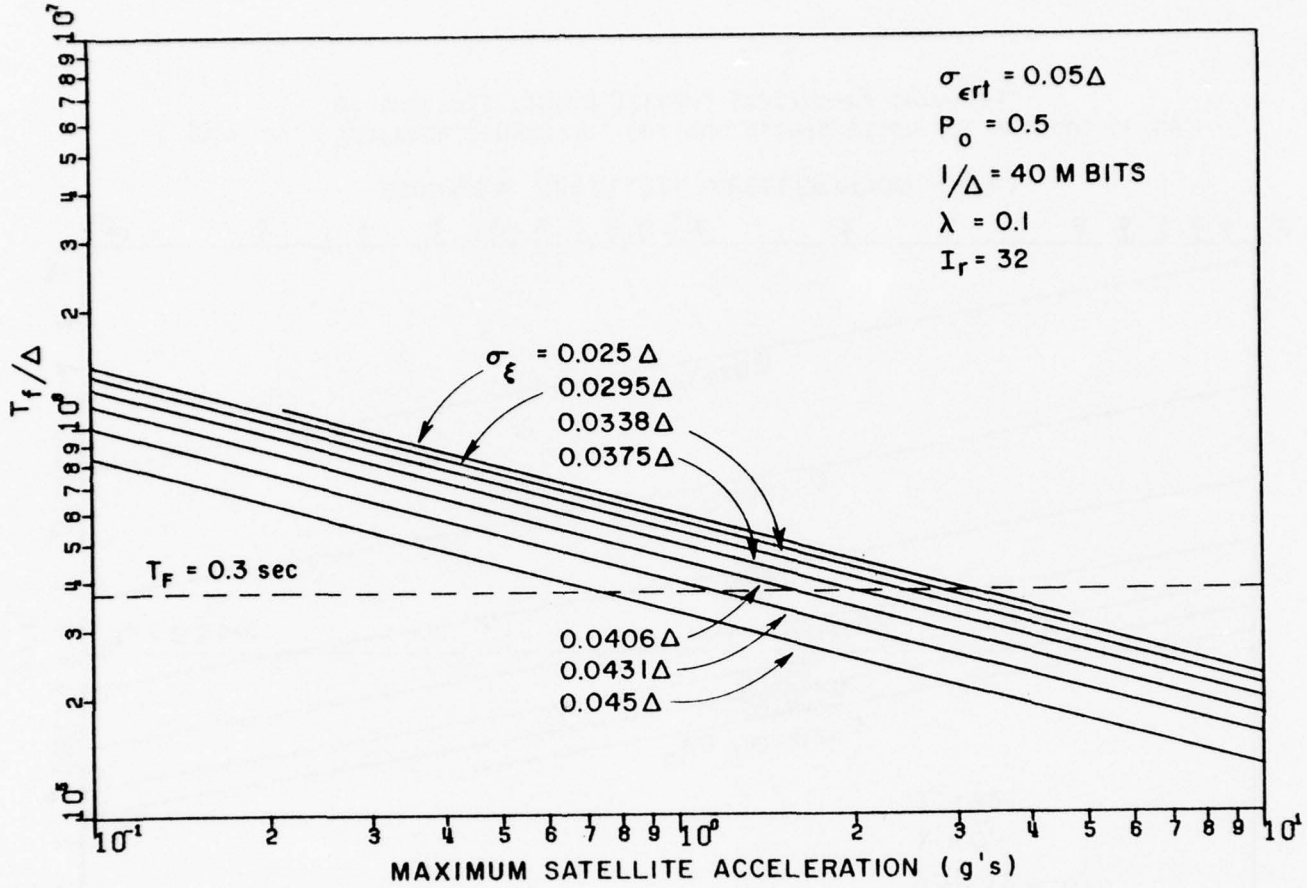

Figure 60. Subframe length vs. maximum acceleration for various values of measurement noise, stationary terminal.

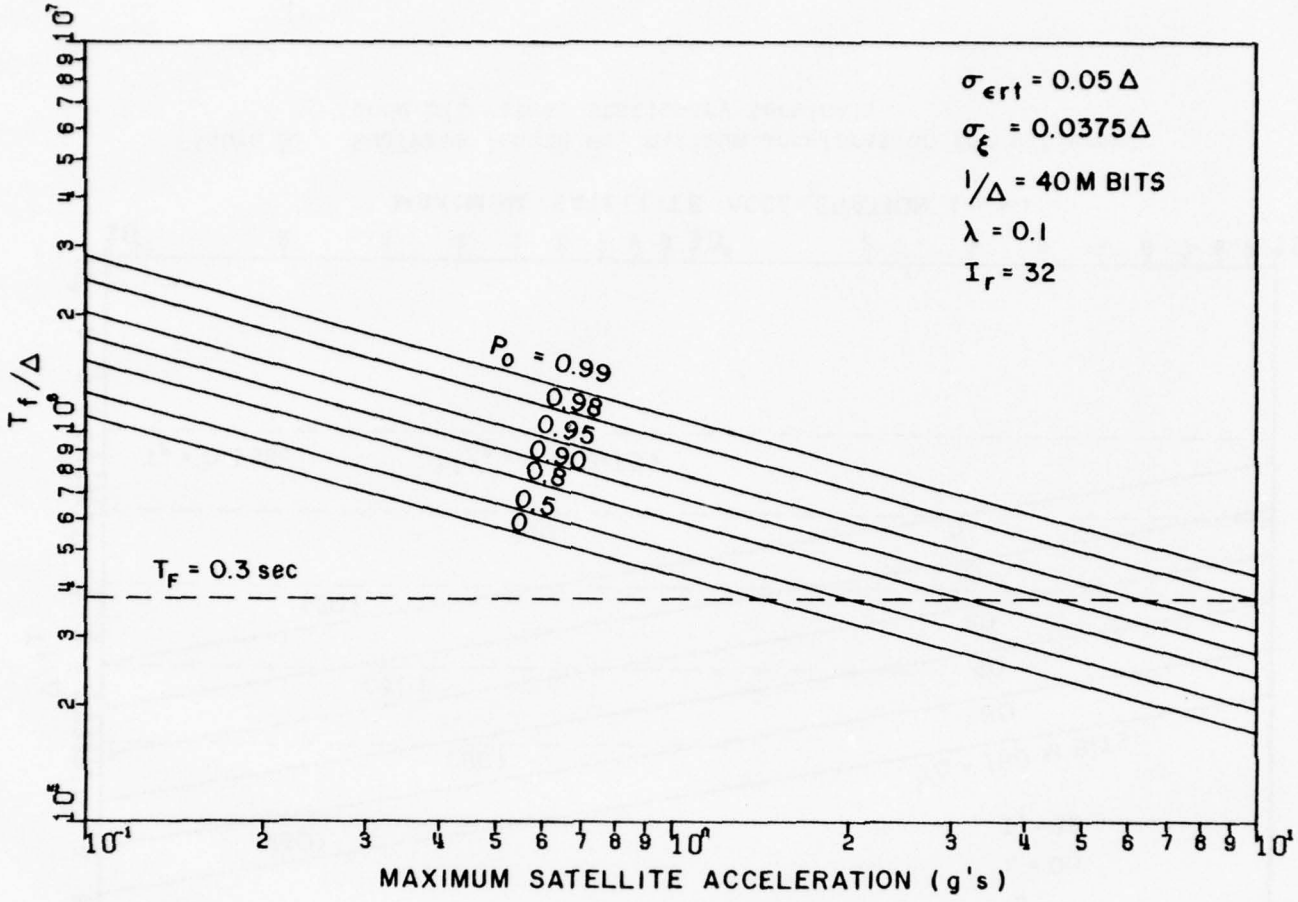

Figure 61. Subframe length vs. maximum acceleration for different maneuver probabilities, stationary terminal.

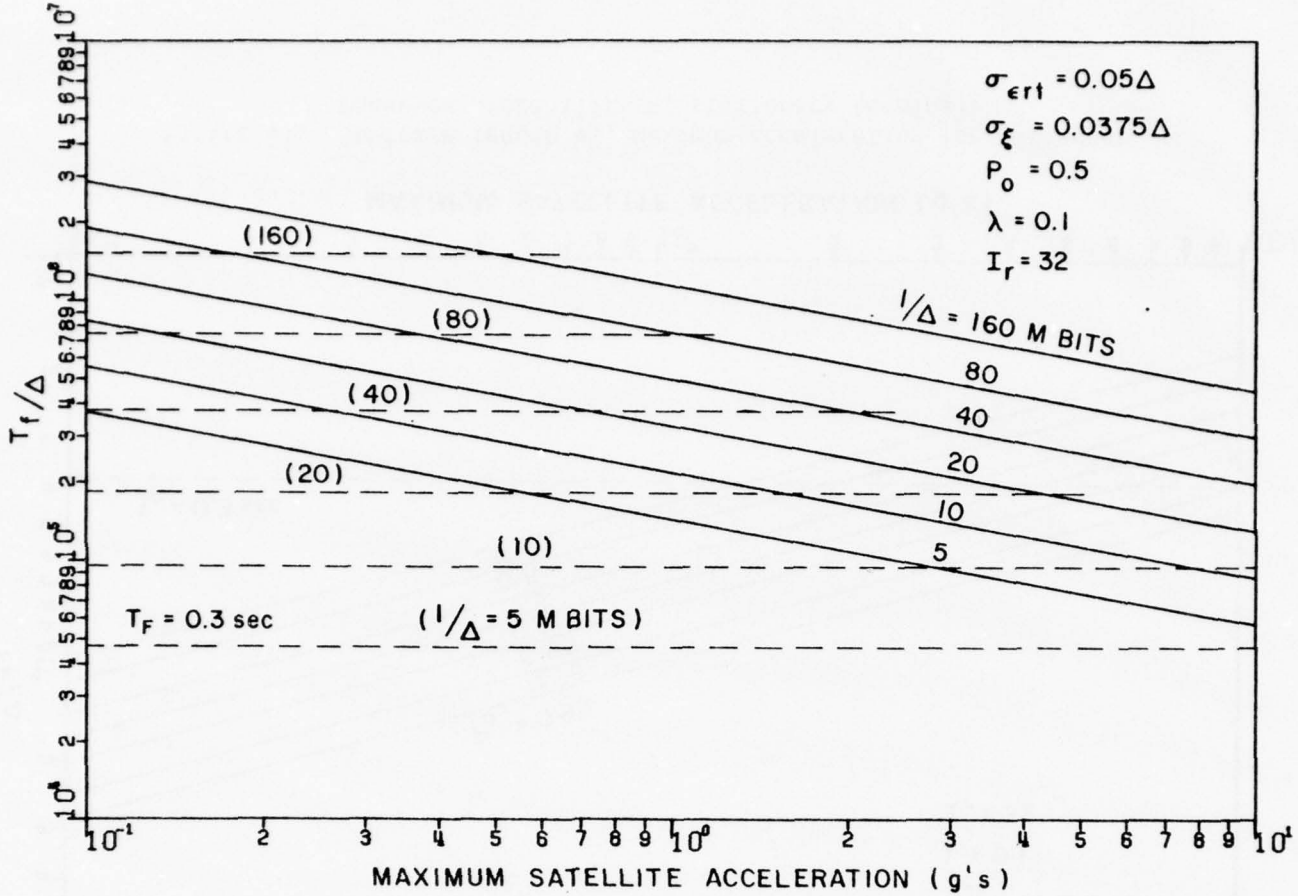

Figure 62. Subframe length vs. maximum acceleration for different code bit rates, stationary terminal.

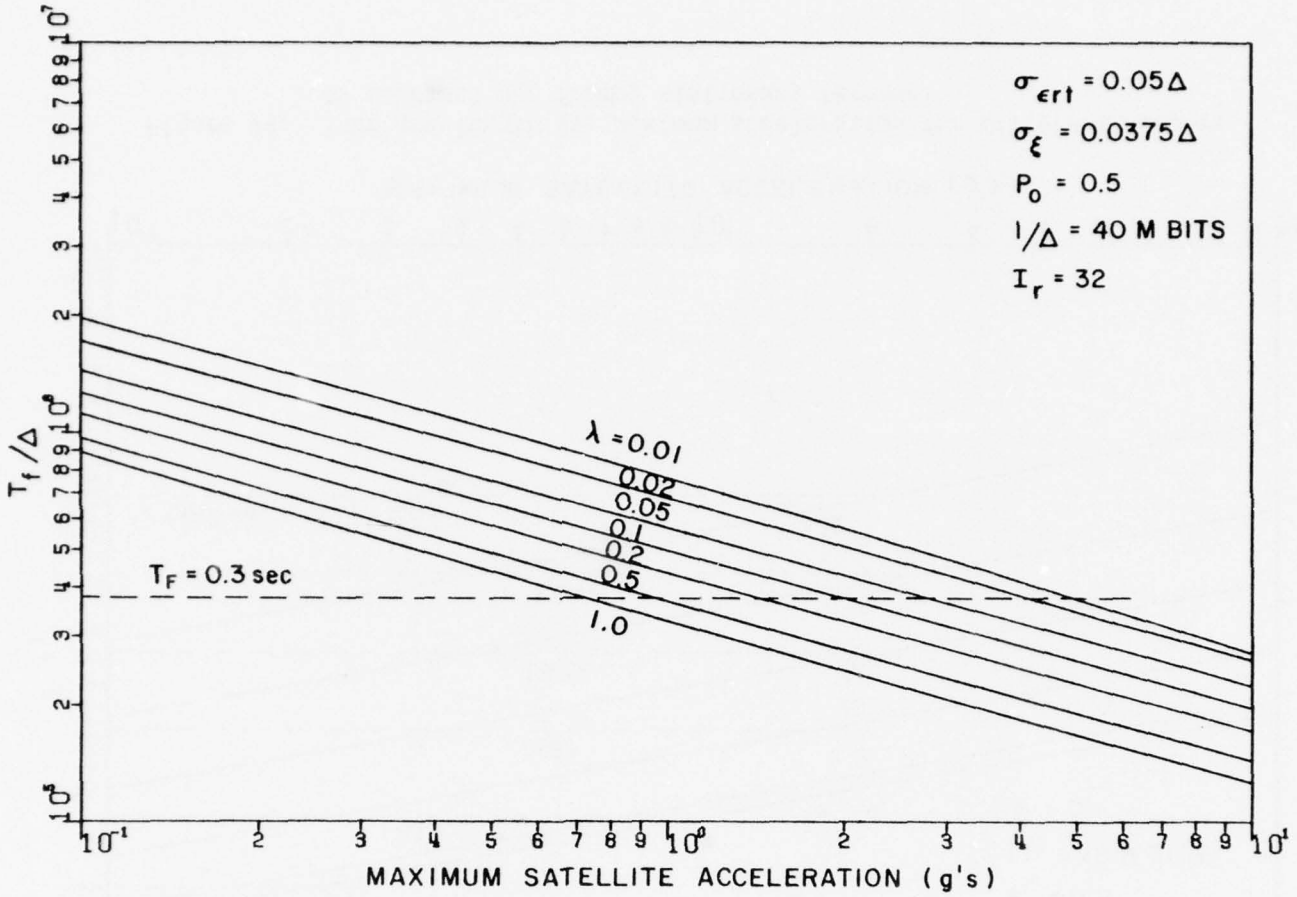

Figure 63. Subframe length vs. maximum acceleration for different maneuver rates, stationary terminal.

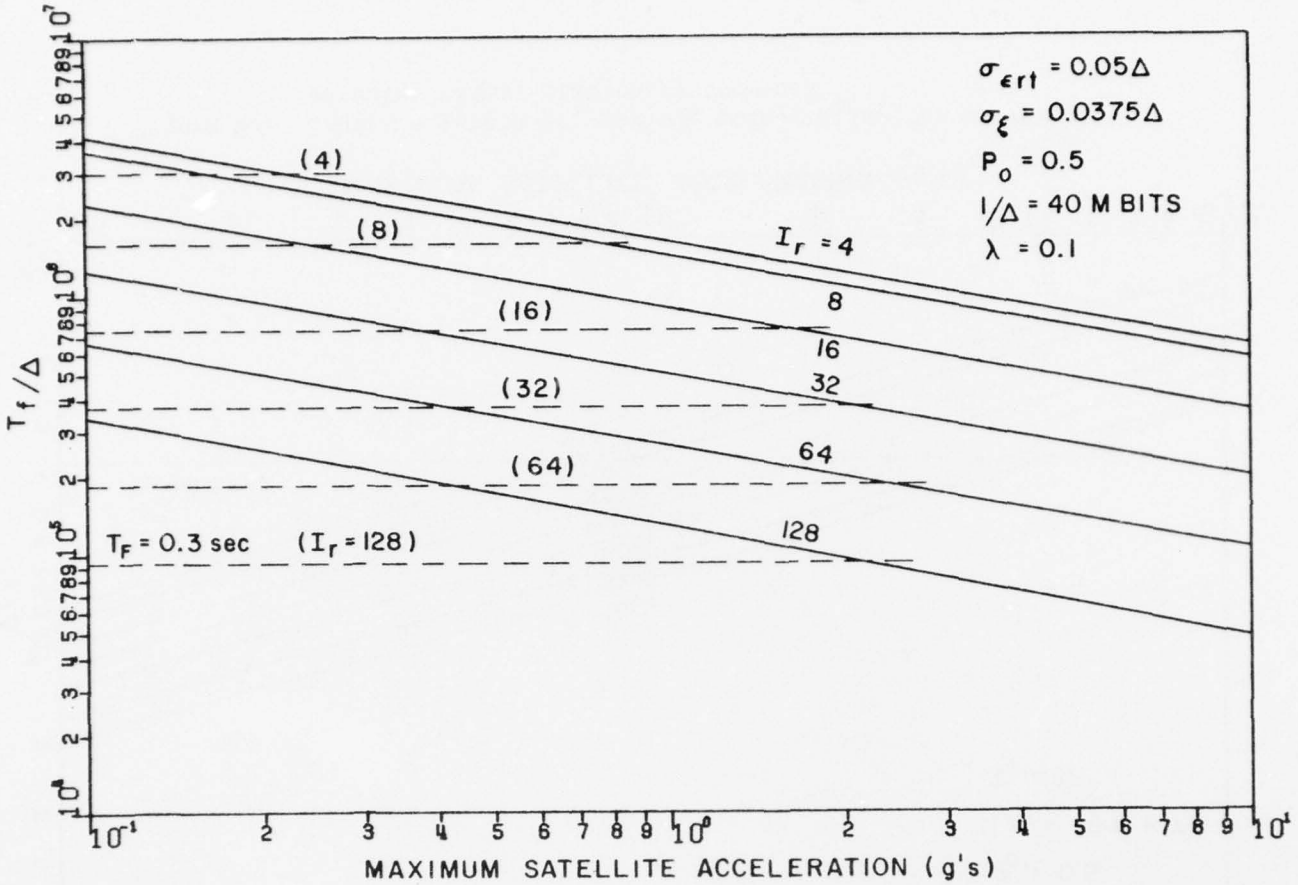

Figure 64. Subframe length vs. maximum acceleration for different numbers of subrames per frame, stationary terminal.

obtained via an iteration technique using Equation (444). As for the analogous curves (Figures 50 to 55) of the previous section (stationary-satellite maneuvering-terminal) the maximum usable subframe time is given by the appropriate curve of each family while the lower limit is set by the round trip path delay ($\approx$ 0.3 sec, for a synchronous satellite).

It is evident from these figures that the maximum usable subframe time for the maneuvering satellite case is considerably less than that for the corresponding case of the stationary satellite (as would be expected). Hence, since the lower bound ($T_F \approx .3$ sec) remains fixed, the range of parameters within the permissible operating range is correspondingly reduced. For example, from Figure 59, if the minimum permissible value for the subframe time ($T_f/\Delta \approx 3.75 \cdot 10^5$) is chosen, then a maximum satellite relay acceleration of approximately 2g. can be accommodated in order to maintain $\sigma_{\varepsilon_{rt}} \leq .05\Delta$, as compared to considerably more than 10g. terminal acceleration for the corresponding case with a stationary satellite.

As noted in the previous section the lower bound on subframe time is not applicable for essentially earth-bound relays where propagation delay becomes negligible. Also, as noted previously, the degradation in performance for the case of the maneuvering satellite relative to that of the stationary satellite arises because changes in satellite motion are not known at the terminal (where timing measurements and corrections are made) until after the (one-way) propagation delay. Hence, for an airborne relay where propagation delay is negligible, applicable system parameters must approach those of the previous section (i.e., the stationary satellite case) regardless of whether the terminal or the relay (or both) are maneuvering. Thus, for an atmospheric airborne relay, considerably greater maneuverability is permissible than for a satellite relay while maintaining the same transmit timing error variance. This is indeed fortunate since in the forseeable future airborne relays appear much more likely to be highly maneuverable than do satellites.

SECTION VII
SIMULATION STUDIES

This section presents typical examples of results obtained from the simulation studies performed to investigate the clock loop transient response and the filter performance under conditions of no terminal motion (zero X-vector) to check the validity of the Kalman filter model.

A. Transient Response

The transient response of the clock loop filter derived in Example 1 of Section IV is given in Figures 65 and 66. The parameters for this filter were given previously in Table 2. At time t=0 (0 iterations), when the filter is first turned on, there is a 1/2 chip delay in the system clock waveform. The filter, starting from zero delay, proceeds to acquire the delay as shown in Figure 65a. Measurement noise (σ_ξ=.05Δ) is included in the response shown in this figure, hence this curve represents the actual transient performance of the filter, at each iteration (i.e., following the processing of each data sample), for parameters as specified in table 2. Figure 65b shows the filter response for the same situation except the actual measurement noise has been reduced to zero so that the filter's transient response is more readily seen. Figure 66 illustrates a similar situation except that in this case the Kalman gains have reached steady state prior to the introduction of a 1/2 chip offset in delay. (This is equivalent to replacing the Kalman filter of the above example by the corresponding Wiener filter.) The initial response to the offset is seen to be somewhat slower, but the overshoot is also somewhat less, resulting in a total effective settling time not much different from that of the previous example. Hence, for this system there appears to be little advantage in employing a Kalman filter. The simpler Wiener filter would perform nearly as well.

An example for which the Kalman filter with variable gains may have a definite advantage over the fixed gain Wiener filter is shown, with and without measurement noise, in Figures 67 and 68. Parameters for this filter (which approximate the parameters of the present modems operating in the lower rate format [6], but with greatly increased measurement noise) are given in Table 4. In this case, the settling time for the Kalman filter (Figure 67) is considerably shorter than for the Wiener filter (Figure 68). However, the overshoot is somewhat greater and the effects of noise spikes just after turn on (when the Kalman gain is high) are very severe, which could cause problems with lock-up. Note, However, that the measurement noise variance used for this example is much greater than would normally be used in a practical system, therefore the effects of noise spikes in a practical system would be significantly smaller. If violent maneuvers (or sudden offsets in the clock oscillators) are expected during normal operation, then some

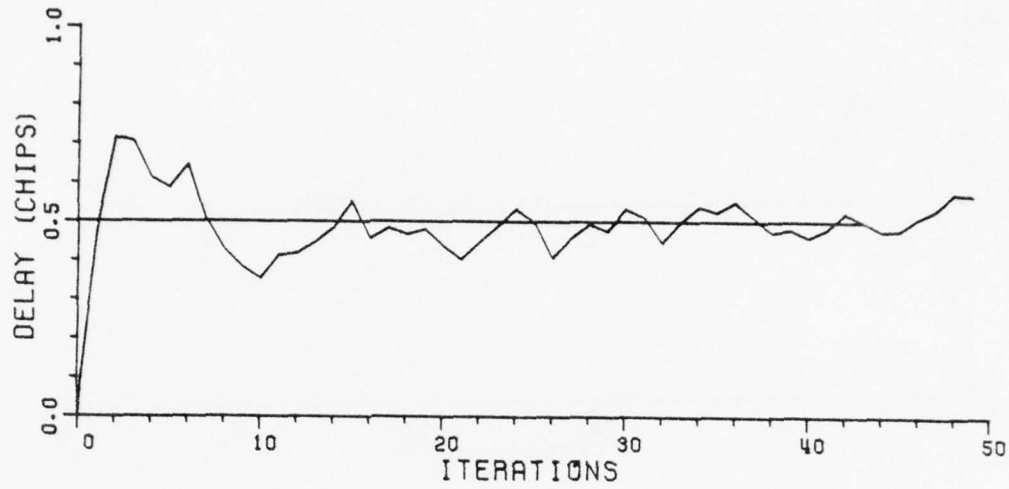

(a)

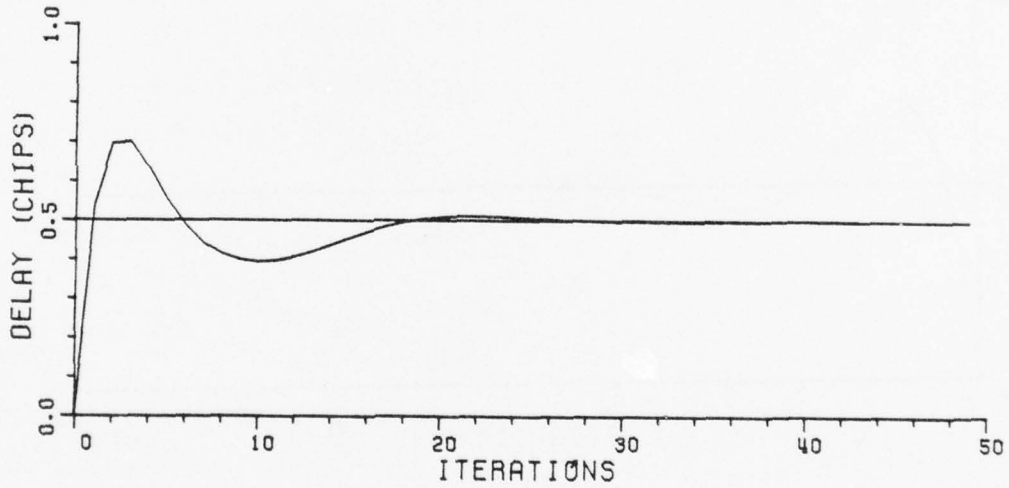

(b)

Figure 65. Transient response of the Kalman filter of Example 1.
(a) With noise (b) No measurement noise

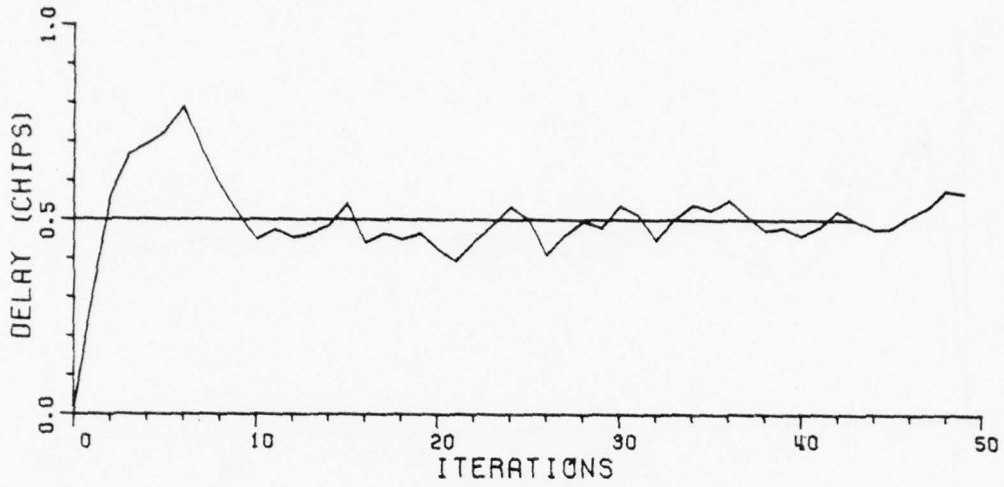

(a)

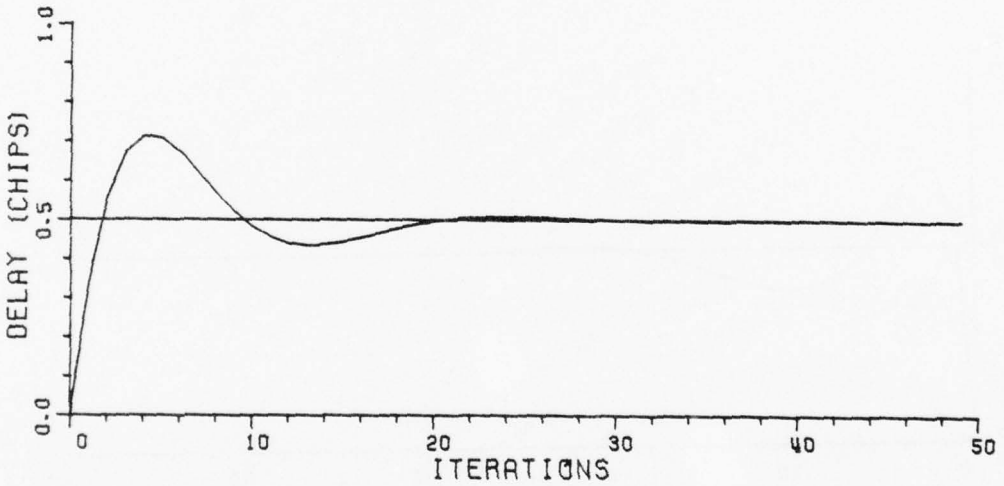

(b)

Figure 66. Transient response of the Kalman filter of Example 1 with fixed steady state (Wiener Filter) gains.

(a) With noise (b) No measurement noise

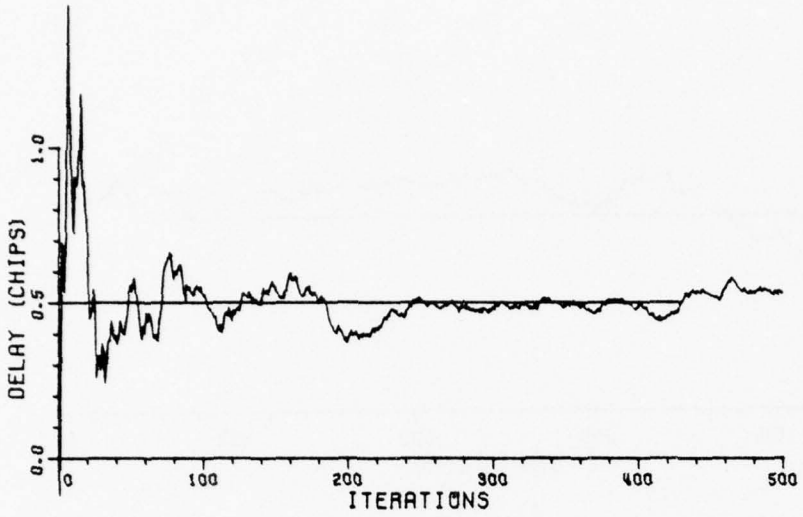

(a)

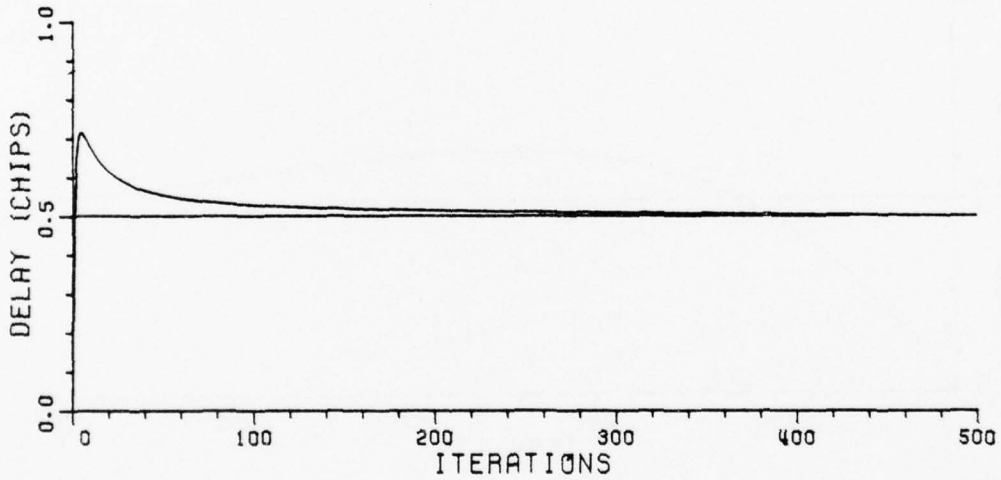

(b)

Figure 67. Transient response of the Kalman filter specified in Table 4.
(a) With noise (b) No measurement noise

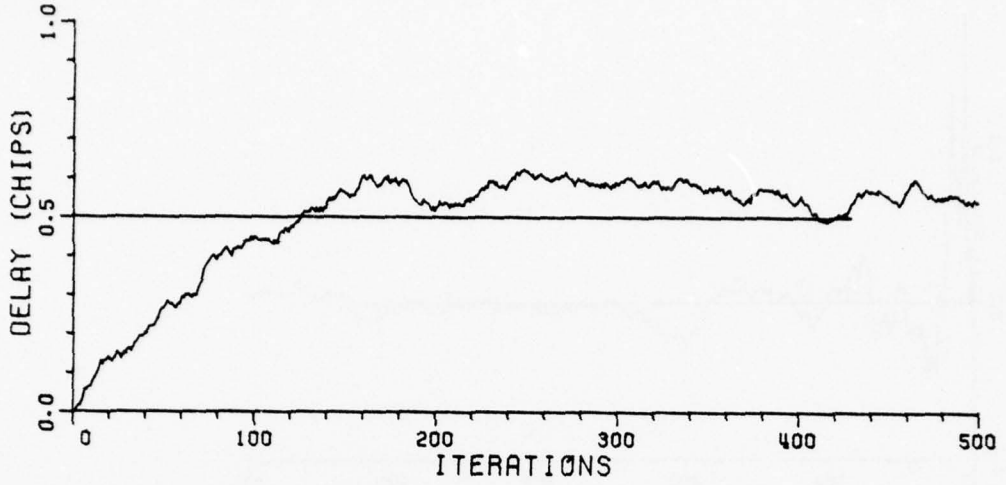

(a)

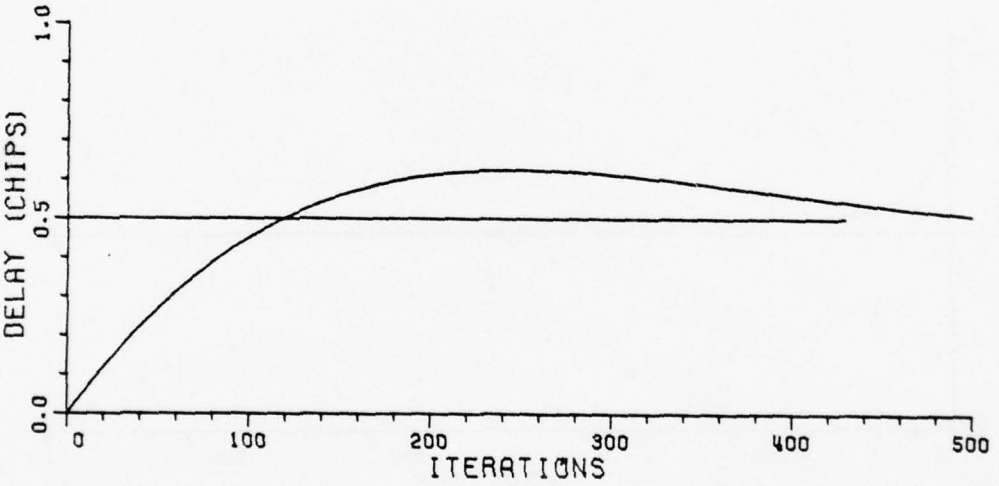

(b)

Figure 68. Transient response of the Kalman filter specified in Table 4 with fixed steady state (Wiener Filter) gains.

(a) With noise (b) No measurement noise

Table 4

Filter Parameters for the Response Curves of Figures 67 and 68.

Code Rate ($1/\Delta$)	140 Kbps
Max Timing Error Std. Dev. $(\tilde{P}_1)^{1/2}$	$.056\Delta$
Measurement Noise Std. Dev. (σ_ξ)	$.5\Delta$
Max. Terminal Acceleration (A)	5 g.
Maneuver Rate (λ)	.2 maneuvers/sec.
Subframe Time (T_f)	.0267 sec.
E/N_o	2.9 dB
$r_s = \frac{\sigma_\xi \lambda^2}{\sigma_a}$	4.80
K_T (steady state range gain)	.013
$K_{\dot{T}}$ (steady state velocity gain)	$2.97 \cdot 10^{-3}$
$K_{\ddot{T}}$ (steady state acceleration gain)	$2.52 \cdot 10^{-4}$

means of re-initializing the filter gains at those times must be incorporated; otherwise, any advantages of the Kalman filter over the steady state (Wiener) filter will be lost after initial system turn-on.

B. Steady State Zero Motion Response

Consider a Kalman filter which has been uniquely determined by specifying the process and measurement models according to Equations (4) and (5) of Section III, i.e.,

$$Z_{n+1} = \Phi Z_n + \Gamma u_n \tag{474}$$

$$X_n = H Z_n + \xi_n \quad . \tag{475}$$

The Kalman predictor algorithm uses Φ, Γ, H, and the variances σ_ξ^2 and σ_u^2 to obtain a prediction of the state Z via the equation

$$\hat{Z}_{n+1} = \Phi \hat{Z}_n + \underline{K}_n [X_n - H \hat{Z}_n] \tag{476}$$

where $\underline{K}_n$ is the prediction gain vector ($\underline{K}_n = \Phi K(n)$ of Section III). At the n+1 stage, the error in the prediction is given by

$$\bar{Z}_{n+1} = Z_{n+1} - \tilde{Z}_{n+1} \tag{477}$$

Upon substituting Equations (297) and (299) into (300), one obtains

$$\bar{Z}_{n+1} = \Phi Z_n + \Gamma u_n - \Phi \tilde{Z}_n - \underline{K}_n[X_n - H\tilde{Z}_n] \tag{478}$$

Under the constraint of zero motion, Equations (300) and (301) reduce to

$$\bar{Z}_{n+1} = - \tilde{Z}_{n+1} \tag{479}$$

$$\bar{Z}_{n+1} = - (\Phi - \underline{K}_n H) \tilde{Z}_n - \underline{K}_n \xi_n \quad . \tag{480}$$

The estimation error variance under this constraint is given by

$$\tilde{P}_{n+1} = E[\bar{Z}_{n+1} \cdot \bar{Z}_{n+1}^T] = (\Phi - \underline{K}_n H) \tilde{P}_n (\Phi - \underline{K}_n H)^T + \underline{K}_n \sigma_\xi^2 \underline{K}_n^T \tag{481}$$

since the measurement noise at the n^{th} sample is uncorrelated with the estimate at the n^{th} sample (Equations (475) and (476)). If a steady-state exists (as it does for the models of interest here), then in the steady-state $\tilde{P}_{n+1} = \tilde{P}_n = \tilde{P}$ and $\underline{K}_{n+1} = \underline{K}_n = \underline{K}$, so Equation (481) becomes

$$\tilde{P} = (\Phi \cdot \underline{K}H) \tilde{P} (\Phi - \underline{K}H)^T + \underline{K} \sigma_\xi^2 \underline{K}^T \tag{482}$$

Equation (482) is linear in $\tilde{P}$ and can easily be solved by a computer. Figure 69 shows the variation in the normalized standard deviation of the prediction error $\sqrt{\tilde{P}_1}/\sigma_\xi$, as a function of the parameter $r_s = \sigma_\xi \lambda^2/\sigma_a$ for various λT_f. The solid lines are general Kalman filter results (no constraints) as obtained in Section IV, and given here for comparison, while the dotted lines are the solutions under the zero motion constraint. Note that the error standard deviation is reduced under the zero motion constraint as stated previously, although the filter is no longer optimum for this condition.

The results of Figure 69, for zero motion constraints, were verified by a computer simulation in which the filter is given a noise input and the error variance is observed. Φ, Γ, H, and the prior statistics σ_ξ^2, and σ_u^2 were specified and the filter was iterated with no input until steady state was achieved. After steady state was

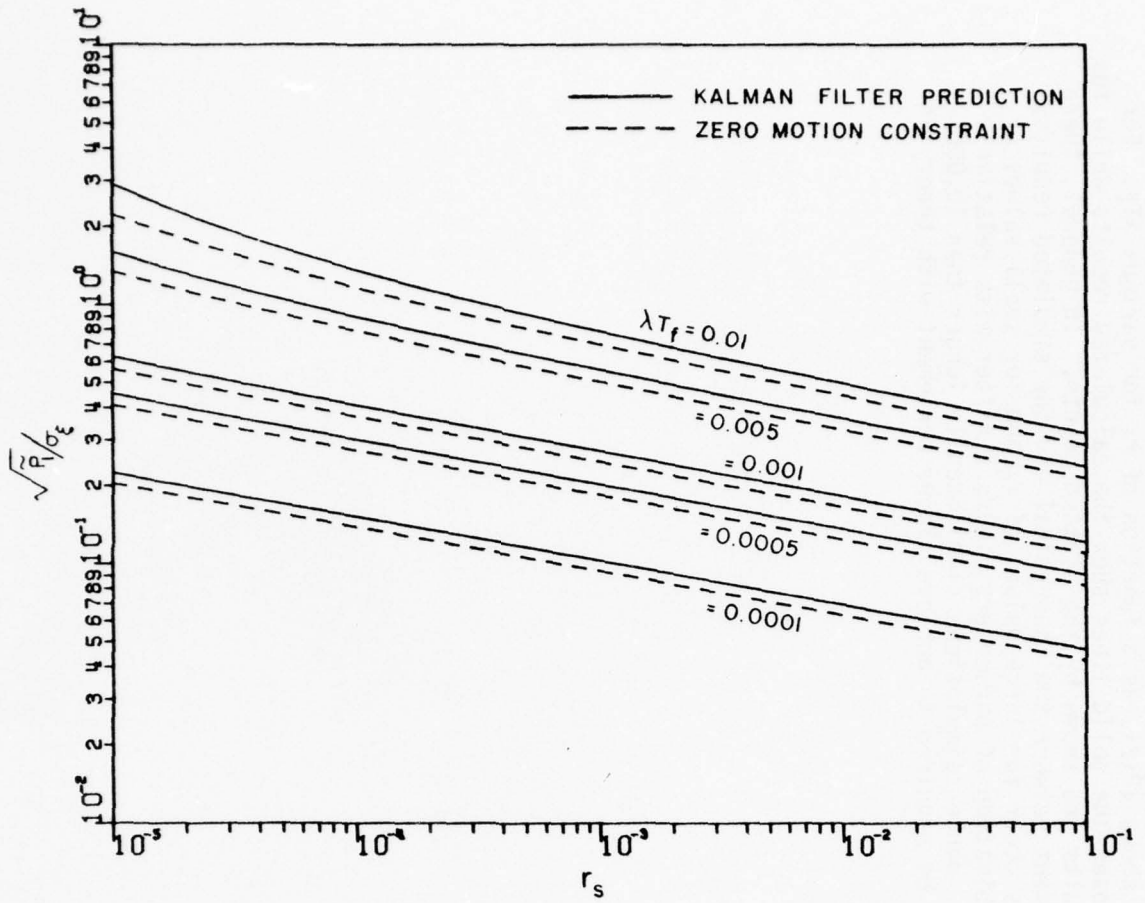

Figure 69. Analytic solution for the Kalman filter prediction error standard deviation vs. r_s with zero motion constraint.

achieved, the filter was given an input of Gaussian noise with variance σ_ξ^2 and iterated for an additional 10,000 iterations. A running sum of the squared prediction error was kept and after the 10,000 iterations the sum was divided by 10,000 to yield the error variance.

Figure 70 shows $\sqrt{\tilde{P}_1}/\sigma_\xi$ as a function of r_s for various λT_f. For reference purposes the solid lines show the calculated results while the simulation results are shown by the plotted points. In general, there is close agreement between the theoretical and the simulated results. The differences occur for large values of r_s and for small values of λT_f. This combination of parameters yields a filter with relatively slow response. Hence, simulations significantly longer than 10,000 iterations may be required to achieve closer agreement with theory in these cases.

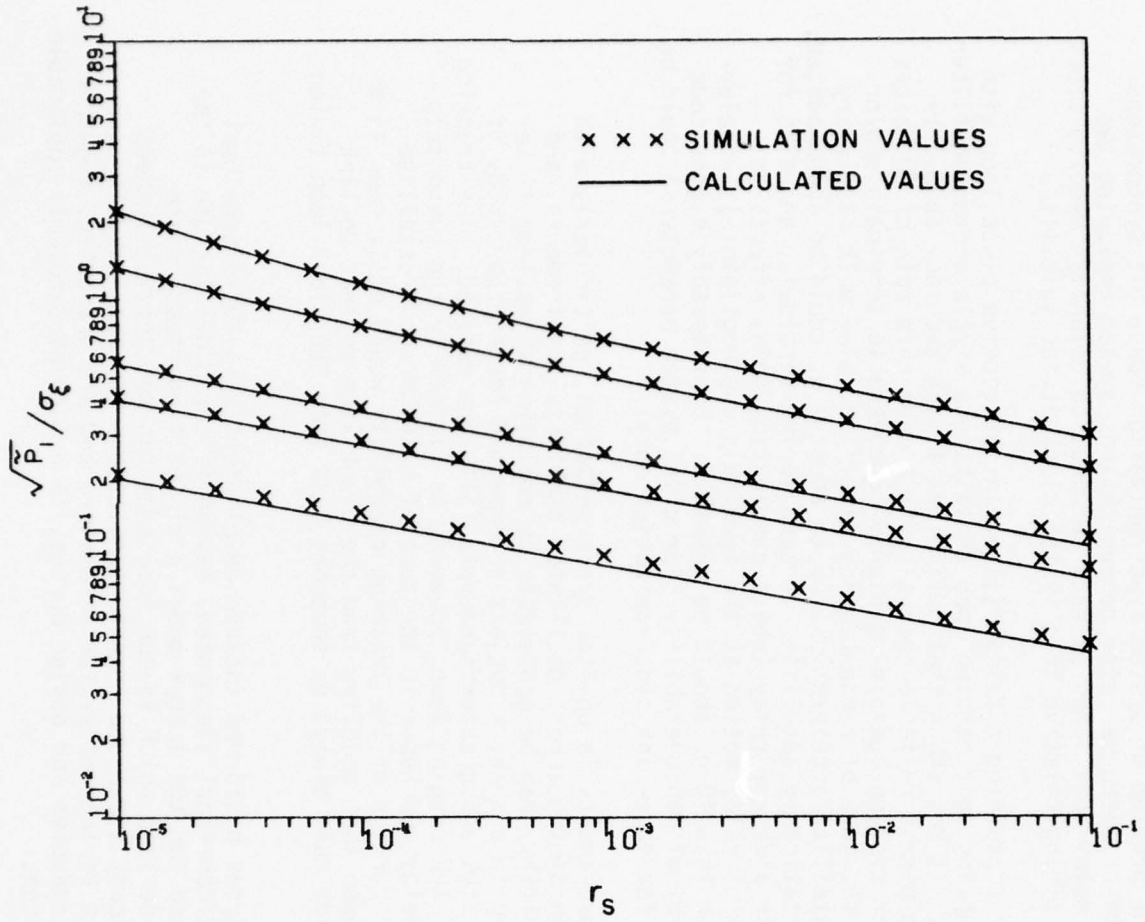

Figure 70. Simulation results for the Kalman filter prediction error standard deviation vs. r_s, with zero motion constraint.

SECTION VIII
CONCLUSIONS

Optimum linear recursive (Kalman) filter techniques have been applied to the problem of system synchronization for a bit synchronous TDMA satellite or airborne relay communications system employing two sampled data delay lock loops at each terminal to establish receive clock and transmit timing relative to a system clock at the satellite.

A system containing a Kalman filter in the receive clock loop with open loop coupling to a ranging loop containing a simple averaging filter was analyzed. It was shown that sufficient timing accuracy should be achievable to permit reliable operation at a code chip rate of 40 Mbit/s or greater for systems containing highly maneuverable terminals and/or relays. For the case of a maneuvering satellite relay with stationary terminals, satellite accelerations up to about 2 g. could be accommodated; while for a stationary satellite and maneuvering terminals, and also for the case of an airborne relay (where propagation delay effects on determination of relay motion at the terminals are negligible), accelerations greater than 10 g. should be possible. Considerably higher code rates and terminal maneuverability (for given system parameters) could be accommodated for down-link synchronization only.

Some improvements in up-link synchronization, particularly with regard to mean timing error, oscillator stability requirements, and lock-up capability, may be achievable by employing an optimum filter in the ranging loop also, a subject recommended for further study if higher code rates and greater maneuverability are desired. The tracking capability of the ranging loop, however, is limited by the round trip propagation delay and hence in the case of a synchronous satellite relay a major portion of the tracking capability would still need to be provided by open loop coupling from the clock loop so that up-link timing accuracy must always be somewhat less than the clock loop timing accuracy.

The analyses performed include development of a two-dimensional and a three-dimensional (augmented) Kalman filter model for use in the clock loop, and for the latter model a closed form steady state solution was derived which to our knowledge has not perviously been obtained. Steady state and transient solutions for these models were computed for a variety of system parameters and are presented, together with typical examples and design curves, in a form particularly applicable to system design.

Simulation studies were also performed to further investigate transient response, to compare the performance of the variable gain Kalman filter to that of the fixed gain Wiener filter, and to verify the models and the analytical results obtained. Simulation results were

in good agreement with analytical results in all cases, and it was found that for high data rate systems of this type, the fixed gain Wiener filter often performs nearly as well as the variable gain Kalman filter. There may be significant differences in lock-up capability however, and this is the subject of current investigation.

Recommendations for future work in this area include design, breadboarding, and testing of critical parts of the proposed TDMA timing system, particularly the clock loop Kalman filter; followed by eventual construction and testing of a complete timing system including both the clock loop and ranging loop. (An incremental time base shifter applicable to this system for local clock timing corrections is currently being developed under this contract.) Current theoretical studies involving lock-up characteristics and transient response should be continued and an investigation of the possible advantages (primarily in lock-up and transient response) of incorporating an optimum filter in the ranging loop is also suggested.

REFERENCES

[1] R. J. Huff, "An Investigation of Time Division Multiple Access Space Communications System," Ph.D. Dissertation, The Ohio State University, 1969.

[2] R. J. Huff, D. C. Upp and K. L. Reinhard, "The Synchronization of Time Division Multiple Access Systems -- An Analytical and Experimental Study," Report 2358-9, January 1969, The Ohio State University ElectroScience Laboratory, Department of Electrical Engineering; prepared under Contract F30602-67-C-0119 for Rome Air Development Center. (AD 689223)

[3] R. J. Huff, "TDMA Space Communications Systems: Concepts and Practical Techniques," Bulletin 206, Engineering Experiment Station, The Ohio State University, Columbus, Ohio 43210.

[4] R. J. Huff, "Multifunction TDMA Techniques," Report 3364-3, August 1974, The Ohio State University ElectroScience Laboratory, Department of Electrical Engineering; prepared under Contract F30602-72-C-0162 for Rome Air Development Center. (RADC-TR-74-327) (AD/A 004196)

[5] T. W. Miller, R. Caldecott and R. J. Huff, "A Satellite Simulator With a TDMA-System Compatible Adaptive Array," Report 3364-4, January 1976, The Ohio State University ElectroScience Laboratory, Department of Electrical Engineering; prepared under Contract F30602-72-C-0162 for Rome Air Development Center. (RADC-TR-76-98) (AD-B011048L)

[6] R. C. Taylor and R. J. Huff, "A Modem/Controller for TDMA Communications Systems," Report 3364-5, August 1976, The Ohio State University ElectroScience Laboratory, Department of Electrical Engineering; prepared under Contract F30602-72-C-0162 for Rome Air Development Center.

[7] A. P. Sage and J. L. Melsa, Estimation Theory with Applications to Communications and Control, New York: McGraw Hill Book Company, 1971.

[8] N. E. Nahi, Estimation Theory and Applications, New York: John Wiley and Sons, Inc., 1969.

[9] Bernard Friedland, "Optimum Steady-State Position and Velocity Estimation Using Noisy Sampled Position Data," IEEE Transactions on Aerospace and Electronic Systems, Vol. AES-9, No. 6, November 1973, pp. 906-911.

AD-A062 992 OHIO STATE UNIV RESEARCH FOUNDATION COLUMBUS F/G 17/2
TDMA TIMING LOOPS FOR HIGH DATA RATE SYSTEMS.(U)
NOV 78 W G SWARNER, C W CHUANG, R J HUFF F30602-75-C-0061
UNCLASSIFIED OSURF-710300-1(ESL) RADC-TR-78-238 NL

3 OF 3
AD
A062992

END
DATE
FILMED
3 -79
DDC

[10] R. A. Singer and K. W. Behnke, "Real Time Tracking Filter Evaluation and Selection for Tactical Applications," IEEE Transactions on Aerospace and Electronic Systems, Vol. AES-7, No. 1, January 1971, pp. 100-110.

[11] M. Abramowitz and I. A. Stegun, Handbook of Mathematical Functions with Formulas, Graphs, and Mathematical Tables, U. S. Department of Commerce, National Bureau of Standards, Applied Mathematical Series 55, 1964, pp. 17-18.

[12] S. M. Selby, Standard Mathematical Tables, 15th Edition, The Chemical Rubber Co., Cleveland, Ohio, 1967, p. 88.

MISSION
of
Rome Air Development Center

RADC plans and conducts research, exploratory and advanced development programs in command, control, and communications (C^3) activities, and in the C^3 areas of information sciences and intelligence. The principal technical mission areas are communications, electromagnetic guidance and control, surveillance of ground and aerospace objects, intelligence data collection and handling, information system technology, ionospheric propagation, solid state sciences, microwave physics and electronic reliability, maintainability and compatibility.